Milk Extracellular Vesicles-Mediated Oral Delivery of TNFα RNA Interference for Inflammatory Bowel Disease (IBD)

Zhang, Yunyue

Awarding institution:
King's College London

Milk Extracellular Vesicles-Mediated Oral Delivery of TNFα RNA Interference for Inflammatory Bowel Disease (IBD)

by

Yunyue Zhang

A thesis submitted to King's College London

in partial fulfilment for the degree of

Doctor of Philosophy

Supervisors:

Dr. Driton Vllasaliu

Dr. Maya Thanou

Faculty of Life Sciences & Medicine

School of Cancer and Pharmaceutical Sciences

2024

This thesis is dedicated to my family.

ABSTRACT

Inflammatory bowel disease (IBD) is a chronic and progressive disorder with destructive inflammation in the gastrointestinal tract (GIT). RNA interference, which is mediated by small interfering RNA (siRNA), has been recognized as an efficient approach for downregulating the expression of tumour necrosis factor α (TNFα) at inflamed intestinal mucosa, thereby reduces inflammation and restores the damaged mucosa. Considering the site of drug action in IBD resides within the GIT itself, oral administration of medication is naturally the preferred and most efficacious choice. However, oral administration of siRNA is currently not possible since the physiological barriers in GIT pose significant challenges. Milk extracellular vesicles (mEVs), which could potentially resist *in vitro* digestion and possess the ability to transport across the intestinal epithelium, may serve as vehicles for oral delivery of anti-TNFα siRNA in IBD.

This work focuses on the development of mEVs-based systems for oral siRNA delivery and the investigation of their potential for IBD therapy. Initially, mEVs were isolated by ultracentrifugation from bovine milk and purified by size exclusion chromatography (SEC). Expected size, remarkable yield, high purity, characteristic protein markers and typical morphology were exhibited among isolated mEVs. Thereafter, various strategies were assessed for loading siRNA into mEVs, and the most effective method (using a commercial transfection kit) achieved a loading efficiency above 20%.

The potential of mEVs as oral delivery systems for siRNA in IBD therapy was investigated in this study. The results showed that mEVs efficiently translocate across the Caco-2 intestinal epithelial model, which is not compromised by treatment with simulated intestinal fluids. Significantly, two relevant *in vitro* human intestinal epithelial organoids (IEOs) models were initially created: a 3D apical-out IEO model and an IEO monolayer model. Unlike the conventional culture of IEOs whereby the apical surface is shielded in the interior of organoids,

these models enabled the investigation of the apical-to-basolateral permeability of mEVs. mEVs demonstrated similar permeability through these highly human relevant models, demonstrating their potential for oral delivery. Furthermore, mEVs loaded with siRNA successfully induced (glyceraldehyde 3-phosphate dehydrogenase, GAPDH) gene silencing in J774A.1 macrophages, confirming the therapeutic potential of mEVs delivery systems.

To improve the siRNA loading efficiency of mEVs, hybrid nanovesicles ('hybridosomes') based on mEVs and liposomes were developed in this work. Hybridosomes were fabricated using two related methods based on freeze-thawing fusion of mEVs and cationic liposomes. The systems were 180-230 nm and demonstrated efficient loading of siRNA cargo. Hybridosomes exhibited significantly lower cytotoxicity in intestinal Caco-2 cells and superior stability in a fed-state simulated intestinal fluid compared to cationic liposomes. Furthermore, these systems significantly increased the transport of siRNA across the *in vitro* intestinal model, and hybridosomes loaded with GAPDH siRNA successfully induced transfection in J774A.1 macrophages. Importantly, anti-TNFα siRNA loaded-hybridosomes and -mEVs were both able to downregulate TNFα levels and relieve inflammation in an *in vitro* co-culture model of intestinal inflammation.

In conclusion, this work demonstrates that mEVs and mEVs-mediated hybridosomes can either act as safe and effective systems for potential oral delivery of siRNA therapies in IBD.

Table of Contents

List of Relevant Publications

[1] **Yunyue Zhang**, Xiang Luo, Ning Ding, Mona Belaid, Maya Thanou, Driton Vllasaliu (2024). Hybrid milk extracellular vesicles as potential systems for oral delivery of siRNA. *Advanced Therapeutics*, 2300335.

[2] **Yunyue Zhang,** Mona Belaid, Xiang Luo, Armond Daci, Rinë Limani, Julia Mantaj, Matthias Zilbauer, Komal Nayak, Driton Vllasaliu (2023). Probing milk extracellular vesicles for intestinal delivery of RNA therapies. *Journal of Nanobiotechnology, 21*, 406.

[3] **Yunyue Zhang,** Maya Thanou, Driton Vllasaliu (2020). Exploiting disease-induced changes for targeted oral delivery of biologics and nanomedicines in inflammatory bowel disease. *European Journal of Pharmaceutics and Biopharmaceutics, 155,* 128-138.

[4] Shilpa Lekhraj Peswani Sajnani, **Yunyue Zhang,** Driton Vllasaliu (2021). Exosome-based therapies for mucosal delivery. *International Journal of Pharmaceutics, 608,* 121087.

ACKNOWLEDGEMENTS

First and foremost, I would like to express my deepest gratitude to my primary supervisor, Dr. Driton Vllasaliu, who encouraged and directed me throughout the PhD study. Dr. Vllasaliu consistently has an open mind towards my ideas and supports my bold attempt in research. I am also deeply thankful to my second supervisor Dr. Maya Thanou for her exemplary guidance and valuable ideas during my project, and her enthusiasm to science research deeply affected me.

I would like to thank my lab group members: Dr Julia Mataj, Elliott Higgin, Mona Belaid, Xiang Luo, Sa Feng and Ding Ning, for their invaluable assistance and enriching my PhD journey with enjoyable experiences. I am particularly thankful for Dr. Mataj's guidance in intestinal organoid culturing, as well as all her support from the inception of my first-year PhD research. I wish to express my thanks to Mona Belaid and Sa Feng for their contributions to the co-culture model development, and in particular, thanks Mona Belaid for her patience and support in our Cambridge project. Working with these wonderful colleagues not only brings me professional rewarding but also joy and happiness to my PhD life.

I will forever be grateful to my family members for their unwavering love and support. My husband Leyan Li, the closest person to my life, gives me all his unconditional love and encouragement, especially during challenging times in my PhD research. I am extremely thankful to my father Mr. Xuedong Zhang, who is the first hero in my life. His dedication to the pursuit of truth, his patience in work, and his indomitable spirit have always inspired me to move forward and stay strong. My mother, Mrs. Hua Nie, has been consistently offering her most gentle words to support both my study and life. I would like to express my gratitude to my new-born son, Oliver Wu Li, whose arrival makes my life shining and I hope to have made him proud.

Finally, I extend my sincere thanks to my friends: Qing Guo, Wanqing Zhu, Lin Zhang, Weiqi Zhang, Wenjing Hu, Chubin Zhang and Yiran Wang for their assistance on my research, and their uplifting conversations and encouragement throughout my PhD journey added vibrancy and happiness to my life.

ABBREVIATIONS

18:0 PEG2000 PE	1,2-Distearoyl-*sn*-glycero-3-phosphoethanolamine-*N*-[methoxy(polyethylene glycol)-2000] (ammonium salt)
ALIX	ALG-2-interacting protein X
ANXA5	Annexin A5
BM	Basement membrane
BME	Basement membrane extract
CaP	Calcium phosphate
CD	Crohn's Disease
CD14	Cluster of differentiation 14
CPP	Cell-penetrating peptide
DDM	*n*-Dodecyl-*β*-D-maltoside
DLS	Dynamic light scattering
DMEM	Dulbecco's Modified Eagle Medium
DMF	Dimethylformamide
DODAG	*N′*,*N′*-Dioctadecyl-*N*-4,8-diaza-10-aminodecanoylglycine amide
DOPC	1,2-Dioleoyl-*sn*-glycero-3-phosphocholine
DOPE	1,2-Dioleoyl-*sn*-glycero-3-phosphoethanolamine
DPH	1,6-Diphenyl-1,3,5-hexatriene
DPPC	1,2-Dipalmitoyl-*sn*-glycero-3-phosphocholine
DSS	Dextran sulfate sodium
Duo	Duodenum
ECACC	European Collection of Cell Cultures
ECM	Extracellular matrix
eEPR	Epithelial enhanced permeability and retention
EGF	Epidermal growth factor
Em	Emission wavelength
EpCAM	Epithelial cell adhesion molecule
Ex	Excitation wavelength
FaSSIF	Fasted-State Simulated Intestinal Fluids
FBS	Fetal bovine serum
FcRn	Neonatal Fc receptor
FD10	Fluorescein isothiocyanate–dextran with molecular weight of 10k
FDA	Food and Drug Administration
FeSSIF	Fed-State Simulated Intestinal Fluids
FRET	Fluorescence resonance energy transfer
GalNAc	N-Acetylgalactosamine
GAPDH	Glyceraldehyde 3-phosphate dehydrogenase
GIT	Gastrointestinal tract
H&E	Haematoxylin and eosin
HBSS	Hank's Balanced Salt Solution
HSC70	Heat shock cognate 71 kDa protein
HSP90β	Heat shock protein 90β
IBD	Inflammatory bowel disease
ICAM	Intercellular Adhesion Molecule-1
IEOs	Intestinal epithelial organoids
IFN-γ	Interferon-γ

IL	Interleukin
ILVs	Intraluminal vesicles
ISEV	International Society for Extracellular Vesicles
JNK	c-Jun N-terminal kinases
LDL	Low-density lipoprotein
LN2	Liquid nitrogen
LPS	Lipopolysaccharides
M cells	Microfold cells
MDP	Muramyl dipeptide
mEVs	Milk extracellular vesicles
miRNA	Micro RNA
MTS	(3-(4,5-Dimethylthiazol-2-yl)-5-(3-carboxymethoxyphenyl)-2-(4-sulfophenyl)-2H-tetrazolium)
MUC2	Mucin 2
MVBs	Multivesicular bodies
MVs	Microvesicles
NBD-DSPE	1,2-Distearoyl-*sn*-glycero-3-phosphoethanolamine-*N*-(7-nitro-2-1,3-benzoxadiazol-4-yl) (ammonium salt)
NF-κB	Nuclear factor kappa B
NIRF	Near-infrared fluorescence
NOD2	Nucleotide-binding oligomerization domain 2
NPs	Nanoparticles
NTA	Nanoparticle Tracking Analysis
P_{app}	Apparent permeability coefficient
PdI	Polydispersity index
PEG	Polyethylene glycol
PEI	Polyethyleneimine
PepT1	Peptide transporter 1
PGA	Poly glycolic acid
PLA	Polylactide
PLGA	poly(D,L-Lactide-co-glycolide acid)
PMA	Phorbol 12-myristate 12-acetate
PSG-1	Ganoderma atrum polysaccharides
Rho-PE	1,2-Dioleoyl-*sn*-glycero-3-phosphoethanolamine-*N*-(lissamine rhodamine B sulfonyl) (ammonium salt)
RIP2	Receptor interacting protein-2
RISC	RNA-induced silencing complex
ROS	Reactive oxygen species
RPMI	Roswell Park Memorial Institute
RT	Room temperature
SC	Sigmoid colon
SCI	Spinal cord injury
SD	Standard deviation
SDS	Sodium dodecyl sulfate
SEC	Size exclusion chromatography
SIFs	Simulated intestinal fluids
siPAK4	P21-Activated kinase 4 siRNA
siRNA	Small interfering RNA

sTNF-α	Soluble TNF-α
sTNFR	Soluble TNF-α receptors
SUV	Small unilamellar vesicles
TE	Tris-EDTA
TEER	Trans-epithelial electrical resistance
TEM	Transmission electron microscopy
TfR	Transferrin receptor
TGF-β	Transforming growth factor β
Th 17	Type 17 T helper
Th 2	Type 2 T helper
Th1	Type 1 T helper
TI	Terminal ileum
TK	Transfection kit
TLR4	Toll-like Receptor 4
tmTNF-α	Transmembrane TNF-α
TNBS	4,6-Trinitrobenzene-sulfonic acid
TNF	Tumor necrosis factor
TNFR1	TNF receptor 1
TNFR2	TNF receptor 2
TNFα	Tumor necrosis factor α
TR	Transfection reagent
TSG101	Tumor Susceptibility Gene 101
UC	Ulcerative Colitis
US	The United States
ZO-1	Zonula occludens-1

1. Introduction

1.1. Inflammatory Bowel Disease (IBD) and Treatment

1.1.1. Pathophysiology of IBD

Inflammatory bowel disease (IBD) is a type of progressive, chronic, and immune-mediated disorder, which is characterized by destructive inflammation in small and/or large intestines. The prevalence of IBD in developed countries although is stable at approximately 1%; the incidence and prevalence are still increasing in developing countries across Africa, Asia, and South America due to their rapid economic growth and urbanization [1-4]. For instance, the prevalence of Ulcerative Colitis (UC, a subtype of IBD) in India was increased from 21.10 to 44.30 per 100,000 person between 1990 and 2016 [2] . Therefore, IBD has emerged as a global disease in the 21st century [1-4]. The management costs for IBD are substantial by healthcare system and society, e.g., in the United States (US), the healthcare costs for IBD patients are 3 times higher than those for non-IBD patients [4].

Two main forms of IBD include Crohn's Disease (CD) and UC, which show overlapping and specific clinical signs and symptoms. The overlapping features of both CD and UC include weight loss, abdominal pain, diarrhea and malnutrition [5]. However, CD often influences the entire gastrointestinal tract (GIT) from mouth all the way down to the anus and may appear in discontinuous intestinal sites featuring skip lesions, whereas UC is always restricted to large bowel, displaying a continuous pattern without skip lesions [6, 7]. In addition, UC can be diagnosed earlier than CD by the hematochezia with mucus and the primarily inflammation which is focused on mucosal surface. In contrast, CD usually gets delayed diagnosis due to more insidious onset, and the inflammation is usually transmural [5]. Importantly, IBD has a high potential to progress to colorectal cancers if the inflammation remains uncontrolled or untreated [8], and timely and effective management of inflammation for IBD is crucial to

mitigate the risk of disease progression. Therefore, due to the severe symptoms and long disease course of IBD, this condition significantly impacts every aspect of the sufferer's life and requires life-long therapy to manage and improve their life quality [9].

The pathophysiology of IBD is complicated and currently remains only partially understood. Nevertheless, research has provided evidence and insight into the underlying causes and progression of IBD. Generally, IBD is associated with multiple factors, including genetic susceptibility of the host, various environmental elements, and alteration of intestinal microbiota which may lead to immunological abnormalities. These disorders are considered to be related to the dysfunction of the intestinal epithelial barrier. However, whether the epithelial dysfunction precedes the development of IBD or caused by inflammation is still not clear **(Figure 1-1)** [10, 11].

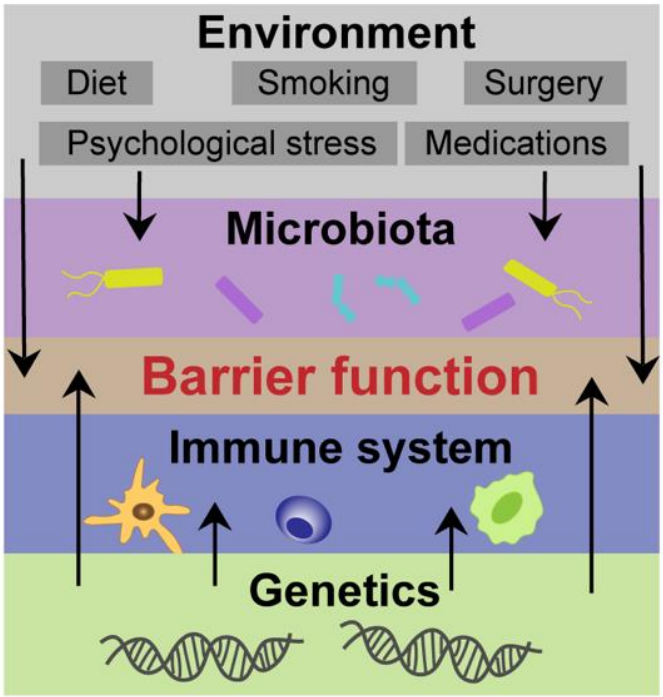

Figure 1-1. Inflammatory bowel disease (IBD) is influenced and developed by multiple factors. Environmental factors can impact the intestinal microbiota and barrier function, and genetics and the immune system also play a role in barrier dysfunction.

Gene analysis has identified over 240 nonoverlapping genetic risk loci which therein approximately 30 genetic loci are shared between CD and UC [12, 13]. Nucleotide-binding oligomerization domain 2 (NOD2) is the first gene found to be associated with CD. NOD2 could recognize the muramyl dipeptide (MDP) which is the minimal bioactive fragment of peptidoglycan found in the surface wall of bacteria [14, 15]. After binding to MDP, there is a conformational change of NOD2 and then binding to the receptor interacting protein-2 (RIP2), which activates nuclear factor kappa B (NF-κB), resulting in the secretion of proinflammatory cytokines [14, 15]. In addition, there are several risk genetic loci associated with both UC and CD development, including ATG16L1 and IRGM which are related to autophagy, and IL23R, associated with the immune response [16, 17]. However, ECM1, which regulates the epithelial barrier, was reported to have no association with CD, while certain loci such as those encoding genes ICOSLG and CCR6 were identified as CD-specific and showed no evidence of association with UC [18]. It should be noted that some of the risk genetic loci show heterogenicity between populations, while some individuals may carry the genetic risk loci associated with IBD, but do not necessarily develop the condition [19]. This also indicates that the genetic predisposition is only one of several contributing factors to IBD and other factors should be considered.

Previous studies have revealed that different environmental conditions are associated with IBD pathogenesis. Food and diet are considered as important factors. Intake of fruit and vegetables decreases the risk of CD, while food rich in fat and sugar may speed up the development of IBD [20, 21]. The impact of diet also indicates why the prevalence of IBD in developed countries is higher than in others [20, 21]. Generally, the modern western diet, characterized by a high intake of processed foods, refined sugars, unhealthy fats, and low intake of fruits and vegetables, has been associated with an increased risk of IBD [20, 21]. In addition, other environmental conditions such as smoking, psychological stress, appendectomy or medications

are also regarded as relevant factors affecting IBD development [22]. However, the relevance of these environmental factors with the risk of IBD was demonstrated complicated. For instance, active smoking was reported to have a protective effect against UC but pose a risk for CD [23], and appendectomy was associated with subsequent CD, yet the risk diminished when more than 5 years elapsed between the appendectomy and the CD diagnosis [24]. Interestingly, maintaining a favourable lifestyle, including a healthy diet and regular physical activity, has been associated with an approximately 50% lower risk of IBD among participants at a high genetic risk, which indicates the complex pathophysiology of IBD and the interactions between various risk factors [25].

Gut microbiota which contains 1000-5000 different species plays an important role in intestinal homeostasis and function, as well as develops and differentiates local and systemic immune systems [26]. Numerous studies have demonstrated that the changes in the composition of microbiota and termed dysbiosis could be observed under IBD progression [17]. Collectively, both CD and UC are associated with a decreased diversity of gut microbiota [17]. A previous study in animals has demonstrated that the intestinal microbiota may have dual roles in the development of IBD, with the potential to exhibit both pro-inflammatory and anti-inflammatory effects in disease pathogenesis [27]. In human studies, it is difficult to conclude whether a definitive cause-effect relationship between microbiota and IBD exists, but the intestinal microbiota clearly promotes the development of IBD [28].

Immunological abnormalities are considered as essential factors related to IBD development. GIT immune system is divided into innate and adaptive immunity. Innate immunity composes the intestinal barrier, defensins, acid environment, immune cells including macrophages, dendritic cells and natural killer T cells, as well as innate cytokines (interleukin-1 (IL-1), tumour necrosis factor (TNF), etc.) [29]. The adaptive immunity, including T and B cells, is pathogen-specific, and they are activated when innate immune response is unable to circumvent

the stimulation of pathogens [29]. The immune response in GIT is strictly regulated by immune systems, and this regulation determines the balance of the infection tolerance and the defensive inflammatory response. Disturbance of this maintained balance can lead to IBD development [30]. Specifically, the intestinal epithelial barrier integrity is disturbed due to the trigger of proinflammatory cytokines which regulate tight junctions and promote apoptosis [31]. The epithelial goblet cells are also dysregulated under IBD, potentially resulting in the disruption of integrity of tight junctions *via* downregulation of WFDC2, an antiprotease molecule which is expressed by goblet cells and preserves the integrity of tight junctions [32]. Dendritic cells, known as the most potent antigen-presenting cells in both innate and adaptive immune responses, have been shown to accumulate at the site of inflammation throughout the lamina propria and mesenteric lymph nodes under IBD [33]. Intestinal epithelium cells from 70% of patients with CD cannot control the dendritic cell-mediated proinflammatory response and this can lead to upregulated production of IL-12, which polarizes Type 1 T helper (Th1) responses [34]. In UC, there is a positive correlation between the circulating number of activated and mature dendritic cells with disease activities [35].

Macrophages are found underneath the intestinal epithelial layer in the lamina propria [36]. In IBD patients, the number of macrophages was found to increase in the inflamed mucosa, which can initiate a rapid response to luminal microbial antigens [33, 37]. The aberrant cluster of differentiation 14 (CD14)-expressing macrophages isolated from the mucosa of IBD patients was observed to produce high levels of IL-12 and IL-23 *in vitro* under microbial stimulation [38]. In IBD animal models, there is an obvious influx of immature macrophages into the gut mucosa, where these macrophages are arrested for further differentiation during inflammation. This leads to the secretion of a large amount of proinflammatory mediators like TNF, IL-6 and nitric oxide [39]. Furthermore, the dysregulation of the innate immune system could result in functional abnormalities of the adaptive immune system, leading to various characteristics of

chronic inflammation observed in IBD [33]. Previous studies have demonstrated that CD is caused by an overly aggressive Th1 immune response and recently it was found that in genetically predisposed individuals, there is an excessive activation of the IL-23/Type 17 T helper (Th 17) pathway in response to bacterial antigens [40], while UC is usually consisted as a "Type 2 T helper (Th 2)-like" disease characterized by the increased amount of IL-5 and IL-13 [41].

In IBD, increased secretion of various nonspecific inflammatory mediators is observed, such as free radicals, leukotrienes, chemokines, and proinflammatory cytokines (including TNF-related, IL-6 family cytokines and transforming growth factor β (TGF-β)).

TNF-related cytokines are proinflammatory cytokines with molecular weight of 17 kDa, which are mainly secreted by macrophages and monocytes. TNF-related cytokines are associated with various biological functions such as proliferation, differentiation, stimulation of the acute phase response, or cytotoxicity [42]. Secreted TNF-related cytokines can bind to two distinct cell surface receptors: TNF receptor 1 (TNFR1) and TNF receptor 2 (TNFR2). This binding leads to activation of one of the three pathways: a death domain pathway results in apoptosis; activation c-Jun N-terminal kinases (JNK) involved in cell differentiation and proliferation; or activation NF-κB [11, 43]. The soluble forms of both cell surface TNF receptors, known as soluble TNF receptors, are generated through proteolytic cleavage of the extracellular domains of the surface receptors and are subsequently released into circulation [44]. Significantly increased concentration of soluble TNF receptors was observed in acute or chronic inflammatory conditions, binding with TNF-related cytokines and activating their biological activities [45]. Previous studies have revealed that the TNF-related cytokine level is increased in the intestinal mucosa and shows a correlation with disease activity in patients with CD [43]. TNF-related cytokines have the potential to increase epithelial permeability by destroying tight junctions and promoting apoptosis, thereby compromising epithelial integrity and exacerbating

inflammation [31]. TNFα is the typical proinflammatory cytokine in TNF family and previous studies have shown that the inhibition of TNFα (e.g. application of anti-TNFα monoclonal antibodies) can dramatically reduce inflammatory markers and restore the damaged structure of mucosa, which elicited beneficial responses in IBD patients [46]. **Figure 1-2** illustrates how TNF inhibitors can neutralize TNF-α–mediated signalling [47]. Therefore, inhibiting or reducing inflammatory cytokines such as TNFα represents an effective approach to manage inflammation and restore intestinal barrier function, and then achieve the purpose of IBD therapy [43].

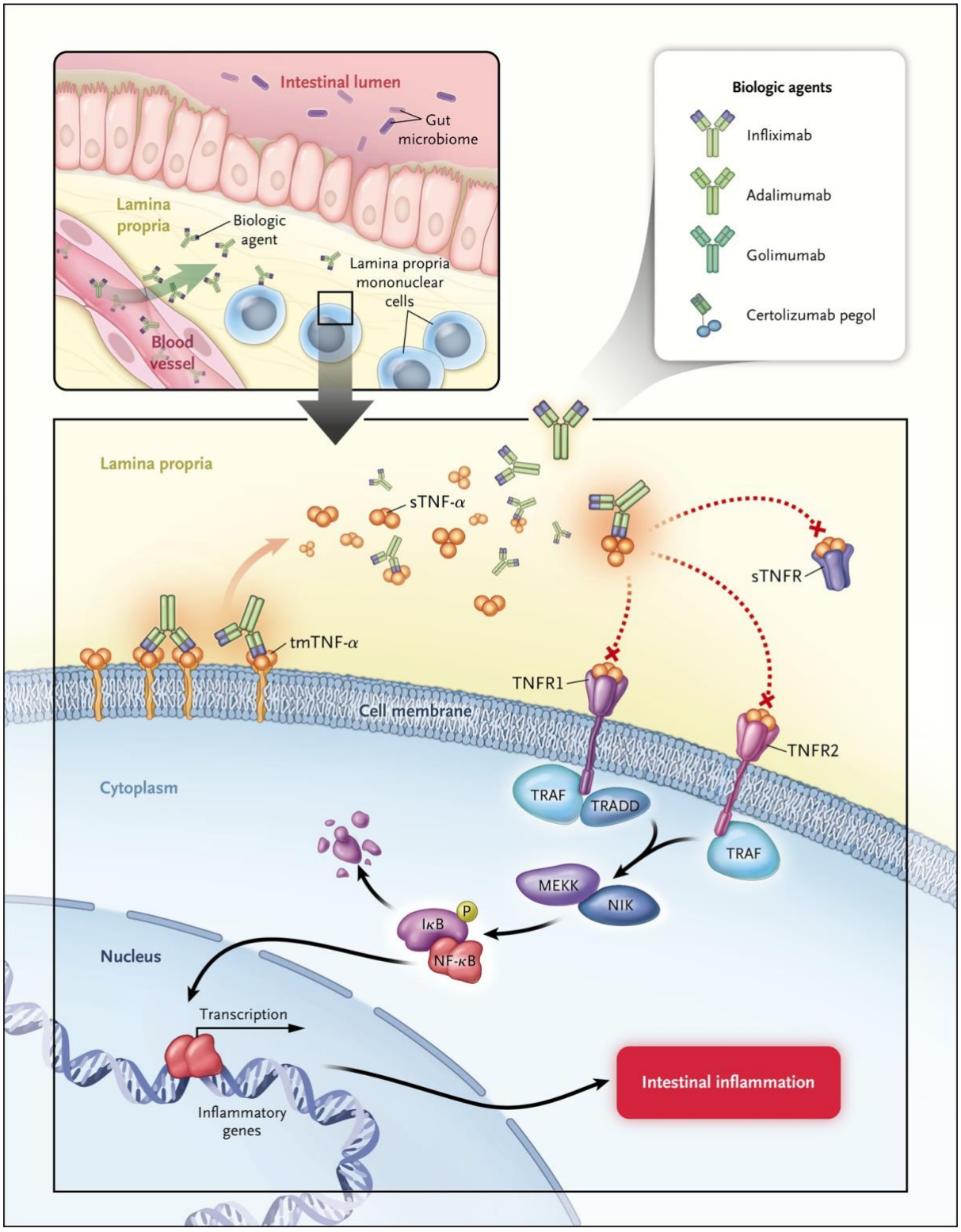

Figure 1-2. Mechanism of therapeutic effect of anti–tumor necrosis factor α (TNF-α) antibodies in inflammatory bowel disease. Anti–TNF-α antibodies bind to two types of homotrimeric TNF-α: the precursor transmembrane TNF-α (tmTNF-α) and the soluble TNF-α (sTNF-α), which is processed from tmTNF-α. Thus, these biologic agents block the interaction between TNF-α molecules and TNF-α

receptor type 1 and type 2 (TNFR1 and TNFR2) as well as soluble TNF-α receptors (sTNFR), neutralizing TNF-α–mediated proinflammatory cell signalling and inhibiting the expression of inflammatory genes. Infliximab, the first TNF inhibitor on the market, is used as an example in this figure. IκB denotes inhibitor of κB, MEKK mitogen-activated protein kinase kinase, NF-κB nuclear factor κB, NIK NF-κB–inducing kinase, P phosphorylated protein, TRADD TNFR1-associated death domain protein, and TRAF TNFR-associated factor [47].

1.1.2. Conventional treatment and demand of alternative therapeutic approaches for IBD

There are three categories of conventional medication for IBD: a) non-steroidal anti-inflammatory drugs, such as mesalamine, sulfasalazine and olsalazine, which are able to inhibit the secretion of leukotriene, free radicals and prostaglandin E (thermoregulator) to regulate immune responses; b) glucocorticoids, such as budesonide, which are able to block the metabolic pathways of arachidonic acid (a key inflammatory intermediate), show efficient anti-inflammatory and immunosuppressive effects; c) synthetic immunosuppressants, such as cyclosporine, azathioprine and tacrolimus, which induce the T-lymphocytes apoptosis and could relieve inflammation [48, 49]. Conventional therapies are capable of relieving symptoms to some extent, but fail to address the cause of underlying inflammation, and are also limited by their toxicity during long-term administration [50, 51]. For instance, there is an uncertain efficacy of amino salicylates on CD, and the toxicity of corticosteroids is still unacceptable. Immunosuppressants on the other hand are associated with a slow response and adverse events like lymphomas [52, 53]. Therefore, an alternative therapeutic approach is highly demanded for IBD treatment.

1.1.3. Monoclonal antibodies for IBD treatment

Biologics, which refer to products derived from living organisms or those containing components of living organisms (such as peptides, antibodies, and fragments of nucleic acids), have been expanding rapidly in the past two decades. Biologics have revolutionized the management of various diseases, presenting powerful treatment options for patients [54].

Monoclonal antibodies are a major class of biologics used in IBD. Anti-TNF monoclonal antibodies such as infliximab, adalimumab and certolizumab pegol have been used successfully in IBD treatment (**Figure 1-2**). These antibodies are able to downregulate pro-inflammatory cytokines, including TNF-α. Infliximab, which is approved by the European Union for the treatment of CD of adults and children and UC in adults, produces clinical remission and mucosal healing. Ustekinumab and guselkumab are monoclonal antibodies against IL-12/IL-23, which is a heterodimeric cytokine involved in pro-inflammation. Additionally, natalizumab is a monoclonal antibody which targets α4β1 (an integrin protein on white blood cells involved in inflammation) and is used as a therapy option in CD [55, 56]. These monoclonal antibodies as biological therapies have remarkably improved the management of IBD refractory to conventional medications, although their use is not without issues. Specifically, these treatments may produce serious adverse effects such as infection, infusion reaction and lymphomas, which need to be carefully monitored [53]. Furthermore, the resistance to mAb therapy in IBD is a significant concern. It occurs when patients exhibit inadequate responses to mAb treatment and may suffer a relapse, often resulting from factors including drug pharmacokinetics, pharmacodynamics, or immunogenicity [57, 58] .

1.2. Small Interference RNA (siRNA) as a Treatment Approach for IBD

1.2.1. siRNA mechanism of action

siRNA is a kind of double-strand nucleic acids with 21-23 pairs of nucleotides and about 7.5 nm length. The molecular weight of siRNA is about 13 kDa, and the phosphate groups in their backbone make them possess negative charge [59]. It is important to note that siRNA is categorized distinctively from typical biologics. Unlike conventional biologics, which are derived from living organisms, siRNA is chemically synthesized nucleic acid molecules and is recognized as a separate class of therapeutic agents, which stands alongside small molecules and biologics, offering a novel modality for disease treatment and intervention [60, 61]. Therapy by siRNA is one of the RNA interfering-based systems belonging to gene therapy. Specifically, duplex siRNA contains two strands including a passenger strand (sense strand) and a guide strand (antisense strand). Once transferred into cells, siRNA in cytoplasm gets incorporated into a ribonucleoprotein called RNA-induced silencing complex (RISC), resulting in duplex unwinding and the passenger strand is degraded. Thereafter, the remained guide strand could bind to the complementary sequence of target mRNA, and guide RISC to cleave the mRNA then inhibit its protein translation **(Figure 1-3)** [62, 63].

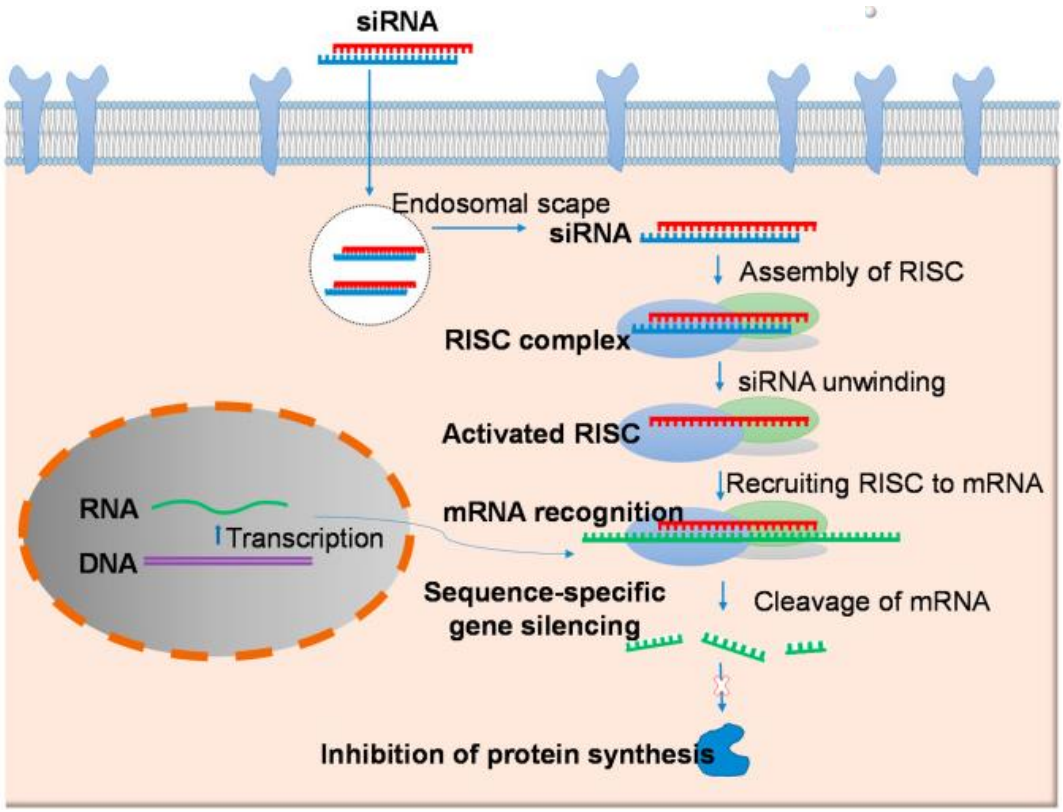

Figure 1-3. Mechanism of siRNA action, 1) The delivery of siRNA into the cell by a suitable nanocarrier, 2) Inside the cytoplasm the siRNA binds to a ribonucleoprotein called RNA-induced silencing complex (RISC), 3) The guided strand of siRNA is maintained by Argonaute protein in the (RISC) and the passenger strand is degraded, 4) The activated RISC recognizes the complementary mRNA of the targeted gene and induce mRNA degradation [62].

Following the discovery of the RNA interference mechanism two decades ago, several siRNA based-drugs have been approved for clinical use by the US FDA (Food and Drug Administration) or the European Medicines Agency between 2018 to 2022, including Givosiran (Givlaari®) for acute hepatic porphyria, Patisiran (Onpattro®) for transthyretin-mediated amyloidosis, Inclisiran (Leqvio®) for hypercholesterolemia, Vutrisiran (Amvuttra®) for transthyretin-mediated amyloidosis, and Lumasiran (Oxluma®) for primary hyperoxaluria type 1. All of them are applied based on the delivery systems of N-acetylgalactosamine (GalNAc) conjugate or lipid nanoparticles (DLin-MC3-DMA) *via* subcutaneous or intravenous [64], due to the instability (rapid enzymatic or non-enzymatic degradation), short half-life in

blood stream, and low cellular uptake of siRNA [65]. Specifically, Givosiran is administered by subcutaneous injection with a dosage of 2.5 mg/kg once per month, and the long-term administration (24-month) demonstrated a sustained decrease of δ-aminolevulinic acid and porphobilinogen [66]. Importantly, with Givosiran treatment, the reduction of attack frequency and serious daily pain improved the life quality of patients with acute hepatic porphyria [66]. Patisiran is recommended to be administered *via* an intravenous injection every 3 weeks with the dose of 0.3 mg/kg, and with an 18-month period treatment. 81% decrease of serum transthyretin and obvious improvement in polyneuropathy were observed [64]. Patients with heterozygous familial hypercholesterolemia received the treatment of Inclisiran *via* subcutaneous injections with dose of 300 mg at day 1, followed by subsequent doses on days 90, 270, 450, and this treatment resulted in a reduction of PCSK9 levels by over 60% as well as a sustained decreasing in low-density lipoprotein cholesterol by 51% [67]. Therefore, siRNA therapies demonstrate the potential as long-term treatments capable of long-lasting effects on various diseases. Additionally, numerous other siRNA drugs, relying on various delivery systems, are currently undergoing clinical studies. These are targeted for different diseases, such as metabolic diseases, infectious diseases, and oncology ocular diseases, etc [64].

1.2.2. siRNA delivery systems for IBD management

Compared with conventional therapeutic approaches for IBD, siRNA therapy offers distinct advantages. Firstly, siRNA holds the potential to exert on-site therapeutic effects at the sites of intestinal tissue when carefully designed for targeting and correctly administered, aiming to minimize immunosuppression throughout the whole body, and this targeted approach relieves inflammation from the underlying cause of disease instead of only the symptoms [51]. Importantly, siRNA therapy has the capacity to modulate the secretion of proinflammatory cytokines associated with IBD (such as anti-TNFα siRNA) by interfering with their gene

expression. As a result, it can restore the mucosa and recover the immune balance at the sites of diseases [43]. In addition to siRNAs targeting pro-inflammatory cytokines, research has demonstrated that siRNA against CD98 significantly reduces CD98 expression in a dextran sodium sulfate-induced colitis mouse model, thereby contributing to the alleviation of colitis by modulating both homeostatic functions and innate immune responses [68]. Cyclin D1, a molecule integral to cell cycle regulation which is often elevated in cases of colonic inflammation, can be targeted by siRNA to potentially mitigate colitis [69]. Research indicates that Cyclin D1 siRNA, when administered through intravenous nanoparticles, can attenuate colitis in murine models by downregulating inflammatory markers, demonstrating alleviation of inflammation [70]. Importantly, compared to monoclonal antibodies for IBD, siRNA therapy can directly reduce the secretion of pro-inflammatory markers at the source by silencing mRNA before protein production, and siRNA is more flexible for targeting any gene *via* sequence selection, which stands in contrast to the need for antibodies to recognize complex protein structures [71]. Furthermore, the biggest problem is that antibody therapies have strong immunogenicity [72], and many patients with Crohn's disease gradually developed resistance to therapy through the generation of anti-antibodies, whereas siRNA is considered to potentially have a safer therapeutic profile [73]. Though siRNA has significant potential for the management of IBD, one of the main limitations of siRNA application currently is the lack of safe, effective and patient-friendly delivery options.

1.2.3. The obstacles of oral administration of siRNA for IBD treatment [incorporated publication 3]

(**Statement:** The contents in section (1.2.3.) is based in part on the previously published review article:

Yunyue Zhang, Maya Thanou, Driton Vllasaliu (2020). Exploiting disease-induced changes for targeted oral delivery of biologics and nanomedicines in inflammatory bowel disease. *European Journal of Pharmaceutics and Biopharmaceutics, 155,* 128-138. Authors contributions: Yunyue Zhang (the candidate) contributes to the designing of the subject, writing and revision of the manuscript. Maya Thanou contributes to the revision of the manuscript, and Driton Vllasaliu contributes to the concept, supervision and revision of this work. I have permission from my co-authors/publishers to use the work in my thesis.)

Oral administration is a convenient, familiar, painless and the most accepted route of siRNA administration. Given that the site of drug action in IBD is the GIT itself, administration *via* the oral route is an obvious choice. However, siRNA is not stable and prone to degradation in GIT due to its sensitivity and the harsh environment in the GIT, such as stomach acid, which could lead to denaturation and depurination of nucleic acids over time and reduce their effectiveness in unprotected form [54, 74]. The presence of nucleases in the GIT is also considered as a major obstacle, resulting in degradation of siRNA before reaching the disease sites [75, 76]. Additionally, due to the high molecular weight and strong negative charge, siRNA is not capable of overcoming the biological barriers in the GIT, which include, amongst others, microbiota-mediated metabolism, mucus, intestinal epithelium and basement membrane (BM) (**Figure 1-4A**) [77]. Therefore, oral administration of siRNA is currently remaining an unsolved challenge.

In disease states such as IBD, physiological barriers to oral siRNA delivery may undergo alterations. IBD is a disease caused by multiple factors (as mentioned in Section 1.1.1), including genetic factors and excessive immune response to altered intestinal microbiota, leading to – crucially – dysfunction in epithelial barrier [10]. Barrier dysfunction has become the most common characteristic of IBD and this arises from increased permeability, alterations in tight junctions, reduced antimicrobial secretions, altered mucus composition and amount,

reduced number of secretory cells and even complete loss of the area of ulcerated epithelium (**Figure 1-4B**) [77, 78]. Previous studies using non-invasive techniques have demonstrated an increase in intestinal permeability in CD [79]. Furthermore, intestinal permeability can be considered as a potential contributor to disease progression and is also a predictor of relapse in CD patients [80]. In patients with UC, intestinal permeability was also increased in remission [81]. The following sections explore the distinct biological barriers associated with the oral administration of siRNA, as well as the alterations observed in each under IBD conditions.

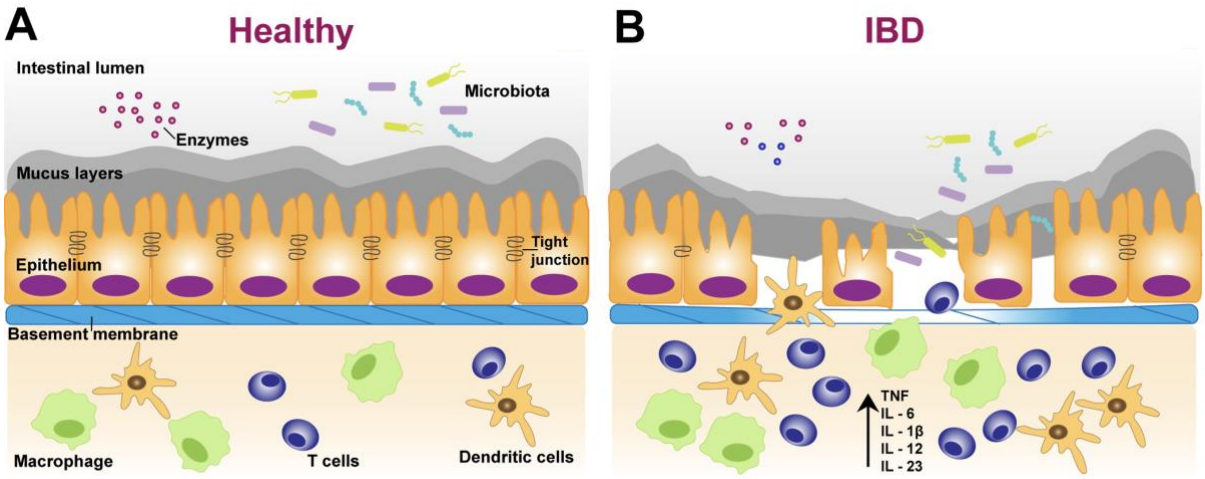

Figure 1-4. Physiological intestinal barriers and typical changes in inflammatory bowel disease (IBD). The homeostasis of healthy intestine is maintained by various barriers, including enzymes, microbiota-mediated metabolism, mucus layer, intestinal epithelium, basement membrane and immune cells (A). In IBD, all of these barriers are altered, including alteration of enzymes activity, wrong location and changed diversity of microbiota, alterations of mucus composition and amount, increased epithelial permeability, alterations in tight junctions and stimulated immune cells (B) [77].

1.2.3.1. Biochemical barrier

The stomach pH ranges from 1.0 to 2.5, and this rises to 6.6 to 7.5 in small and large intestine [82]. The harsh acidic environment of the GIT is not compatible with the labile nature of siRNA therapies. In addition, the GIT is rich in the presence of degradative enzymes, such as pepsin

in the stomach [83] and amylase, trypsin, chymotrypsin and lipase in the small intestine. Pancreatic juices also comprise various enzymes which degrade nucleic acids and proteins [84]. In IBD, there may be disease-induced changes in pH and degradative enzymes of the GIT. For UC patients, the pH in stomach is slightly higher, whereas in the small intestine there are no significant changes compared with healthy subjects. On the other hand, the change in colonic pH of UC patients has been reported inconsistently in the literature, with a mainly observed decrease [85]. For CD patients, the pH in the stomach was usually found to be higher compared to control (healthy) subjects, which correlated with decreased gastric acid secretion. No significant differences were observed in the median pH of the small intestine. Finally, the colonic pH values in patients with CD were found to fluctuate with a large range of values reported in different studies [85]. On the other hand, the changes of pH can vary from individuals and disease states [86]. A previous study has revealed that the colon environment in patients with IBD can be significantly more acidic (pH 2.3-5.5) than that in healthy states (pH 7.0 ± 0.7) [87]. For degradative enzymes, significant decreases of activity of amylase (33-85%), lipase (28-80%) and trypsin (29%) were observed in CD patients compared with controls [88, 89]. Previous studies have also revealed that a large number of proteases, such as metalloproteinases and elastase, are upregulated in IBD and this relates to the degradation of proteins in tight junctions, increasing intestinal permeability [90]. In addition, it has been increasingly recognised that alterations in the microbiota usually happen in IBD patients. The decrease in diversity and a shift of microbiota to potentially more inflammatory and less protective species in IBD could affect the drug-metabolising enzymes they secret [91, 92]. It has been revealed that the activity of proteinase from microbiota increases in patients with CD and UC compared to controls [93, 94].

1.2.3.2. Mucus

Mucus in the GIT, which ranges between 10-800 μm in thickness, is secreted by goblet cells allocated on the intestinal epithelium [95, 96]. Mucus is a semipermeable fibrous network (average pore size between 5-500 nm), which is governed by the main functional component – mucin glycoproteins (1-5% content) with extensive intermolecular interactions [74, 97, 98]. Other components of mucus are water (90-95%), proteins, enzymes, lipids and immune factors [99]. Mucus allows the transport of water, gasses, nutrients and hormones, but limits the transit of most bacteria, therefore playing an important role in maintaining intestinal homeostasis [99, 100]. The dense network structure of mucus results in a size-dependent hinderance of the diffusion of drug from the intestinal lumen to the underlying surface of epithelium [74], and it was found that the diffusion mobility of particles decreased with the increasing particle size (**Figure 1-5**) [101, 102]. It has been demonstrated that the effective diffusion decreased 2.9-fold with the increase in particle size from 100 to 500 nm [103], and particles larger than 200 nm were observed to accumulate within the mucus [99], which were thought to be too large to undergo rapid diffusional transport through the mucus barrier [104]. In addition to size hinderance, the negative charge of mucins is considered as an important factor affecting the transport of molecules through mucus. It is reasonable to speculate that the naked negatively charged siRNA might be repelled by the mucin fibres due to the similar charge characteristics [105]. However, in principle, positively charged molecules or delivery systems might interact with the negatively charged mucus and get trapped. A previous study demonstrated that the negatively charged nanoparticles (NPs) with Zeta-potential of -19 ± 2 mV exhibited higher permeation ability compared to positively charged NPs (26 ± 6 mV), while the highest diffusion was observed for neutral NPs (0.9 ± 2 mV) [106]. Additionally, there were observed differences in both thickness and components among various segments in the intestinal mucus, and the mucus heterogeneity provides numerous potential sites for chemical and physical interaction

with macromolecules (**Figure 1-5**) [101]. In the small intestine the mucus appears as a single layer residing on top of the epithelium, whereas in the large intestine the mucus blanket has two layers: the outer is relatively loose and can be adhered by bacteria; while the inner is tight and is normally sterile [96, 107]. The mucus layer was found to be thicker in the large intestine compared to the small intestine which exhibited the thinnest mucus lining throughout the GI tract [108]. Additionally, the viscosity of mucus in colon is considerably higher than that in small intestine [109], consistent with a reported observation of higher mucin concentration (30 mg/ml) in the large intestine compared to the lower mucin concentration (20 mg/ml) in the small intestine in pig [110]. It was found that the particles with the size of 100 nm demonstrated higher diffusion through small intestinal mucus compared with colonic mucus [111]. Therefore, considering the variations in mucus characteristics between the small and large intestines, the design of delivery systems should be meticulously tailored for specific segments, such as systems for drugs absorption in small intestine followed by blood circulation, or therapeutic systems intended for the small/large intestine such as in the treatment of IBD.

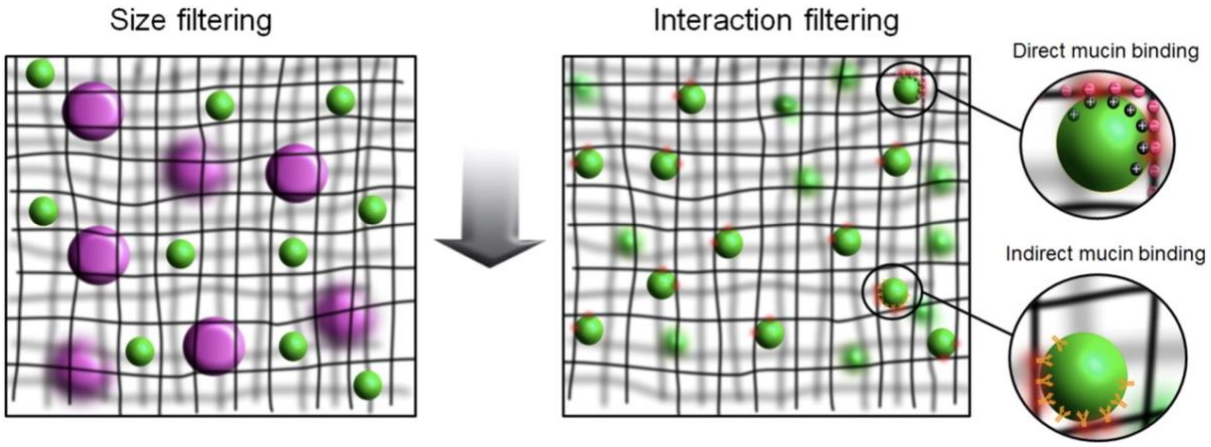

Figure 1-5. Schematic representation of the filtering properties of the mucus barrier. The size filtering mechanism of mucus is depicted on the left side: purple particles are trapped by the network due to their bigger size than the mesh spacing, while green particles can diffuse through the pores relying on their smaller size compared to mesh spacing. However, the interaction filtering mechanism of mucus (right side) allows interceptions of smaller particles through different interactions, such as direct

electrostatic interactions between particles and mucins or indirect binding mediated by non-mucin proteins and other mucus constituents [101].

In IBD, there are alterations in mucus amount, thickness and composition. CD is associated with goblet cell hypertrophy and therefore mucus formation is increased, leading to increased thickness of the mucus layer in colon and rectum compared with controls [112]. Although in CD the expression of Mucin 2 (MUC2) is increased irrespective of inflammation [113], the structure of MUC2 is however altered as a result of reduction of the oligosaccharide chain length by around 50% [114], and although the production of MUC2 increases, the altered structure leads to a loss of its viscoelasticity and an overall reduced barrier function. On the contrary, UC is characterized with a reduction and depletion of goblet cells, which leads to decreased mucin production and a diminished mucus barrier. The thickness of mucus layers in colon and rectum was found to be reduced in patients with UC compared to controls [112]. In more active colitis, the mucus layer is even completely lost [115]. Mucus diarrhoea, which is one of the main clinical symptoms in UC, may indicate poor mucus quality leading to decreased retention at the mucosal surface [78]. Apart from the amount and the thickness of mucus layer, the composition of mucus is also altered in conditions under IBD. Studies have revealed that the expression of antimicrobial peptides, which prevent bacteria from contacting the epithelial surface, decreased in the mucus of CD patients [116, 117]. Additionally, phosphatidylcholine, a crucial constituent for normal function of mucus barrier, was reportedly significantly reduced in the colonic mucus of UC patients (-70%); phosphatidylcholine used in treatment of UC has produced benefits [118-120]. Another change concerns the carbohydrate content of glycoproteins in mucus, which has been found to be reduced in patients with active UC compared to healthy controls [121]. Besides, colonic mucins from healthy mucosa display a negative charge due to the sulfate and sialic acid residues. However, in conditions of chronic

inflammation, glycans that have a shorter structure and decreased sulfation confer a less negative charge to mucins [122]. It is worth mentioning that reactive oxygen species (ROS) can be produced by macrophages and neutrophils into mucus and intestinal lumen under inflammatory conditions. It has been reported that the concentrations of mucosal ROS are 10- to 100-fold higher in UC patients compared with controls [123]. These changes in GIT mucus in IBD patients must be fully understood and considered when designing and developing drug delivery systems. Many formulations designed for oral delivery of siRNA employ mucus-penetrating or mucoadhesive systems, which are typically tested in healthy mucus (or more typically mucus models). More research is therefore needed to evaluate the performance of such systems in situations where mucus is altered [124].

1.2.3.3. Intestinal epithelium

Intestinal epithelium, which consists of a near-continuous layer of epithelial cells, is the largest and most crucial barrier for siRNA permeation. There are different epithelial cell subtypes within this barrier, such as enterocytes (the main component), goblet cells, Paneth cells, enteroendocrine cells, stem cells, tuft cells and microfold (M) cells. Enterocytes possess biochemically and functionally distinct apical and basolateral membrane domains, which are responsible for water and nutrient transportation from the intestinal lumen into the bloodstream [125]. These cells also provide opportunities for macromolecules to traverse the intestinal epithelium *via* transcytosis by enterocytes or M cells [80]. There are also junctional complexes including tight junctions and adherens junctions (estimated pore radius of 0.8–1.3 nm) between enterocytes, which restrict the transport of most ions and molecules which are larger than 2 nm (termed paracellular transport). Therefore, siRNA is not capable of permeating the epithelial barrier *via* the paracellular pathway under normal situations.

In IBD, it has been shown that the intestinal epithelial cells undergoing apoptosis are constantly shed from the epithelial surface, leaving transient gaps, which are subsequently filled by migration of surrounding cells. This shedding can be observed by fluorescein leakage (using confocal endomicroscopic techniques) into the intestinal lumen following intravenous administration (a common method to investigate intestinal epithelial barrier defects), indicating a loss of continuous epithelium (**Figure 1-6**) [126]. In both CD and UC, this shedding is increased and has been shown to predict subsequent relapse in both cases [127]. Epithelial apoptosis was found to be upregulated and mediated by TNF-α (reversible by anti-TNF-α antibody treatment) in the colon in CD, and this is a structural correlation of epithelial barrier dysfunction [128]. An increased rate of epithelial apoptosis has also been reported in UC [129]. Furthermore, in mild inflammation without epithelial lesions, leaks turned out to be foci of epithelial apoptosis, while in moderate-to-severe inflammation, leaks were associated with epithelial erosion/ulcerative lesions or crypt abscesses [130].

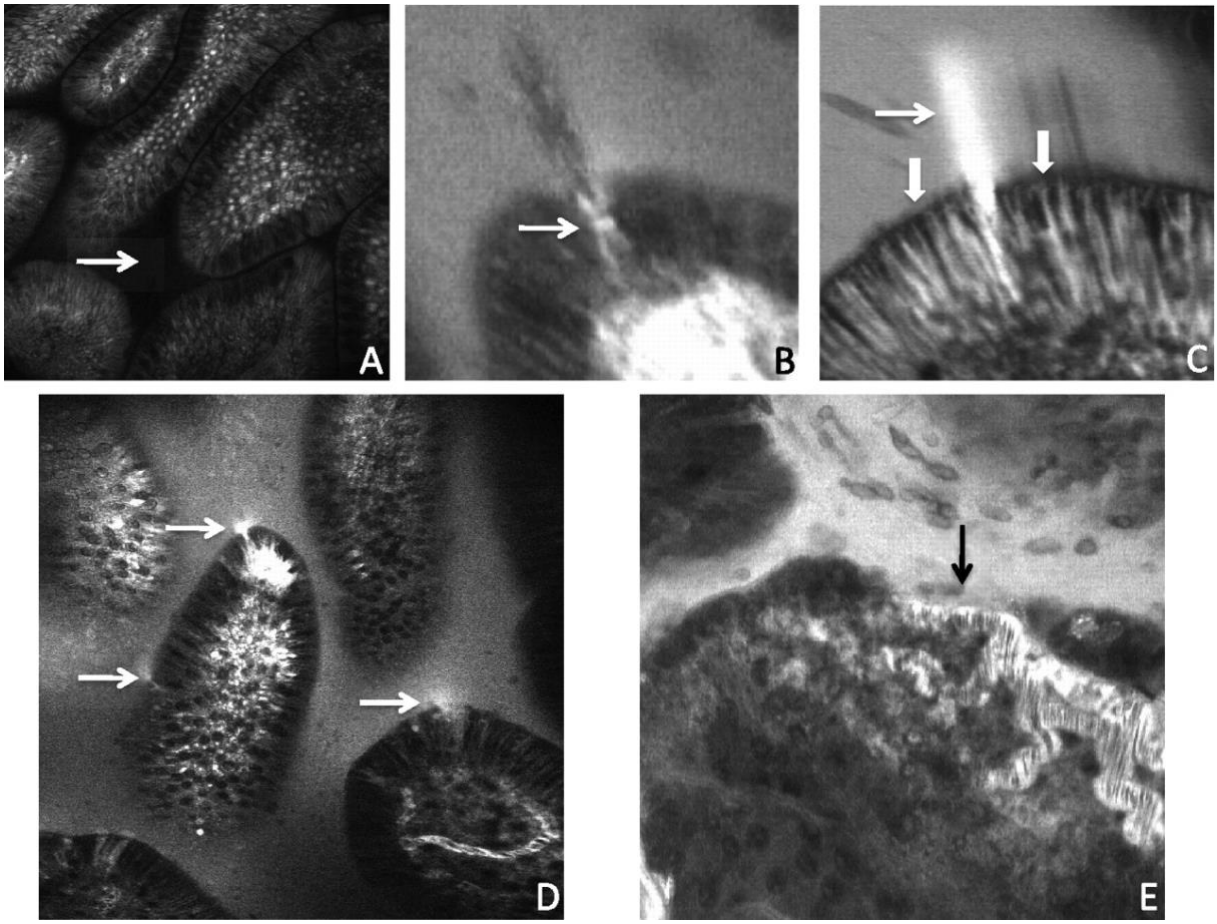

Figure 1-6. Loss of barrier function visualized by confocal endomicroscopy. (A) Intact barrier function with no escape of fluorescein into the gut lumen (arrow). (B) Fluorescein in the gap in the epithelium left by a shedding cell (arrow). Cellular debris from the shedding cell can be seen in the lumen. (C) Efflux of fluorescein out of blood vessels (block arrow) into the lateral intercellular space. Efflux into the lumen is constrained at the apical border (block arrows). A plume of fluorescein effluxing through the gap left behind a shedding cell (line arrow). (D) Multiple sites of efflux of fluorescein through the epithelium into gut lumen (arrows). Note the increased fluorescence in the gut lumen. (E) Microerosion (arrow) where more than one epithelial cell has been lost at one site exposing a capillary to the lumen. Note the functional relevance of this lesion as there is efflux of fluorescein into the lumen [131].

Damage of epithelial tight junctions is an important characteristic in active IBD [132]. The increased permeability of tight junctions in IBD has been attributed to the changes in

expression, structure and location of tight junction proteins, possibly as a result of changes in the expression of pro-inflammatory cytokines, such as TNF-α and Interferon-γ (IFN-γ) [10, 133]. In CD, tight junction protein claudin 2 was found to be upregulated, whereas claudin 5 and 8 (seal-forming tight junction proteins) were reported to be downregulated [132]. Murine models of CD, such as the SAMP1/YitFc model, demonstrated an increase in paracellular permeability of intestinal epithelium at early stages of disease [134]. Impaired tight junction function is also seen in UC, which could be due to the upregulation of cytokines, such as TNF-α, IL-1β and IL-13 [78, 79]. Increased expression of the tight junction protein claudin 2 and decreased expression of claudin 4 and 7 was demonstrated and thought to contribute to the development of epithelial barrier dysfunction in UC [135, 136].

Epithelial shedding and impaired paracellular epithelial barrier in IBD could theoretically result in a higher intestinal absorption of macromolecules at sites of inflammation – an outcome that would allow targeted delivery of siRNA following oral administration. siRNA or delivery systems may be able to penetrate through the leaks among epithelial cells. This has been termed epithelial enhanced permeability and retention (eEPR) effect [137, 138]. Disruption of epithelium also causes the exposure of positively charged proteins, such as transferrin, bactericidal/permeability-increasing proteins and anti-microbial peptides [139, 140]. This leads to a localised build-up of positively charged components at the damaged epithelial surface, and provides an opportunity for targeted drug delivery mediated by electrostatic interaction, e.g. *via* negatively-charged drug carriers [139]. However, with regards to the tight junction-regulated paracellular barrier, this is not expected impaired to a degree to allow significantly higher absorption of macromolecules across the inflamed mucosa compared to the healthy tissue.

Differential expression of epithelial trafficking receptors in intestinal epithelial cells may also create opportunities for improving intestinal translocation of biological delivery systems *via*

transcytosis, in addition to enabling targeted absorption at the sites of inflammation. A number of biological transport systems expressed in the intestinal epithelium have been shown to possess potential for transepithelial delivery of macromolecules. Transferrin receptor (TfR) is a membrane glycoprotein found on epithelial cells, involved in the intestinal absorption of ions by binding to Transferrins (Tfs) through transcytosis [141]. Tfs has been utilized to modify NPs so to increase their permeation through the intestinal epithelial barrier [142], and it has been found that the expression of TfR increases in colonic enterocytes of rats with colitis and patients with UC [143]. CD98 transporter, responsible for the uptake of essential amino acids across biological barriers, has been reported to be significantly upregulated in intestinal epithelial cells in inflammation and increased at the surface of intestinal immune cells, including B cells, $CD4^+$ T cells and $CD8^+$ T cells in IBD [144]. Similarly, the PepT1 (an oligopeptide transporter) is also observed to be overexpressed in the colon epithelial cells of IBD patients [145]. Therefore, these changes could present opportunities for the use of CD98 antibodies or dipeptides (such as valine-glycine and tyrosine-valine) as targeting ligands to direct a delivery system such as NPs to the sites of intestinal inflammation. Further, CD44 receptor has also been found to be upregulated at the surface of epithelial cells and activated inflammatory cells [146]. Hyaluronic acid as a natural anionic polysaccharide has a high affinity to CD44 receptor and has been used as a ligand to modify NPs for targeted drug (including biologics) delivery in IBD. In addition, there are various carbohydrate receptors, such as mannose and galactose receptors, which are expressed by cells of the intestinal epithelium and immune system [147]. The mannose and galactose receptors are also been observed to be exclusively expressed on the macrophages surface [148]. Studies have therefore attempted to present saccharide moieties on NPs surface for selective macrophage targeting and internalization [149, 150]. Neonatal Fc receptor (FcRn) was identified as an IgG receptor on the intestinal epithelial cells, which facilitates the transport of IgG across the intestinal epithelium through transcytosis by interacting with the Fc portion

of IgG [151]. NPs featuring surface-modified IgG Fc have been applied for the delivery of insulin across the intestinal epithelium [152]. Interestingly, FcRn may have an essential role in the intestinal absorption of mEVs, where the antibodies presented on mEVs could be recognized by FcRn expressed on intestinal epithelial cells, facilitating their transcytosis across this barrier [153, 154]. These receptor systems may serve as biological gateways for inflammation-targeted oral delivery of siRNA, although the role or efficiency of these systems in promoting apical-to-basolateral translocation of siRNA is currently not clear.

1.2.3.4. Basement membrane (BM)

Epithelial BM is a thin structure formed from sheets of extracellular matrix (ECM) and located between epithelium and connective tissue (**Figure 1-7**). The composition of BM includes collagen, laminins, nidogen and perlecan [74]. Collagen as the main BM protein is cross-linked by various bonds, such as disulfide and hydrogen bonds [155, 156]. Laminin also supports the networks of BM and tightly associates to the cell surface [157]. Additional ECM proteins, such as nidogen and perlecan, link the independent collagen and laminin networks to form the integral BM structure. BM is associated with several functions, such as cell and tissue polarity coordination, function as signalling platforms by sequestering many growth factors and other ligands, as well as playing a critical role in cell differentiation. BM has also been reported to possess a barrier function, displaying selective permeability (size- and charge-dependent) of molecules across this barrier [157, 158]. Mantaj et al. [159] measured the permeability of macromolecules (dextrans) and 100 nm nanoparticles through the BM. They found that the BM did not affect the movement of dextran, but severely hindered the diffusion of nanoparticles. The BM barrier effect with respect to macromolecule diffusion was also shown by a study by Alfanon et al. [160]. The diffusion of inulin (molecular weight 5kDa) was impeded by the oral mucosal epithelial BM, while that of a larger macromolecule dextran (20kDa), was not

influenced. The possible reason for this observation was suggested to be the binding of smaller molecules to the structural components of BM or the possibility of these molecules being caught in the finer interstices, similar to the mechanism of gel permeation chromatography.

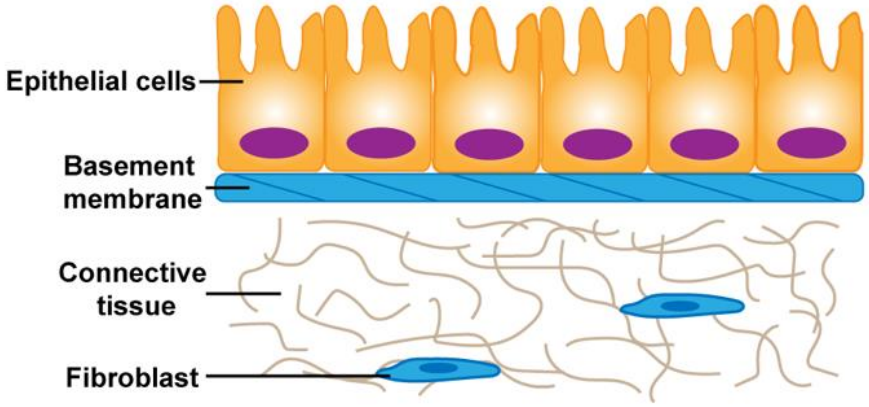

Figure 1-7. Epithelial basement membrane is a thin structure formed from sheets of extracellular matrix and located between epithelium and connective tissue.

In IBD, it has been shown that the ECM plays an important role in the interaction with the immune system [161]. In the inflamed tissues, the ECM is influenced by the activated resident cells of tissue and infiltrating immune cells. This leads to a remodelled or abnormal ECM microenvironment with high concentrations of proinflammatory cytokines (such as IFNs and TNF-α), esterases, matrix metalloproteinases (MMP), myeloperoxidase, and ROS [162]. The remodelling of ECM, characterized by increased degradation of ECM components and the development of excessive intestinal fibrosis, is a significant feature in the progression of IBD [163]. Specifically, ECM macromolecules (such as type I collagen) can be selectively cleaved by MMP into small bioactive peptides [164]. In addition to the increased activity of degradation enzymes, ECM remodelling during IBD is also relevant to the excessive ECM formation. This involves a substantial increase of the synthesis of fibre-forming collagens, contributing to progressive intestinal fibrosis and subsequent narrowing of the intestinal lumen [163, 165]. Therefore, in IBD, the imbalanced and dysregulated remodeling of ECM results in the

breakdown of the BM barrier and contribute to the development of fistulas, eventually leading to intestinal perforation [163]. It has been found that the immunosuppressive treatment, such as anti-TNFα agents or corticosteroids, contributed to the improvement, including enhanced wound-healing response *via* decreasing of MMP-9 and MMP-26 positive neutrophils and stromal TIMP-1 and TIMP-3, in patients with CD [166]. Furthermore, infliximab (anti-TNFα monoclonal antibodies) has been shown to potentially impede subclinical fibrosis related to ECM remodeling in CD [167]. Additionally, the elevated presence of enzymes, such as MMP, in the ECM of the inflamed colon during IBD provides an opportunity for degradation-mediated targeting delivery system to the site of inflammation. Various MMP-sensitive delivery systems have been developed [168], including hydrogels formed by cross-linking polymeric chains with specific amino acid fragments, which result in the polymer biodegradation through enzymatic cleavage, subsequently facilitating drug release [169, 170]. Therefore, in IBD, the structural damage of BM may further compromise the overall mucosal barrier either directly or indirectly. Indirect effects arise from a clear effect of BM on intestinal epithelial cells, including morphology and tight junction barrier, above the BM [159].

1.2.3.5. Intracellular Barriers

Beyond the biological barriers mentioned above, a critical challenge in achieving effective RNA interference therapy for IBD lies in the inefficiency of siRNA delivery across the cellular and endosomal membranes to reach the cytoplasm of immune cells [171]. The cellular membrane is typically composed of negatively charged phospholipids, causing disruptions in the intracellular trafficking of anionic siRNA due to repulsive interactions [172]. Various delivery systems have been developed to facilitate the intracellular trafficking of siRNA through the endocytosis route. However, once these systems, such as NPs, are endocytosed, they encounter entrapment within endosomal vesicles [173]. Early endosomes (pH 6-6.5)

gradually transition into more acidic late endosomes (pH 5-5.5), and eventually fuse with lysosomes (pH 4.5-5) for degradation [174]. Part of the endosomes may undergo exocytosis (recycling back to the membrane), leading to the excretion of cargos from the cells [175]. It has been reported that only 0.3% of endocytosed GalNAc-siRNA conjugate was present in the cytoplasm *in vivo* [176]. Therefore, escaping from endosomes following enabling the release of siRNA into the cytoplasm after endocytosis, is the critical capacity of siRNA delivery systems for efficient gene silencing. Different strategies for endosomal escape proposed in siRNA delivery systems, such as "proton sponge effect", endosomes membrane disruption, or fusion with endosomes, were elaborated upon in Section 1.3.

1.3. Nanoparticles (NPs)-Based siRNA Oral Delivery Systems for IBD Treatment

As indicated in Section 1.2.3., the physiochemical properties of siRNA and physiological barriers in GIT pose challenges for the oral administration of naked siRNA. Chemical modifications on siRNA, such as focusing on phosphodiester bond of RNA backbone, 2'-ribose and binding siRNA with peptide, polyethylene glycol (PEG) or cholesterol, could promote the resistance to rapid degradation by ribonuclease to a certain degree [177, 178]. However, most of these modifications are not enough for siRNA to permeate through physiological intestinal barriers efficiently. Viral vectors as a delivery strategy could improve the transfection efficiency of siRNA, while several limitations such as high production costs, immunotoxicity and gene insertion on host chromosomes are still hindering their application [178, 179]. The cargo loading capacity into viral vectors can still vary widely depending on the type of virus. Adenoviral vectors, for instance, have been demonstrated to carry large transgene cassettes, and are reorganized as effective carriers for siRNA [180]. However, a significant challenge lies in the inefficient siRNA release from the endosome to the cytoplasm [180]. Adeno-associated virus, characterized by non-immunogenic and non-pathogenic features, however compromised

with small packaging capacity which is generally considered to be < 5kb [181]. In contrast, herpesviral vectors offer a higher packaging capacity (40 kb-150kb), but may trigger a robust inflammatory response [181]. Even though being one of the promising carriers for gene therapy delivery [182, 183], viral vectors are typically administered *via* systemic delivery such as intravenous route instead of oral administration, due to the harsh environment of GIT, including the acidic conditions in the stomach, proteolytic conditions in the intestine, and the high turnover rate of enterocytes, which could lead to the denaturation of viral surface proteins, compromising viral structural integrity [184]. In addition, oral administration of viral vectors may trigger an immune response from the immune components in the gastrointestinal mucosa, while the mucosal immune responses provide an opportunity for the application of recombinant adeno-associated virus vectors in the development of oral vaccines [185-187].

Non-viral NPs-based oral delivery systems for siRNA therapy have been developing fast in recent years, and numerous nanomaterials have been tested to encapsulate or complex siRNA to overcome the obstacles for its oral delivery, including enteric-coated systems (e.g. Eudragit®), polymers (polylactide(PLA)-based NPs, poly(D,L-lactide-co-glycolide acid) (PLGA)-based nanoparticles), liposomes and natural macromolecules (e.g. extracellular vesicles or exosomes), etc.

1.3.1. Polymer-based NPs

Polymer-based NPs such as PLA-based and PLGA-based NPs have been investigated as systems for loading and delivery of siRNA in IBD. PLA is an aliphatic thermoplastic polyester which shows non-toxicity, biocompatibility and biodegradability in human and has been approved by FDA for use in oral drug delivery systems [188]. PLGA, a copolymer composed by PLA with poly glycolic acid (PGA), has been widely applied as oral drug delivery carrier and has been approved by FDA and European Medicines Agency owing to its biodegradable

and nontoxic characteristics [189]. Polymer-based NPs possess flexibility of controlled release profile design to reduce the adverse effects or dosing frequency, and the incorporation of ligands to enable targeted delivery. Polymer-based NPs delivery systems have been developed for different diseases *via* various administration routes depending on the therapeutic requirement. Intravenous injection is widely used for targeting tumors or providing system treatment, and subcutaneous and intramuscular injection are also applied for the delivery of these systems. Additionally, some other routes such as inhalation, ocular, and transdermal applications have also been explored [190, 191]. Importantly, there has been development in polymer-based NPs delivery systems specifically for the oral administration of siRNA in the treatment of IBD. Laroui et al. [192] designed PLA-PEG NPs loaded with TNFα siRNA for potential IBD therapy. This delivery system's surface was modified with antigen-binding (Fab') portion to improve targeting ability, and the siRNA was mixed with polyethyleneimine (PEI) to form a complex which promotes siRNA lysosome-escape ability [192]. The *in vivo* study (delivery system orally administered in dextran sulfate sodium (DSS)-mice) showed this system was capable of targeting colonic macrophages and relieving inflammation [192]. Huang et al. [193] used PLGA NPs as nanocarriers to load TNFα siRNA and modified them with galactosylated chitosan on the surface to improve mucus adhesion and targeting ability to macrophages. *In vivo* study demonstrated that this delivery system could target colitis tissues of mice and alleviate inflammation effectively *via* oral administration [193].

Multi-shell polymer-based NPs have been investigated, where different functional layers or ligands were incorporated, and these layers effectively carry a specific function for the oral delivery of siRNA in the treatment of IBD. Merlin et al. [194] designed a delivery system by loading PEI/TNF-α siRNA complexes into PLA NPs, and polyvinyl alcohol was added to coat these complexes. The complexes were subsequently encapsulated into alginate and chitosan for collapsing in intestinal pH and targeting to inflamed colon for IBD therapy [194]. According

to the results of pretreatment by this multi-layer NPs system to mice with UC (induced with lipopolysaccharides (LPS)), TNF-α expression level was significantly reduced compared with blank NPs [194]. Frede et al. [195] engineered an oral delivery system - TNF-α siRNA loaded multi-layer NPs for IBD therapy. Specifically, TNF-α siRNA was loaded into a calcium phosphate (CaP) core which was subsequently coated with PLGA. PLGA-CaP-siRNA complexes were further encapsulated into PEI for early endosomal release of siRNA. Intrarectal administration of this delivery system in DSS-induced mice led to a significantly decrease of TNF-α expression and colonic biopsies along with recovery [195]. Lichen et al. [196] synthesized an asymmetric tri-block copolymer, poly(ethylene glycol)-b-poly(trimethylenecar-bonate-co-dithiolane trimethylene carbonate)-b-polyethyl-enimine (PEG-P(TMC-DTC)-PEI) (RCP), that can self-assemble to redox-sensitive polymersomes with an inner PEI core and PEGylated surface. This system could electrostatically interact with TNF-α siRNA, as well as encapsulate the dexamethasone sodium phosphate. Their results from an *in vivo* study showed that these delivery systems were able to relieve intestinal inflammation effectively [196].

1.3.2. Liposomes

Liposomes are composed of a phospholipid bilayer, offering the benefits of biocompatibility with cell membranes, and the hydrophilic core in liposomes facilitates a high loading efficiency of siRNA. The flexible fabrication of liposomes with various lipid types or ligands incorporation also enables liposomes to be modified for targeted delivery. Liposomes have been developed for different therapeutic delivery using multiple routes of administration, including parenteral (intravenous), ocular, pulmonary and transdermal pathways [197, 198]. Specifically, liposomal delivery systems for siRNA targeting IBD therapy *via* oral or rectal administration have been developed fast in recent years.

Commercially available liposomes such as Lipofectin® and Lipofectamine™ 2000 have been widely applied for loading siRNA as delivery systems, which facilitates binding and fusion with the cellular membrane to release the siRNA in cells [199]. Zhang et al. [200] prepared a liposome complex by encapsulating siRNA with Lipofectamine™ 2000, and the siRNA mediated gene-silencing efficiency and therapeutic effect on a murine IBD model were evaluated. The results revealed that rectal administration of this delivery system decreased corresponding mRNA levels by 72% compared to control groups and the inflammation was observed to be relieved. Guo et al. [201] designed ROS-responsive liposomes (with the lipids of ZnDPA-R) which could combine ROS reduction and siRNA delivery capacity for colitis treatment. The *in vitro* study showed that the TNF-α siRNA loaded-liposomes efficiently reduced the expression level of TNF-α mRNA in macrophages and the *in vivo* study proved that the delivery system could not only treat inflammation by ROS reduction, but also relieve inflammatory symptoms by reducing inflammatory factors [201]. Furthermore, biocompatible natural source-derived cationic lipoplexes have been identified to encapsulate siRNA for IBD therapy through oral administration. Zhang et al. [202] found that the lipid nanoparticles with positive charge derived from ginger were able to form complexes with CD98-siRNA. Remarkably, orally administered CD98-siRNA loaded-lipid nanoparticles demonstrated targeted delivery to colon tissues, resulting in a decreasing expression of CD98. Importantly, the efficacy of gene silencing by siRNA loaded-lipoplexes or lipid nanoparticles relies on their capacity for endosomal escape. Image visualization has observed siRNA release from these complexes during endosomal maturation, which subsequently initiates the autophagic isolation of the releasing endosome [203].

Even though the siRNA loading efficiency and transfection efficiency of liposome delivery systems are relatively high, toxicity arising from cationic (positively charged) lipids, which are essential for complexing with negatively charged siRNA, is the unignorable limitation for their

general application [204]. Furthermore, it has been observed that liposomes exhibit limited stability in the in GIT (e.g. lipid can be digested in the small intestine and the digested products would associate with bile salts to form mixed micelles) [76]. Efforts have been dedicated to enhancing the GIT stability of liposomes by adjusting their formulations. It has been found that phospholipids, the primary components of liposomes, exhibit greater stability when they possess longer fatty acid chains and a higher degree of saturation in their hydrocarbon chains [205]. Additionally, cholesterol has been identified as an effective lipid component to increase the structural stability of liposomal membranes against harsh GIT environment, attributing to hydrogen bonds formed by cholesterol with phospholipids and increase the rigidity of membranes [205, 206].

Though artificially synthesized NPs with various modified strategies have been widely investigated for siRNA oral delivery, most synthetic NPs suffer from poor delivery across the highly effective, multi-component intestinal mucosal barrier [207]. An ideal carrier for safe and effective oral delivery of siRNA is one that successfully protects the cargo and tackles the physiological barriers in the GIT without toxicity. However, such a system is yet to be identified. The current technology based on conventional lipid nanoparticles (i.e. those utilized for the COVID-19 vaccines) is not suitable for oral administration due to the instability of these particles in the complex gut environment [208] and the need for the formulation to address mucus diffusion [209]. Therefore, the search for effective technologies for oral delivery of siRNA is still highly demanded.

1.3.3. Extracellular vesicles (EVs)

1.3.3.1. The source, components, and functions of EVs

EVs are membrane-bound vesicles secreted by a variety of cell types to extracellular environment. The three major types of EVs are exosomes (30 nm -150 nm), microvesicles

(MVs, 100 nm – 1 μm) and apoptotic bodies (50 nm – 5 μm), which can be distinguished by their size, biogenesis and functions (**Figure 1-8**) [210-212]. Exosomes form through a process involving the endosomal system (**Figure 1-9**) [213]. Briefly, this process begins with the inward budding of plasma membrane forming early endosomes. Then the early endosomes mature into multivesicular bodies (MVBs) and lead the formation of intraluminal vesicles (ILVs) inside them *via* inward budding of MVBs membrane. In the process, certain molecules, including specific proteins, lipids, and nucleic acids, are selectively incorporated into the ILVs. Depending on the surface protein of MVBs, most of them serve as 'delivery trucks', fusing with plasma membrane to release ILVs into the extracellular space, which are then termed exosomes. A small proportion of MVBs function as 'garbage trucks', directing their cargo towards lysosomes for degradation [214]. Apoptotic bodies are derived from disassembly of apoptotic cells [215], and microvesicles are directedly budded from plasma membrane of live cells [212].

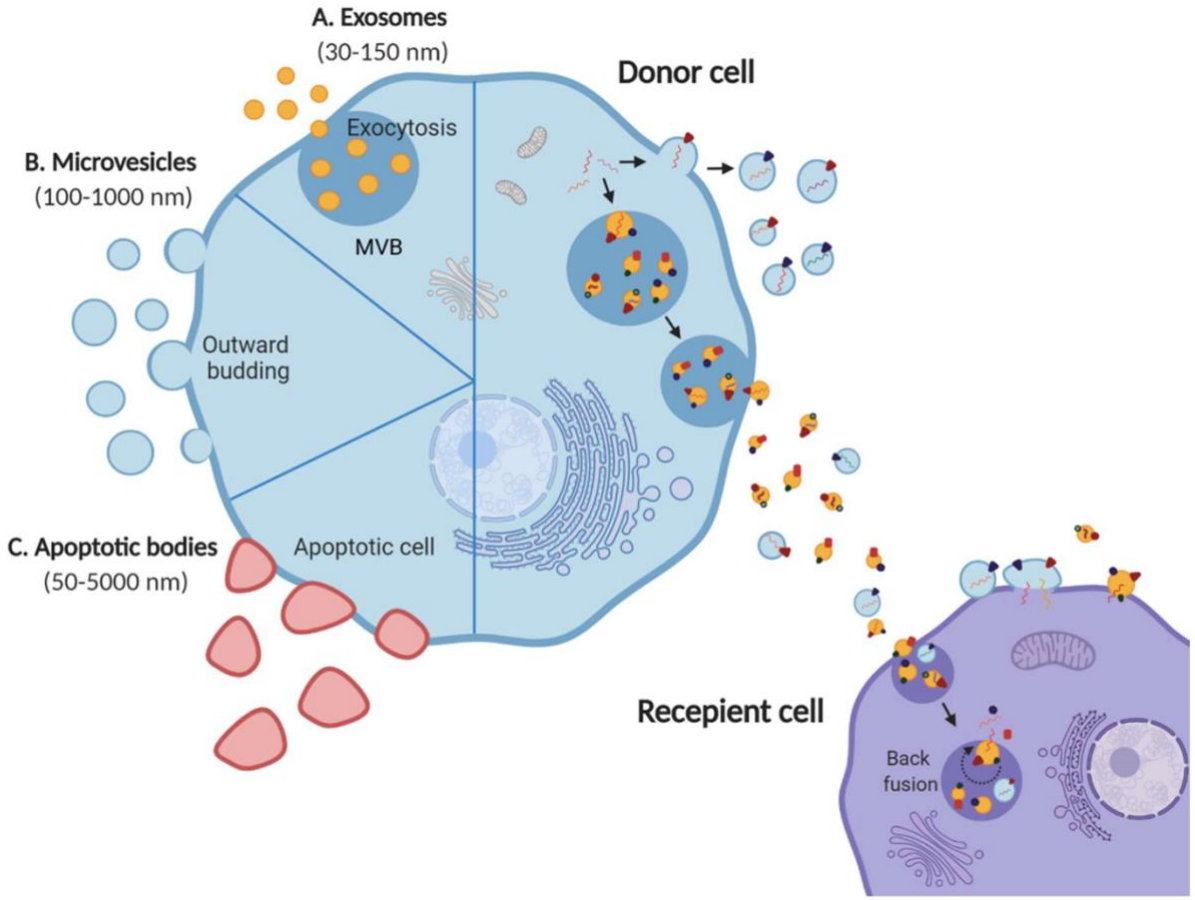

Figure 1-8. EV subtypes and role in mediating cellular crosstalk. Schematic representation of three main EV subtypes; **(A)** exosomes, **(B)** microvesicles, **(C)** apoptotic bodies released by all cell types into the extracellular space. Exosomes and microvesicles are released by live cells *via* exocytosis and outward budding, respectively. Apoptotic bodies, on the contrary, are released by apoptotic cells. EVs are known to mediate intercellular communication by carrying a diverse cargo of proteins, nucleic acids and lipids from the donor cell to the recipient [212].

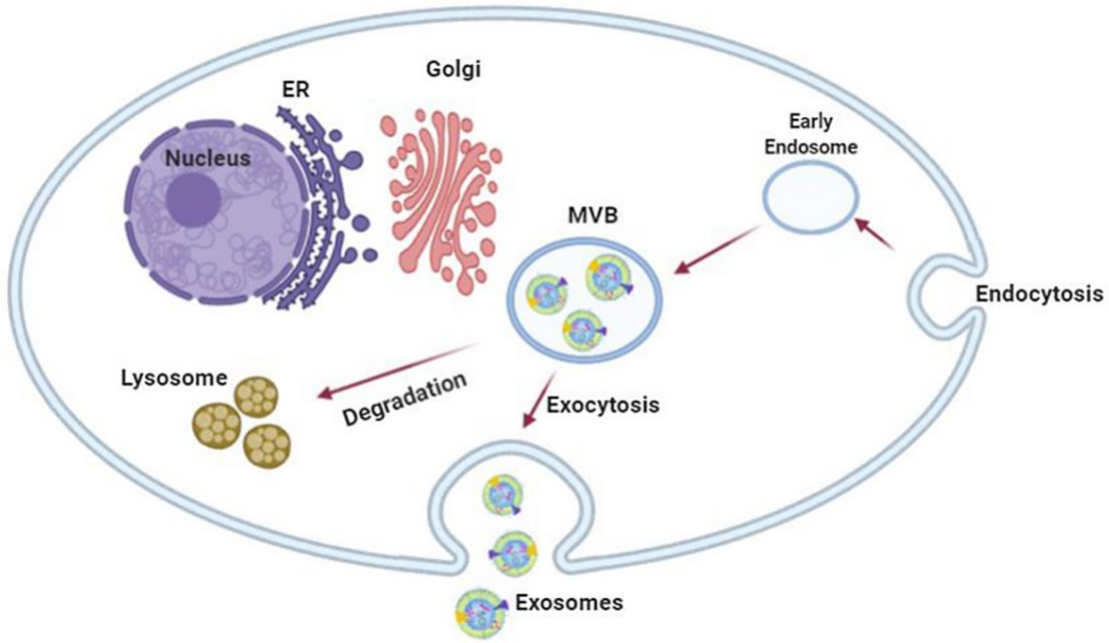

Figure 1-9. Process of exosome formation in cells [213].

EVs are found in different types of biofluids including blood, urine, saliva, breast milk, cerebrospinal liquid, ascitic fluid and amniotic fluid [216, 217]. The composition of EVs includes lipids, proteins, and nucleic acids **(Figure 1-10)**. The bilayer structure of EVs is composed of phospholipids, glycerophospholipids, cholesterol, diglycerides and sphingolipids [216]. Due to endosomal origin, exosomes possess proteins include Alix, tumor susceptibility gene 101 protein (TSG101), heat shock cognate 71 kDa protein (HSC70), heat shock protein 90β (HSP90β), and tetraspanin family protein including CD9, CD63 and CD81, which are often termed “exosomal marker proteins” [210], while microvesicles and apoptotic bodies always contain signaling proteins and actin-myosin cytoskeleton proteins [218]. Exosomes are also carriers of various nucleic acids, including DNA, mRNA and micro RNA (miRNA, a type of small non-coding RNA) that regulate gene expression [216]. Apoptotic bodies also contain nucleic acid fragments, inclusive of DNA and RNA, derived from cellular apoptotic processes [219], whereas microvesicles always include a diverse array of nucleic acids from the parent cell [220].

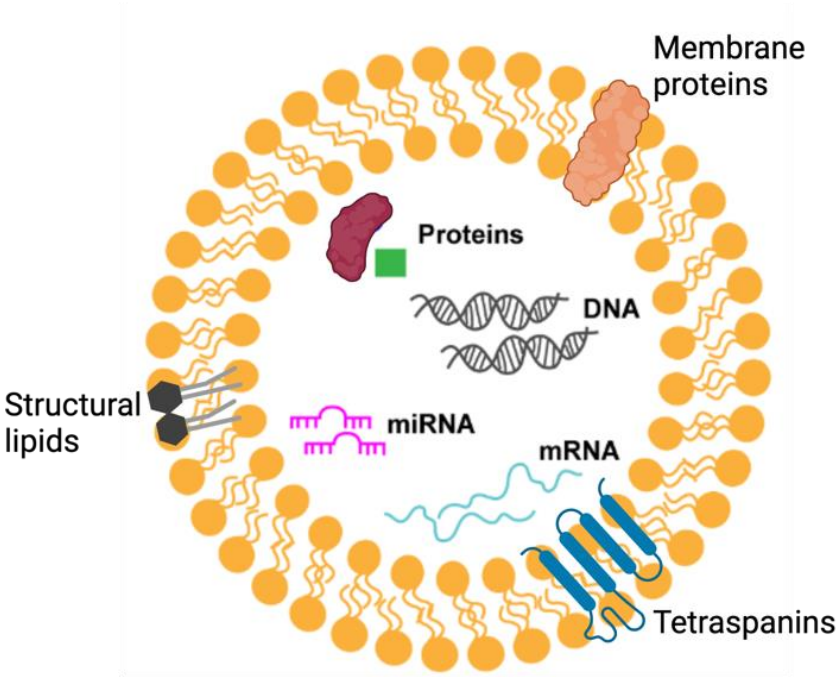

Figure 1-10. Phospholipids bilayer structure and contents of extracellular vesicles.

EVs from different sources exhibit different compositions of lipids and proteins, along with various nucleic acid fragments, which potentially affect their functions. Various cell types capable of secreting EVs have been explored, including mesenchymal stem cells, haematopoietic cells such as reticulocytes, T cells and macrophages, and non-haematopoietic origin such as intestinal epithelial cells, neurons and tumor cells [216]. Previous studies demonstrated that EVs secreted from immune cells were especially good at immune phagocytosis from immune system, and these EVs have longer circulation time [221]. However, EVs from dendritic cells were found to induce antigen-specific effector immune responses [222]. EVs derived from mesenchymal stem cells have been applied in clinical studies [223]. These EVs exhibit low-immunogenicity and have the potential to treat tissue fibrosis, in addition to demonstrating the capacity to promote tissue regeneration in some instances [224]. Moreover, mesenchymal stem cells derived-EVs are regarded as promising therapeutic agents

to mediate immunomodulation [224]. Tumor cell-derived EVs have also attracted a lot attention in recent years due to their specific targeting capabilities, relying on specific molecules on their surface that originate from the parent tumor cells, which allow them to interact with corresponding receptors on tumor cells [225]. For instance, use of ovarian cancer cell-derived EVs as delivery vehicles for CRISPR/Cas9 plasmid have demonstrated effectively delivery and accumulation in ovarian cancer cells, resulting in a decreased expression of PARP-1 gene, and sensitizing the tumor cells to cisplatin treatment [226]. However, EVs from certain cell types including colorectal cancer, pancreatic cancer and kidney adenocarcinoma tumor cells have also demonstrated limitations such as induction of apoptosis in activated cytotoxic T cells, [227], and tumor cell-derived EVs (such as cholangiocarcinoma) potentially induced a pro-inflammatory microenvironment, which may aggravate a patient's malignancy [228, 229]. In addition, the need for long-term cell culture (potential effects by cell status and growth conditions) and low yield of cell-derived EVs (depending on cell types) also pose obstacles to their application [230]. Considering the limitations of cell-derived EVs mentioned above, EVs isolated from dietary sources such as milk or plants have been explored for their potential functions. There are two main reasons to choose dietary EVs: (1) they originate from edible sources and thus potentially have a better safety profile, (2) cost-effectiveness and scalability [228].

Raimondo et al. [231] found that the EVs isolated from *Citrus limon* juice were able to inhibit the cell proliferation of tumor cell lines including lung carcinoma, chronic myeloid leukemia, and colorectal adenocarcinoma, and no effect from these EVs was observed on normal cell lines. In a recent study conducted by the same research team, it was found that the consumption of lemon EVs (isolation was conducted at an industrial scale) as a dietary supplement led to a decrease of low-density lipoprotein (LDL) cholesterol levels in healthy volunteers [232]. Ju et al. [233] isolated exosome-like NPs from grapes, and found that these NPs could target to

intestinal stem cells and protect against DSS-induced colitis. Wang et al. [234] revealed that the grapefruit-derived nanovectors coated with inflammation-related receptors could enhance the targeting ability to inflammatory tumor tissues and can more directly deliver therapeutic agents to inflamed tumor sites.

1.3.3.2. The application of EVs for siRNA delivery

Due to the variety of potential functions exhibited by EVs originating from various sources (mentioned above), EVs (particularly exosomes) have attracted significant interest for therapeutic (and diagnostic) purposes, with around 70 EV-based companies emerging globally in recent years, roughly 10 of them are engaged in researching the delivery capacity of EVs for therapeutic molecules such as anti-cancer drugs or RNA therapies [235]. 6 companies are focusing on investigating the inflammation inhibition capabilities of EVs derived from various sources [235]. Among over 200 active or recruiting clinical trials investigating EVs/exosomes (as of Jan. 2024), 7 trials are specifically investigating the potential of EVs/exosomes for IBD therapy [236]. Interestingly, mEVs *per se* have been investigated for their therapeutic potential in IBD and were found to ameliorate colitis in a murine model of the disease [237]. This therapeutic effect of mEVs is thought to arise from beneficial miRNA and cytokine cargo, such as miRNA-148 [238] and TGF-β (an immune-suppressive cytokine) [239]. However, the significant potential of EVs is currently underexplored for oral drug delivery.

Originally, EVs were regarded as a mechanism of cellular dumping or maintenance. However, in recent decades, research revealed that EVs are involved in cell-cell communication between local and distant cells. It has been observed that EVs are able to transfer their cargo (such as protein, nucleic acids and lipids) to nearby or distant recipient cells [240]. Numerous studies have demonstrated the potential of EVs as nanocarriers for siRNA delivery, where their advantages include small size and similarity with cell membranes ensuring effective cell uptake,

as well as long circulation with their slightly negative Zeta-potential [228]. Wahlgren et al. [241] found that exosome vesicles derived from human peripheral blood can deliver exogenous siRNA (encapsulated *via* electroporation) to human mononuclear blood cells (monocytes and lymphocytes), leading to selective gene silencing of corresponding proteins. In a recent research reported by Rong et al. [242], EVs isolated from induced neural stem cells modified with peptide CAQK were targeted to spinal cord injury (SCI) region and taken up by target cells (*via* tail vein injection in a SCI rat model), and the electroporated CCL2-siRNA cargo demonstrated anti-inflammatory and neuroreparative functions to promote the therapeutic effect of siRNA loaded-EVs against SCI *in vivo*. Interestingly, EVs were found to deliver cargo to recipient cells more efficiently than lipid nanoparticles. It was observed that the P21-activated kinase 4 (PAK4) siRNA (siPAK4) loaded-EVs (derived from PANC-1 cells) had significant higher gene silencing efficiency compared to siPAK4 encapsulated-Lipofectamine^{TM} which has been commercially used for transfection, and the intra-tumoral administration of siPAK4 loaded-EVs decreased tumor growth *in vivo* then promoted mice survival ($p < 0.001$) [243]. A similar result was reported in another study, showing EVs could deliver approximately 10-30% of RNA cargo to the cytosol of recipient cells, whereas only 1-2% of RNA cargo could be delivered by lipid nanoparticles [244]. This result indicated the promising potential of EVs as siRNA carriers, capable of inducing effective gene silencing.

1.3.3.3. Advantages and potential of bovine milk EVs (mEVs) for siRNA oral delivery

Considering the limited yield and the possibility of immune responses associated with EVs derived from cell lines, bovine milk has been revealed as a scalable source of EVs with low immunogenicity and high cross-species tolerance [245]. mEVs are observed to be stable in the gut biofluid including saliva, gastric, pancreatic and bile juices [246]. In addition, the

remarkable ability of EVs to cross biological barriers is regarded as a promising attribute for oral delivery of siRNA [247-249]. Rani et al. [250] revealed that the natural miRNA in milk exosomes did not affected by simulated digestion *in vitro* and could permeate through the intestinal monolayer. The bioactive function of miRNA in exosomes was still valid after simulated digestion process. The same results were also observed in another research. Liao et al. [251] found that the top 15 exosomal miRNAs in human milk maintained their stabilities after simulated gastric/pancreatic digestion process. Another study tried to load curcumin into milk exosomes by incubating curcumin with milk whey overnight at 4°C, and the results showed a loading efficiency of 70.46%, indicating a significant loading capacity of milk exosomes for hydrophobic molecules [252]. With loading into milk exosomes, the solubility and stability of curcumin were increased, and milk exosomes were able to protect curcumin against GIT digestion as well as promote their intestinal permeability *in vitro* [252]. The permeability of mEVs through Caco-2 cells was demonstrated to be mediated by endocytosis and associated with mEVs surface glycoproteins [247]. Similarly, mEVs could transport through the human vascular endothelial cells by endocytosis to deliver their cargo to the peripheral tissues [253]. Matsuda et al. [254] loaded siRNA into mEVs *via* Lipofectamine™ transfection reagents, and found that these siRNA loaded-mEVs are able to be uptaken by hepatocellular carcinoma cells *in vitro*, showing significant target gene silencing efficiency. However, this study did not demonstrate the loading efficiency of siRNA into mEVs. Importantly, significant progress has been made in mEV isolation methods that are amenable to industrial-scale production of purified, high-quality EVs as drug delivery vehicles [255]. Therefore, mEVs are potentially ideal, safe, effective and inexpensive carriers to enhance the intestinal uptake of therapeutic RNAs (siRNA), without toxicity/immunogenicity issues [239, 256].

1.3.3.4. Methods for mEV isolation from milk

Milk is a complex mixture of different constituents which should be removed in the process of mEV isolation. Various methods for mEVs isolation from milk have been developed in recent decades. Common isolation methods, including differential ultracentrifugation, density centrifugation, filtration centrifugation, immunoaffinity capture, microfluidic chip, size exclusion chromatography (SEC) and commercial precipitation kits, are applied separately or combinedly to isolate and increase the purity of mEVs (**Figure 1-11**) [245, 257].

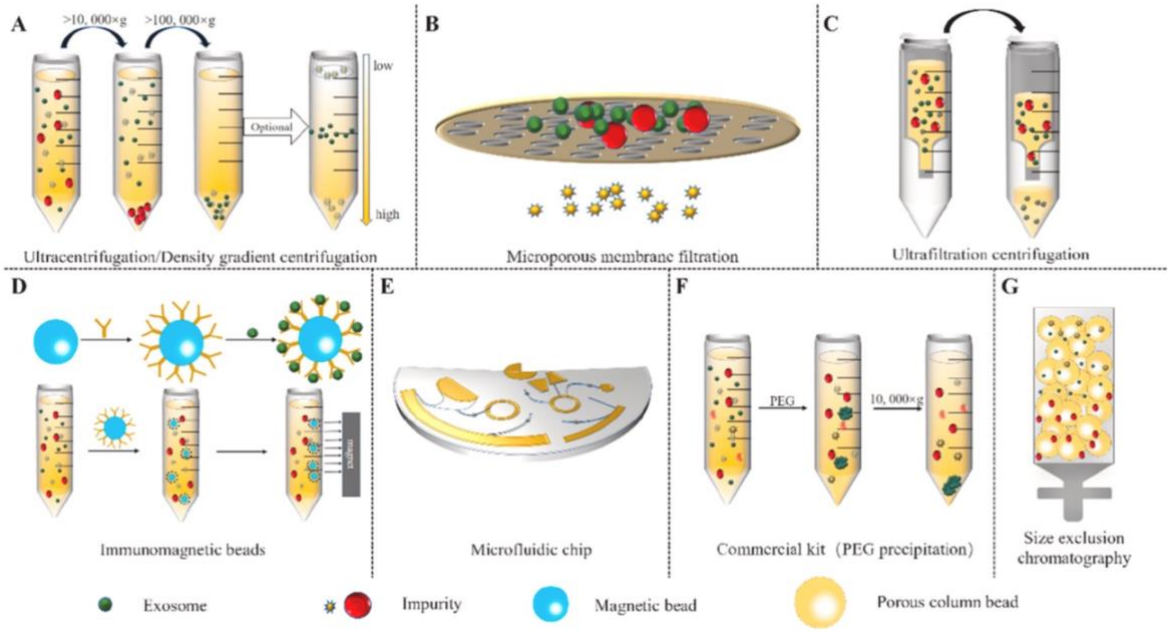

Figure 1-11. Isolation techniques for extracellular vesicles (EVs) [245].

Differential ultracentrifugation, which is cost-effective and amenable to handling large volumes of mEV sources, is currently the most widely used technology to isolate mEVs from milk. This method is based on several ultracentrifugation steps with different speed to remove untargeted components in milk and finally collect mEVs. The first spin normally utilizes low speed (~ 10,000 × g) to remove fat globules, casein aggregates, somatic cells and other large debris in milk. The higher spin speeds (~ 100,000 × g) are subsequently applied to remove large

particles and macrovesicles, and the final mEVs pellets are obtained *via* a high speed of spin (~ 130,000 × g). During or after spin, the mEVs supernatant is usually filtered with 0.22 μm membrane to remove large particles and provide sterilization [154, 247, 258, 259]. The differential ultracentrifugation can enable the isolation of mEVs from substantial milk volumes, which in turn improves the yield of mEVs. Normally, the initial volume of milk applied to ultracentrifugation exceeds 100 mL (relying on large-volume tubes compatible with spin rotor), significantly larger than several milliliters processed by commercial kits [260]. However, disadvantages of differential ultracentrifugation include the fact that it is time consuming, affords a low yield (to volume) and low purity [261]. Therefore, additional steps are always followed to ultracentrifugation to improve the purity of mEVs.

Density gradient centrifugation is another method to isolate mEVs from milk, which enriches mEVs to a specific density layer made from sucrose or iohexol. Briefly, gradient concentrations of sucrose or iohexol are loaded in a centrifugal tube with density increasing from top to bottom, and the sample loaded on the top travels through the gradient when centrifugation is applied. The sucrose gradient is created by layering decreasing concentrations of sucrose solution, such as 0, 64, 58, 52, 46, 40, 34, 28, 16 and 10%. With centrifugation, the layer with density range of 1.13-1.19 g/mL enriched with purified mEVs is collected [262]. With this method, the purity of mEVs is improved, but the steps such as sucrose solution with different concentrations preparation are complicated and time-consuming. Therefore, one specific concentration of sucrose cushion was reported to be applied following ultracentrifugation to purify mEVs [261, 263, 264]. 25% - 30% sucrose density ultracentrifugation is usually applied to remove non-mEVs particles including apoptotic bodies or Golgi-derived vesicles, and protein contaminations. The density of mEVs is equivalent to the density of 30% sucrose (1.12. to 1.18 g/mL), thereby a cushioning produced by sucrose separates protein contaminants of high density (1.22 g/mL) and also maintains the integrity of mEVs [265].

SEC technique (e.g. qEV column), applied to isolate mEVs from milk, is based on the relationship between particle size and the pore size of the stationary phase with porous beads. Specifically, particles with larger size such as mEVs in an aqueous solution flow out of the column firstly, and components with smaller size such as protein contaminants would go into and pass through the beads and stay longer in the column [266]. Even though SEC is associated with long-running time, in addition to not being suitable for large-scale purification and resulting in some loss of mEVs during the process, this process provides high purity based on the selective eluted fractions and maintains the integrity of mEVs [267]. Therefore, SEC is often used in combination with differential ultracentrifugation or other methods to improve the purity and integrity of mEVs [268].

Commercial precipitation kit is another choice for mEVs isolation from milk, such as the ExoQuick™ reagent [269]. These precipitation reagents are based on polymers such as PEG, which competitively bind with free water molecules and co-precipitate the hydrophobic proteins and lipid molecules [270]. The kit requires simpler equipment (low-speed centrifugation) and less professional operation. However, the method based on precipitation technique performs poorly in purity of mEVs [267], and the kit, which is expensive, could be only applied for limited volumes of milk or other sources (1 mL to 100 mL), resulting in low yield [261].

In addition to the methods mentioned above, there are techniques in current development. Immunoaffinity capture, which is based on the capture of magnetic beads coated with monoclonal antibodies to specific protein markers on EVs surface, shows high specificity and can maintain the morphological integrity of mEVs [271]. However, the high costs of immunomagnetic beads and small scale production are still limitations of this technology [272]. Ultrafiltration based on the centrifugation through membranes with specific molecular weight cutoff, has been applied to separate mEVs from other macromolecules in milk, however, the

contaminations possessing same molecular weight as mEVs cannot be removed [273]. Overall, various methods for isolating mEVs each come with their own advantages and disadvantages, and currently, a universally standard technique for the isolation and purification of mEVs is lacking. It is worth noting that lipoproteins, another phospholipid-based nanoparticles, are extensively assessed as contaminants in isolated EVs derived from blood plasma, due to the approximately 6 orders of magnitude of lipoproteins more abundant than EVs [274]. Even though the composition of lipoproteins in milk is not as abundant as in plasma, their existence should not be overlooked, especially a recent research has indicated that the interactions between EVs and lipoproteins may affect the bioactivities of EVs [275, 276]. However, the overlap of size and density between EVs and lipoproteins makes it a challenge to separate lipoproteins from EVs efficiently *via* traditional separation technologies such as SEC [277]. Various technologies have been explored to remove lipoproteins from EVs, such as ELISA [278], acoustofluidic-based separation technique [279], agarose gel electrophoresis [280], and a chemical method (styrene-maleic acid copolymer) involving the breakdown of lipoproteins [274], which could be considered as additional steps in isolation procedures to enhance the overall purity of mEVs.

1.3.3.5. Methods for drug loading into EVs

Various methods for drug loading into EVs have been researched (**Figure 1-12**) [281]. The simplest and most straightforward method is co-incubation (mixing) of EVs with the drug [282]. Due to the lipid bilayer structure of EVs, some hydrophobic drugs such as paclitaxel and curcumin can passively incorporate into the vesicles. Electroporation, which is based on the creation of temporary pores on EV membrane *via* high-intensity electric pulses, is commonly employed for nucleic acid loading into EVs, which is discussed specifically in the subsequent Section. Similarly, the ultrasonic energy from sonication also leads the formation of transient

pores in EVs membrane and allows efficient loading of drugs [283]. Both freeze/thaw cycles and extrusion are methods relying on the temporary disruption of the lipid bilayer structure of EVs, enabling the encapsulation of drugs [281]. In addition to these physical loading technologies, chemical conjugation has also been attempted to load drugs into EVs. Drugs can be chemically conjugated to lipids or other molecules that have an affinity for EV membranes [284]. These modified molecules are then incorporated into the EVs during their biogenesis. Given the inherent advantages and disadvantages associated with various loading techniques, it is important to consider the nature of drugs (hydrophilicity, size, surface charge, and stability), the types of EVs, and the intended therapeutic application when choosing a loading method. The subsequent section discusses specifically siRNA loading methods into mEVs.

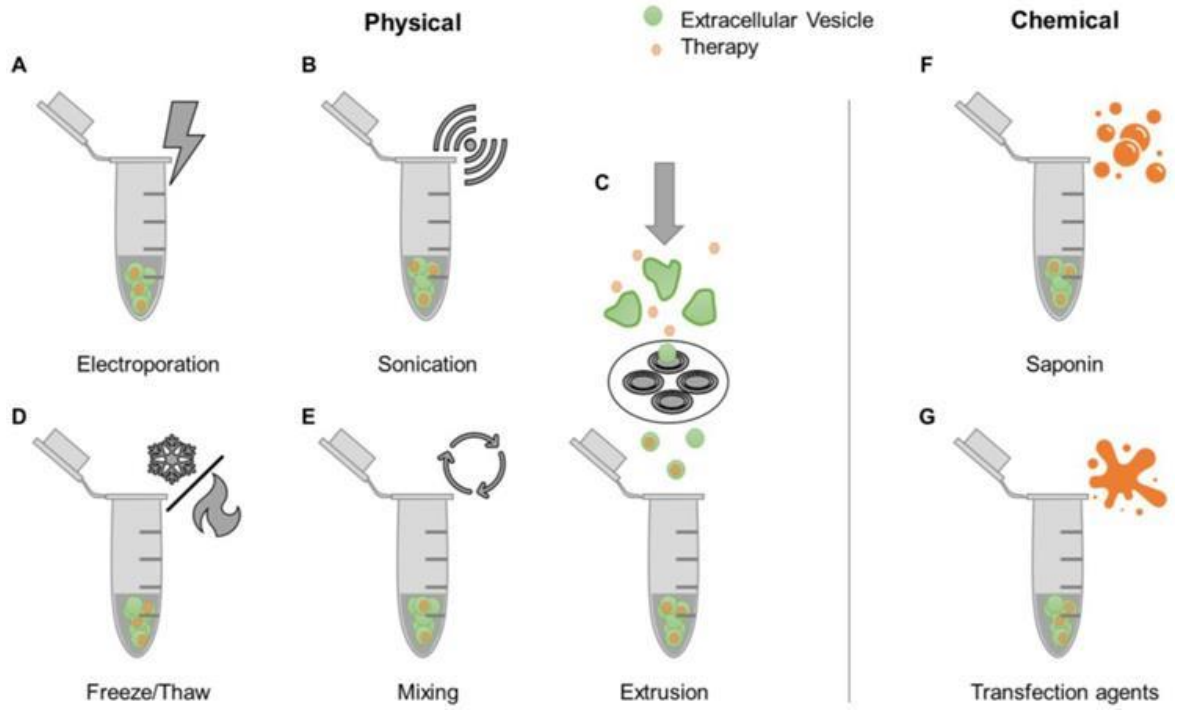

Figure 1-12. Examples of drug loading methods post-extracellular vesicles (EVs) isolation. After EVs have been isolated from biological sources, drugs can be loaded into EVs through various physical [e.g. electroporation **(A)**, sonication **(B)**, freeze/thaw cycles **(D)**, mixing **(E)**, and extrusion **(C)**] or chemical methods [e.g. use of saponin **(F)** and transfection reagents **(G)**] [281].

1.3.3.6. Methods for siRNA loading into mEVs

Even though mEVs are potentially ideal nanocarriers of siRNA, the key impediment to the clinical development of mEVs for RNA delivery is the current lack of non-destructive methods for efficient loading of macromolecules. Several approaches for siRNA loading into EVs have been reported, which are generally classified as endogenous or exogenous loading strategies [285].

Endogenous loading strategies

Endogenous loading approach concerns the genetic engineering of EV-producing cells to facilitate the intracellular production and loading of molecules by co-opting the EVs biosynthesis machinery [286]. Overexpression of exogenous nucleic acids has been widely applied for loading miRNA into EVs. Briefly, the donor cells which secret EVs are transfected by commercial transfection reagents to increase the production of RNAs that could be involved into pre-secreted EVs [211]. For instance, NIH3T3 cells were transduced with shRNA against human MYC and the EVs secreted by cells were generated and collected [287]. To evaluate the loading of siRNA, secreted EVs were added to λ820 cells expressing human c-MYC, and the results showed that c-MYC expression from cells was decreased in both mRNA and protein levels, which indicated that efficient endogenous loading of siRNA [287]. However, endogenous loading strategy is more suitable for cell-derived EVs due to the mechanism of cell modification, while this approach is not applicable to mEVs.

Exogenous loading strategies

Electroporation is the most widely used technology to load siRNA into mEVs. The mechanism of electroporation is based on the electrical pulse to create temporary pores on mEVs

membrane and small siRNA molecules could following diffuse into the interior [228]. After pulsing, mEVs are placed on ice to restore the mEV membrane and complete siRNA loading. This method is straightforward and typically used for loading of siRNA, which due to its hydrophilic and macromolecular nature cannot be loaded through simple incubation (in a similar way to hydrophobic or small molecules) [228]. However, electroporation is prone to inducing siRNA aggregation, affects mEV membrane integrity and exhibits a low loading efficiency for siRNA [288, 289].

siRNA loading into mEVs can also be achieved *via* transfection reagents due to the similar bilayer structure of mEVs and cells [248, 290, 291]. The transfection reagent is typically a cationic lipid-based product such as lipofectamine, or cationic polymers (ExoFect™ transfection kit), *etc.* Condensed siRNA-transfection reagent complexes are formed *via* electrostatic interaction between positively charged reagent and negatively charged siRNA [292]. The ExoFect™ siRNA/miRNA transfection kit was utilized to facilitate the loading of siRNA into mEVs, resulting in a several-fold increase in loading efficiency compared to electroporation [293]. Additionally, unlike electroporation, transfection reagents for introducing siRNA into mEVs does not require specialized equipment and the operation steps are user-friendly.

In addition to electroporation and transfection, additional methods have been reported to load siRNA into EVs. For instance, simple incubation was attempted in an effort to load siRNA into EVs, where the hydrophobic siRNA was modified with cholesterol and phosphonothioate for internalizing the siRNA across EV membranes [294]. Sonication is based on the sonoporation phenomenon, which uses low-frequency ultrasound to induce microbubble burst and allows siRNA to cross into EVs [295, 296]. However, loading siRNA into EVs *via* sonication requires consideration of the damage from ultrasound force to both siRNA and EVs.

1.3.4. Development of hybridosomes as a technique to achieve macromolecule loading into EVs

Various methods have been used to load siRNA into EVs (mentioned above), however, these strategies are highly inefficient [297, 298]. Some of these (exogenous loading) are associated with a plethora of adverse effects, including the denaturing of drugs or proteins on EV surface, EV aggregation, compromised tissue-penetrating properties of native EVs and potential toxic residual impurities [299]. Importantly, most current methods produce orders of magnitude lower RNA loading into EVs compared to what can be achieved in synthetic delivery systems [300], presenting a significant barrier to clinical translation of EVs as delivery vehicles for macromolecules.

The fusion of EVs with liposomes to create novel bioinspired delivery systems that merge the advantages of both EVs and liposomes has recently emerged as a strategy to overcome some of the obstacles associated with EVs (**Figure 1-13**) [301, 302]. Hybrids have found application in various diseases including cancer therapy (tumor-targeted drug delivery), drug delivery to fibrosis, anabolic therapy for bone loss, and gene delivery, etc [302]. These systems, which are generated *via* different approaches, overcome the poor drug loading of EVs, enable easier surface functionalization to confer beneficial properties, such as theranostics or targeting capabilities (functionalizing the surface of native EVs is challenging), and are endowed with high biocompatibility and low immunogenicity of EVs [302]. For example, it was recently demonstrated that the loading efficiency of siRNA into EV-liposome hybrids can reach up to ~50% [303]. As a result of these advantages, a number of recent studies have reported the generation of different EV-liposome hybrid systems, which are comprehensively reviewed by Liu et al. [302].

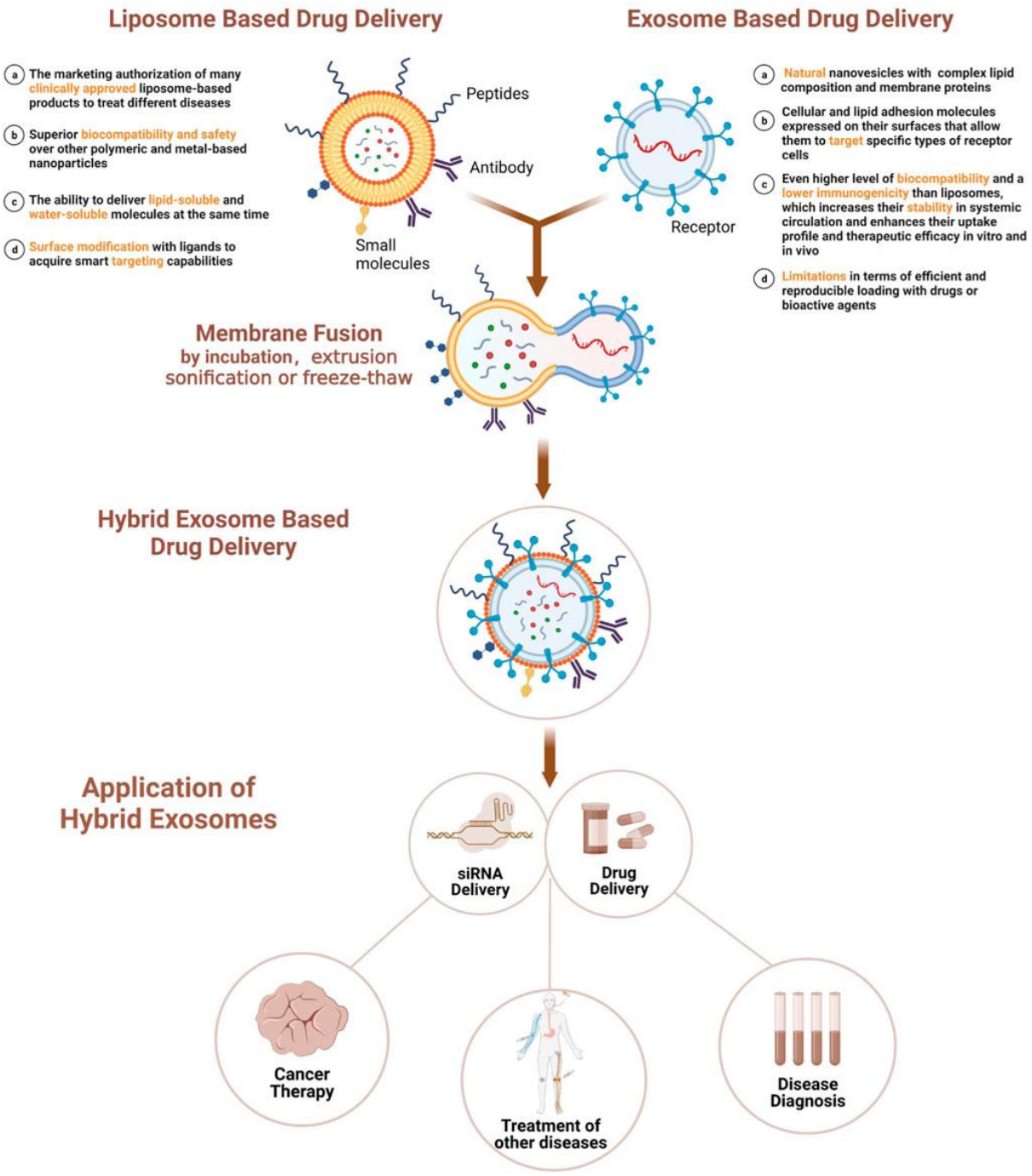

Figure 1-13. Membrane fusion-based hybrid exosome preparation and applications [302].

Various methods can be employed to fuse liposomes with EVs. When selecting an appropriate fusion method, various factors should be considered, such as fusion efficiency, impact on bioavailability, drug loading efficiency, and the practicality of the process.

Freeze-thaw cycles

The freeze-thaw method is the most commonly used fusion approach, relying on the disruption and reassembly of lipids bilayers of liposomes and EVs. During the freezing phase, ice crystals formed from water induce disruption of the lipid bilayers. Upon thawing the frozen mixture, the lipids from the disrupted liposomes and EVs can reassemble, driven by their hydrophobic properties. Cheng et al. designed a hybrid fused by genetically engineered exosomes (a type of EVs) with heat-sensitive liposomes *via* three freeze-thaw cycles [304]. The fusion efficiency was shown to be 97.4% and the hybrids possessed properties suitable for a combination of photothermal therapy and immunotherapy for cancer [304].

Incubation

It was also found that spontaneous membrane fusion of liposomes and EVs can occur through incubation, based on the similarity in lipid bilayer structures between liposomes and EVs. Lin et al. [305] designed hybrids by simply incubating EVs with liposomes at 37℃ for 12 h to provide a delivery system for CRISPR-Cas9. However, even though this method is safe and straightforward, it is associated with relatively low fusion efficiency.

Polyethylene glycol (PEG)-mediated fusion

PEG has been widely applied to induce cell-cell fusion mediated by the close contact and dehydration of lipid bilayer structures. Piffoux et al. [306] fused EVs with functionalized liposomes *via* PEG trigger to develop a smart biosynthetic hybrid. The hybrids enable EVs to encapsulate exogenous compounds efficiently, and the hybrids improved 3-4 folds of cellular delivery efficiency of a therapeutic compound compared to free drug or drug-loaded liposomes [306].

Extrusion

The membrane extrusion method for fusion of liposomes with EVs refers to the simultaneous extrusion of these nanoparticles through membrane pores with controllable size. The mechanical pressure on the lipid bilayers causes them to deform and pass through the pores

and on the other side of the membrane the mixed vesicles reform to hybrids. A number of studies have used the extrusion method to prepare hybrids [307-309]. Briefly, EVs and liposomes were mixed in various ratios and the mixtures were subsequently vortexed and/or sonicated for several minutes to solvate and homogenize the nanoparticles in solution. Thereafter, the mixtures were extruded through the membranes with various pore size of 400 nm, 200 nm and/or 100 nm.

1.4. Research Aim & Objectives

Research Aim

This work explored the potential of bovine milk extracellular vesicles (mEVs) and mEVs-mediated systems for the oral delivery of anti-TNFα siRNA as a new therapeutic approach for IBD.

Research Objectives

In pursuit of the aim, the following specific research objectives have been defined:

Objective 1 (Chapter 3): To optimize the methods for isolation, purification and siRNA loading into mEVs from skimmed bovine milk. The target is to achieve a high yield and purity of mEVs, and achieve similar or higher siRNA loading efficiency compared with previous studies employing similar techniques.

Objective 2 (Chapter 4): To determine the drug delivery potential of mEVs by testing their stability in simulated intestinal fluids, uptake and transport across the intestinal epithelium, gene silencing effect of siRNA-loaded mEVs on macrophages. The target is to achieve these performances of mEVs demonstrating better than siRNA delivered either unaided or *via* liposome delivery systems.

Objective 3 (Chapter 5): To optimise siRNA loading into mEVs through the development of 'hybridosomes' – hybrid particles formed *via* the fusion of mEVs and liposomes (aim to achieve a higher loading efficiency compared to existing loading methods), and assess their anti-TNFα siRNA delivery potential in *in vitro* co-culture inflamed intestinal models.

2. Materials and General Methods

2.1. Materials

Bovine pasteurized skimmed milk was purchased from a local grocery (Sainsbury's). QuantiPro™ BCA Assay Kit, Triton X-100, Sodium Dodecyl Sulfate (SDS), *N*,*N*-Dimethylforamide Dulbecco's Modified Eagle's Medium (DMEM), Hank's Balanced Salt Solution (HBSS), fetal bovine serum (FBS, non-USA origin), non-essential amino acids, antibiotic/antimycotic solution, N-Acetyl-L-cysteine, Nicotinamide, Gastrin I human, paraformaldehyde, Fluoroshield™ DAPI, low temperature gelling agarose, fluorescein isothiocyanate–dextran with molecular weight of 10k (FD10), MISSION® siRNA Fluorescent Universal Negative Control #1, Cyanine 5 and X-tremeGENE™ 360 Transfection Reagent were obtained from Merck (Dorset, UK). qEV original 35 nm size exclusion chromatography (SEC) was purchased from Izon Science (Lyon, France). Fasted- and Fed-State Simulated Intestinal Fluids (FaSSIF and FeSSIF, respectively) were purchased from Biorelevant (London, UK). TrypLE™ Express Enzyme, Ambion™ Nuclease-Free Water, TRIzol® reagent, Advanced DMEM/F-12, HEPES (1 M), GlutaMAX™, Penicillin-Streptomycin, B-27™ Supplement (50X), Human Epidermal Growth Factor (EGF) Recombinant Protein, A83-01, Opti-MEM™ I Reduced Serum Medium, KDalert™ GAPDH Assay Kit, Silencer™ Select GAPDH Positive Control siRNA, Silencer™ Select Negative Control siRNA, ZO-1 polyclonal antibody and chicken anti-rabbit IgG (H+L) cross-adsorbed secondary antibody, Alexa Fluor™ 488 were bought from Thermo Fisher Scientific (Waltham, MA, USA). Goat Anti-Mouse IgG H&L (Alexa Fluor™ 594) was purchased from Abcam (Cambridge, UK). Tris-EDTA (TE) buffer and QuantiFluor® RNA System were purchased from Promega (Southampton, UK). Caco-2 cells and macrophages (J774A.1) were purchased from European Collection of Cell

Cultures (ECACC, Salisbury, UK). ExoGlow™-Protein EV Labeling Kit (Red), ExoQuick™ reagent and Exo-Check™ Exosome Antibody Array kit were purchased from System Biosciences (Palo Alto, CA, USA). 6.5 mm Transwell® with 0.4 μm pore polycarbonate membrane inserts and Corning® Matrigel® Growth Factor Reduced Basement Membrane Matrix were purchased from Corning (Glendale, AZ, USA). Recombinant Human Noggin was purchased from PeproTech (London, UK). IntestiCult™ Organoid Growth Medium (Human), SB202190, and Y27632 were purchased from STEMCELL Technologies (Cambridge, UK). 24-well PET inserts with 0.4 μm pore size were purchased from SARSTEDT (Nümbrecht, Germany). Cultrex® Reduced Growth Factor Basement Membrane Extract Type 2, PathClear® (BME2) and DAPT were purchased from Bio-Techne Ltd. (Oxford, UK).

2.2. General Methods

2.2.1. Isolation and purification of mEVs

mEVs were isolated from skimmed bovine milk by differential ultracentrifugation process according to the methods described by previous studies [259, 310]. Briefly, 70 mL of milk was centrifuged at 13,000 × g for 30 min at 4 ºC with Optima XPN-80 Ultracentrifuge (Beckman Coulter, Type 45 Ti fixed angle rotor) to remove fats and casein. The whey was then centrifuged at 100,000 × g for 60 min to pellet large particles. The supernatant was filtered by 0.2 μm filter to remove large particles and further centrifuged at 135,000 × g for 90 min, producing mEVs pellets which were washed with PBS once and resuspended in 1 mL sterile PBS. Resuspended mEVs were then purified by SEC. Specifically, the qEV original column was equilibrated in room temperature for 30 min and flushed with 20 mL filtered sterile PBS or HEPES buffer. Then 500 mL of raw mEVs suspension was immediately loaded onto the loading frit and the elution was collected. When all the samples entered the loading frit, the column was topped up with 500 mL buffer and elution was collected again. The same procedure was repeated and 20

fractions were collected in total. The protein level in each fraction was compared with the absorbance of plasma protein (280 nm) by a plate reader. The fractions containing purified mEVs were used for downstream application. Purified mEVs in sterile PBS or HEPES buffer could be stored at -80 ºC for up to 3 months.

2.2.2. Fluorescent labelling of mEVs

To image and quantify the cell uptake and transport, mEVs were labelled using an ExoGlow™-protein EV labeling kit (Red). Briefly, 1 μL of the labelling dye was added to 500 μL mEVs suspension (0.4-1.0 mg/mL, protein concentration) and incubated at 37°C for 20 min with shaking. Thereafter, 167 μL ExoQuick™ reagent was added to the mixture and incubated at 4°C overnight to precipitate mEVs. The mixture was centrifuged with 10,000 × rpm for 10 min to remove excess labelling dye and pellet the labelled mEVs which were then resuspended in sterile PBS.

2.2.3. Preparation of liposomes

Liposomes were formulated by different lipid compositions. Firstly, lipids were dissolved in different organic solvents depending on their solubility in a round bottom flask, and the organic solvent was evaporated by a rotary evaporator to create a lipid film, which was dried under vacuum overnight. Thereafter, the lipid film was hydrated with HEPES buffer (4 mM, pH 7.4) at a final lipid concentration of 1 mg/mL. 10 freeze-thaw cycles (freezing in liquid nitrogen and thawing by sonication at 40 ℃ for ∼5 minutes) were applied to develop and homogenize the liposomes.

2.2.4. Characterization of EVs, liposomes and hybrid EVs

The size and surface charge (Zeta-potential) of NPs (including EVs, liposomes and hybrid EVs) were measured by Malvern Zetasizer (Malvern, UK). Following isolation or synthesis, the NPs were diluted 100× using either 0.01 M PBS or 4 mM HEPES buffer (pH 7.4) for the purpose of measurement. Nanoparticle Tracking Analysis (NTA, Malvern Nanosight LM-10, UK) was used to determine the size and nanoparticle concentration (yield, nanoparticles count/mL). To conduct NTA, nanoparticles were diluted with filtered (0.2 μm) 0.01 M PBS or 4 mM HEPES buffer (pH 7.4) to a concentration which allowed the count rate to stabilize at 20-80 particles/frame.

The morphological features of mEVs were examined by transmission electron microscopy (TEM). Briefly, 300-mesh carbon-coated copper grids were pre-treated by glow discharge (negative charge). 3 μl of mEVs were applied onto the grids and incubated at room temperature for 1 min, after which were stained with 3% uranyl formate for additional 1min. Images were acquired on JEM-1400 flash (JEOL, Japan) at an acceleration voltage of 80 kV.

Total protein concentration and protein markers of mEV samples were determined by QuantiPro™ BCA Assay Kit and Exo-Check™ Array, respectively, following the manufacturers' instructions.

2.2.5. Cell culture

2.2.5.1. General culture of Caco-2 cells and macrophages

Caco-2 cells were maintained in DMEM supplemented with 10% FBS (v/v), 1% non-essential amino acids (v/v), and 1× Antibiotic-Antimycotic in T-75 cell culture flasks at 37 °C and 5% CO_2 atmosphere. When the cells were above 80% confluent, the medium was removed by aspiration and cells were washed with 5 mL sterile PBS. 2 mL TrypLE™ was added to the

flask and incubated for 10 min at 37 °C and 5% CO_2 atmosphere to detach the cells from flasks. After detachment, 8 mL culture medium was added, and cell suspension was centrifuged at 1500 × rpm for 5 min. Thereafter, the cell pellets were resuspended in 5 mL culture medium and 1 ml of cell suspension (1:5 splitting ratio) was added to a new T-75 culture flask with 14 mL culture medium involved. The culture medium was changed every 2 days. Caco-2 cells were used between 10 to 80 passages, after which they were discarded, and a new batch was defrosted. Macrophages (J774A.1) were maintained in the same culture medium and splitting procedure as above, except the detachment of macrophages was operated by scraping. Macrophages were used between 10 to 30 passages, after which they were discarded, and a new batch was defrosted.

2.2.5.2. Culture of Caco-2 monolayers and transport experiments

To establish differentiated Caco-2 monolayers, cells were seeded on 12-well polycarbonate Transwell inserts (0.4 µm pore size) at 100,000 cells/well (500 µL/well) density and cultured for 21 days (changed culture medium every 2-3 days), with measurement of trans-epithelial electrical resistance (TEER) by EVOM (World Precision Instruments, Sarasota, FL, USA) to monitor the monolayer barrier integrity.

Prior to the transport study, the culture medium in both apical and basolateral sides was replaced with HBSS and incubated for 45 min at 37°C and 5% CO_2 atmosphere for equilibration. Thereafter, 500 µL of tested samples dissolved in HBSS were added to the apical side of monolayers for a certain period of incubation. During the incubation, 100 µL basolateral solution was sampled regularly (at 30 min or 40 min intervals), with the sampled solution replaced with HBSS.

2.2.6. Statistical analysis

Data were analyzed using GraphPad Prism® 9. Data is presented using the mean ± standard deviation (SD) using at least three technical replicates and repeat experiments. Statistical analysis was performed by unpaired Student's t-test or ANOVA, and the normality distribution of data was checked before analysis. Differences with a *p*-value lower than 0.05 were taken as significant. The * and ** nomenclature were used to indicate $p < 0.05$ and $p < 0.01$, respectively.

3. mEV Isolation, Characterization and Loading siRNA into mEVs

3.1. Introduction

mEVs, which are designed by nature for delivery of cargos to cells, have been shown to have unique characteristics for lipid membrane-enclosed nanosystems, which comprise a combination of stability in GIT and the ability to cross biological barriers [247-249]. Importantly, the milk origin of mEVs renders them cost-effective and suitable for large-scale production by the dairy industry, compared with other EVs sources such as cell culture medium [311]. These advantages position mEVs as promising candidates for oral delivery carriers. However, milk as a source of natural nutrients, comprises complicated components including a plethora of carbohydrates, proteins, lipids, minerals, and vitamins, which poses challenges to isolating pure mEVs from milk [257].

Many studies have focused on isolation of mEVs from milk reproducibly, utilizing various techniques (as mentioned in Section 1.3.3.4.). However, the yield and purity of mEVs are still highly variable due to the presence of contaminations from milk such as proteins/nucleic acids, other vesicles or cellular components [312]. The lack of gold standard methods for mEVs isolation and purification is the main obstacle for mEVs application. In recent years, the International Society for Extracellular Vesicles (ISEV) has worked actively to improve the standardization of EVs research, and released the first Minimal Information for Studies of Extracellular Vesicles (MISEV) guidelines in 2014 (renewed in 2018) [313], which provides guidance in standardization of protocols and reporting in EVs filed. However, as the study of mEVs is still rapidly evolving, methods for isolating or purifying EVs are frequently updated or advanced, leading to variations in outcomes compared to earlier findings. Therefore, reliable methods for mEVs isolation and purification are highly demanded, and the obtained mEVs need to be well characterized for downstream application.

Upon obtaining purified mEVs, the efficient loading of siRNA into them becomes a pivotal step in the development of a siRNA delivery system. Several approaches for siRNA loading into EVs have been reported, which are generally classified as exogenous or endogenous loading strategies (described in Section 1.3.3.5). Different loading technologies possess their own advantages and disadvantages. For instance, commercial transfection reagent provides relatively high loading efficiency, while their toxicity and high cost should be considered [293]. Electroporation, as the most widely used technology, enables encapsulation of siRNA into mEVs in a straightforward and efficient manner [228]. However, the pulse of electroporation could cause siRNA aggregation and destroy the mEVs membrane integrity [288, 289]. Therefore, different loading methods need to be carefully considered not only for achieving a high loading efficiency but also to maintain subsequent bioactivities of siRNA-loaded mEVs.

3.2. Study Objectives

The aim of this Chapter is to isolate mEVs from bovine milk and load siRNA into mEVs. Described in this Chapter are studies on: i) Optimizing mEV isolation methods and conditions, including using commercial kit (Invitrogen™ Total Exosome Isolation Reagent (from other body fluids)) and ultracentrifugation, as well as SEC to increase the purification of mEVs; ii) Characterizing mEVs with various parameters, including size, PdI, Zeta-potential, yield, morphology and protein markers; iii) Optimizing methods for siRNA loading into mEVs, including using transfection reagents (X-tremeGENE^{TM} 360 Transfection Reagent and Exo-Fect^{TM} siRNA/miRNA Transfection Kit), surfactant-saponin, and electroporation.

The objectives of this Chapter are:

1. To isolate, purify and characterize mEVs from bovine milk.
2. To load siRNA into mEVs efficiently.

3.3. Methods

3.3.1. mEVs isolated by a commercial kit

In addition to isolation and purification of mEVs from bovine milk *via* ultracentrifugation and SEC (General Methods Section 2.2.1.), a potentially alternative isolation method, namely a commercial kit (Invitrogen™ Total Exosome Isolation Reagent (from other body fluids)), was also investigated in this chapter. According to the manufacture's instruction, 1 mL bovine milk was centrifuged at 2000 × g for 10 min to remove the bigger debris, then the supernatant was centrifuged at 10,000 × g for 30 min and with another 10 min to remove the upper layer and lower debris pellet. The middle layer was carefully moved to a new tube followed by the addition of 1 volume of PBS and 1 volume of isolation reagent. Thereafter, the solution was mixed and incubated for 30 min at room temperature. Then the mixture was centrifuged at 10,000 × g for 10 min to collect the pellet which contained the mEVs. The pellets were then resuspended in 50 μL PBS and centrifuged at 10,000 × g for 5 min to remove non-organic particles in the pellets and the supernatant containing mEVs was used for downstream application.

Characterization of mEVs was conducted according to General Methods, Section 2.2.4.

3.3.2. siRNA loading into mEVs

3.3.2.1. Loading siRNA into mEVs by transfection reagent

To optimize the loading conditions, siRNA Fluorescent Universal Negative Control #1 containing Cyanine 3 (Merck, St. Louis, MO, USA) was loaded into mEVs. X-tremeGENE™ 360 Transfection Reagent was used according to the methods described by previous studies [290, 314]. Briefly, siRNA was dissolved in 50 μL Opti-MEM reduced serum medium, and the transfection reagent was mixed with 100 μL Opti-MEM medium. Then the siRNA and

transfection reagent solution were mixed gently and incubated for 15 min at room temperature. Thereafter, 200 µL of mEVs resuspended in Opti-MEM medium were added to the siRNA-transfection reagent mixture, followed by additional incubation at room temperature or 37°C. Unloaded siRNA was removed *via* centrifugal ultrafiltration with 100 kDa Amicon Ultra-0.5 Centrifugal Filter Unit (Merck, Dorset, UK) by four sequential centrifugations for 10 minutes each at 10,000 × rpm. 500 µL of PBS was added between each spin to wash off the remaining unloaded siRNA from the mEVs suspension. After ultrafiltration, siRNA loaded-mEVs were collected and resuspended in 100 µL PBS for downstream application. ExoQuick™ reagent, which precipitates mEVs, was another approach to remove unloaded siRNA. Briefly, 167 µL ExoQuick™ reagent was added to 500 µL siRNA loaded-mEVs solution and mixed completely. The mixture was then incubated at 4°C overnight or on ice for 30 min followed by a centrifugation with 10,000 × rpm for 10 min. siRNA loaded-mEVs pellets were then resuspended in 250 µL sterile PBS for downstream application.

After loading siRNA into mEVs, the fluorescent signal of loaded siRNA was measured by a plate reader with excitation wavelength (Ex) of 555 nm and emission wavelength (Em) of 605 nm. The amount of loaded siRNA was calculated based on the fluorescence-to-concentration standard curve. The loading efficiency of siRNA into mEVs was calculated by **Equation 3-1**:

$$\%\ loading\ efficiency = 100 \times \frac{amount\ of\ loaded\ siRNA}{amount\ of\ added\ siRNA} \qquad (3-1)$$

Loading of siRNA into mEVs by the Exo-Fect^{TM} siRNA/miRNA Transfection Kit was conducted according to the manufacturer's instructions. Briefly, positive control siRNA (Cy3-labeled siRNA, provided within the Kit) or Cy5-labeled siRNA was mixed with transfection reagent and transfection buffer according to the recommended amounts (by the manufacturer), following incubation for 15 min at room temperature in dark. Thereafter, mEVs (50-300 µg in 100 µL) were added to the mixture and incubated for 1 hour at 37°C in the dark. After transfection, the ExoQuick™ reagent was applied to precipitate siRNA loaded-mEVs and

remove unloaded siRNA. Fluorescence of Cy3-labeled siRNA and Cy5-labeled siRNA was measured by a plate reader at Ex/Em: 555 nm/605 nm and 640 nm/676 nm, respectively. The loading efficiency was calculated by **Equation 3-1**.

3.3.2.2. Loading of siRNA into mEVs by saponin

mEVs were initially diluted to a concentration of 0.5 mg/mL with PBS. 1 nmol siRNA (dissolved in 20 μL nuclease-free water) was added to mEVs solution (300 μL). Thereafter, the mixture of siRNA and mEVs was supplemented with 0.2% (m/v) saponin and incubated for 20 min at room temperature. After loading, the unloaded siRNA was removed *via* ultrafiltration and loading efficiency was calculated as mentioned above.

3.3.2.3. Loading of siRNA into mEVs by electroporation

Electroporation was applied to load siRNA into mEVs using parameters that were optimized based on previous reports [289]. Specifically, 150 μg mEVs were mixed with 0.5 nmol siRNA, followed by the addition of electroporation buffer (1:1 v/v ratio to mEVs-siRNA mixture, and total volume was 400-500 μL). The electroporation cuvette (4 mm) was incubated on ice for 10 min before pulsing. Electroporation was performed at various voltages and capacitances on a Gene pulser System (Bio-Rad Laboratories, Watford, UK). Unloaded siRNA was removed *via* ExoQuick™ reagent or ultracentrifugation (135,000 × g for 90 min).

3.4. Results and Discussion

3.4.1. mEV isolation and characterization

3.4.1.1. mEV isolation by a commercial kit

Commercial kit (Invitrogen™ Total Exosome Isolation Reagent (from other body fluids)) was applied to isolate mEVs from pasteurized skim bovine milk. Dynamic Light Scattering (DLS) and NTA were both used to identify the size of mEVs. According to the results shown in **Table 3-1**, the size of mEVs measured by NTA (144.3 ± 7.00 nm) was slightly lower than that given by DLS (173.8 ± 3.50), which could be a result of variations in the optical detection mechanism. DLS delivers an intensity-weighted measurement by analyzing fluctuations in light scattering intensity from particles due to Brownian motion, disproportionately emphasizing larger particles because they scatter more light [315]. In contrast, NTA provides a number-weighted distribution by tracking Brownian motion of individual particles using a microscope camera system, assigning equal significance to each particle, regardless of size, which allows for a more balanced representation of all particles present in the sample [315, 316]. The low PdI value measured by DLS indicated good dispersibility of isolated mEVs and without aggregations (**Table 3-1**). Commercial pasteurized skim bovine milk served as the source of mEVs in this study for several reasons: a) Quality control: commercial milk often has standardized compositions, enhancing the reliability and reproducibility of mEVs isolation; b) Reduced contamination: the production procedure of commercial milk includes steps to remove some contaminations such as microorganisms; c) Availability and convenience: the commercial milk can be easily procured from groceries, making it readily accessible for research. However, whether the pasteurization process has effect on mEVs remains to be fully investigated. Previous reports have demonstrated that the pasteurization does not appear to adversely affect the integrity and biological function of mEVs, and pasteurized mEVs are shown to be as

functionally beneficial as raw milk EVs [317, 318]. Research into the specific marker proteins of goat mEVs has revealed little effect due to pasteurization [319]. Another study showed that the pasteurization process might decrease mEVs concentration from bovine milk, and some types of original miRNA in EVs may be affected by pasteurization [320]. Therefore, though comprehensive research for the effect of pasteurization on mEVs is warranted, the focus of this study on the delivery potential of mEVs, which related to their integrity and protein instead of bioactive components such as miRNAs, indicates a minimal impact of pasteurization on the mEVs used for delivery purposes.

As abundant proteins existed on mEVs surface, protein concentration measured by BCA assay was a straightforward way to quantify mEVs [321], and the results showed a high protein concentration (1.07 mg/mL, resuspended in 50 μL PBS) of mEVs isolated by commercial kit from 1 mL bovine milk. However, considering that the accuracy of this assay may be compromised by protein contamination, particle count should be also involved to evaluate mEVs yield [321], which is shown as $2.74 \times 10^{11} \pm 9.02 \times 10^{9}$ particles/mL (**Table 3-1**). Importantly, the purity of mEVs is always determined by the ratio of particle to protein concentration [322]. Herein, isolated by commercial kit, the mEVs ratio of particle/protein concentration was calculated as 2.56×10^{8} particles/μg, which indicated the impurity of mEVs and protein contaminations existence (according to the reported standard: ratios > 3×10^{10} particles/μg equate to high EVs purity, ratios of 2×10^{9} to 2×10^{10} particles/μg represent low purity, and any ratios below 1.5×10^{9} Particles/μg are impure [323]).

Determining the expression of mEV protein markers (*via* the Exo-Check™ Array kit), **Figure 3-1** shows that the general markers of EVs were expressed in mEVs, such as: a) non-tissue specific tetraspanins including CD63 and CD81, which are proteins associated to plasma membrane and/or endosomes, b) ICAM (*Intercellular* Adhesion Molecule-1) which is a cell surface glycoprotein involved in cell-cell adhesion, c) FLOT 1 (Flotillin 1) and TSG101 (Tumor

Susceptibility Gene 101), which are cytosolic proteins recovered in EVs [324]. ALIX (ALG-2-interacting *protein* X, cytosolic proteins) is not apparent, as this protein exists in EVs from colostrum and not mature milk [325]. Epithelial cell adhesion molecule (EpCAM), which is a cell/tissue specific protein marker and often found in epithelial cells-derived EVs, was also not apparent in mEVs. The staining of GM130 (Cis-golgi matrix protein) suggests some contamination of intracellular proteins (arising from apoptosis) during mEVs preparation [326-328]. According to MISEV 2018 guidelines, the protein markers highlighted in our results serve to confirm the nature of EVs and the successful isolation of mEVs from milk [324]. However, it is recommended for future studies to include a purity control protein marker for major components of non-EV co-isolated structures, such as lipoproteins (Apolipoproteins A1/2 and B (APOA1/2, APOB); APOB100; albumin (ALB)) [324]. In addition to Western blotting, several other technologies are available for the identification and quantification of protein markers in mEVs. Flow cytometry, for instance, allows to quantify the subpopulations of EVs expressing protein markers upon immunofluorescent staining [329, 330]. ELISA, available in both direct and sandwich assay formats, is a well-established technique with high specificity for quantification of EVs protein, and several kits have been commercially available [331, 332]. Similarly, sandwich immunoassay employing fluorescence scanning to quantify EVs binding to an antibody-coated surface, offers additional options [333]. Mass spectrometry has been utilized for the simultaneous measurement of numerous membrane-bound and intra-vesicular proteins within mEVs [334]. Furthermore, innovative techniques for mEV protein quantification, which offer high specificity and sensitivity, are under development, including various microfluidic methods [334, 335], and immune-electron microscopy with gold-labeled antibodies, allowing to confirm and quantify specific protein expression on individual EVs [336, 337].

Table 3-1. Physicochemical parameters of bovine milk extracellular vesicles isolated by commercial kit.

Parameter & Measurement method	**Value**
Size (nm) (DLS)[a)]	173.8 ± 3.50
PdI[b)] (DLS)	0.221 ± 0.006
Size (nm) (NTA)[c)]	144.3 ± 7.00
Yield (particles/mL) (NTA) [d)]	$2.74 \times 10^{11} \pm 9.02 \times 10^{9}$
Zeta-potential (mV)	-8.68 ± 0.69
Protein concentration (mg/mL)[d)]	1.07

[a)] DLS: Dynamic Light Scattering; [b)] PdI: polydispersity index. [c)] NTA: Nanoparticle Tracking Analysis. [d)] Yield and protein concentration were determined for mEVs isolated from 1 mL of bovine milk and subsequently resuspended in 50 μL of PBS. Data presented as mean ± SD (n=3).

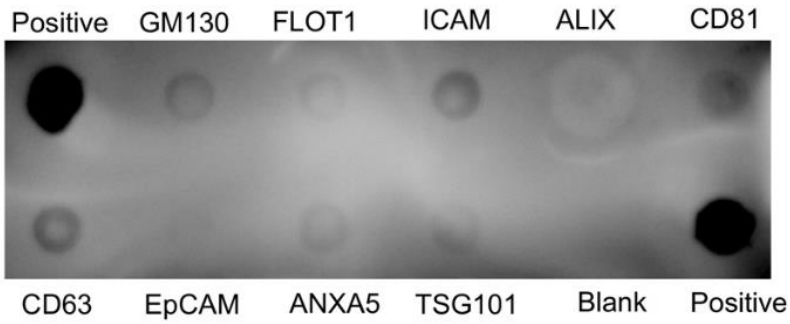

Figure 3-1. Expression of standard protein markers in bovine milk extracellular vesicles isolated from commercial kit, as determined by the Exo-Check™ Array. Protein marker tested: FLOT1 (Flotillin 1), ICAM (Intercellular Adhesion Molecule-1), CD81, CD63, ANXA5 (Annexin A5) and TSG101 (Tumour Susceptibility Gene 101). 'Positive' denotes labelled positive control for horseradish peroxidase detection which indicates that the detection reagents were working properly, and the blank spot serves as a background control.

3.4.1.2. mEV isolation by differential ultracentrifugation and purification by size exclusion chromatography (SEC)

Considering the high cost and low purity of using commercial kit for mEVs isolation, it was decided that differential ultracentrifugation would be attempted as a long-term technique for mEVs isolation. This approach is one of the most widely used ones for EVs isolation. **Figure 3-2** shows the steps of mEV isolation by differential ultracentrifugation and purification with qEV original 35 nm SEC. The protein content of mEV eluted fractions is shown in **Figure 3-3**. The major protein peak was observed at fractions 7, 8, 9, where the mEV particles existed, and the fractions of mEVs existing were consistent with the manufacturer's guidelines of SEC column. The protein existed in fraction 10-20 was considered as the protein contaminations from bovine milk, which should be discarded. Therefore, purified mEVs in fractions 7, 8, 9 (characterization was shown in **Table 3-2**) were used for downstream applications. Notably, we did not present particle numbers included for each fraction, but a positive correlation between the particle numbers and protein levels of fractions 7, 8, 9 was observed in **Table 3-2**,

thus confirming the existence of mEVs. However, to exclude the existence of protein aggregations in mEVs fractions, particle numbers for each fraction should be measured in future research. The size of purified mEVs falls within the range of those reported previously [239]. The low PdI value indicated good dispersibility of mEVs, and the Zeta-potential value showed a negative surface charge. Importantly, the particle-to-protein ratio of mEVs from fraction 7, 8, 9 were all above 3×10^{10} particles/µg, which indicated high mEVs purity [323]. It is worth noting that the size of mEVs isolated by commercial kit was larger than mEVs isolated by ultracentrifugation. This could be attributed to the mechanism of commercial kit, which relies on a water-excluding polymer to "tie-up" water molecules and the reagent forces less-soluble components out of the solution. As a result, not only mEVs were precipitated from the solution by the reagent, but also larger nanoparticles, contributing to an increased average size [210]. mEVs that were isolated using ultracentrifugation and subsequently purified through SEC demonstrated higher purity in comparison to mEVs isolated using commercial kit, which was attributed to the effective exclusion of protein contaminants achieved through SEC. Moreover, ultracentrifugation offers the advantage of large-scale mEVs isolation, utilizing sizable volume spin tubes and appropriate facilities. Therefore, the mEVs isolated by ultracentrifugation and purified by SEC were applied for downstream application. However, it is worth noting that lipoproteins were assessed as contaminations in our isolated mEVs due to the overlap of size and density between them, as discussed in Section 1.3.3.4, and the characterizations in our study including particle-to-protein ratio and Western blotting cannot exclude the existence of lipoproteins. Therefore, future research should explore additional isolation procedures to improve the overall purity of mEVs, as highlighted in Section 1.3.3.4.

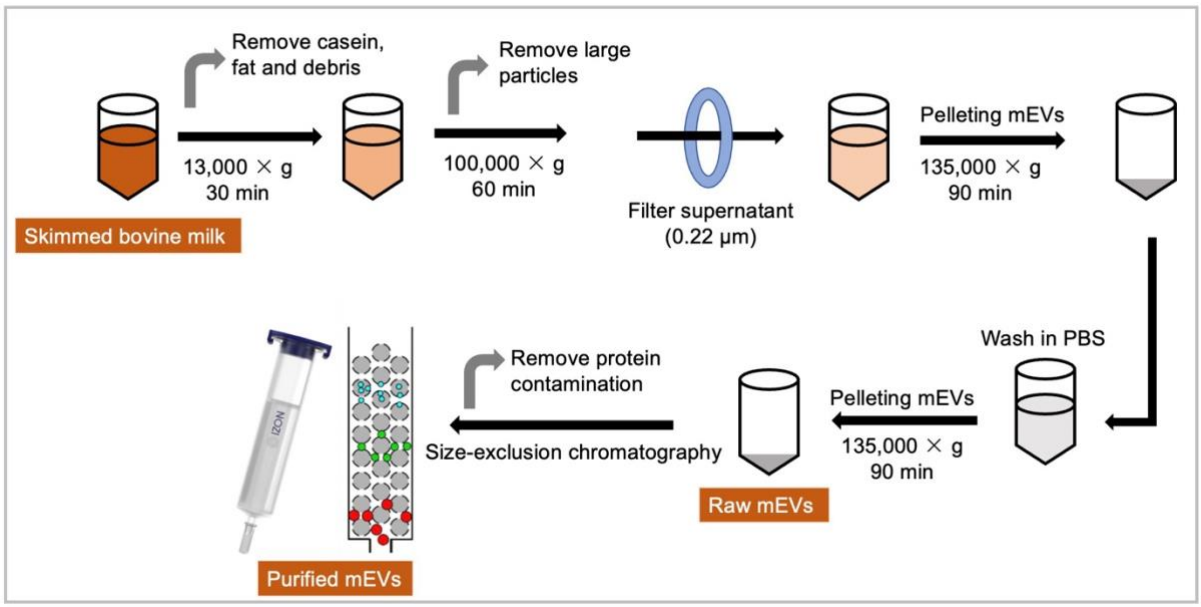

Figure 3-2. The schematic isolation process of bovine milk extracellular vesicles (mEVs) from skimmed bovine milk. Casein, fat, debris, and large particles in milk were removed *via* differential ultracentrifugation and 0.22 μm filter. mEV pellets were resuspended in sterile PBS and purified by size-exclusion chromatography to remove protein contaminations.

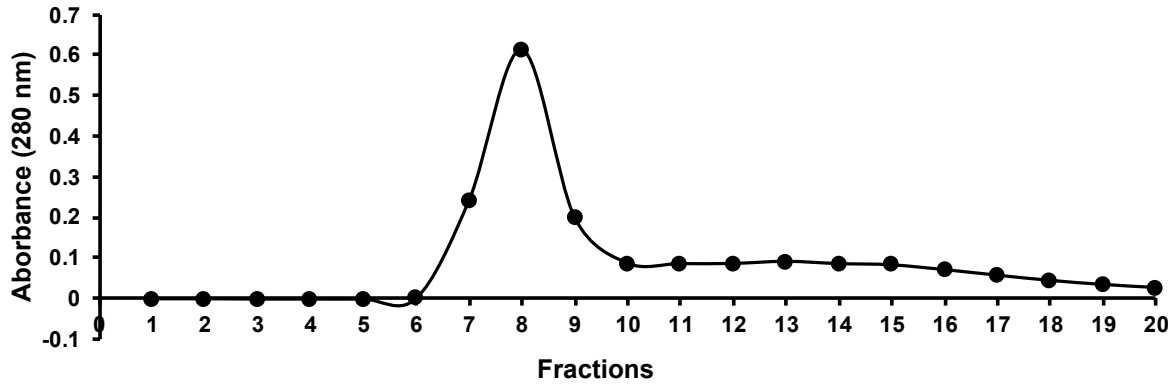

Figure 3-3. Purification of bovine milk extracellular vesicles (mEVs) by size exclusion chromatography. Protein content of eluted fractions was measured at 280 nm absorbance.

Table 3-2. Physicochemical parameters of bovine milk extracellular vesicles (mEVs) isolated by differential ultracentrifugation and purified by size exclusion chromatography (SEC).

Parameter & Measurement method	**Fraction 7**[a)]	**Fraction 8**	**Fraction 9**
Size (nm) (DLS)[b)]	163.1 ± 6.60	161.5 ± 5.45	156.4 ± 1.72
PdI[c)] (DLS)	0.064 ± 0.054	0.124 ± 0.063	0.086 ± 0.107
Size (nm) (NTA)[d)]	158.9 ± 2.40	132.5 ± 6.00	142.0 ± 12.2
Yield (particles/mL) (NTA)[e)]	$3.58 \times 10^{14} \pm 1.04 \times 10^{12}$	$1.14 \times 10^{15} \pm 2.84 \times 10^{13}$	$9.45 \times 10^{14} \pm 5.92 \times 10^{12}$
Zeta-potential (mV)	-8.61 ± 1.40	-9.90 ± 1.32	-8.95 ± 0.85
Protein concentration (mg/mL)[e)]	1.17	2.74	2.26

[a)] Fraction 7, 8, 9: mEVs eluted fractions by SEC; [b)] DLS: Dynamic Light Scattering; [c)] PdI: polydispersity index. [d)] NTA: Nanoparticle Tracking Analysis; [e)] Yield and protein concentration were determined for mEVs isolated from 70 mL of bovine milk and subsequently resuspended in 1.0 mL of PBS (with 0.5 mL of mEVs used for each SEC purification). Data presented as mean ± SD (n=3).

Transmission electron microscopy (TEM) was used to image the morphology of mEVs isolated by ultracentrifugation. **Figure 3-4A** depicts the typical cup-shaped structure of mEVs under negative staining [338]. EV marker protein characterization by Exo-Check Array for mEVs isolated by ultracentrifugation is shown in **Figure 3-4B**. Mirroring the data obtained with mEVs isolated by the commercial kit, the general proteins including CD63, CD81, ICAM and TSG101 were expressed, while ALIX and EpCAM were not found in mEVs (detailed in Section 3.4.1.1). Notably, given that mEVs were derived from dairy product-commercial milk, the heterogeneity of mEVs preparation should be considered, which may affect the

standardization of experiments and the reproducibility of results. As discussed in Section 3.4.1.1, the standardized compositions of commercial skim milk have enhanced the reliability and reproducibility of mEVs isolation. However, variations between different batches of milk and their levels of freshness may still introduce variability in the mEVs obtained. Therefore, we have quantified and characterized the isolated mEVs across multiple preparations and found that their size distribution, concentrations (particles and protein), and protein markers fall within a comparable range, although assessing bioactivity variation remains an unaddressed challenge. We applied the quantification after each isolation of mEVs as a quality control to manage the inherent heterogeneity of mEVs.

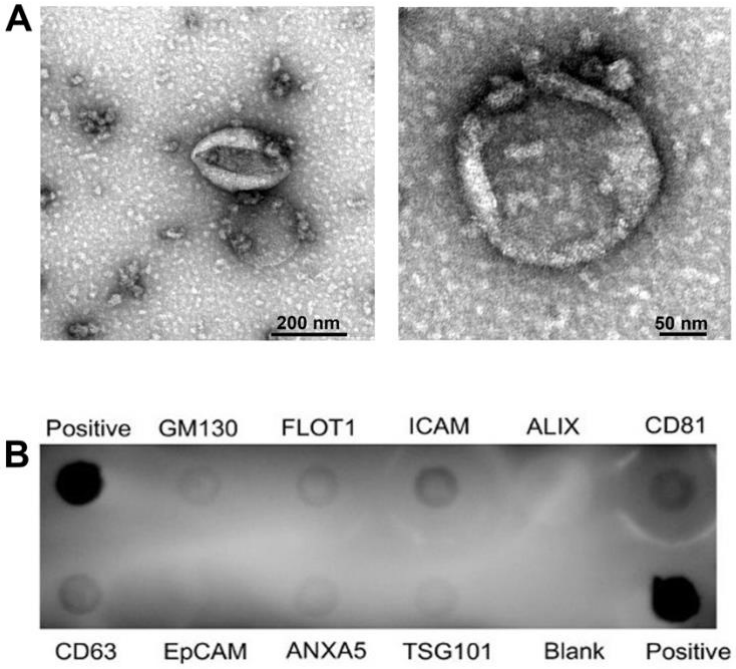

Figure 3-4. Characterisation of bovine milk extracellular vesicles (mEVs) isolated by ultracentrifugation and purified by size exclusion chromatography (SEC). (A) Morphological characterisation of mEVs by transmission electronic microscopy (TEM). **(B)** Expression of standard protein markers in mEVs, as determined by the Exo-Check™ Array. Protein marker tested: FLOT1 (Flotillin 1), ICAM (Intercellular Adhesion Molecule-1), CD81, CD63, ANXA5 (Annexin A5) and TSG101 (Tumour Susceptibility Gene 101). 'Positive' denotes labelled positive control for horseradish

peroxidase detection which indicates that the detection reagents were working properly, and the blank spot serves as a background control.

3.4.2. Loading of siRNA into mEVs by different methods

3.4.2.1. Loading siRNA into mEVs by transfection reagent

X-tremeGENE™ 360 Transfection Reagent was used as an exemplary commercial reagent to load siRNA into mEVs. To determine the efficiency of this transfection reagent, fluorescent siRNA loading was evaluated with and without the transfection reagent (replaced by ethanol which was the solvent of transfection reagent). The range of siRNA to mEVs ratios for loading by transfection reagents has been reported widely in previous studies. For instance, one study applied 5×10^{-14} nmol of siRNA per mEVs particle for loading using Lipofectamine 2000 [254], while another study used 2.5×10^{-13} nmol/particle for loading by the same transfection reagent [248]. In a different research, a range of 0.33 nmol/mg – 1 nmol/mg of mEVs (based on protein concentration) was applied to load by Exo-Fect transfection reagent [339]. Theoretically, studies have found from one miRNA per EV to one miRNA per 100 EVs [340], and knowing that miRNA represent 0.9% of RNA reads in EVs RNA deep sequencing, it can be anticipated that approximately 1 to 100 RNAs are present in each EV [341], which suggests the potential loading amounts of siRNA into EVs. In our study, the amount of siRNA added was 0.25 nmol, and volume of transfection reagent and ethanol were 8 μL. The siRNA-transfection reagent mixture was then added into mEVs solution (0.06 mg mEVs resuspended in 200 μL Opti-MEM medium). According to the calculation of mEVs particle concentrations and protein concentrations (**Table 3-2**), the concentration of siRNA applied was determined to be 1×10^{-14} nmol/particle, and 4.17 nmol/mg (protein concentration), which closely aligns with previous reports and optimizations were following conducted to achieve higher loading efficiency. Notably, we kept a consistent concentration of mEVs to ensure comparable loading efficiency

under the condition of siRNA overdose. Following the removal of unloaded siRNA, the loading efficiency of siRNA using the transfection reagent was calculated to be 7.0%, which was significantly higher than the absence of transfection reagent (2.1%).

In order to achieve a higher siRNA loading efficiency into mEVs by the transfection reagent, various loading conditions were optimized in this study. Firstly, the amount of transfection reagent used was optimized. As shown in **Table 3-3 (Group 1 and 2)**, doubling the amount of transfection reagent increased the loading efficiency by 4.7%. However, higher transfection reagent amounts led to aggregation of mEVs and increased the particle size. Therefore, 8 μL transfection reagent was used in downstream application. Thereafter, considering the possibility of mEVs loss while using ultrafiltration to remove unloaded siRNA (where the mEVs could attach to the ultrafiltration column membrane) [342, 343], the ExoQuick™ reagent was used. The ExoQuick™ reagent can "tie-up" the water molecules and precipitate mEVs; this approach led to an enhancement in loading efficiency due to the collection of more mEVs (**Table 3-3 Group 3**). Considering the potential presence of lipoprotein contaminants, albeit in small quantities, in our isolated mEV samples (as discussed in Section 1.3.3.4), the interactions between lipoproteins and siRNA should not be ignored. While lipoproteins possess a net negative charge, resulting in minimal interaction with negatively charged siRNA [344], the possibility of interaction between lipoproteins and siRNA-transfection reagent complexes, which typically carry a positive charge, cannot be disregarded. Therefore, it is essential to remove lipoproteins during the isolation stage. Furthermore, although the ExoQuick™ reagent facilitates increased mEVs yield, scalability limitations arise due to its high cost for large-scale EVs precipitation (mEVs used here have been purified by SEC during isolation, thus the limitation of specificity of this commercial precipitation reagent is not a primary concern). Therefore, ultrafiltration remained employed in certain downstream applications to remove free siRNA, with additional washing steps (flashing to the membrane by pipette) implemented

to minimize mEV loss. The loading efficiency was also influenced by the time and temperature of siRNA-mEVs incubation. As shown in **Table 3-3 (Group 4 and 5**), shorter incubation time (30 min) was associated with a significantly increased loading efficiency compared with 3 h incubation, and the efficiency of room temperature incubation was slightly higher than that of 37°C.

Table 3-3. Optimization for loading siRNA into bovine milk extracellular vesicles (mEVs) by X-tremeGENE™ 360 Transfection Reagent (TR).

Group	siRNA (nmol)	TR (μL)	mEVs (mg)	Incubation	Remove siRNA[a)]	Size	Loading efficiency
1	0.25	8	0.06	3 h, 37°C	ultrafiltration	186.6±1.06	7.0%
2	0.25	16	0.06	3 h, 37°C	ultrafiltration	405.6±31.11	11.7%
3	0.25	8	0.06	3 h, 37°C	ExoQuick™	284.6±6.20	11.9%
4	0.25	8	0.06	30 min, 37°C	ExoQuick™	192.6±5.45	24.5%
5	0.25	8	0.06	30 min, RT[b)]	ExoQuick™	215.9±0.07	27.5%

[a)] The method to remove unloaded siRNA; [b)] RT: room temperature.

Exo-Fect™ siRNA/miRNA Transfection Kit is another transfection reagent applied in this study which specifies for siRNA loading to EVs. This transfection reagent was based on the proprietary Cell-Penetrating Peptide (CPP) technology which enables siRNA to be transferred into EVs. As shown in **Table 3-4**, two types of siRNA (positive siRNA provided by this Kit and fluorescent Cy5 siRNA) were applied to evaluate the efficiency of transfection regent. As directed by the manufacturer's instructions, the recommended amount of siRNA was 0.02 nmol,

which corresponded to the quantity of 0.17 mg mEVs. The loading efficiency of positive siRNA and Cy5 siRNA into mEVs was calculated to be 12.9% and 5.9%, respectively. In order to increase the loading efficiency, a higher siRNA amount (0.05 nmol) was added, however, there was no observed increase in the loading efficiency. Compared with X-tremeGENE^{TM} 360 Transfection Reagent, the loading efficiency of Exo-Fect^{TM} siRNA/miRNA Transfection Kit was lower by approximately 15%, furthermore, reduced siRNA amount added in Exo-Fect^{TM} mediated loading resulted in a notably lower loading of siRNA into mEVs.

Table 3-4. Optimization for loading siRNA into bovine milk extracellular vesicles (mEVs) by Exo-Fect^{TM} siRNA/miRNA Transfection Kit (TK).

Group	siRNA (nmol)	TK (μL)	mEVs (mg)	Size (nm)	Loading efficiency
1	0.00	10	0.17	216.4 ± 0.71	-
2	0.02 (P [a)])	10	0.17	312.5 ± 16.9	12.9%
3	0.05 (P)	10	0.17	223.4 ± 5.60	9.3%
4	0.02 (Cy5 [b)])	10	0.17	315.8 ± 4.20	5.9%
5	0.05 (Cy5)	10	0.17	353.4 ± 14.2	3.5%

[a)] P: positive siRNA in Transfection Kit; [b)] Cy5: fluorescent Cy5 siRNA.

3.4.2.2. Loading siRNA into mEVs by saponin

Saponin, a versatile surfactant soluble in both water and oil phases, has been applied for efficient loading of various drugs, including porphyrins and catalase, into mEVs [221, 284]. The amphipathic property of saponin enables it to form complexes with cholesterol on the membrane of mEVs, potentially generating pores and increasing membrane permeability of mEVs [345]. Upon saponin-assisted loading, the loading efficiency of siRNA into mEVs was calculated to be 2.3%. The low loading efficiency was attributed to the high hydrophilicity of

siRNA. Notably, previous studies achieving high loading efficiency predominantly involved the encapsulation of hydrophobic compounds such as porphyrins, characterized by their substantial hydrophobic properties [284].

3.4.2.3. Loading siRNA into mEVs by electroporation

Electroporation was applied to load siRNA into mEVs. To achieve higher loading efficiency, various conditions were optimized, encompassing factors such as voltage, capacitance of pulse, and times of pulse during electroporation. As shown in **Table 3-5**, voltage of 150 V and capacitance of 100 μF were used, however, both employing a single pulse and applying two consecutive pulses resulted in low loading efficiency (< 2.5%). Increasing the voltage value was reported as an efficient way to promote loading efficiency *via* electroporation [346, 347]. With a voltage of 400 V and a single pulse, the loading efficiency increased to 3.38%. However, when two consecutive pulses were attempted to further improve the loading efficiency, it was observed that the size of siRNA loaded-mEVs increased to nearly 300 nm, which is attributed to aggregation during the intensive electroporation process. We considered a size below 200 nm as the ideal size for oral delivery systems because NPs below this threshold have been observed to be more readily absorbed by the GI tract [348, 349]. Specifically, concerning various intestinal barriers, it has been found that particles larger than 200 nm can accumulate within the intestinal mucus [99], and the effective mucus diffusion decreases by 2.9-fold with an increase in particle size from 100 to 500 nm [103]. Moreover, smaller-sized particles are more easily absorbed by intestinal epithelial cells (e.g., particles smaller than 300 nm can be taken up by enterocytes [350], and the uptake of 50 nm particles by Caco-2 cells was higher than 200 nm particles [351]). Therefore, 300 nm exceeds our target and is deemed unacceptable. Furthermore, continuing to increase the Voltage (Group 5 with 800 V in **Table 3-5**) did not significantly increase the loading efficiency (2.55%). Thereafter, various capacitance values

were tested to improve loading efficiency (Group 6, 7, 8 in **Table 3-5**). It was observed that the loading efficiency improved with the increase in capacitance value, however, the size (over 300 nm) exceeded our intended target when a capacitance of 250 μF was used. Pulse times were not optimized here to avoid the potential increase in the size of mEVs, but this factor should be considered in future research. Therefore, the voltage of 400 V, and capacitance of 200 μF with single pulse was chosen to load siRNA into mEVs for downstream application (with loading efficiency of 5.05%). Even though transfection reagents can achieve a loading efficiency of up to 27.5%, surpassing that of electroporation, their high cost and potential toxicity remain significant obstacles in the large-scale production of siRNA-loaded mEVs. Consequently, electroporation has found favour in downstream applications due to its cost-effectiveness and reduced adverse effects.

Table 3-5. Optimization for loading siRNA into bovine milk extracellular vesicles (mEVs) by electroporation.

Group	Voltage (V)	Capacitance (μF)	Times[a)]	Size (nm)	PdI[b)]	Loading efficiency
1	150	100	1	178.5 ± 5.6	0.338	1.65%
2	150	100	2	158.2 ± 3.5	0.280	2.45%
3	400	100	1	174.6 ± 1.1	0.387	3.38%
4	400	100	2	296.5 ± 25.5	0.576	8.50%
5	800	100	1	240.2 ± 12.5	0.403	2.55%
6	400	150	1	197.5 ± 10.3	0.305	3.71%
7	400	200	1	208.6 ± 4.2	0.376	5.05%
8	400	250	1	307.4 ± 30.2	0.497	9.85%

[a)] Times: times of pulse in electroporation; [b)] PdI: polydispersity index.

3.5. Conclusion

In summary, this chapter details the isolation of mEVs from bovine milk using two typical methods: a commercial precipitation kit, and ultracentrifugation followed by subsequent purification through SEC. mEVs obtained through ultracentrifugation and SEC purification exhibited a size falling within the standard mEVs range and their low PdI value attested to their good dispersibility. Characteristic protein markers for these mEVs were observed and the high particle-to-protein ratio indicated their high purity. Therefore, mEVs isolated by ultracentrifugation and purified by SEC were used for downstream work. However, the possibility of the existence of lipoprotein contaminations, though in small quantities, cannot be entirely excluded based on our current characterization, which requires further investigation and clarification in future research. Various strategies were assessed for loading siRNA into mEVs. The employment of a commercial kit yielded a loading efficiency of over 20%, whereas the use of saponin resulted in a 2.3% efficiency. Furthermore, electroporation resulted in a encapsulation of 5.05% siRNA into mEVs. Even though the commercial kit yielded the highest loading efficiency of siRNA into mEVs compared to other methods, this efficiency remains notably lower than what can be achieved in synthetic delivery systems. Moreover, the cost and potential toxicity of the loading reagent must be taken into consideration and subjected to further evaluation. Therefore, there remains a demand for EV drug loading methods that are cost-effective and can deliver a high loading efficiency.

4. Bovine Milk Extracellular Vesicles (mEVs) as Systems for Oral Delivery of siRNA [incorporated publication 2]

(**Statement:** This Chapter is based in part on the previously published article:

Yunyue Zhang, Mona Belaid, Xiang Luo, Armond Daci, Rinë Limani, Julia Mantaj, Matthias Zilbauer, Komal Nayak, Driton Vllasaliu (2023). Probing milk extracellular vesicles for intestinal delivery of RNA therapies. *Journal of Nanobiotechnology,* Accepted.

Authors contributions: Yunyue Zhang (the candidate) designed the subject, performed the experiments and data analysis, wrote and revised the manuscript. Mona Belaid, Xiang Luo and Julia Mantaj performed part of the experiments and data analysis. Armond Daci, Rinë Limani designed and performed the *in vivo* studies. Matthias Zilbauer and Komal Nayak analysed and discussed the results. Driton Vllasaliu designed and supervised the work, wrote and revised the manuscript.)

4.1. Introduction

Oral administration of siRNA is the most preferred route of treatment mode. In addition to offering significant benefits in terms of access to medicines and patient convenience, oral administration is also amenable to effective local drug delivery in the GIT as part of the therapeutic management of GIT diseases, such as IBD. However, the oral bioavailability of siRNA is limited due to inefficient penetration across biochemical and physical barriers of the GIT [352]. Nanomedicine-based approaches have been investigated for oral delivery of siRNA in intestinal inflammation [353-355], but most synthetic nanoparticles tend to suffer from poor stability in, and inefficient penetration across, the challenging biochemical and physical barriers of the GIT [352].

As discussed in Section 1.3.3.3, mEVs are potentially ideal carriers for siRNA oral delivery for IBD therapy, based on their stability in intestine and permeability across intestinal mucosa

[247-249]. However, previous assessments of intestinal permeability of mEVs were predominantly conducted on simple *in vitro* intestinal epithelial models, which are not able to replicate the intricate characteristics of natural intestinal epithelia. The intestinal epithelium is a complex tissue composed of different cell types working together to control the absorption of nutrients while protecting the body from potentially harmful material, including microorganisms, present in the intestinal lumen [356]. One of the most important barriers in oral drug delivery is the intestinal epithelium. Over the years, numerous *in vitro* intestinal epithelium models have been developed to study intestinal physiology and assess oral drug delivery systems. Intestinal epithelium models can be divided into different types, including cell line-based systems (derived from tumors), organoids constructed from primary intestinal cells, and co-culture models that involve different cell types. *In vitro* intestinal epithelium models are not just more efficient and cost-effective in comparison *to in vivo* animal models, but they also offer accessibility for exploring drug transport mechanisms, such as identifying cellular receptors involved in transcytosis [357].

Caco-2 monolayer model

Intestinal epithelial models based on epithelial tumor cells are traditional and most widely used in oral drug delivery assessment. A large number of cell lines have been developed to build these models such as Caco-2, HT-29, T84 or SW 480, etc., which are highly proliferative and relatively easy and cheap to culture. Among them, Caco-2 cells represent the most commonly applied model for drug permeability and absorption experiments. Caco-2 cells cultured on Transwell inserts can be differentiated/polarized, forming tight junctions and microvilli, resembling the intestinal enterocytes **(Figure 4-1A)** [358]. However, this model has several disadvantages due to their limited resemblance to the *in vivo* epithelium. The Caco-2 monolayer model fails to represent the interaction between different cell types (including enterocytes, Paneth cells, enteroendocrine cells, and goblet cells, etc.) and the recapitulation of realistic

tissue architecture is not achievable. Moreover, the Caco-2 monolayer as an intestinal epithelial model has their limitations in use such as underestimated paracellular absorption, abnormally high TEER, or abnormal expression of metabolizing enzymes [359]. To overcome the limit of Caco-2 monolayers, co-culture models of Caco-2 cells with mucus-producing HT29-MTX cells were developed, which mimic both enterocytes and goblet cells [360-362]. However, this model is also not realistic due to the lack of other cell types.

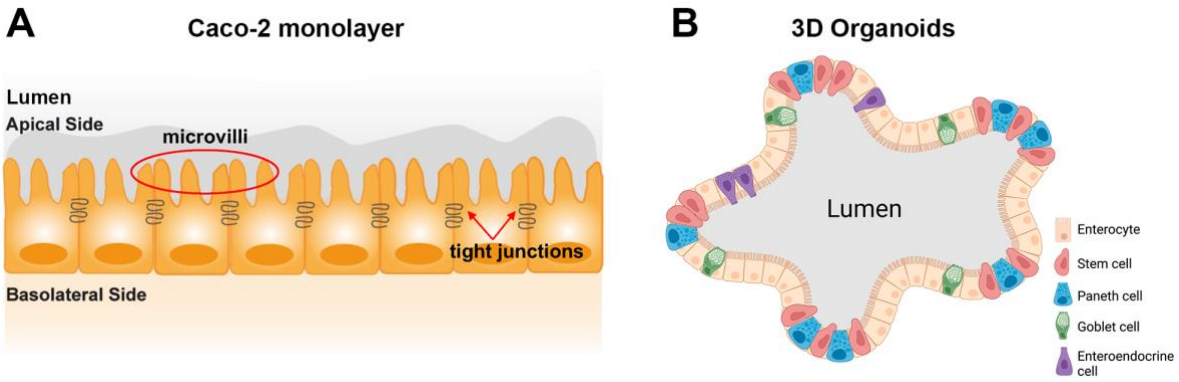

Figure 4-1. Schematic representation of Caco-2 monolayer (A) and 3D intestinal organoid (B).

Intestinal organoids models

With the development of cell culture technology, 3D organoids are emerging as a novel *in vitro* model to investigate disease, drug absorption and toxicity, and human organ development [363]. Intestinal epithelial organoids (IEOs) are derived from intestinal isolated $Lgr5^+$ stem cells or dissociated crypts, which organize into 3D structures when embedded in Matrigel (an extracellular matrix rich in laminin and collagen) covered with essential biochemical factors mimicking the *in vivo* niche. The key niche signals include R-Spondin (a Wnt agonist that maintains stem cell population), Noggin (a BMP inhibitor which limits differentiation), and epidermal growth factor (EGF, to promote cell proliferation). Crypt cells as stem cells have permitted the self-renewal and differentiation capacities of IEOs, and IEOs capability of maintaining highly similar protein expression to freshly isolated crypts for several months

enables this model to be stable in a long-term culture, which contributes to the repeatability and reliability in application of biological assessment [364, 365].

IEOs recapitulate the physiology, genetic signature, and multicellular nature of the native intestinal epithelium [366]. The representation of all types of terminally differentiated intestinal epithelial cells and the crypt-villus structures with stratified epithelium, which serve important functions in barrier regulation, material absorption, mucus secretion, interaction with microbiota, gut-brain communication and host defense [367], are key advantages of IEOs over cell line alternatives for modelling the intestinal epithelium **(Figure 2-1 B)**. IEOs are spherical structures with budding formations. Each of buds recapitulates the crypt structure located in stem cells including $Lgr5^+$ stem cells and Paneth cells. Between the budding locations, cells mimic the villus structures, composed with enterocytes and other types of cells [364, 365]. These crypt/villi-like domains form a central lumen structure, and dead cells from constantly renewed epithelial layer are extruded into the lumen area [368].

However, the conventional culture of IEOs currently limits their application in the field of drug delivery since the apical/luminal side is not accessible by the user (the center of the IEOs corresponds to the intestinal lumen where directly contacts dietary factors). Currently, the highly challenging and disruptive micro-injection technology is used to access the lumen of IEOs [369], which is required in the fields of drug development and nutrition. To overcome this obstacle, recent studies have reported the culture of IEOs with exposed apical surfaces. To this end, a few studies have reported the culture of organoids monolayers or 3D apical-out human enteroids [370, 371].

The main obstacle to developing organoids monolayers is the selection of substrates that ensure cell adhesion and stem cell maintenance, while preventing 3D organoid structure formation. Several culture systems have been reported to support organoid monolayers, including a thin layer of gelatin [372], thin layer of Matrigel or basement membrane extract (BME) on solid

surface or porous Transwell membranes [373, 374], and a thick layer of collagen [375]. The monolayers could form to a polarized morphology and self-organize into stem cell areas and differentiated cell areas, akin to 3D organoids [373, 374]. Moreover, when the organoid monolayers are cultured on porous Transwell membranes, these systems enable access to both apical (luminal) and basolateral sides, which enable the assessment of drug or nutrients absorption/transport, as well as the influence of host-pathogen interaction on epithelium. In addition, 3D apical-out human enteroids, which reverse the conventional basal-out enteroid polarity, were explored as another model to overcome the obstacles of accessing to apical epithelium in biological applications. Co et al. [370, 371] have developed a series of apical-out enteroid models which can maintain the 3D spheroid structure and at the same time enable apical surface to be accessible to experimental applications. To produce this model, briefly, conventional spheroids were first released from matrix (BME) and resuspended in EDTA where the chelates cations can depolymerize matrix proteins. The organoids were subsequently washed and resuspended culturing in culture media. Culturing without BME, the basolateral β-1 integrin receptors on organoids cannot interact with extracellular matrix, thereafter, triggering morphogenetic rearrangement of epithelium, leading to eversion of organoid polarity. This model enables nutritional compounds or microbes to interact with organoids apical surface by simply adding these materials to culture media. Therefore, intestinal organoid monolayers and apical-out organoid models represent novel and potentially highly human-relevant models for evaluation of permeability of drugs and performance of drug delivery systems. However, IEOs have not previously been used to study the intestinal translocation of EVs, or indeed any other NPs, probably due to the basolateral-out nature of IEOs.

In this Chapter, we examine the interaction between mEVs with the intestinal biofluid and epithelium, followed by probing their potential for oral delivery of siRNA. mEVs were characterized after exposure to simulated intestinal fluids. Intestinal cell uptake and transport

of mEVs were then confirmed in Caco-2 cells as an established *in vitro* intestinal model, together with assessing the effect of simulated intestinal fluid on their epithelial transport. Importantly, using novel IEOs models of the human intestinal epithelium, we demonstrate epithelial translocation of mEVs in this highly biorelevant intestinal epithelial model. We show that mEVs efficiently transport across Caco-2 cells, which was not affected by their treatment with simulated intestinal fluids. We further demonstrate apical-to-basolateral translocation of mEVs in two separate human tissue-derived IEO models, which were, unconventionally, cultured with an exposed apical surface. When loaded with a model siRNA molecule (anti glyceraldehyde-3-phosphate dehydrogenase, GAPDH) by electroporation, mEVs induced gene silencing in a macrophage cell line, which was employed here given the central role of these immune system cells in mediating inflammation in IBD. The work in this Chapter therefore clearly highlights that mEVs could serve as highly effective carriers or inform the design of bio-inspired synthetic systems for oral delivery of siRNA.

4.2. Study Objectives

The aim of this Chapter is to explore the potential of mEVs for oral delivery of siRNA.

The objectives of this Chapter are:

1. To investigate the effect of simulated intestinal fluids (SIFs) on mEVs stability and intestinal permeability.
2. To establish *in vitro* intestinal epithelial models based on IEO monolayers and 3D 'apical-out' IEOs, followed by the assessment of apical-to-basolateral translocation of mEVs in these models.
3. To evaluate the gene silencing of siRNA-loaded mEVs in a macrophage cell line.

4.3. Methods

4.3.1. Effect of Simulated Intestinal Fluids (SIFs) on mEV physicochemical characteristics

Fasted state simulated intestinal fluid (FaSSIF, pH 6.5) and fed state simulated intestinal fluid (FeSSIF, pH 5.0) were used as simple, commercially available models of small intestinal fluids. SIFs were prepared according to the manufacturer's instructions. The composition of FaSSIF includes 3 mM taurocholate, 0.75 mM phospholipids, 148 mM sodium, 106 mM chloride, and 29 mM phosphate. FeSSIF comprises 15 mM taurocholate, 3.75 mM phospholipids, 319 mM sodium, 203 mM chloride, and 144 mM acetic acid. 100 µL of mEV suspension at 1 mg/mL protein concentration was incubated in 400 µL of SIFs at 37ºC with gentle shaking for 1.5 hours. After digestion, mEVs were recovered *via* centrifugal ultrafiltration with 100 kDa Amicon Ultra-0.5 Centrifugal Filter Unit (Merck, Dorset, UK) by four sequential centrifugations for 10 minutes each at 10,000 × rpm. 500 µL of PBS was added between each spin to wash off the remaining debris from the digestion solutions. Post-treatment with SSIFs, mEVs were resuspended in 200 µL PBS and characterized for size and Zeta-potential.

4.3.2. Effect of SIFs on RNA release from mEVs

Following the exposure of mEVs to SIFs, RNA was quantified to establish whether SIFs induced a damage to mEV membranes and hence release of mEV RNA content. RNA was quantified following an ultrafiltration recovery step of mEVs post digestion, and RNA was isolated with TRIzol® reagent according to the manufacturer's instructions. RNA pellets were resuspended in Nuclease-free water, and the final RNA concentration was quantified using QuantiFluor® RNA System. 15 µL of resuspended RNA was mixed with the buffer and RNA dye according to the manufacturer's instructions on a black 96-well plate and fluorescence intensity was measured by a plate reader (excitation 492 nm; emission 540 nm).

4.3.3. Cell uptake and transport of nanoparticles in intestinal Caco-2 monolayers

4.3.3.1. mEV uptake and transport in intestinal Caco-2 monolayers

Caco-2 monolayer culture and transport experiments were conducted in a manner mentioned in General Methods Section 2.2.5.2, with the labelled mEVs dissolved in HBSS as tested samples. During the incubation, mEVs in the sampled basolateral solution were quantified by fluorescence using a plate reader with excitation wavelength of 565 nm and emission wavelength of 615 nm. After 3 hours, mEV samples were removed, cells washed with HBSS, detached from inserts and permeabilised with trypsin and 1% v/v Triton X-100 (1:4 v/v). Thereafter, cells were pelleted by centrifugation with 5,000 × g for 5 min and mEVs in supernatant were quantified by fluorescence to determine the cell uptake efficiency.

The cell uptake of mEVs in Caco-2 monolayers was also imaged by confocal microscopy. For this purpose, following the transport study (i.e. 3 hours after mEV application), Caco-2 cells cultured on Transwell membranes were washed with PBS three times and fixed with 4% paraformaldehyde for 20 min at room temperature, followed with Fluoroshield™ DAPI to stain nuclei. For imaging, Transwell membranes were cut and placed on a 24-well plate with a polymer coverslip bottom (µ-Plate 24 Well Black ID 14 mm, Ibidi, Gräfelfing, Germany). Thereafter, 0.5% (w/v) low-temperature gelling agarose at 30 °C was added drop-wise to cover and immobilize the membrane. Images were collected by the 20 X water objective on Opera Phenix™ High Content Screening System (PerkinElmer, Waltham, MA, US).

4.3.3.2. Comparison of transport of mEVs and liposomes in intestinal Caco-2 monolayers

The purpose of these studies was to compare the intestinal epithelial transport of mEVs versus a synthetic lipid nanoparticle system, namely liposomes of similar size (~100 nm). A comparison was also made with the free fluorescent dye which was used to label mEVs.

Liposomes were prepared using the following lipids: 1,2-dipalmitoyl-*sn*-glycero-3-phosphocholine (DPPC) which is widely employed in liposome formulation for enhancing membrane rigidity and increasing structural integrity [376]; 1,2-dioleoyl-*sn*-glycero-3-phosphoethanolamine (DOPE) for enhancing the membrane fluidity and promoting fusogenicity [377]; 1,2-distearoyl-*sn*-glycero-3-phosphoethanolamine-*N*-(7-nitro-2-1,3-benzoxadiazol-4-yl) (ammonium salt) (NBD-DSPE); and 1,2-dioleoyl-*sn*-glycero-3-phosphoethanolamine-*N*-(lissamine rhodamine B sulfonyl) (ammonium salt) (Rho-PE), with the molar ratio of 67%:30%:1.5%:1.5%. All lipids were dissolved in chloroform and the preparation procedure of liposomes was conducted in the same way as that mentioned in General Methods Section 2.2.3.

Epithelial transport was determined in differentiated intestinal Caco-2 monolayers. Caco-2 monolayer culture and transport experiments were conducted in the same way as that mentioned in General Methods Section 2.2.5.2, except for the tested samples, which were as follows: 500 μL of labelled mEVs at 0.05 mg/mL protein concentration, liposomes at 0.05 mg/mL lipid concentration, and fluorescent dye, the concentration of which was adjusted to produce same fluorescent signal as that of mEVs. Samples were added to the apical side of monolayers for 120 minutes. mEVs and labelling dye in the sampled basolateral solution were quantified by fluorescence using plate reader (excitation 565 nm; emission 615 nm), and liposomes were quantified through Rhodamine fluorescence using excitation wavelength of 530 nm and emission wavelength of 588 nm.

4.3.3.3. Effect of SIFs on mEVs transport across Caco-2 monolayers

mEVs were exposed to SIFs and harvested by centrifugal ultrafiltration. mEVs were then labelled to enable quantitation of cell uptake and transport using plate reader (excitation 565 nm; emission 615 nm). To determine the effect of SIFs on mEVs transport across intestinal

epithelial cells, differentiated Caco-2 monolayers were used as an intestinal model. Caco-2 monolayer culture and testing of transport followed methods mentioned in General Methods Section 2.2.5.2, except for the tested samples, which consisted of 500 µL of labelled mEVs at 0.05 mg/mL protein concentration that were previously treated with SIFs or PBS (control), added to the apical side of monolayers for 90 minutes.

4.3.4. mEV transport across IBD-intestinal epithelial organoids (IEOs) monolayer model

4.3.4.1. Culture of typical IBD-IEOs

IEOs were generated from mucosal biopsies (i.e. duodenum, terminal ileum, sigmoid colon) obtained from a patient with mild chronic gastritis. Ethical approval for the study was obtained (Research Ethics Committee reference 17/EE/0265). IEOs ('IBD-IEOs') were cultured as previously reported [378], with minor modifications. Briefly, IEOs were defrosted from liquid nitrogen stock at 37°C, then immediately added to warm AF+++ medium (Advanced DMEM/F-12 with 10 mM HEPES, 1X GlutaMAX™, and 1% Penicillin-Streptomycin (v/v)). After centrifugation at 800 × g for 5 min, IEO pellets were resuspended in Matrigel and seeded on pre-warmed 48 wells plate (3548, Corning) with 20 µL droplet per well and supplemented with 0.25 mL IntestiCult™ Organoid Growth Medium (Human) (growth medium). The growth medium was changed every 2 to 3 days. IEOs were passaged every 7-10 days, and 10 µM Y-27632 was added to the growth medium for the first 2 to 3 days after passage. Following culture for 4-5 days in the growth medium, IEOs were differentiated by differentiation medium for another 3-4 days. Differentiation media was prepared by AF+++ medium supplemented with 50 ng/mL Human EGF Recombinant Protein, 100 ng/mL Recombinant Human Noggin, 10 nM Gastrin I human, 500 nM A83-01, 10 µM Y27632, 5 µM DAPT, 1 mM N-Acetyl-L-cysteine and 1X B27 [371]. The differentiation medium was changed every 2 days.

4.3.4.2. Culture of IBD-IEO monolayer model

IEO monolayers were generated as previously reported, with some modifications [379]. Firstly, 6.5 mm transwell inserts (PET for imaging and polycarbonate for transport study) were coated with 40X diluted BME2. Specifically, BME2 was diluted with cold AF+++ medium by 40X and 150 µL of diluted BME2 was added to each well followed by incubation at 37°C for 1-2 h. Diluted BME2 medium mixture was removed from wells before adding the cells. IEOs which were not excessively large were used to generate monolayer model. Briefly, IEOs in Matrigel were broken up and resuspended in cold AF+++ medium. After centrifugation (800 x g, 5 min), organoid pellets were resuspended in TrypLE™ with 250 µL/well and incubated in 37°C for 10 min to disassociate them into single cells. The suspension was pipetted during the incubation to help with the disassociation of organoids. Thereafter, cold AF+++ medium was added to the TrypLE™ mixture and centrifuged at 800 × g for 5 min. IEO cell pellets were resuspended in cold AF+++ medium and filtered with 70 µm cells strainer. After centrifugation, cells were resuspended in growth medium. To develop IEO monolayers, 0.8 – 1.5 × 10^6 cells/mL were added to the apical side of transwell inserts (150 µL/well) and 600 - 800 µL growth medium (depending on plate types) was added basolaterally. The growth medium was changed every 2 to 3 days, and 10 µM Y-27632 was added for the first 2 to 3 days after seeding. Differentiation of IEO monolayers was induced as mentioned above. Cell monolayer growth and integrity were monitored by measuring TEER.

4.3.4.3. Confocal immunofluorescence imaging of IEO monolayer model

IEOs cultured in Matrigel and IEO monolayers were washed with 0.01 M PBS (3 times) and fixed with 4% paraformaldehyde for 20 min at room temperature, followed by permeabilization with 0.1% Triton-X 100 for 5 min. Thereafter, IEOs were blocked with blocking buffer (5% (w/v) skimmed dry milk powder with 0.5% Triton-X 100 in 0.01M PBS) for 1 hour. IEOs were

then incubated with primary antibodies (1:150 ZO-1 polyclonal antibody and 1:150 MUC2 monoclonal antibody diluted in 1% (w/v) skimmed dry milk powder with 0.5% Triton-X 100) at 4°C overnight and then incubated with secondary antibodies (1:500 goat anti-rabbit Alexa Fluor™ 488 lgG and 1:500 goat anti-mouse Alexa Fluor™ 594 IgG diluted in 1% (w/v) skimmed dry milk powder with 0.05% Triton-X 100) for 1 hour at room temperature. Finally, IEOs were treated with Fluoreshield™ DAPI to stain nuclei. To enable imaging, transwell membrane-supported IEOs were cut off and placed on a 24-well plate with a polymer coverslip bottom (µ-Plate 24 Well Black ID 14 mm, Ibidi, Gräfelfing, Germany). Then, 0.5% (w/v) low-temperature gelling agarose at 30 °C was added drop-wise to cover and immobilize the membrane. IEOs cultured in Matrigel were imaged directly after immunostaining. Images were collected by the 20 X or 40 X water objective on Opera Phenix™ High Content Screening System (PerkinElmer, Waltham, MA, US).

4.3.4.4. mEV transport across IEOs monolayer model

Prior to the study of mEV transport across IEOs monolayers, the integrity of monolayers was evaluated by determining FD10 permeability. To do this, the culture medium was replaced by HBSS and monolayers were incubated for 45 min at 37°C and 5% CO_2 atmosphere for equilibration. Thereafter, 150 µL of 1 mg/mL FD10 in HBSS was added to the apical side of monolayers for 160 min. During the incubation, 100 µL basolateral solution was sampled regularly (at 40 min intervals), with the sampled solution replaced with HBSS. FD10 was quantified by fluorescence at 490 nm/520 nm of excitation/emission wavelengths. The transport of labelled mEVs through IEO monolayers was determined in a similar manner, with labelled mEVs quantitation using fluorescence at excitation wavelength of 565 nm and emission wavelength of 615 nm. For confocal imaging of the IEO monolayers after mEV

transport, cells on Transwell inserts were processed for immunostaining and confocal imaging as mentioned at Section 4.3.4.3.

4.3.5. mEV transport in 3D 'apical-out' intestinal epithelial organoids (IEOs)

4.3.5.1. Culture of typical colon IEOs

Colon IEOs were a kind gift from Dr Vivian Li (Francis Crick Institute, London, UK). They were generated by Dr Li from tissues collected from a 2-year-old female patient with ethical approval (Research Ethics Committee reference 04/Q0508/79). IEOs were defrosted from liquid nitrogen stock at 37°C and then centrifuged at 800 × g for 5 min immediately. IEOs pellets were resuspended in Matrigel and seeded on pre-warmed 24 wells plate with 50 µL droplet per well and supplemented with 0.5 mL IEOs growth medium: Advanced DMEM/F-12 with 10 mM HEPES, 1X GlutaMAX™, 50% WNT3A conditioned medium (in house production), 20% R-Spondin-1 conditioned medium (in house production), 1.25 mM N-Acetyl-L-cysteine, 10 mM Nicotinamide, 1X B-27™ Supplement, 150 ng/mL Recombinant Human Noggin, 50 ng/mL Human EGF Recombinant Protein, 10 nM Gastrin I human, 0.5 µM A83-01 and 10 µM SB202190. The growth medium was changed every 2 to 3 days. IEO cultures were passaged every 7 to 10 days, and 10 µM Y-27632 was added to the growth medium for the first 2 to 3 days after passage.

4.3.5.2. Culture of 3D 'apical-out' colon IEOs model

Apical-out 3D IEOs were generated by non-Matrigel culturing. PET inserts with 0.4 µm pore size were used for this purpose. Briefly, IEOs in Matrigel were broken up by pipette tip gently and centrifuged at 800 × g for 5 min to remove the medium and most of Matrigel. IEOs pellets were resuspended in TrypLE™ with 500 µL/well and incubated in 37°C for 10 min to disassociate IEOs into single cells. Thereafter, IEOs were centrifuged again to remove

TrypLE™ and the pellets were resuspended in IEOs growth medium. A 70 μm cell strainer was used to filter the suspension and single IEOs cells were collected. To develop apical-out IEOs, dissociated cells were seeded on 24-well PET inserts with $1.0 \times 10^5 – 5.0 \times 10^5$ cells/well (100 μL/well) and cultured for 10 days. The growth medium was changed every 2 to 3 days and 10 μM Y-27632 was added for the first 2 to 3 days after seeding. To create conventional, basolateral-out IEOs on the same inserts, 25 μL/well Matrigel was used to coat the surface of inserts. After incubating the coated inserts at 37 °C for 15 min, IEOs single cells were seeded and cultured on inserts with same procedures as apical-out IEOs.

4.3.5.3. mEV transport in 3D 'apical-out' IEOs model

To evaluate the transport of mEVs through 3D apical-out IEOs, labelled mEVs were diluted in IEOs growth medium to 0.05 mg/mL and applied to 3D apical-out IEOs for 4 hours incubation at 37°C and 5% CO_2 atmosphere. Thereafter, the growth medium containing mEVs was removed. The process of immobilizing membranes and confocal imaging was described in Section 4.3.4.3.

4.3.6. Transfection efficiency of GAPDH siRNA loaded-mEVs in macrophages

J774A.1 macrophage cells were seeded on 96-wells plates with 5000 cells/well and cultured for 24 hours to ~50% confluence. GAPDH siRNA loaded-mEVs were diluted to 0.08, 0.05 and 0.02 mg/mL (corresponding to the siRNA concentration of 0.016, 0.010 and 0.004 nmol/mL calculated by the loading efficiency) with Opti-MEM™ I Reduced Serum Medium and incubated with cells for 48 hours at 37°C and 5% CO_2 atmosphere. Thereafter, GAPDH activity was measured by KDalert™ GAPDH Assay Kit according to the manufacturer's instructions. Negative siRNA loaded-mEVs were applied as the negative control group, and GAPDH siRNA transfected with commercial transfection reagent (X-tremeGENE™ 360 Transfection Reagent,

2.5 μl/mL) was applied as the positive control group. The % remaining GAPDH gene expression was calculated with **Equation (4-1)**:

$$\%\ remaining\ expression\ = 100\ \times \frac{\Delta fluorescence\ of\ GAPDH}{\Delta\ fluorescence\ of\ Negative} \qquad (4-1)$$

Where Δ*fluorescence of GAPDH* and Δ*fluorescence of Negative* are fluorescence increases within 4 min for samples and negative control group, respectively.

4.4. Results and Discussion

4.4.1. Effect of intestinal fluids on mEVs stability

The stability of mEVs in intestinal fluids was determined *via* size, surface charge and RNA cargo measurements. We intentionally focused on intestinal rather than gastric fluids given that the most appropriate way in which mEVs or mEV-like synthetic delivery systems would be administered orally is *via* enteric-coated capsules so to ensure that membrane-associated proteins of mEVs are protected in the harsh environment of stomach biofluid.

There is evidence that cargo in mEVs (e.g. miRNAs) remains protected against degradation by low pH, RNases and treatment that mimics digestion in the GIT [380, 381]. However, studies reporting on the stability of mEVs and their content in the gut (which mainly come from the field of nutrition) tend to expose milk, rather than isolated EVs, to digestive conditions [380]. **Figure 4-2A** shows that while mEVs treated with fasted state simulated intestinal fluid (FaSSIF) displayed a similar size to those in PBS, fed state simulated intestinal fluid (FeSSIF) treatment resulted in a decreased diameter of mEVs. The surface charge (Zeta-potential) of mEVs was not compromised by simulated intestinal fluids (SIFs) digestion (**Figure 4-2B**). This observation is similar to the findings reported by Kokkona et al [382]. on the effect of sodium cholate on the mean diameter of liposomes containing phosphatidylcholine and cholesterol, which decreased by approximately 20% in the presence of sodium cholate. The effect of SIFs

on natural RNA cargo of mEVs was also evaluated, hence signifying vesicle damage and leakage of encapsulated mEVs content (**Figure 4-2C**). mEVs were treated with SIFs, followed by recovery with ultrafiltration and lysis with Trizol. The RNA fluorescence-based kit was applied to quantify the concentration of RNA in mEVs. The results demonstrated that the mEVs subjected to FaSSIF and PBS controls had similar RNA concentrations, indicating no loss of RNA cargo after exposure to FaSSIF. A significant decrease of mEVs RNA concentration was observed in the FeSSIF-exposed group compared to the PBS control, which indicated vesicle damage and RNA release upon exposure to FeSSIF. The effect of SIFs on quantity and functionality of mEVs surface proteins remains unexplored in this study. The quantity and species alteration of surface proteins could be investigated by BCA assay and Western blot, while their function could be reflected by our mEVs intestinal epithelium uptake and transport studies (**Figure 4-6**), which rely on the functions of their surface proteins [154].

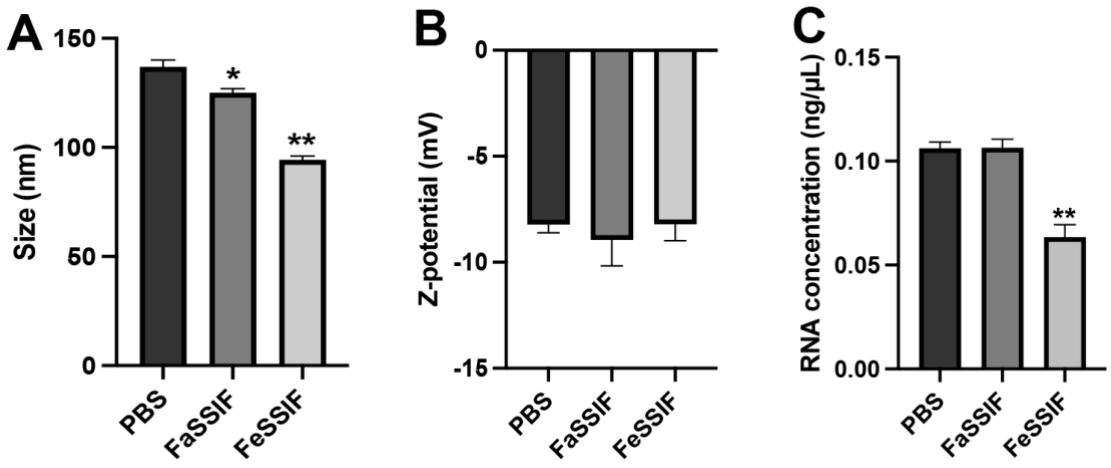

Figure 4-2. Effect of simulated intestinal fluids on bovine milk extracellular vesicles (mEVs). (A) size, (B) Zeta-potential, and (C) RNA cargo. mEVs were treated with simulated intestinal fluids for 90 minutes. RNA concentration was measured by QuantiFluor® RNA System. FaSSIF: Fasted State Simulated Intestinal Fluid; FeSSIF: Fed State Simulated Intestinal Fluid. Data shown as the mean ± SD, n=3. * and ** indicate $p < 0.05$ and $p < 0.01$ compared with PBS group, respectively.

It is noted that the SIFs employed in this work are simple models of the intestinal biofluid. They do not fully represent the complexity of the natural composition, although they contain the surfactants (bile salt and phospholipid), and they are adjusted to reflect the average pH and osmolarity of the intestinal environment. As such, they are derived of vital intraluminal components; for example, whilst native human intestinal fluid harbours a variety of bile salts, the SIFs used here comprise pure sodium taurocholate only [383]. These fluids additionally fail to replicate the intricate ultrastructure of postprandial human intestinal fluid (which includes mixed micelles and vesicles), likely due to the absence of lipids and lipolysis products. Furthermore, the intestinal movement and enzymatic degradation of food (which impact colloid formation) within the gastrointestinal tract are unaccounted for [384, 385]. Furthermore, the variation of intestinal environment between individuals, particularly the alterations of biochemical components associated with IBD conditions, is a critical consideration in future studies[77]. Although this study supports previous evidence on the stability of mEVs in the GIT, the ultimate evidence of the ability of mEVs to survive digestion should come from *in vivo* studies in the future.

4.4.2. mEV uptake and transport in intestinal Caco-2 monolayers

Caco-2 cells were seeded on Transwell inserts and cultured for 21 days to develop the monolayers. TEER, which reflects the ionic conductance of the paracellular pathway (tight junction dynamics), refers to the assessment of electrical resistance across a cellular monolayer in real-time, serving as a very sensitive and dependable technique to monitor the monolayer integrity and permeability [386]. As shown in **Figure 4-3A**, the TEER value increased in the first 17 days and became stable after 17 days until 22 days (reached ~1500 Ω and ~1339 Ω cm^2 calculated to account the surface area, 1.12 cm^2 , of 12-well polycarbonate Transwell inserts). The TEER value obtained after 21 days of culture was consistent with previous studies

which used the same type of Transwell inserts, suggesting the formation and integrity of monolayers [386, 387]. Caco-2 monolayers with well-established tight junctions typically exhibit high TEER values (>500 Ω cm^2) [388], but the values within this range may fluctuate due to variations in medium composition, temperature, or detection equipment [389]. In order to assess the potential impact of mEVs incubation on the integrity of Caco-2 monolayers, the TEER value of monolayers was detected both before and after the incubation period (0 h and 3 h). As shown in **Figure 4-3B**, the TEER value of the monolayers remained unchanged before and after the incubation with mEVs at two different concentrations, which indicated that the mEVs had no impact on the integrity of the monolayers due to the low toxicity [386].

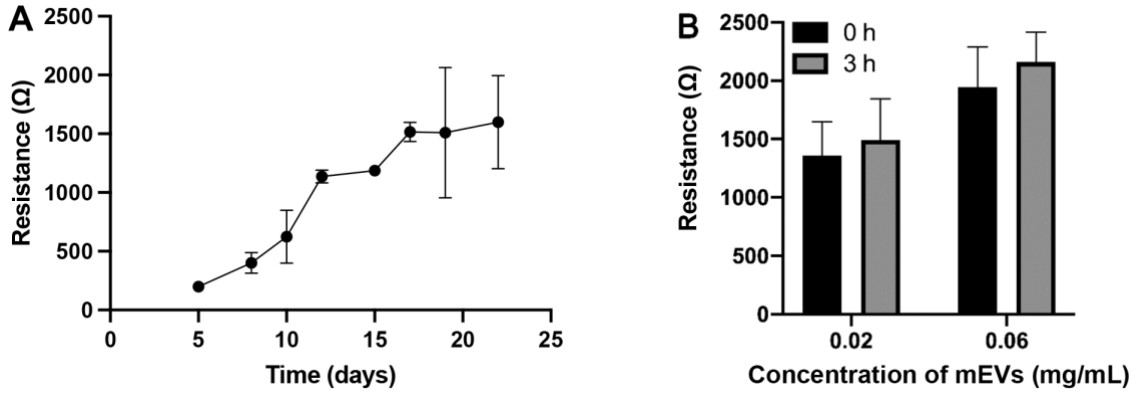

Figure 4-3. The transepithelial electrical resistance (TEER) values of Caco-2 cell monolayers for 21 days culture (A), and the TEER values before and after treatment with milk extracellular vesicles (mEVs) solutions (B). Data shown as the mean ± SD (n=3).

Figure 4-4 shows the cell uptake of mEVs by differentiated intestinal epithelial Caco-2 cells (Caco-2 monolayers). Cell uptake was around 6% when mEVs were applied at 0.02 mg/mL and approximately 4% at 0.06 mg/mL, but without significant difference (**Figure 4-4A**). Note that because cell uptake is expressed as percentage of applied mEVs, the overall uptake of mEVs in amount terms is higher with 0.06 mg/mL application. This result is consistent with

our previous study [249], and correlates with another research which demonstrated the cell uptake of mEVs by Caco-2 cells was lower than 10% when quantified by EVs fluorescence intensity during the first 3-hour incubation. However, this uptake increased to approximately 40% after 8 hours [390]. Therefore, the modest cell uptake of mEVs by Caco-2 cells in this study may be due to the limited incubation time. Additionally, the method of measuring mEVs fluorescence intensity following cell lysis could result in suboptimal signal detection of supernatant, potentially because mEVs are entrapped in cellular debris. To overcome this, alternative quantification techniques, such as confocal imaging with quantification analysis or flow cytometry, should be considered for more accurate assessment [153, 391]. **Figure 4-4B** shows a confocal image of the cell uptake of mEVs, whereby a fluorescence signal associated with mEVs is clearly apparent. We recognize the omission of dye-only controls in our confocal imaging studies, which are essential for establishing baseline fluorescence and should be incorporated into future experimental designs. Despite this, we have quantitatively measured cell uptake as presented in **Figure 4-4A**, which was achieved through fluorescence quantification using a plate reader after cell lysis. This alternative methodological approach corroborates the uptake of mEVs by Caco-2 cells. Furthermore, the observed heterogeneous distribution of mEVs, illustrated in **Figure 4-4B**, could potentially be attributed to mEVs aggregation during incubation with the cells. The fluorescent dye we used for mEVs labelling is ExoGlow™-protein EV labelling kit (Red), which specifically and covalently labels EVs proteins, leading to low levels of background. While DiO is commonly employed for EVs membrane lipids labelling, the excess dye might bind to cell components such as phospholipids bilayers [392]. Additionally, both DiO and another labelling dye, SYTO® (specific to EVs RNA), might suffer the risk of non-specific dye transfer from labelled EVs to cell components after prolonged incubation (24h) [153]. In terms of transepithelial transport of mEVs, there was an overall trend of gradual accumulation of mEVs in the basolateral side through 3 hours, and

overall transport reached approximately 10% (**Figure 4-4C**). In addition, comparisons of the mEVs transport across Caco-2 monolayers were made with liposomes of similar size (~100 nm), as well as the fluorescent dye alone which was used to label mEVs. **Figure 4-5** shows that the extent of transport was notably higher for mEVs compared to liposomes (over an order of magnitude) or the dye alone. Notably, in this transport study, the concentrations of mEVs and liposomes applied were 0.05 mg/mL (protein) and 0.05 mg/mL (lipids), respectively. To ensure comparability, we determined the particles/mg concentration for each, resulting in 4.16 $\times 10^{14}$ particles/mg (protein-mEVs) and 5.35 $\times 10^{14}$ particles/mg (lipids-liposomes). Therefore, the similar particles/mg concentration of mEVs and liposomes validates the use of mg/mL concentration to represent the comparable number of particles applied.

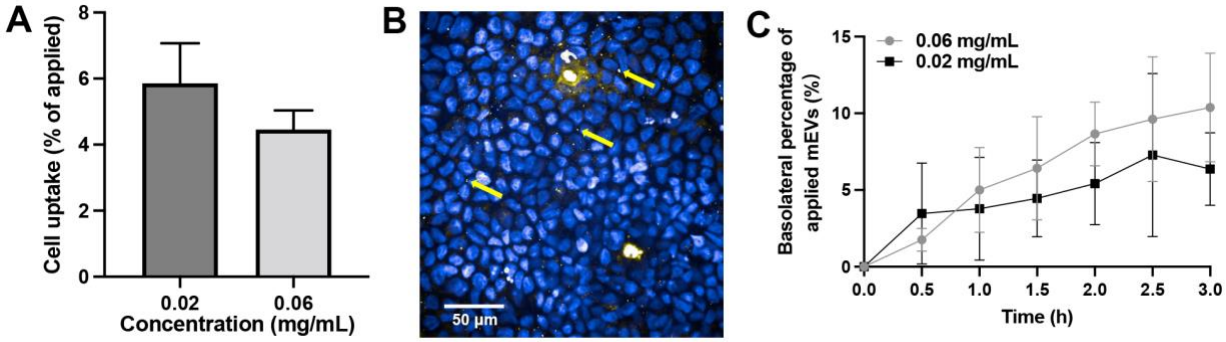

Figure 4-4. Uptake and transport of milk extracellular vesicles (mEVs) in intestinal Caco-2 monolayers. (A) mEVs uptake in differentiated (polarised) Caco-2 cells (3-hour incubation). **(B)** High content confocal image of mEVs cell uptake by differentiated Caco-2 cells. Nuclei in blue and mEVs in yellow (arrows). **(C)** mEVs transport across differentiated Caco-2 monolayers (cultured for 21 days on Transwell inserts). Data shown as the mean ± SD (n=3).

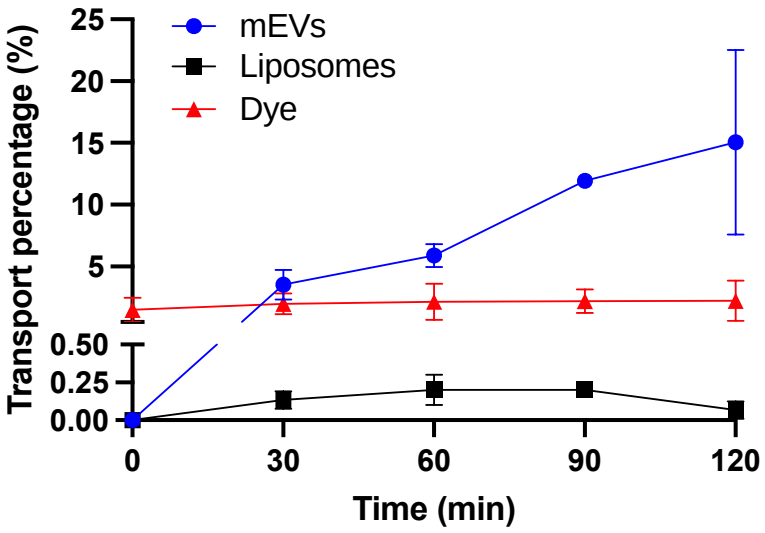

Figure 4-5. Transport of bovine milk extracellular vesicles (mEVs), liposomes and labelling dye alone (for mEVs) across differentiated intestinal epithelial Caco-2 monolayers. Data shown as the mean ± SD, n=3.

We next sought to understand whether the ability of mEVs to translocate across the intestinal epithelium is compromised upon treatment with SIFs. **Figure 4-6A** shows the uptake of digested mEVs into differentiated Caco-2 cells after 3 hours incubation. Around 4.5% of FeSSIF-digested mEVs and FaSSIF-treated mEVs were taken up by cells. Control (PBS incubated) mEVs demonstrated a lower uptake (2.5%). **Figure 4-6B** shows the transport of mEVs, post-treatment with SIFs, across polarised/differentiated Caco-2 monolayers. In all three groups, mEVs showed a remarkable ability to permeate across the Caco-2 monolayers. Interestingly, FeSSIF-treated mEVs possessed a slightly higher transport through the monolayers compared to FaSSIF-treated and untreated control. Specifically, approximately, 18% of FeSSIF-treated mEVs translocated across cell monolayers in 90 minutes, while FaSSIF-treated and untreated control showed a lower level of translocation, amounting to 10% of applied mEVs after 90 minutes. The calculated rate of mEV transport across intestinal epithelial monolayers was 12.0, 6.7 and 7.9% per hour for FeSSIF-treated, FaSSIF-treated and untreated

mEVs, respectively, with the difference between FeSSIF-treated and untreated mEVs being statistically significant (p=0.026).

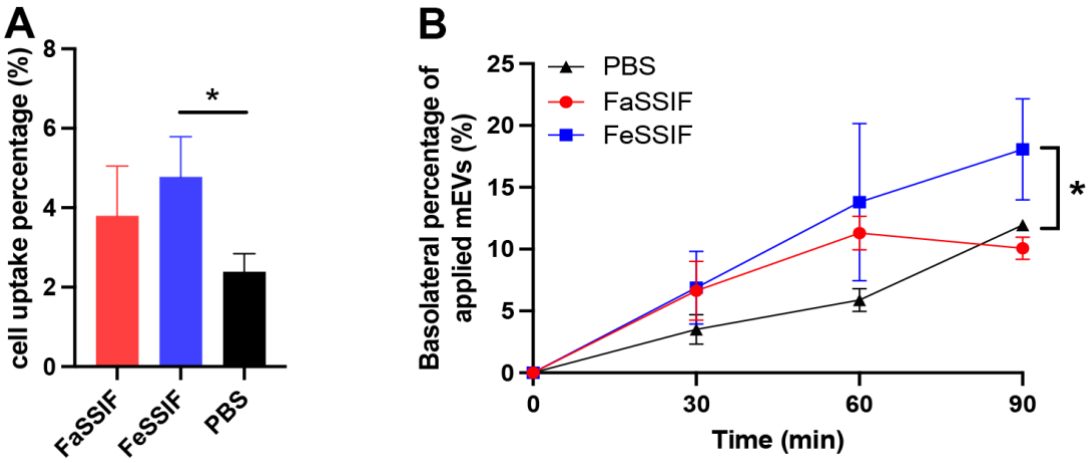

Figure 4-6. Effect of simulated intestinal fluids on bovine milk extracellular vesicles (mEVs) cell uptake (A) and transport (B) across differentiated intestinal epithelial Caco-2 monolayers. mEVs were treated with simulated intestinal fluids for 90 minutes. FaSSIF: Fasted State Simulated Intestinal Fluid; FeSSIF: Fed State Simulated Intestinal Fluid. Data shown as the mean ± SD, n=4. * indicates $p < 0.05$ compared with PBS group.

Interestingly, it was observed that mEVs treated with FeSSIF displayed a higher uptake and transport across Caco-2 monolayers in comparison to FaSSIF-treated group and control (untreated with SIFs) (**Figure 4-6**). It is reasonable to assume that epithelial uptake and transport of mEVs is dependent upon their stability and integrity of membrane, particularly since there is evidence of the potential existence of a receptor-mediated epithelial transport process for mEVs, such as IgG - FcRn dependent transcytosis [153, 154]. Besides, glycoproteins, especially Galectin-3 and its galactose ligands on mEVs, have been identified as critical for the efficient absorption and transport of mEVs across epithelial cells [393]. Therefore, the receptor-mediated transport process would obviously rely on an interaction of mEVs having intact membranes and ligands on their surfaces with cell receptors and any

disruption of mEVs membranes could influence such interaction and overall cell uptake and transport. It is therefore presently unclear how an apparent compromised membrane integrity of mEVs upon treatment in FeSSIF does not result in a loss of mEVs capacity to transport across intestinal epithelial monolayers. However, one has to be careful in drawing any conclusions from this study on the possible effect of FeSSIF on intestinal uptake and translocation of mEVs given the fluorescence-based quantitation method employed here, meaning that a scenario whereby the component of mEVs is uptaking or transporting across the cell monolayers, cannot be excluded. While this phenomenon requires further study (e.g. *via* characterisation of basolateral mEVs, or the use of multiple labels), our findings bare significant importance in highlighting that mEVs may undergo structural damage in the fed-state intestinal fluid, releasing its cargo, which would preclude their usefulness for oral delivery of siRNA.

Overall, the stability experiments convincingly point to a conclusion that mEVs are stable in FaSSIF but not in FeSSIF. The mEVs membrane-disrupting effect of FeSSIF can probably be attributed to one of its key components, namely the bile salt sodium taurocholate (present at 15 mM concentration). Although to our knowledge there are no previous published studies investigating the effect of simulated (or native) gastrointestinal fluids on mEVs stability, research on liposomes highlighted that these structures are susceptible to detrimental effects of components of GIT fluids, including bile salts [394-396]. A study by Richards et al. showed that sodium taurocholate (and sodium glycocholate) at concentrations in the range encountered in the human intestine have a significant effect on the structural integrity of liposomes of different lipid compositions [397]. Specifically, in the presence of 10 mM bile salts at pH 7.4, liposomes were totally disrupted, with their entire contents released. Similar observations were reported by Kokkona et al. [398] confirming instability of small unilamellar vesicles (SUV) liposomes in the presence of cholates. Furthermore, the osmotic balance within EVs can be

influenced by variations in environmental ionic strength, potentially leading to their swelling or shrinkage based on osmotic potential which is contingent upon the structural integrity of the EVs [399]. Consequently, it is conceivable that bile salts may compromise the structural integrity of EVs, leading to increased membrane permeability and resulting in the efflux of internal ions and small molecules. Such alterations would attenuate the osmotic gradient between the interior of the EVs and the external environment, ultimately reducing their osmotic potential.

4.4.3. mEV transport across IBD-IEOs monolayer model

4.4.3.1. Culture and differentiation of typical IBD-IEOs

To evaluate the transport of mEVs across IEOs, we first cultured IEOs using a typical culture condition, and using DAPT, we induced differentiation of IEOs so to promote the production of mucus [371]. IEOs were generated from intestinal crypts isolated from mucosal biopsies of a patient with mild chronic gastritis and were cultured in Matrigel covered with IEOs growth medium. Matrigel, an ECM mixture secreted by mouse tumor, provides abundant factors including laminin, nidogen, collagen IV, heparan sulfate, entactin, various growth factors etc., which mimics the basement membrane structure *in vivo* and enables attachment and differentiation of epithelial stem cells [400]. The components of the complex IEOs growth medium perform different roles in maintaining the development of IEOs. For instance, the Wnt and R-Spondin in medium are key factors to keep stem cells in an undifferentiated state and drive proliferation, and EGF possesses the effect of mitogenic [401]. Noggin could provide a suitable environment for crypt formation by inhibiting the BMP pathway, since BMP signaling is a negative regulator of crypts [402]. Furthermore, the inclusion of nicotinamide, A83-01 (a selective TGFβ type I receptor kinase (ALK) inhibitor), and SB202190 (a p38 inhibitor) were essential for the sustained growth and expansion of both human small and colon organoids

[402]. When inducing IEOs differentiation, the medium components responsible for maintaining the undifferentiated state of stem cells were excluded and 5 μM DAPT was introduced to inhibit the Notch pathway and enhance neuronal differentiation [403].

IEOs from different intestinal segments demonstrated different morphologies. **Figure 4-7A** and **4-7D** show representative brightfield images of duodenum ('Duo') and terminal ileum ('TI') IEOs, respectively. Duodenal IEOs showed a cystic morphology with a bright lumen, while terminal ileum IEOs produced more buds with an irregular shape. Immunofluorescence images (confocal microscopy) of undifferentiated Duo IEOs are shown in **Figure 4-7B**, whereas **Figure 4-7C** shows Duo IEOs following differentiation. The fluorescence signal associated with immunostaining of apical zonula occludens (ZO-1) tight junction proteins appears to be similar in both differentiated and undifferentiated Duo IEOs, while that of MUC2 mucin, which is secreted by goblet cells, was increased following differentiation. **Figure 4-7D and 4-7E** show undifferentiated TI IEOs, with the latter depicting immunofluorescence of ZO-1 and MUC2. The immunofluorescence-based determination of expression of these proteins is also shown in **Figure 4-7F** for differentiated TI IEOs. Similarly to Duo IEOs, the figure clearly indicates that differentiation of TI IEOs promotes MUC2 expression, as confirmed by a visibly increased fluorescence signal.

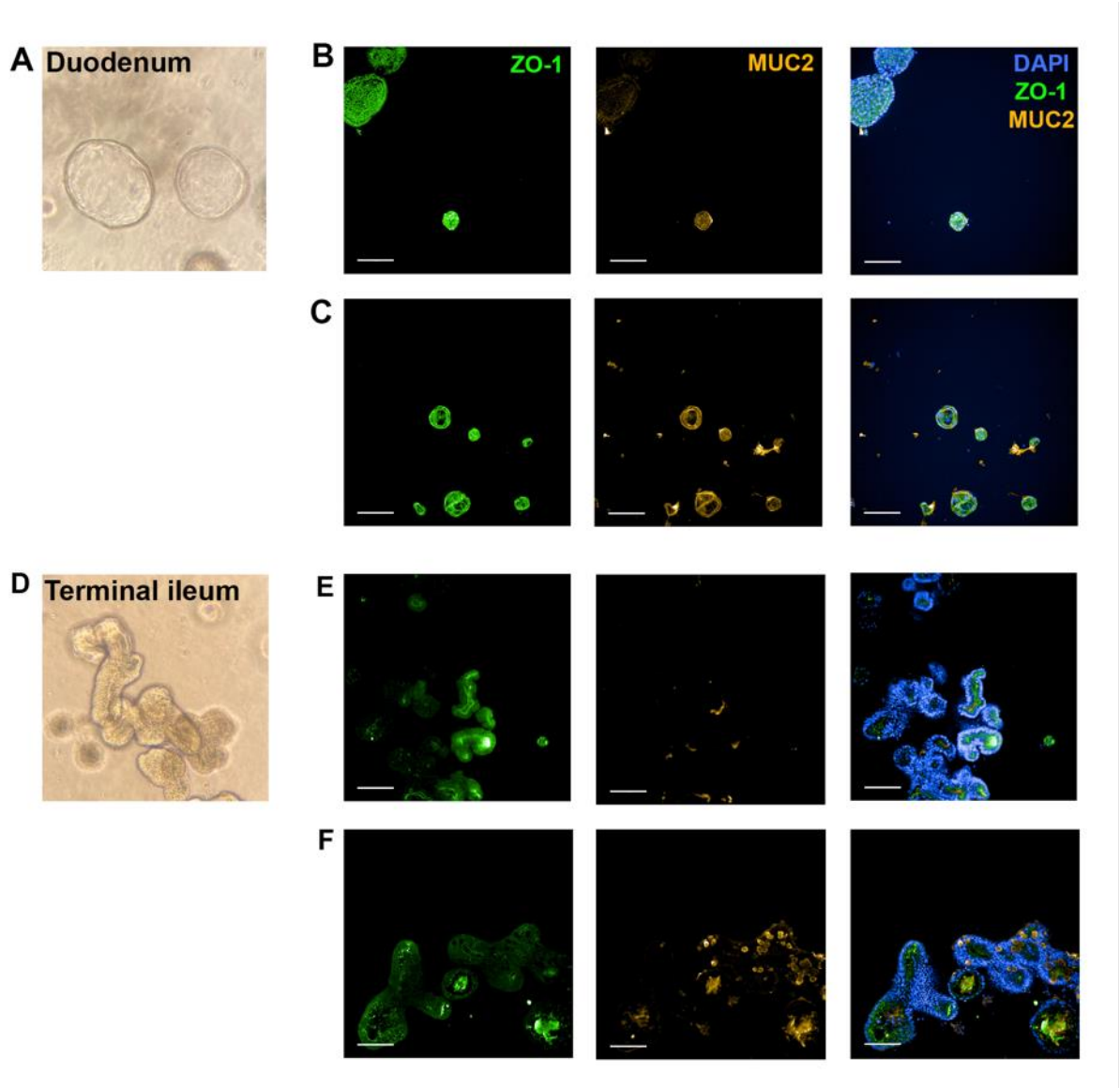

Figure 4-7. Human (biopsy-derived) intestinal epithelial organoids (IEOs) cultured in Matrigel extracellular matrix. (A) Brightfield image of duodenum IEOs. **(B)** Confocal immunofluorescent staining images of undifferentiated duodenum IEOs for apical zonula occludens (ZO-1) tight junction protein (green), MUC2 mucin (orange) and cell nucleus (DAPI, blue). **(C)** Confocal immunofluorescent staining images of differentiated duodenum IEOs. **(D)** Brightfield image of terminal ileum IEOs. **(E)** Confocal immunofluorescent staining images of undifferentiated terminal ileum IEOs. **(F)** Confocal immunofluorescent staining images of differentiated terminal ileum IEOs. Scale bars: 100 μm.

4.4.3.2. mEV transport across IBD-IEOs monolayer model

Apical-to-basolateral transport of mEVs in IEOs monolayers originating from different gut segments (i.e. duodenum (Duo), terminal ileum (TI) and sigmoid colon (SC)) was determined. 2D monolayers enable easy access to the apical and basolateral sides and therefore the determination of transintestinal transport of material. To achieve this system, IEOs cultured in Matrigel were harvested for monolayer preparation at an optimized culture period, dissociated and single cells seeded on Transwell inserts. **Figure 4-8** depicts the growth of IEO monolayers over a period of seven days, whereby the differentiation medium was added on day 5 and differentiated confluent IEOs monolayers developed by day 7. **Figure 4-9A** shows immunofluorescence staining images of Duo, TI and SC IEOs monolayers. ZO-1 fluorescence signal displays a characteristic 'chicken-wire' distribution of tight junctions. MUC2 signal is absent in Duo and TI monolayers, while it is weak in SC monolayers. The secretion of the mucin protein MUC2 is higher in the colon than in the small intestine (Duo and TI), which is attributed to the colon's dual-layer mucus system, as opposed to the single, less dense mucus layer found in the small intestine [404]. However, the relatively low level of MUC2 expression in organoid monolayers may stem from less effective goblet cell differentiation, and the absence of a 3D architecture could also affect the expression of MUC2 [405]. Optimizing the differentiated conditions specifically for organoid monolayers could potentially enhance the goblet cell quantity and MUC2 expression in future studies. The formation of electrically tight monolayers was also confirmed *via* TEER measurement. **Figure 4-9B** shows that the TEER values of Duo, TI and SC monolayers increased gradually with time during the first five days with culture in normal growth medium, while after the addition of differentiation medium on day 5, the TEER of monolayers from all three intestinal regions increased significantly, reaching beyond 200 $\Omega * cm^2$. The TEER values observed for Duo and TI monolayers after differentiation were consistent with previous studies where monolayers derived from small

intestinal organoids exhibited TEER values ranging from 200 to 400 Ω·cm² [406, 407]. The TEER value for the SC was significantly higher, reaching 2000 Ω * cm^2, consistent with another investigation that reported similar values for monolayers developed from mouse proximal and distal colon organoids [408]. A previous study also reported that the TEER value (~ 1300 Ω * cm^2) for colon monolayers was significantly higher than that of small intestinal monolayers (~ 480 Ω * cm^2) [409], which due to the differences in permeability of respective intestinal segments *in vivo*, with the colonic epithelium forming a robust paracellular barrier compared to that of the small intestine [410]. To probe the barrier of IEOs monolayers, we determined FD10 permeability in this system. **Figure 4-9C** shows a significantly lower permeability of FD10 across IEOs monolayers compared with blank (no cell) inserts (coated with diluted BME2, similarly to cell-containing counterparts), and the apparent permeability coefficient (P_{app}) of FD10 through IEOs monolayers were lower than 10^{-7} cm/s, which confirms the barrier integrity of monolayers. Overall, the distribution of ZO-1 tight junction protein, high TEER and low permeability of FD10 together demonstrate the successful development of polarised Duo, TI and SC IEOs monolayers which are electrically tight and pose a barrier to transepithelial diffusion of a model macromolecule.

The data in **Figure 4-9D** show mEVs accumulation on the basolateral side over time, reaching approximately 3% and 5% after 160 min across Duo and TI IEO monolayers, respectively (upside). The cellular localization of mEVs following their incubation with IEO monolayers is shown on confocal images (**Figure 4-9D**, bottom). The fluorescence signal associated with mEVs can be observed in the cell interior and across the vertical cross-sections of the monolayers, with a more prominent distribution of fluorescence on the apical side. The accumulation of red mEVs fluorescence in TI monolayers was higher than Duo monolayers, which was consistent with the transport quantitation. As shown in **Figure 4-9D, SC**, both the

quantitative transport measurement and 3D confocal images show that mEVs transport across SC monolayers is the least efficient (compared to Duo and TI monolayers).

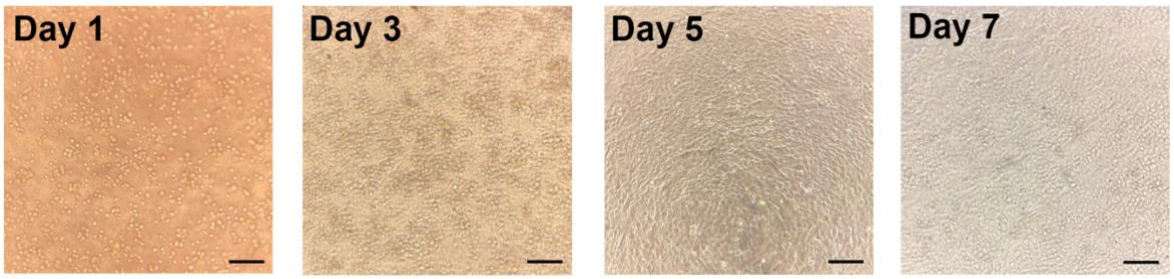

Figure 4-8. Brightfield images of human terminal ileum epithelial organoids (IEOs) as 2D monolayers on Transwell inserts of 1 day, 3 days, 5 days, and 7 days culturing after seeding (differentiated at day 5). Scale bars: 100 μm.

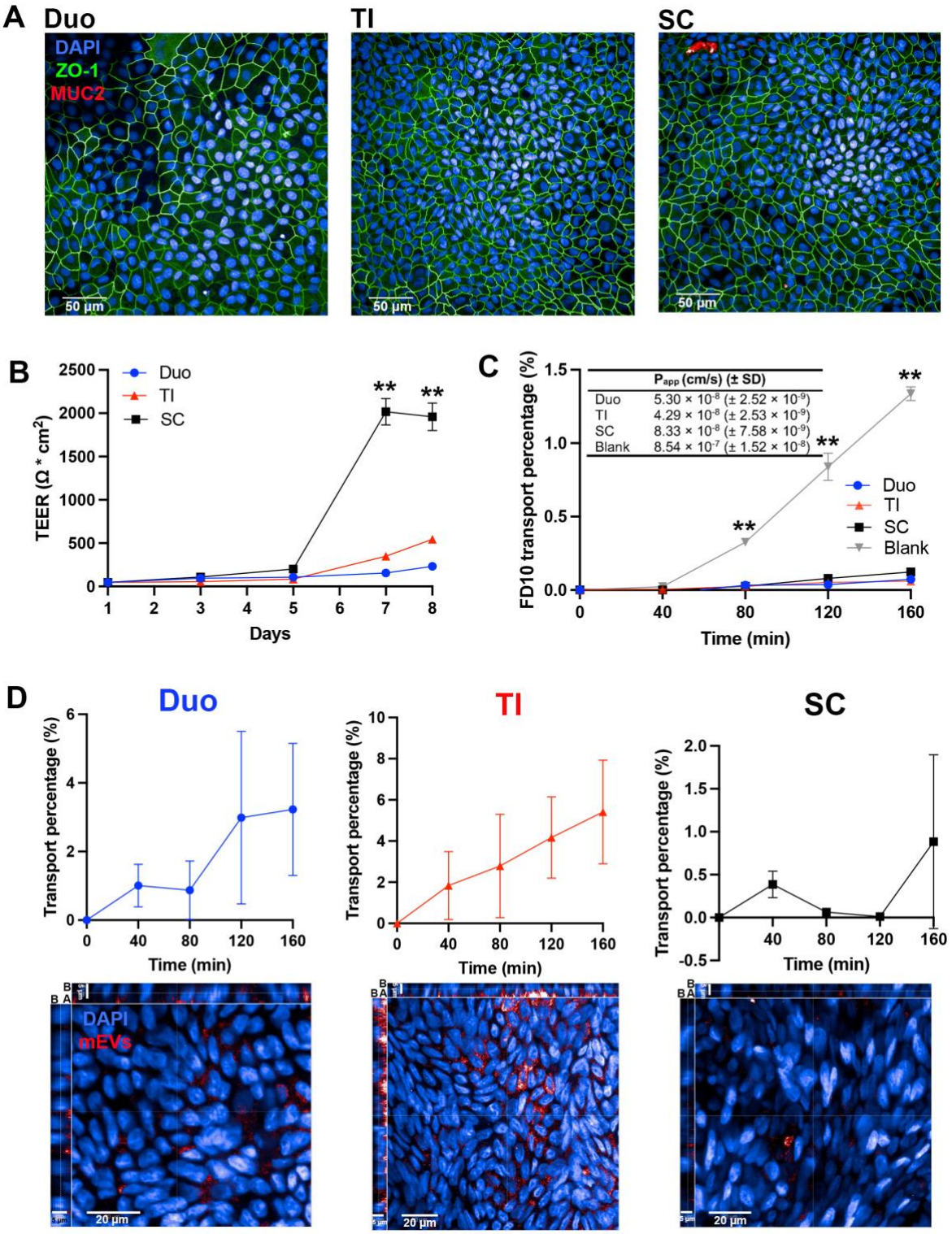

Figure 4-9. Culture of human intestinal epithelial organoids (IEOs) as 2D monolayers on Transwell inserts and epithelial transport of milk extracellular vesicle (mEVs). (A) Confocal immunofluorescent staining images of IEOs monolayers cultured on Transwell inserts for 8 days (differentiated at day 5), immunostained for the apical zonula occludens (ZO-1) tight junction protein

(green), MUC2 mucin (red) and cell nucleus (DAPI, blue). **(B)** Transepithelial electrical resistance (TEER) of IEOs cultured as monolayers. **(C)** Transport percentage of fluorescein isothiocyanate–dextran with molecular weight of 10k (FD10) through IEOs monolayers and blank inserts with diluted basement membrane extract (BME2) coating, and insert table shows apparent permeability coefficient (P_{app}) of FD10 through monolayers. **(D)** mEVs transport across IEOs monolayers including transport percentage shown on the upside and 3D confocal images on the bottom, where the apical side of the cells is marked by 'A' and the basolateral side 'B'. Nuclei appear in blue and mEVs in red. IEOs were derived from biopsied tissue from different regions of human gastrointestinal system ('Duo': duodenum; 'TI': terminal ileum; and 'SC': sigmoid colon). Data shown as the mean ± SD, n=4. ** indicates $p < 0.01$.

4.4.4. mEV transport across 3D 'apical-out' IEOs model

Based on a modified method reported by Co et al., we initially cultured 3D IEOs derived colon tissue with reversed polarity [370, 371]. The process of achieving successful *in vitro* culture of apical-out IEOs is shown in **Figure 4-10A**. The single cells dissociated from typical basal-out IEOs cultured in Matrigel could self-assemble to apical-out IEOs on naked Transwell inserts without Matrigel or BME2. Confocal imaging revealed that when compared to typical basal-out IEOs, which have apical tight junction ZO-1 protein expression in the interior of the cell clusters, in apical-out IEOs, apical ZO-1 is distributed on the surface of IEOs clusters, facing outward (**Figure 4-10B and C**), which confirmed the successful development of 3D apical-out IEOs model. We then applied fluorescently labelled mEVs to the apical-out IEOs model for four hours, followed by confocal imaging of uptake (**Figure 4-10D**). In these systems, the fluorescence signal (red) of mEVs was clearly apparent within the interior of apical-out IEOs, which indicates transepithelial transport of mEVs from the exterior facing of 3D IEOs into their basolateral lumen. We attempted to quantify the transport of mEVs through 3D IEOs by dissociating the IEOs and measuring the fluorescence intensity of released mEVs using a plate

reader. However, the sensitivity of the equipment was insufficient for detecting the low-level fluorescence signals from the samples. In future studies, increasing the sample size, such as pooling multiple wells containing IEOs, may be a viable approach to enhance detectability.

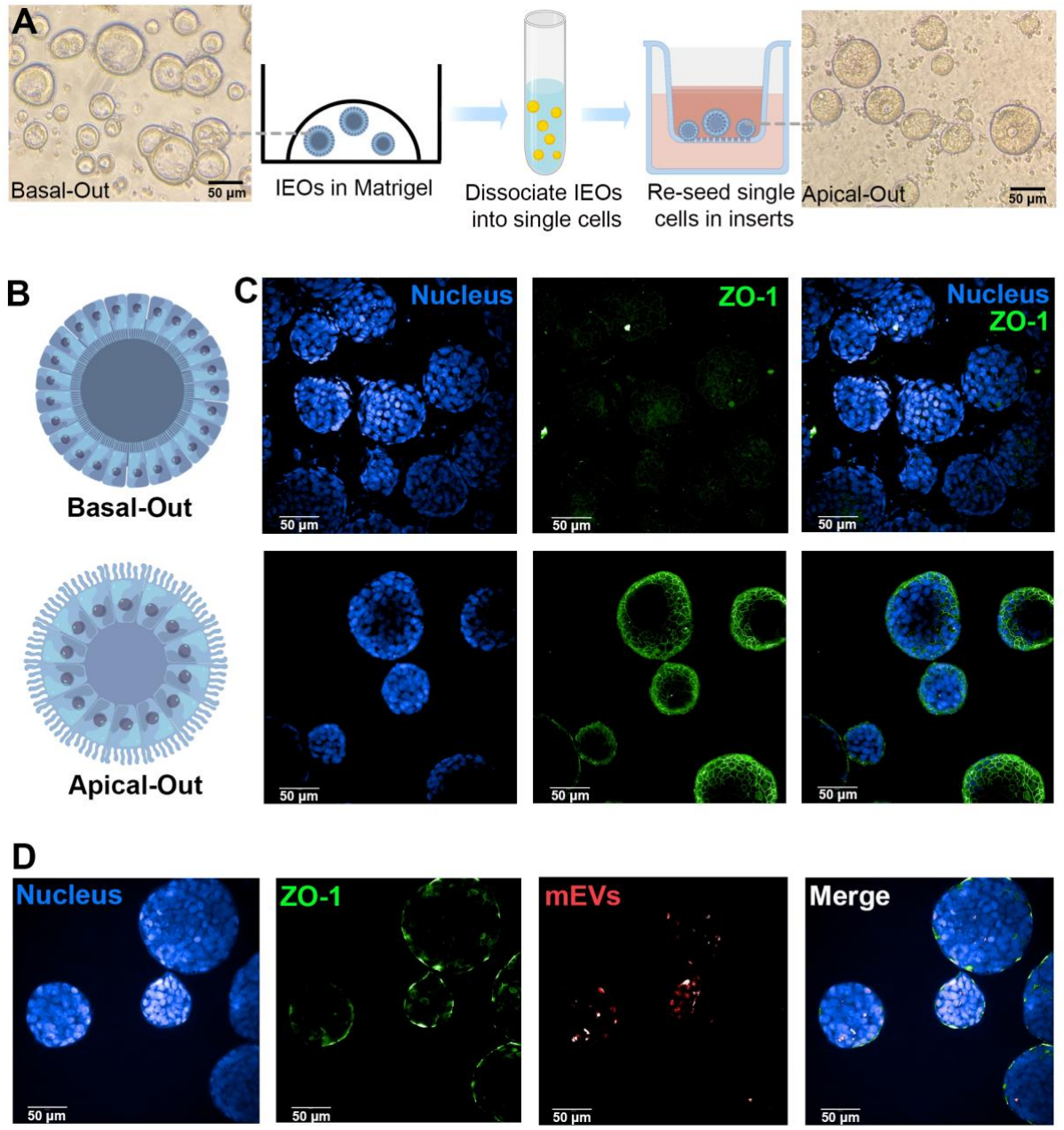

Figure 4-10. Apical-out culture of human (biopsy-derived) colon intestinal epithelial organoids (IEOs) and transport of milk extracellular vesicles (mEVs). (A) Brightfield image of IEOs cultured in Matrigel (basal-out) and PET transwells inserts (apical-out), and the schematic for development of apical-out IEOs from basal-out polarity. **(B)** Depicted schematic of basal-out and apical-out IEOs. **(C)**

Confocal immunofluorescent staining images of IEOs with apical-out and basal-out polarity. **(D)** Confocal immunofluorescent staining images of mEVs transporting across apical-out IEOs after incubation for 4 hours. Nucleus in blue (DAPI), apical zonula occludens (ZO-1) tight junction protein in green, and mEVs in red. Schematics were drawn by Figdraw.

Data in **Figure 4-9** confirms the intestinal epithelium crossing characteristic of mEVs, also demonstrated in Caco-2 monolayers (**Figure 4-4**) and 'apical-out' 3D IEOs (**Figure 4-10**). Additionally and importantly, the data highlights that mEV transport across Duo- and TI-derived IEO monolayers is significantly higher than that in SC-derived monolayers. Although it is relatively well established that the intestinal barrier is more 'leaky' in the small intestine compared to the colon [411], attributed to differential expression of tight junctions [412], a markedly different transport profile of mEVs in SC compared to Duo and TI IEOs cannot be compared with the permeability of small molecular weight drugs, or indeed macromolecules. However, it has been reported that the permeability of actively transported compounds, D-glucose and L-leucine, is dramatically lower in the colon compared to the small intestine in a study utilizing human tissue in Ussing chambers [413]. This provides an interesting comparison, as although the mechanisms of intestinal epithelial transport of particulate mEVs are expected to be facilitated by different mechanisms to actively-transported molecules, it may be the case that the lower transport of mEVs in SC is linked to lower expression levels of the cellular machinery involved in their trafficking, although presently this is only a speculation and needs confirming in future studies. Notably, constrained by resource limitations and the high cost of organoids culturing, the use of N=1 patient number (IEOs obtained from one patient) was acknowledged as a limitation in the IEOs-related research. Therefore, further investigation into inter-person variation is warranted in future studies.

IEOs monolayers and 3D 'apical-out' IEOs were established in this Chapter, providing comprehensive *in vitro* intestinal models for investigation of drug delivery systems. IEOs

monolayers present a 2D structure which facilitates the quantification of transport of delivery systems across epithelium, while 3D apical-out IEOs mimic the nature tissue morphology but compromise direct quantification of transport. Combining the strengths of both these models in future research has the potential to yield a more relevant *in vitro* epithelial model. Technical approaches to produce 3D architectures for the monolayers (including photolithography, soft-lithography, 3D printing and microfluidics) have been developing in recent years [414]. It has been revealed that 3D architectures strongly affect cell proliferation, differentiation, and metabolism [414]. Scaffolds reproducing intestinal villi based on a combination of molding techniques were used for Caco-2 cells culturing to develop a 3D intestinal epithelial model [415]. This model showed more similarity to human native small intestine compared with 2D Caco-2 monolayers in drug transport studies, and the TEER was closer to that physiologically observed in tissue [416]. Moreover, the Caco-2 cells grown on 3D collagen scaffolds have been found to produce more differentiation markers and mucins (MUC17) compared with 2D Caco-2 monolayers [417]. Scaffolds in synthetic materials like PLGA has been developed to support the co-culture of Caco-2 cells and HT29-MTX cells, and this system promote differentiation and spatial organization of intestinal cells [417]. The aim of these technologies was to transition 2D Caco-2 monolayers into 3D structures, and this same concept and technology can be extended to IEO monolayers which consist of multiple cell types. 3D architecture provides a more natural and realistic structure as nature tissues. In this context, 3D printing was also applied to develop a 3D model of intestinal tissue with two printed layers: a supporting layer of intestinal fibroblasts and an epithelial layer with epithelial cells (which can be IEOs monolayers). This model could recapitulate some key features of native tissue like differentiation markers secretion and tight junction establishment [418]. Recently, studies focused on scaffolds reproducing not only villus, but also crypt architectures were reported [419]. The system was integrated into two inserts with opposite growth factors: proliferative

factors in the basal reservoir to maintain the growth of crypts; and the differentiation factors in the upper compartment to promote villi differentiation [419]. In addition to 3D architectures, the 'gut-on-chip' was also introduced to build a more accurate *in vitro* model of intestine. 'gut-on-chip' was one of the concepts of 'organ-on-chip' which is defined as "microfluidics devices for culturing cells in continuously perfused, micrometer sized chambers in order to model physiological function of tissues and organs" [420]. This 'gut-on-chip' system could reproduce the dynamic mechanical stimulation created by shear stress from lumen, and the flow of intestinal fluids, which simulates the real digestion process. A co-culture system of Caco-2 cells with normal microbes on a chip was used to simulate complicated microbiome-immune interaction in IBD. The blood mononuclear cells were included in the lower channel to simulate the immune compartment, and the introduction of endotoxin to lumen could induce pro-inflammatory cytokines secretion and lead to dysfunction of epithelial barrier, which mimics the inflammation-induced damage [421]. Therefore, by integrating IEOs monolayers onto these bioengineered 3D structures which incorporate dynamic forces, homeostasis, and more key features of tissues, these *in vitro* intestinal epithelial models are able to mimic closer to the physiological and representative aspects of human native tissue.

4.4.5. In vitro transfection efficiency of siRNA-loaded mEVs

To establish whether mEVs could serve as potential systems for siRNA delivery, siRNA was loaded into the vesicles *via* electroporation. The optimized loading efficiency of siRNA into mEVs was calculated as 5.10 ± 0.55% (details in Section 3.3.2.3.). The gene silencing efficiency of siRNA loaded-mEVs was then evaluated on macrophages (J774A.1), given that macrophages in the lamina propria (i.e. under the epithelium) play a key role in inflammatory response in IBD [422] and therefore are a potential target of interest in IBD, achieved by a delivery system that permeates the intestinal barrier, such as mEVs. A model 'housekeeping'

protein, GAPDH, was selected as a target for knock-down as it represents a commonly chosen target for these studies, and the GAPDH activity was measured by KDalert™ GAPDH Assay Kit to determine gene silencing [208, 423]. This GAPDH Assay Kit relies on fluorescence-based method (the conversion of NAD^+ to NADH by GAPDH) for measuring the enzymatic activity of GAPDH produced by cells, therefore it enables the assessment of GAPDH expression and the efficacy of its knockdown at the protein level. Though quantifying mRNA *via* qPCR is a more direct method (siRNA targets mRNA), the low stability of mRNA and the lack of appropriate equipment in lab necessitated our choice to measure the protein level, which offers greater stability and functional relevance [424]. The gene silencing efficiency of GAPDH siRNA-loaded mEVs in macrophages is shown in **Figure 4-11**. 0.05 mg/mL GAPDH siRNA loaded-mEVs (corresponding to 0.010 nmol/mL loaded siRNA) possessed around 50% silencing efficiency (48 h post-transfection), which was significantly higher than siRNA transfected with a commercial transfection reagent (~5% silencing efficiency) and negative control (siRNA alone). The lack of dose dependency with siRNA-loaded mEVs (by electroporation) may be attributed to a complex cell response to EVs at various doses and up-regulated lysosomal activity associated with high doses [425]. The low transfection efficiency of the commercial reagent observed here may be attributed to its varying efficacy across different cell types. Despite adherence to the manufacturer's protocol regarding reagent concentration and experimental conditions, further optimization may be required for specific cell types and target nanoparticles. Previous research has demonstrated that some synthesis nanoparticles such as those modified with PEG, can outperform transfection reagents in the delivery of siRNA, leading to more effective gene silencing [426]. In addition, the decoration of transfection reagents, such as adding diINF-7 fusogenic peptide to Lipofectamine™, could significantly promote the escape of siRNA from endosomes, resulting in greater gene silencing [427]. EVs are known to facilitate efficient endosomal escape *via* fusing with the membrane of

endosomes/lysosomes in an acidification-dependent manner, leading to the release of EVs cargo to the cell cytosol [428, 429], and the cargo release efficiency is reported to be significantly higher, by an order of magnitude, compared to that from lipid nanoparticles [430]. Investigating the correlation between gene silencing efficiency and endosomal escape is valuable to be investigated in future studies. This can be assessed using a variety of techniques such as fluorescent labelling assays (with super-resolution microscopy), leakage assays or membrane lysis assays, providing insights into the mechanisms by which nanoparticles facilitate endosomal escape, directly impacting the efficacy of gene silencing [431, 432].

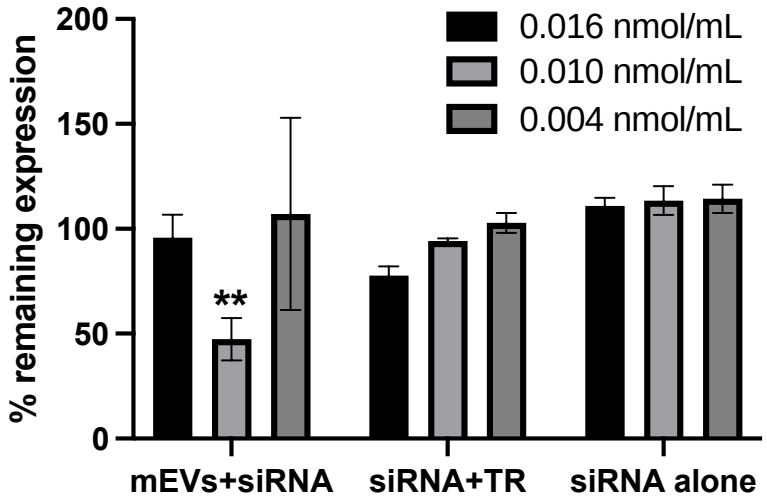

Figure 4-11. Expression levels of GAPDH in macrophages transfected with siRNA-loaded milk extracellular vesicles (mEVs) or siRNA with a commercial transfection reagent (TR), compared with siRNA alone. mEVs concentrations were 0.08, 0.05 and 0.02 mg/mL corresponding to the siRNA concentration of 0.016, 0.010 and 0.004 nmol/mL. Data are presented as mean ± SD (n=3). ** indicates $p < 0.01$ compared with siRNA+TR and siRNA alone group.

4.5. Conclusion

The work in this Chapter confirms that mEVs are highly competent at transporting across the human intestinal epithelium and this property is not compromised by their treatment in intestinal fluids (hence indicating stability). Significantly, the work introduced a novel

approach by utilizing human-derived IEOs as an intestinal epithelium model for the first time to investigate the intestinal permeability of mEVs. To overcome the obstacles associated with typical Matrigel-cultured IEOs (basal-out) application, two advanced models were developed: apical-out IEOs and IEO monolayers, which facilitate easy investigation and quantification of mEVs transport. The permeability observed across these intestinal epithelial models demonstrates the potential of mEVs as nanocarriers for delivering biotherapeutic cargo, such as siRNA, which would otherwise have poor permeability. Furthermore, these two user-friendly IEOs models can find valuable applications in assessing the intestinal permeability of various drug delivery systems. The efficient induction of gene silencing in macrophages by siRNA loaded-mEVs, as well as a clearly efficient ability to permeate the intestinal epithelium indicates the therapeutic potential of mEVs as carriers. In our recent publication, the *in vivo* study showed that administration of anti-TNFα siRNA-loaded mEVs reduced inflammation in a rat model of IBD [433]. Therefore, mEVs could act as safe systems of natural origin that could enable oral delivery of nucleic acid therapies, such as siRNA, or inform the design of synthetic delivery systems for such applications.

5. Hybrid Bovine Milk Extracellular Vesicles (hmEVs) for Oral Delivery of siRNA in IBD [incorporated publication 1]

(**Statement:** This Chapter is based in part on the previously published article:

Yunyue Zhang, Xiang Luo, Ning Ding, Mona Belaid, Maya Thanou, Driton Vllasaliu (2024). Hybrid milk extracellular vesicles as potential systems for oral delivery of siRNA. *Advanced Therapeutics*, 2300335.

Authors contributions: Yunyue Zhang (the candidate) designed the subject, performed the experiments and data analysis, wrote and revised the manuscript. Xiang Luo, Ning Ding and Mona Belaid performed part of the experiments and data analysis. Maya Thanou designed part of the subject and discussed the results. Driton Vllasaliu designed and supervised the work, wrote and revised the manuscript.)

5.1. Introduction

mEVs exhibit some desirable properties to serve as potential carriers for oral delivery of siRNA based on their safety, stability and ability to permeate the intestinal epithelium (Chapter 4). However, one of the key impediments to the clinical development of mEVs for siRNA delivery is the current lack of non-destructive methods for efficient loading of siRNA. In Chapter 3, several approaches for siRNA loading into mEVs were investigated, including the widely used electroporation method, with which we achieved a modest (~5%) loading efficiency; the use of transfection reagents, which showed up to ~25% efficiency; and saponin-mediated loading which demonstrated only ~2% efficiency. Therefore, these are all inefficient for siRNA loading and, in addition, are associated with further issues such as a potentially compromised biological activity (including their function as transport shuttles) of mEVs. Importantly, a successful siRNA response was observed despite the low loading efficiency in mEVs *via* electroporation

in Chapter 4. Therefore, there is an opportunity to improve the therapeutic response of siRNA-loaded mEVs through increasing loading efficiency.

To address these challenges, innovative strategies have been developed to improve the cargo (siRNA)-loading efficiency of mEVs. A promising approach is to achieve cargo loading through the fusion of mEVs with drug-loaded or drug-associated liposomes. Such hybrid systems (also termed 'hybridosomes') potentially merge the advantages of both mEVs and liposomes and overcome the poor siRNA loading of mEVs through the inclusion of cationic lipid(s) to facilitate complexation with or 'loading' of nucleus acids. Importantly, EVs may possess the potential for targeting macrophages, also contributing to the advantages of hybridosomes for siRNA delivery in IBD. EVs derived from serum have been observed to be specifically taken up by macrophages, rather than other phagocytes such as neutrophiles, through interactions with lectin receptors, scavenger receptors, Fc receptors, and adhesion molecules on the macrophage surface, potentially facilitating EVs endocytosis [434, 435]. *In vivo* studies also demonstrate that the predominant accumulation of mEVs in liver and spleen depends on the presence of resident macrophages in these tissues [291], and this targeted accumulation is disrupted when proteins on the mEVs surface are removed with trypsin before oral administration [436]. While the specific targeting of mEVs to macrophages and the underlying mechanisms warrant further investigation, insights from previous studies suggest a potential for mEVs to be preferentially taken up by macrophages, which is beneficial for the delivery of anti-TNFα siRNA in IBD, potentially enabling the downregulation of pro-inflammatory cytokines.

In this chapter, we report the fabrication of a new EV-liposome hybrid system for oral delivery of siRNA. The systems are engineered from the fusion by different methods and optimised ratios of mEVs and cationic liposomes. mEVs were selected for this application based on their highly desirable properties for oral drug delivery. The hybrid nanovesicles were found to

demonstrate superior stability in small intestinal simulated fluids compared to liposomes from which they originate (and similar to native mEVs), efficient association with/loading of siRNA and reduced cytotoxicity compared to cationic liposomes. Crucially, these formulations retain the intestinal epithelial barrier-crossing ability of native mEVs and induce efficient gene silencing in macrophages. Additionally, it was found that anti-TNFα siRNA loaded-hybrids delivery systems were able to downregulate TNFα and relieve inflammation in an *in vitro* co-culture model of intestinal inflammation.

5.2. Study Objectives

This Chapter aims to fabricate mEV-liposome hybrid nanovesicles for oral delivery of siRNA and investigate their potential as a therapeutic approach for IBD.

The objectives of this Chapter are:

1. To fabricate mEV-liposome hybrid nanovesicles (hybridosomes) *via* various fusion techniques to achieve high siRNA loading efficiency.
2. To investigate the stability in simulated intestinal fluids, permeability across intestinal epithelium and cytotoxicity of hybridosomes.
3. To evaluate the gene silencing of siRNA-loaded hybridosomes in a macrophage cell line.
4. To establish an *in vitro* co-culture model of intestinal inflammation and evaluate the effect of anti-TNFα siRNA-loaded hybridosomes on inflammatory response.

5.3. Methods

5.3.1. Development of siRNA-loaded hybridosomes by PEG-mediated fusion

5.3.1.1. Preparation of liposomes

Liposomes were prepared from the following lipids: 1,2-dipalmitoyl-*sn*-glycero-3-phosphocholine (DPPC); 1,2-dioleoyl-*sn*-glycero-3-phosphoethanolamine (DOPE); 1,2-distearoyl-*sn*-glycero-3-phosphoethanolamine-*N*-(7-nitro-2-1,3-benzoxadiazol-4-yl) (ammonium salt) (NBD-DSPE); and 1,2-dioleoyl-*sn*-glycero-3-phosphoethanolamine-*N*-(lissamine rhodamine B sulfonyl) (ammonium salt) (Rho-PE), with the molar ratio of 67%:30%:1.5%:1.5% [306]. All lipids were dissolved in chloroform and the preparation procedure of liposomes was conducted in the same way as that mentioned in General Methods Section 2.2.3.

5.3.1.2. Preparation of hybridosomes by PEG-mediated fusion

Liposomes and mEVs were mixed in a 1.5 mL Eppendorf tube, with the total volume of reaction mixtures of 500 μL (PBS buffer). The final concentration of added PEG-8000 ranged from 2.5% to 30% (w/v). Various ratios of liposomes to mEVs (w/w), as well as incubation temperatures and times, were employed to optimise (increase) the fusion efficiency. Fusion was determined by a FRET based-assay (described at the Results and Discussion Section) and the fusion efficiency was normalized using the following **Equation 5-1** [306]:

$$NBD\ fluorescence\ increase\ (\%) = [NBD - Min(NBD)]/[Max(NBD) - Min(NBD)] \quad \textbf{(5-1)}$$

Where the Min(NBD) is the lowest NBD fluorescence signal value form all time points, and the Max(NBD) is the NBD fluorescence signal when the fusion reaction was stopped by the addition of 10 μL *n*-Dodecyl-*β*-D-maltoside (DDM) to solubilize all liposomes (therefore NBD is free without FRET).

5.3.1.3. Transport and uptake of PEG-fused hybridosomes in Caco-2 monolayers

The comparison of transport and cell uptake of mEVs, liposomes and PEG-mediated hybridosomes in Caco-2 monolayers was tested following the same steps as General Methods Section 2.2.5.2, where the concentration of mEVs and liposomes samples was 0.05 mg/mL (concentration of protein and lipids, respectively), and hybridosomes (with the ratio of liposomes:mEVs 1:9) was 0.045 mg/mL (concentration of protein). mEVs sampled basolateral solution were quantified by fluorescence using a plate reader (excitation 565 nm; emission 615 nm). Liposomes and hybridosomes were quantified by Rhodamine fluorescence with excitation wavelength of 530 nm and emission wavelength of 588 nm.

5.3.2. Preparation of hybridosomes by freeze-thaw mediated fusion

5.3.2.1. Preparation of cationic liposomes

Cationic liposomes were prepared using the following lipids: *N',N'*-dioctadecyl-*N*-4,8-diaza-10-aminodecanoylglycine amide (DODAG), 1,2-Dioleoyl-*sn*-glycero-3-phosphocholine (DOPC), cholesterol, 1,2-distearoyl-*sn*-glycero-3-phosphoethanolamine-*N*-[methoxy(polyethylene glycol)-2000] (ammonium salt) (18:0 PEG2000 PE), 1,2-distearoyl-*sn*-glycero-3-phosphoethanolamine-*N*-(7-nitro-2-1,3-benzoxadiazol-4-yl) (ammonium salt) (NBD-DSPE) and 1,2-dioleoyl-*sn*-glycero-3-phosphoethanolamine-*N*-(lissamine rhodamine B sulfonyl) (ammonium salt) (Rho-PE). All lipids were dissolved in chloroform except, DODAG, which was dissolved in a mixture of chloroform/methanol (1:1; v/v).

DODAG was prepared as before [437]. All the lipids were added to a round bottom flask with the molar ratio of 20:57:20:1:1:1 or 50:27:20:1:1:1 for DODAG:DOPC:cholesterol:PEG2000 PE:NBD-DSPE:Rho-PE. The following preparation procedure of liposomes was conducted in the same way as that mentioned in General Methods Section 2.2.3.

5.3.2.2. Preparation of siRNA-loaded liquid nitrogen (LN2) freeze-thaw hybridosomes

mEVs were mixed with liposomes at different ratios (w/w) and the mixtures were frozen in liquid nitrogen (LN2) and thawed by sonication at 37 ℃ for ~5 minutes; the cycle was repeated 10 times. After preparation of positively charged LN2 freeze-thaw hybridosomes, negatively charged siRNA (0.1 nmol/150 μg hybridosomes) was added and incubated at 37 ℃ for 20 min to form siRNA-loaded LN2 hybridosomes. After encapsulation of siRNA into hybridosomes, the unencapsulated siRNA was removed by centrifugal ultrafiltration with 100 kDa Amicon Ultra-0.5 Centrifugal Filter Unit (Merck, Dorset, UK) by four sequential centrifugations for 10 min each at 10,000 × rpm. 500 μL of HEPES buffer was added between each spin to wash the remaining unencapsulated siRNA. After the recovery of siRNA encapsulated-hybridosomes, the unencapsulated Cyanine 5 fluorescent siRNA in HEPES buffer was quantified by plate reader with Ex/Em: 640 nm/676 nm. The encapsulation efficiency of Cyanine 5 fluorescent siRNA into hybridosomes was calculated by **Equation (5-2)**:

$$\%\ encapsulation\ efficiency = 100 \times \frac{amount\ of\ added\ siRNA - amount\ of\ unencapsulated\ siRNA}{amount\ of\ added\ siRNA} \quad (5-2)$$

5.3.2.3. Preparation of siRNA-loaded -80℃ freeze-thaw hybridosomes

37.5 μg cationic liposomes in 250 μL HEPES buffer were mixed with 0.15 nmol siRNA and incubated at 37 ℃ for 20 minutes. Thereafter, different amounts (protein content) of mEVs:

9.4 µg (liposomes:mEVs 4:1 (w/w)), 18.8 µg (liposomes:mEVs 2:1), 75 µg (liposomes:mEVs 1:2), 112.5 µg (liposomes:mEVs 1:3), 150 µg (liposomes:mEVs 1:4) and 187.5 µg (liposomes:mEVs 1:5) in 250 µL HEPES buffer were added into the siRNA-loaded liposomes and incubated at room temperature for 30 min. Then, the mixtures were frozen at -80 ℃ and thawed at 37 ℃ (incubator) for ~10 minutes. The cycle was repeated 5 times and fusion was established by the FRET assay. After preparation of siRNA-loaded -80 ℃ freeze-thaw hybridosomes, unencapsulated siRNA was removed, and encapsulation efficiency was calculated as mentioned at Section 5.3.2.2. The size, PdI and surface charge (Zeta-potential) of liposomes and hybridosomes were measured by Malvern Zetasizer (Malvern, UK).

5.3.3. Toxicity assay of mEVs, liposomes and hybridosomes

The 3-(4,5-dimethylthiazol-2-yl)-5-(3-carboxymethoxyphenyl)-2-(4-sulfophenyl)-2H-tetrazolium (MTS) assay (CellTiter 96® AQueous One Solution Assay, Promega, Madison, WI, USA) was used to evaluate the toxicity of mEVs, liposomes and hybridosomes in undifferentiated Caco-2 cells. Briefly, Caco-2 cells were seeded on 96-well plates at 10^5 cells/mL (100 µL/well) and cultured at 37°C/5% CO_2 atmosphere for 24 h. Thereafter, mEVs, liposomes and hybridosomes were suspended at different concentrations in Opti-MEM medium, and the culture medium of Caco-2 cells was replaced with these samples. Opti-MEM medium was used as a negative control group and Triton X-100 (1% v/v in Opti-MEM medium) as a positive control. After incubation with samples and controls for 4h or 48 h, Caco-2 cells were washed with PBS and 100 µL/well of opti-MEM medium was added, followed by 20 µL/well of MTS reagent and incubated for 4 h at 37°C/5% CO_2 atmosphere. After incubation, the absorbance at 492 nm was measured by a plate reader. The relative metabolic activity (%) was calculated using **Equation (5-3)**:

$$\%\ Relative\ metabolic\ activity = 100 \times \frac{S - T}{Blank - T} \qquad (5-3)$$

where S is the absorbance of samples, T is the absorbance of Triton X-100, and Blank is the absorbance of the blank (culture medium) group.

5.3.4. Stability of hybridosomes in simulated intestinal fluids

FaSSIF and FeSSIF were prepared according to the manufacturer's instructions. The intestinal digestion process was simulated as follows: 100 µL of mEVs, liposomes and hybridosome suspensions at 1 mg/mL protein or lipid concentration were incubated in 400 µL of SIFs at 37°C with light shaking for 1.5 hours. After digestion, nanoparticles were recovered *via* centrifugal ultrafiltration with 100 kDa Amicon Filter Unit by four sequential centrifugations for 10 minutes each at 10,000 × rpm. 500 µL of HEPES buffer was added between each spin to wash off the remaining debris from the digestion solutions. Finally, digested nanoparticles were resuspended in 200 µL HEPES and used for downstream characterization.

To determine the membrane stability of mEVs, liposomes and hybridosomes following *in vitro* digestion, we used DPH as a fluorescent probe that is highly fluorescent in a lipid environment (such as that of mEVs, liposomes or hybridosome membranes), but is associated with a significant loss of fluorescence signal when present in an aqueous environment [438]. DPH was dissolved in dimethylformamide (DMF) to form a stock solution. Nanoparticles were diluted to a concentration of 0.50 mg/mL (protein and/or lipid concentration) and stained with 2.3 µM of DPH by incubating for 40 minutes at room temperature under gentle shaking in the dark. SSIFs were prepared as described above, and 100 µL of stained sample suspensions were exposed to SSIFs for 1.5 h in the dark at 37°C under gentle shaking. Thereafter, stained nanoparticles were recovered by ultrafiltration and resuspended in HEPES buffer as mentioned above. The fluorescence signal of the recovered nanoparticles was measured by a plate reader at excitation and emission wavelengths of 360 nm and 430 nm, respectively. Control

experiments were carried out under the same conditions, with replacement of SSIFs by PBS buffer (negative control) and SDS (1% w/v) as a known membrane-disrupting agent.

5.3.5. Transport of siRNA-loaded mEVs and hybridosomes across Caco-2 monolayers

To determine the transport of siRNA loaded-mEVs and siRNA-associated hybridosomes, 500 µL of fluorescent (Cy5) siRNA (ALLSTARS NEG. SIRNA AF 647, Qiagen, MD, USA) alone, and siRNA loaded-mEVs (using electroporation), siRNA-associated LN2 freeze-thaw hybridosomes, and siRNA-associated -80℃ freeze-thaw hybridosomes at 0.05 mg/mL concentration were added to the apical side of Caco-2 monolayers for 3 h. The culture of Caco-2 monolayers and transport process were the same as that detailed in Section 2.2.5.2.

5.3.6. Transfection efficiency of GAPDH siRNA-loaded mEVs and hybridosomes in Caco-2 cells and macrophages

Caco-2 cells were seeded at 3000 cells/well (96-well plate) and cultured for 48h prior to transfection. GAPDH siRNA-loaded mEVs, hybridosomes, and liposomes were diluted to 0.08 mg/mL and 0.05 mg/mL with Opti-MEM Medium and incubated with cells for 48 hours at 37 °C and 5% CO_2 atmosphere. After incubation, GAPDH activity was measured by the KDalert™ GAPDH Assay Kit according to the manufacturer's instructions. Negative siRNA loaded-nanoparticles were applied as a negative control group, and GAPDH siRNA transfected with a commercial transfection reagent (X-tremeGENE™ 360 Transfection Reagent, 2.5 µl/mL) was applied as a positive control group. The % remaining GAPDH gene expression was calculated using **Equation (5-4)**:

$$\%\, remaining\ expression\ = 100 \times \frac{\Delta fluorescence\ of\ GAPDH}{\Delta\ fluorescence\ of\ Negative} \qquad (5-4)$$

Where Δ*fluorescence of GAPDH* and Δ*fluorescence of Negative* are fluorescence increases within 4 min for samples and negative control group, respectively.

To evaluate the transfection efficiency of delivery systems in macrophages, J774A.1 macrophage cells were seeded on 96-well plates at 5000 cells/well and cultured for 24 hours to ~50% confluence. GAPDH siRNA loaded-hybridosomes (LN2 freeze-thaw formulation) and siRNA loaded-liposomes (150 μg of cationic liposomes mixed with 0.1 nmol siRNA at 37 ℃ for 20 min), were diluted to 0.05 mg/mL and 0.02 mg/mL with Opti-MEM medium and incubated with cells for 5 hours at 37 °C and 5% CO_2 atmosphere. Thereafter, the samples were replaced with the cell culture medium and incubated for another 43 hours. GAPDH siRNA loaded-hybridosomes (-80 ℃ freeze-thaw formulation) were diluted to 0.08 mg/mL and 0.05 mg/mL with Opti-MEM medium and incubated with cells for 48 hours. After incubation, GAPDH activity was measured by the same process as in Caco-2 cells.

5.3.7. Effect of anti-TNFα siRNA-loaded mEVs and hybridosomes on inflammation in an in vitro co-culture model of intestinal inflammation

To develop an *in vitro* co-culture model of intestinal inflammation, Caco-2 cells were cultured on 12-well Transwell inserts (3 μm pore size; polycarbonate) for 21 days to differentiate into monolayers. Macrophages (J774A.1) were seeded on a 12-well plate at a seeding density of 0.5 × 10^5 cells/mL (1.5 mL/well) and cultured for 24 h. Thereafter, the inserts supporting Caco-2 monolayers were combined with plates seeded with macrophages, and 100 ng/mL LPS was added to the basolateral sides (i.e. to macrophages) to induce inflammation. After 24 h of inflammation stimulation, anti-TNFα siRNA-loaded formulations (including 0.05 mg/mL mEVs, 0.08 mg/mL -80°C freeze-thaw hybridosomes, and 0.05 mg/mL LN2 freeze-thaw hybridosomes) were added to the apical side (i.e. Caco-2 monolayers). The same concentrations of formulations loaded with negative siRNA were applied as negative controls. At the same time, 0.05 mg/mL untreated isolated mEVs without siRNA were also added to the

apical side to evaluate the efficiency of inflammation relief. Cells exposed to the same cell conditions but without the addition of formulations were used as control groups to monitor the inflammation induction from macrophages by LPS ('blank with LPS group') and without LPS ('blank without LPS group'). The samples (100 μL per well) were collected from basolateral sides at 0 h, 24 h, and 48 h after adding the formulations and replaced with 100 uL of fresh culture medium. TNFα in the collected samples was quantified using a RayBio® Mouse TNF-alpha ELISA Kit (RayBiotech Life, Inc. Peachtree Corners, GA, USA) according to the manufacturer's instructions.

5.4. Results and Discussion

5.4.1. Development of siRNA loaded-hybridosomes via PEG-mediated fusion

PEG has previously been applied to facilitate cell-cell membrane fusion based on the mechanism of dehydration and promoting close contact of lipid bilayer structures [439, 440]. Briefly, PEG is a swollen and highly hydrated polymer which is excluded from a region near the lipid bilayer based-vesicle surfaces [441]. This results in a creation of a region involving high-activity water, which is an unfavorable thermodynamic state. Consequently, the vesicles will tend to aggregate to reduce the area containing high-activity water [441]. Therefore, this osmotic pressure drives bilayers into close contact and fusion happens under suitable conditions of temperature and incubation time.

We initially synthesized the liposomes using the formulation of DPPC:DOPE:NBD-DSPE:Rho-PE in a molar ratio of 67%:30%:1.5%:1.5%. This formulation was derived from a previous report where it had been successfully applied for fusion with EVs [306]. The liposomes exhibited a size of 142.3 ± 2.4 nm, along with a desirable PdI of 0.125 ± 0.042, which indicated a favourable diameter and a good level of particle polydispersity.

In order to monitor the fusion of liposomes with mEVs, fluorescence resonance energy transfer (FRET) assay was applied here (**Figure 5-1**). Briefly, two types of fluorescent lipids: NBD-DSPE (Excitation wavelength/Emission wavelength (Ex/Em): 460nm/530nm) and Rho-PE (Ex/Em: 530nm/588nm) were introduced into the liposomes. Upon excitation at 460 nm of NBD-DSPE, part of their emission light (530 nm) would be absorbed by Rho-PE as excitation light to emit at 588 nm. Therefore, when the distance between NBD-DSPE and Rho-PE is increased, which would happen upon membrane fusion with mEVs, the emission fluorescence intensity at 530 nm of NBD-DSPE would be increased and the fluorescence intensity at 588 nm of Rho-PE would be decreased.

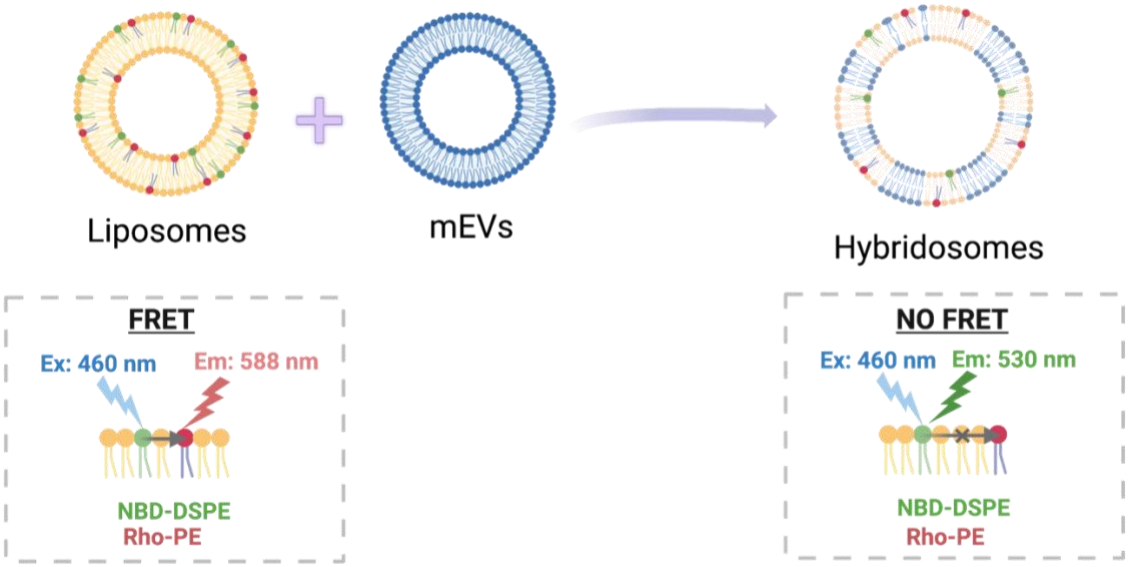

Figure 5-1. Schematic of fluorescence resonance energy transfer (FRET)-based lipid mixing assay to monitor the fusion of liposomes with bovine milk extracellular vesicles (mEVs).

To increase the fusion efficiency of liposomes with mEVs, various factors which could potentially affect the fusion process were subjected to optimisation. The effects of PEG-8000 presence and the ratio of liposomes to mEVs on fusion were investigated first. As shown in **Figure 5-2A**, without PEG-8000, the fusion of liposomes with mEVs at different ratios was largely absent (no NBD fluorescence increase). In contrast, in the presence of 15% (w/v) PEG-

8000, a significant increase of the NBD fluorescence signal was observed when the ratio of liposomes to mEVs amounted to 1:9. This indicates an efficient fusion between liposomes and mEVs at this ratio (**Figure 5-2B**). In the optimization process, the liposome control group, which serves as the source of fluorescence, was excluded due to the negligible impact of the experimental conditions on the inherent fluorescence of the liposomes themselves [306]. The size of hybridosomes obtained under this fusion condition was larger than 1000 nm and the PdI was exceeded 0.5 (measured by DLS), indicating aggregation of particles. As reported by previous research, aggregation can be attributed to PEG, since when the final hybridosome suspension was diluted by 10,000-fold (resulting in a final PEG concentration of 0.001%), the size of the vesicles was observed to increase only slightly and the aggregation was considered potentially reversed [306]. Therefore, to investigate the reversibility of our hybridosomes aggregation, the final solution after fusion was diluted with 1000-fold (with the final PEG concentration of 0.015%) and 10,000-fold (final PEG concentration of 0.0015%), and their size distribution was measured by NTA. As shown in **Figure 5-3**, some particles with sizes exceeding 300 nm were found in the sample diluted to 0.015% PEG **(Figure 5-3A)**, and these larger-sized particles were less apparent in the sample diluted to 0.0015% PEG **(Figure 5-3B)**, which was consistent with the previous report [306]. This result confirmed the reversibility of the hybridosome aggregation post-fusion, and the key point to address the issue of aggregation is to reduce/exclude PEG in the final solution.

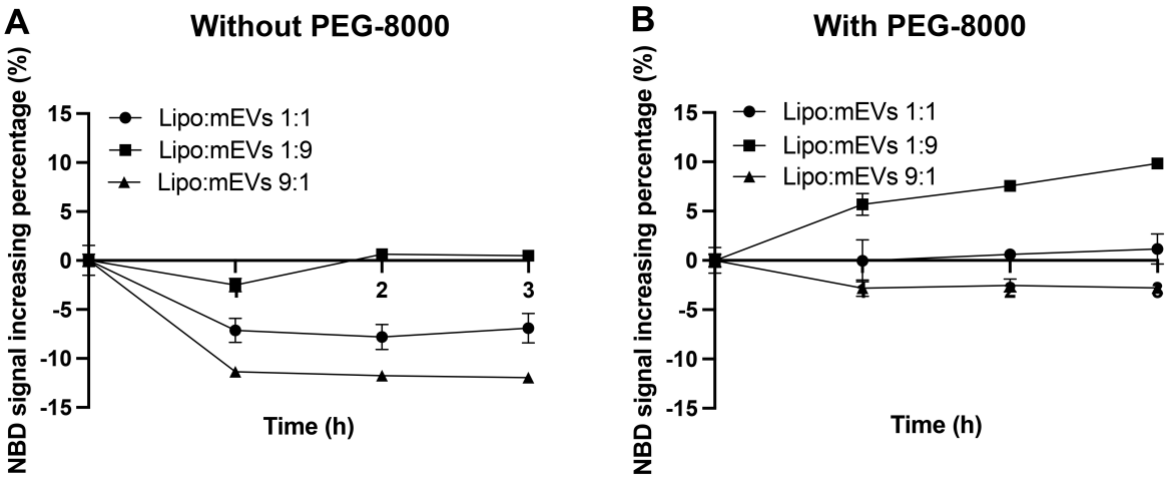

Figure 5-2. NBD fluorescence in liposomes (Lipo) after fusion with bovine milk extracellular vesicles (mEVs) using different ratios of Lipo:mEVs (w/w) in the absence (A) and presence (B) of 15% (w/v) PEG-8000 in solution. Data shown as the mean ± SD (n = 3).

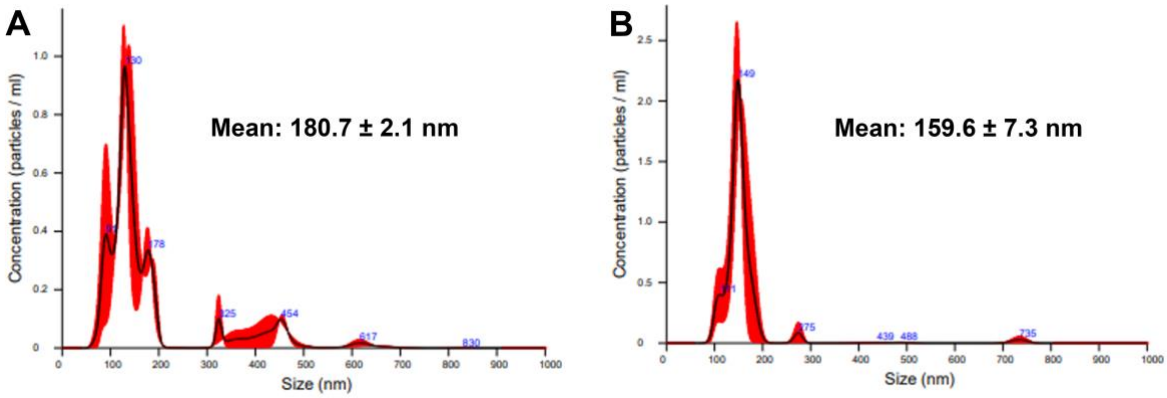

Figure 5-3. Nanoparticle Tracking Analysis (NTA) analyze of hybridosomes fused by liposomes with bovine milk extracellular vesicles (mEVs) using the ratio of Liposomes:mEVs with 1:9 (w/w) in presence of 15% (w/v) PEG-8000 in solution. Final hybridosomes samples were diluted by 1000-folds (with the final PEG concentration of 0.015%) **(A)** and 10,000-folds (with the final PEG concentration of 0.0015%) **(B)**.

To address the aggregation in the final hybridosome suspension we applied sonication. However, despite prolonged sonication (exceeding 30 minutes), the size of the hybridosomes

remained above 800 nm. Therefore, while PEG is a clear mediator of fusion between mEVs and liposomes, it is also the underlying cause of aggregation. Employing a 0.2 μm filter is also inapplicable here, as it would result in the loss of most target aggregated hybridosomes which should be collected, and this approach does not effectively remove PEG. Therefore, either excluding PEG from the final formulation or reducing its concentration is considered as the key point to address aggregation.

Several methods were attempted to exchange the solution buffer and therefore remove PEG. Ultrafiltration with 100 kDa Amicon Ultra-0.5 Centrifugal Filter Unit was one of the methods. This was conducted by four sequential centrifugations for 10 minutes each at 10,000 × rpm, and 500 μL of PBS was added between each spin to wash off extra PEG. Following the washing step, the size of the resulting hybridosomes was measured as 272.0 ± 0.8 nm with the PdI of 0.282 ± 0.010. The results indicated the effective removal of PEG and a significantly reduction in hybridosomes size. However, the size of hybridosomes after washing step was still higher than our target (< 200 nm).

qEV column based on SEC is another technique used in this work to purify hybridosomes and remove PEG. After the collection of sample fractions, the average size of hybridosomes was measured as 281.1 ± 19.5 nm with PdI of 0.309 ± 0.045. This result indicated the lack of efficiency in removing most/all the PEG through qEV column (SEC). Therefore, the combination of these two methods (ultrafiltration and SEC) was considered to potentially remove PEG more efficiently, and the results showed that combining four sequential centrifugation of ultrafiltration following SEC could reduce the size of hybridosomes to 241.8 ± 3.28 nm with the PdI of 0.267 ± 0.003 (significantly smaller than the size of hybridosomes with SEC purification only). It was considered that this is an acceptable hybridosome size at this stage, despite being slightly larger than our target size of under 200 nm for oral delivery system as detailed in Section 3.4.2.3. Particles smaller than 300 nm are still capable of uptake

by enterocytes [350], although their transport efficiency may be modestly hindered within the intestinal mucus [103].

To achieve higher fusion efficiency, various PEG-8000 concentrations, different fusion incubation time and temperature, and various liposomes to mEVs ratios were optimised (**Figure 5-4**). As shown in **Figure 5-4A**, fusion was scarcely observed, as indicated by the NBD fluorescence, when PEG 8000 concentrations were 2.5% and 7.5% (with liposomes to mEVs ratio of 1:9 w/w and incubated at 37°C), while the fusion efficiency was significantly increased with higher PEG-8000 concentration (15% and 30%). However, with 30% PEG concentration, the high concentration of PEG residue in the final formulation presented challenges in removal through the combined purification method (ultrafiltration plus SEC as mentioned above), and the final size of hybridosomes was measured as 358.9 ± 11.3 nm with PdI of 0.416 ± 0.006, indicating existence of aggregations in final formulation.

Different incubation temperature is expected to impact the collision speed of nanoparticles and may affect the fusion efficiency. In this study, the higher incubation temperature significantly increased the fusion efficiency during the first 3 hours of incubation (**Figure 5-4B**). However, after 12 hours incubation, the fusion efficiency at 37°C incubation was the same as that at 40°C incubation, which indicated that the longer incubation time may offset the effect of temperature. Increasing mEV portion in the mixture solution improved the fusion to a certain degree, but there is no significant difference between the liposome to mEV ratio of 1:9 and 1:15 (**Figure 5-4C**).

Therefore, the fusion conditions of 15% PEG-8000 at 1:9 (w/w) liposome to mEV ratio under incubation of 37°C and 12 hours, were chosen for downstream application.

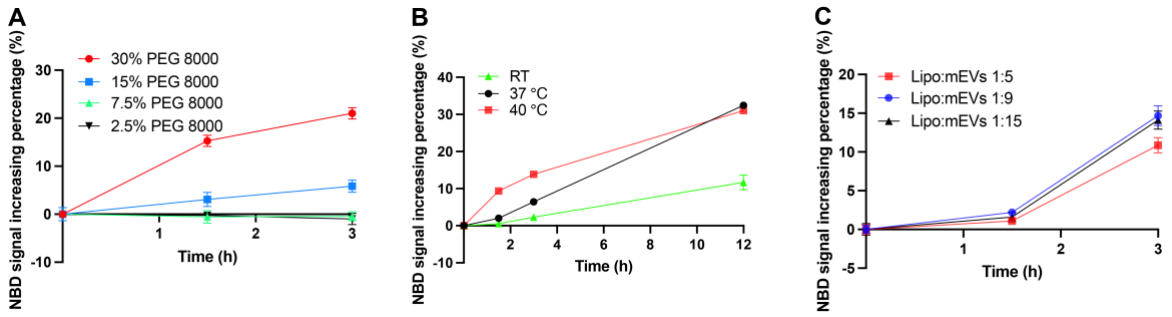

Figure 5-4. Optimization of fusion conditions of liposomes with bovine milk extracellular vesicles (mEVs). (A) Different PEG-8000 concentrations (w/v) in the mixture solution with liposomes to mEVs ratio of 1:9 (w/w) incubated under 37°C. **(B)** Different fusion incubation temperatures with liposomes to mEVs ratio of 1:9 (w/w) and 15% PEG 8000 in mixture solution. **(C)** Different liposomes (Lipo) to mEVs ratios with incubation temperature of 37°C and 15% PEG 8000 in solution. RT: room temperature. Data shown as the mean ± SD (n = 3).

It is important to note here that the fusion was monitored by the percentage change of NBD fluorescence, which relies on the distance of lipids in liposomes. Consequently, a higher mEV proportion for fusion would lead to a greater distance of these lipids, resulting in a seemingly "higher" fusion efficiency. However, it became evident that these changes in percentage of NBD fluorescence did not accurately represent the true fusion efficiency. Therefore, the aim of hybridosome fabrication is to harness the benefits of both mEVs and liposomes effectively instead of pursuing "higher" fusion efficiency, and a balance should be kept with adjusting the hybridosomes' composition such as higher liposomes proportion to attain a positive surface charge and maintaining a specific percentage of mEVs to ensure the permeability through intestinal epithelium. In subsequent investigations, the fluorescent changes of NBD and Rhodamine were chosen instead of the NBD fluorescence signal increasing percentage to monitor the fusion process (confirm the fusion happened). The optimisation of hybridosome formulation should also be based on the physiochemical properties of the resulting systems

such as size, surface charge, the encapsulation efficiency for siRNA, and their bioactivities including the stability in intestine and permeability through intestinal epithelium, etc.

The transport of PEG-mediated hybridosomes across Caco-2 monolayers was investigated to evaluate if the hybridosomes could retain the permeability from mEVs. As shown in **Figure 5-5A,** the transport of mEVs was significantly higher than that of liposomes and hybridosomes, where approximately 5% of mEVs could transport through the monolayers after 3-hour incubation. The intestinal permeation of hybridosomes is higher than that of liposomes (~ 1% versus 0% after 3-hour incubation), which indicated the remaining bioactivity from mEVs in the systems. However, the lower transport percentage compared with mEVs alone indicated that the bioactivity of mEVs in hybridosomes was somewhat compromised upon fusion with liposomes. **Figure 5-5B** showed the Caco-2 cell uptake of mEVs, liposomes and hybridosomes, where there was no significant difference among them. The considerable variability in mEVs uptake may be attributed to the heterogeneity of mEVs isolated from different batches, as discussed in Section 3.4.1.2.

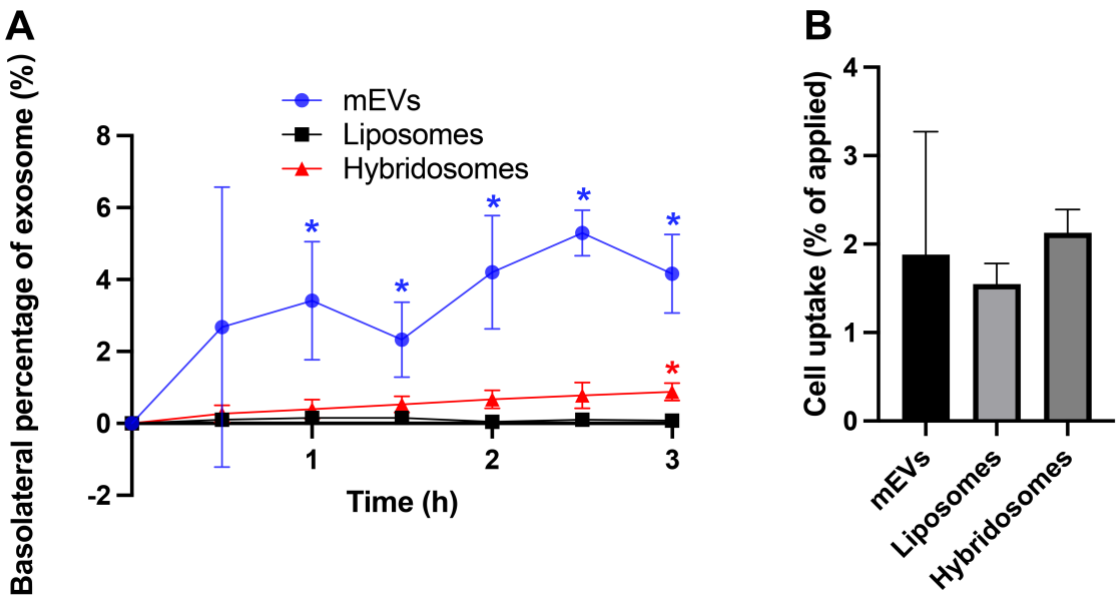

Figure 5-5. Transport and uptake of milk extracellular vesicles (mEVs), liposomes and hybridosomes mediated by PEG-8000 in intestinal Caco-2 monolayers. (A) Transport across differentiated Caco-2 monolayers. **(B)** Uptake in differentiated Caco-2 cells (3-hour incubation). Data shown as the mean ± SD (n=4). * in blue indicates $p < 0.05$ between mEVs and the other two groups, * in red indicates $p < 0.05$ between hybridosomes and liposomes group.

Following the generation of hybridosomes *via* PEG-mediated fusion, an effort was made to encapsulate siRNA. However, the high proportion of mEVs in the hybridosomes (liposomes:mEVs 1:9) resulted in a negative surface charge for the hybridosomes, even with the introduction of cationic liposomes, such as liposomes formulated with DODAG lipids (formulation detailed in Section 5.4.2.1). This negative charge of hybridosomes prevented the association of negatively charged siRNA with the systems *via* electrostatic interaction. Therefore, to address this challenge, as well as the PEG-mediated aggregations mentioned above, alternative fusion methods and formulations to combine mEVs and liposomes should be explored to develop hybridosomes as siRNA carriers.

5.4.2. Development of siRNA loaded-hybridosomes by liquid nitrogen (LN2) and -80°C freeze-thaw cycles

5.4.2.1. Synthesis of cationic liposomes

To prepare cationic liposomes, the cationic lipid *N',N'*-dioctadecyl-*N*-4,8-diaza-10-aminodecanoylglycine amide, known as DODAG, was introduced. DODAG has a cationic head group which is same as a commercially available cationic lipid named CDAN, and a different lipophilic tail which is composed of disteroyl lipidic chains instead of a cholesterol group (**Figure 5-6**) [437]. The cationic liposomes mediated by DODAG were found to have lower *in vitro* cellular toxicity and higher transfection efficiency of siRNA in different cell lines [437]. The formulation optimisation of cationic liposomes was carried out using DODAG, and helper lipids (1,2-Dioleoyl-sn-glycero-3-phosphocholine (DOPC) and cholesterol. The geometry structure of DOPC lipids is more cylindrical allowing smaller liposomes size [442]. Cholesterol was included due to its property of stabilising lipid layers and protecting the liposomes from disruption of surface-adsorption of plasma [442]. The aim of including PEG (18:0 PEG2000 PE) is to increase the polydispersity.

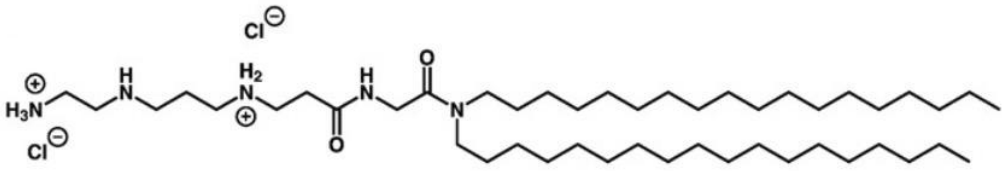

Figure 5-6. Chemical structure of *N',N'*-dioctadecyl-*N*-4,8-diaza-10-aminodecanoylglycine amide (DODAG) lipid.

Two formulations of cationic liposomes were synthesized in this study. The lipid components and ratios are shown in **Table 5-1**. 20% of cationic lipid (DODAG) was applied to form liposomes initially, but subsequently a higher concentration of 50% DODAG was also included

to introduce a more positive charge in hybridosomes. NBD-DSPE and Rho-PE were also applied here to confirm the successful fusion of mEVs with liposomes into hybridosomes. The characterization of these two formulations is summarized in **Table 5-2**. With the lipid film hydration method of preparation of liposomes, both of the low DODAG and high DODAG liposome formulations showed small sizes (<160 nm) and good polydispersity. The formulation with a high DODAG concentration (50%) demonstrated a higher surface charge (Zeta-potential of 43.3 mV) compared with low DODAG formulation, which indicated that increasing the proportion of cationic lipids resulted in an increased liposome surface charge. Therefore, in order to introduce more positive charge in hybridosomes to facilitate the association with negatively charged siRNA, the high DODAG concentration (50%) formulation was used for downstream application.

Table 5-1. Two formulations of cationic liposomes.

Lipid composition (Molar ratio)	**Low DODAG (20%) content liposomes**	**High DODAG (50%) content liposomes**
DODAG [a)]	**20%**	**50%**
DOPC [b)]	57%	27%
Cholesterol	20%	20%
PEG2000-PE [c)]	1%	1%
NBD-DSPE [d)]	1%	1%
Rho-PE [e)]	1%	1%

[a)] DODAG: *N′,N′*-dioctadecyl-*N*-4,8-diaza-10-aminodecanoylglycine amide; [b)] DOPC: 1,2-Dioleoyl-sn-glycero-3-phosphocholine; [c)] PEG2000-PE: 1,2-distearoyl-sn-glycero-3-phosphoethanolamine-N-[methoxy(polyethylene glycol)-2000] (ammonium salt) (18:0); [d)] NBD-DSPE: 1,2-distearoyl-sn-glycero-3-phosphoethanolamine-N-(7-nitro-2-1,3-benzoxadiazol-4-yl) (ammonium salt); [e)] Rho-PE: 1,2-dioleoyl-*sn*-glycero-3-phosphoethanolamine-*N*-(lissamine rhodamine B sulfonyl) (ammonium salt).

Table 5-2. Characterization of cationic liposomes prepared by two formulations.

Parameters	**Low DODAG (20%) content liposomes**	**High DODAG (50%) content liposomes**
Size (nm)	158.9 ± 3.3	145.1 ± 0.89
PdI [a)]	0.148 ± 0.006	0.202 ± 0.027
Zeta-potential (mV)	31.2 ± 1.00	43.3 ± 0.21

[a)] PdI: polydispersity index. Data shown as the mean ± SD (n=3).

5.4.2.2. Development of siRNA-loaded liquid nitrogen (LN2) freeze-thaw hybridosomes

The preparation of novel siRNA-loaded hybridosomes by two separate approaches is shown in **Figure 5-7**. **Figure 5-7A** shows the preparation process of liquid nitrogen (LN2) freeze-thaw hybridosomes. We initially used a liposome to mEV ratio of 1:4 (w/w) (250 µL 0.075 mg/mL of liposomes and 250 µL 0.3 mg/mL mEVs). After mixing the liposome and mEV suspensions and subjecting the mixture to repeated freeze-thaw cycles, the fluorescent signal of NBD-DSPE increased and the signal of Rho-PE decreased (**Figure 5-8**), which indicated that the fluorescent lipids within liposome bilayers were diluted by the fusion with mEVs and the distance of NBD-DSPE to Rho-PE increased. However, the surface charge (Zeta-potential) of this hybridosome formulation was measured as negative (-24.8 ± 1.81 mV), which could not be used for electrostatic association with negatively charged siRNA. Therefore, different ratios of liposomes to mEVs (w/w) were attempted for the preparation of hybridosomes with a positive charge and a diameter below 200 nm. **Table 5-3** shows that when the liposome:mEV ratio decreased to 1.5:1 and 1:1 the size of hybrid vesicles became larger and when ratio was 1:1, the Zeta-potential of hybridosomes decreased to negative. Therefore, to obtain a higher mEV portion in positively charged hybridosomes with an acceptable diameter, we selected the 2:1

liposome:mEV ratio as the final ratio to prepare LN2 freeze-thaw hybridosomes. In addition to size, Zeta-potential and PDI, which were assessed in this study, other nanoparticle characteristics-specifically the fluidity of hybridosomes-warrant consideration for oral drug delivery systems in the future study. The fluidity, influenced by the lipid composition resulting from varying liposome to mEV ratios, could affect their stability and interactions with multiple biological systems such as barrier penetration [443-445]. Importantly, fluidity affects their ability to undergo structural transformations that facilitate membrane fusion and disruption, thereby enabling the release of therapeutic cargo into the cell cytoplasm [446]. Furthermore, while the hybridosomes retained a spherical shape, the morphology of nanoparticles can also influence their biological interactions [349].

After preparation of positively charged LN2 freeze-thaw hybridosomes with a liposome:mEV ratio of 2:1, siRNA was added to the hybridosome suspension and ultrafiltration was applied to remove unloaded siRNA. The final loading efficiency was calculated as 86.9%. After loading of siRNA, the diameter of the hybridosome-siRNA complexes increased to 179.8 ± 0.85 nm, and the Zeta-potential was 17.2 ± 0.27 mV, which was lower than that of the hybrid vesicles without siRNA.

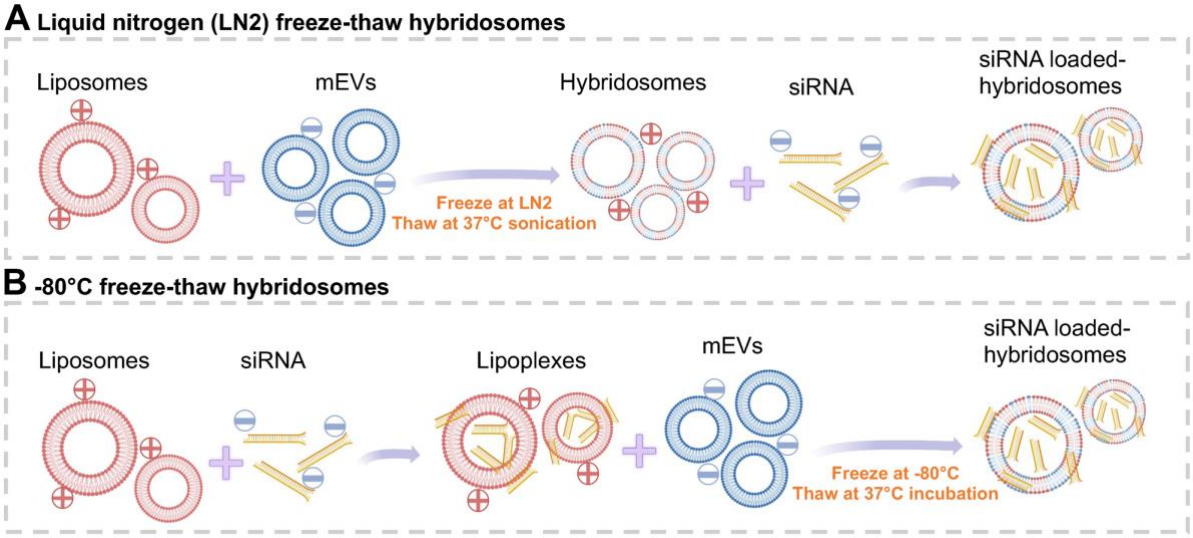

Figure 5-7. Schematic of siRNA loaded-hybridosomes preparation by fusion of bovine milk extracellular vesicles (mEVs) with cationic liposomes. (A) Preparation of siRNA loaded-liquid nitrogen (LN2) freeze-thaw hybridosomes. **(B)** Preparation of siRNA loaded (-80°C freeze-thaw) hybridosomes.

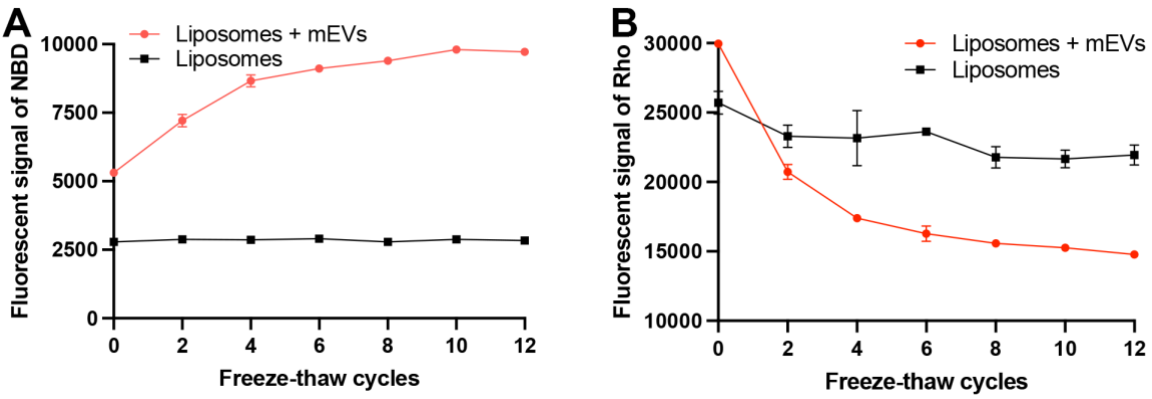

Figure 5-8. Relationship between the number of freeze-thaw cycles with fluorescent signal of liposomes. **(A)** Fluorescent signal of NBD-DSPE with excitation of 460 nm and emission of 530 nm. **(B)** Fluorescent signal of Rho-PE with excitation of 460 nm and emission of 588 nm. The Red line represents the fluorescent signal of liposomes when they were fused with bovine milk extracellular vesicles (mEVs) by liquid nitrogen (LN2) freeze-thaw cycles with liposomes:mEVs ratio of 1:4 (w/w), and the black line represents the fluorescent signal of liposomes alone with the same freeze-thaw condition. Data shown as the mean ± SD (n = 3).

Table 5-3. Characterization of hybridosomes prepared by liquid nitrogen (LN2) freeze-thaw cycles with different liposome to bovine milk extracellular vesicles (mEVs) ratio (w/w).

	6:1	**3:1**	**2:1**	**1.5:1**	**1:1**	**1:4**
Size (nm)	193.9 ± 2.8	130.1 ± 1.48	166.4 ± 3.04	297.9 ± 5.37	1488 ± 214	147.6 ± 0.83
PdI[a)]	0.214 ± 0.003	0.203 ± 0.007	0.125 ± 0.089	0.195 ± 0.013	0.639 ± 0.145	0.211 ± 0.016
Zeta-potential (mV)	22.0 ± 1.04	20.6 ± 0.79	21.4 ± 0.40	24.0 ± 0.59	-3.20 ± 0.61	-24.8 ± 1.81

[a)] PdI: polydispersity index. Data shown as the mean ± SD (n=3).

5.4.2.3. Development of siRNA-loaded -80°C freeze-thaw hybridosomes

The second approach used the for formulation of siRNA-loaded hybridosomes involved freeze-thaw cycles at -80 °C (**Figure 5-7B**). Briefly, negatively charged siRNA was complexed with cationic liposomes first, then the positively charged lipoplexes were fused with negatively charged mEVs by freeze-thawing cycles at -80 °C and 37 °C. Unlike LN2 hybrids, with these formulations the siRNA was introduced prior to hybrid nanovesicle formation, and gentler freeze-thaw operations (-80 °C freeze and thaw without sonication) were applied to protect the integrity and bioactivity of siRNA. Upon prior research, it was ascertained that the structural integrity of siRNA was not compromised after 10 freeze/thaw cycles, which entailed freezing at -20 °C for 12 hours, followed by a subsequent thaw at 21 °C for 30 minutes, through measuring by nondenaturing polyacrylamide gel electrophoresis and functional activity assays [447]. Additionally, the activity of siRNA was preserved following 10 freeze/thaw cycles (liquid nitrogen to 37 °C water bath) [448]. Therefore, siRNA has demonstrated substantial resilience to freeze/thaw processes. Although further investigation is recommended to elucidate the effects of freeze-thaw cycles on siRNA stability, the extant gene silencing activities of siRNA, as explicated in downstream research shown in Section 5.4.6, corroborate the maintained stability and integrity of these molecules. Different ratios of liposomes to mEVs (w/w) were used to optimize this formulation. As shown in **Table 5-4**, the hydrodynamic diameter of the hybrids decreased with the decreasing ratio of liposomes to mEVs, and when the ratio was 1:5, the size was 227.0 nm and the surface charge was -25.2 mV, which we considered as the most desired system for our application. It is important to recognize that the adoption of a negative charge on the hybridosomes is deemed suitable in this instance, as the siRNA has already been encapsulated before hybrids formed within these systems. This encapsulation negates the necessity for a positive surface charge, such as that characteristic of LN2 hybridosomes, which would typically be required to associate with the negatively charged

siRNA. Therefore, the ratio of liposomes to mEVs with 1:5 was used subsequently. The increase in NBD fluorescence and decrease of Rho fluorescence also confirmed the fusion of liposomes with mEVs (**Figure 5-9**). Liposomes control was not measured in Figure 5-9; this is predicated on stable fluorescence during freeze-thaw cycles as demonstrated at Figure 5-8. Ultrafiltration was applied to remove unloaded siRNA and the loading efficiency of siRNA with these systems was calculated as 78.2%. The consistent values of size, Zeta-potential, and loading efficiency of the hybridosomes produced in each batch suggest a high level of reproducibility in their formulation. However, even though the fusions *via* these two methods have been verified by FRET assay, future studies should aim for a more detailed characterization of the composition of hybridosomes, such as using nanoflow cytometry to accurately determine the efficacy of fusion and particle numbers of each vesicle species (mEVs and liposomes) [449].

Table 5-4. Characterisation of hybridosomes prepared by -80°C freeze-thaw cycles with different liposomes to bovine milk extracellular vesicles (mEVs) ratio (w/w).

	4:1	**2:1**	**1:2**	**1:3**	**1:4**	**1:5**
Size (nm)	7218 ± 61.5	4866 ± 730	1499 ± 466	552.2 ± 9.7	269.4 ± 3.7	227.0 ± 5.3
PdI[a)]	1.000 ± 0.00	1.000 ± 0.00	0.900 ± 0.142	0.597 ± 0.001	0.456 ± 0.013	0.249 ± 0.006
Zeta-potential (mV)	-	-	-21.5 ± 0.42	-24.6 ± 0.21	-	-25.2 ± 0.64

[a)] PdI: polydispersity index. Data shown as the mean ± SD (n=3).

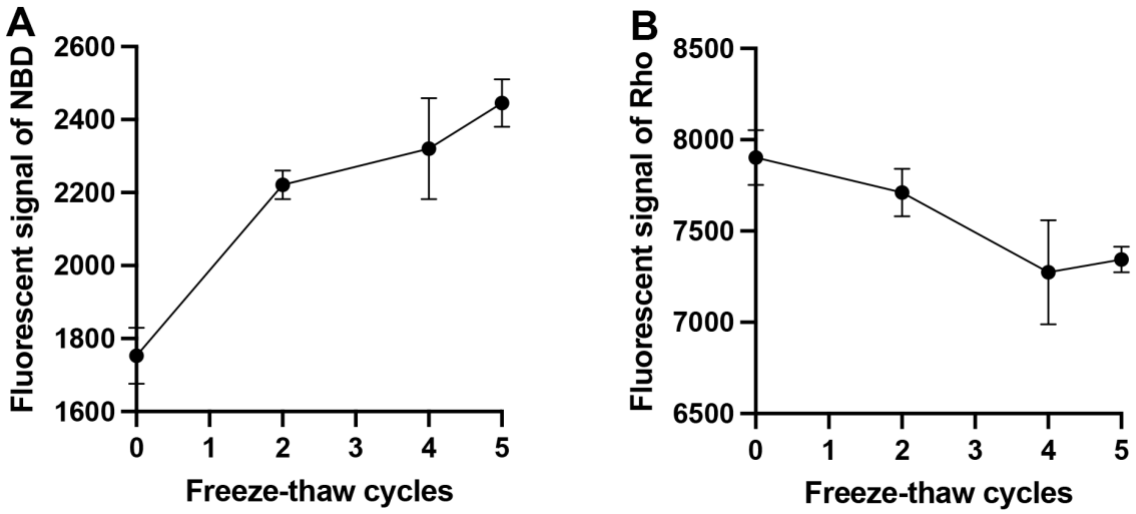

Figure 5-9. Relationship between the number of -80°C freeze-thaw cycles with fluorescent signal of liposomes when they were fused with bovine milk extracellular vesicles (mEVs) with liposome:mEVs ratio of 1:5. (A) Fluorescent signal of NBD-DSPE with excitation of 460 nm and emission of 530 nm. **(B)** Fluorescent signal of Rho-PE with excitation of 460 nm and emission of 588 nm. Data shown as the mean ± SD (n = 3).

5.4.3. Toxicity of mEVs, liposomes and hybridosomes

The toxicity of mEVs, cationic liposomes and hybridosomes in Caco-2 cells was compared, as determined by the MTS assay. A 4-hour incubation period was evaluated initially. As shown in **Figure 5-10A**, no cellular toxicity was observed for all samples within the concentration range of 0.025 mg/mL – 0.20 mg/mL. Additionally, as the transfection procedure normally requires a longer incubation period with the samples of 24 – 48 hours [450, 451], cytotoxicity was also evaluated following 48 h incubation (**Figure 5-10B**). mEVs with surface charge of -9.1 mV demonstrated no toxicity in Caco-2 cells at the concentration range of 0.025 – 0.20 mg/mL for 48h incubation. The two types of formulations of hybridosomes also showed no toxicity at concentration range of 0.025 – 0.10 mg/mL, but demonstrated approximately 40% decrease in Caco-2 cell metabolic activity at 0.20 mg/mL. Cationic liposomes with surface charge of +43.3 mV showed significantly higher toxicity than mEVs and hybridosomes at 0.10 mg/mL,

resulting in around 80% decrease in Caco-2 cell metabolic activity. The results demonstrated that mEVs and hybridosomes are significantly less cytotoxic than cationic liposomes. The toxicity of cationic liposomes is related to the positive surface charge, as it may interfere with the membrane function or integrity (known to be membrane active) of cells [452], and could activate several cellular pathways such as pro-apoptotic and pro-inflammatory cascades [453]. Following the fusion with negatively charged mEVs, the positive charge of cationic liposomes is neutralized to a certain degree and the cytotoxicity is therefore expected to be reduced as a result of this phenomenon. It is worth noting the at relative metabolic activity of cells treated with mEVs and hybridosomes was higher than 100% within the concentration range between 0.025 mg/mL – 0.10 mg/mL (48 h incubation). This could have resulted from a pro cell proliferation property of mEVs, which has been confirmed in previous reports for intestinal cells and macrophages [454, 455].

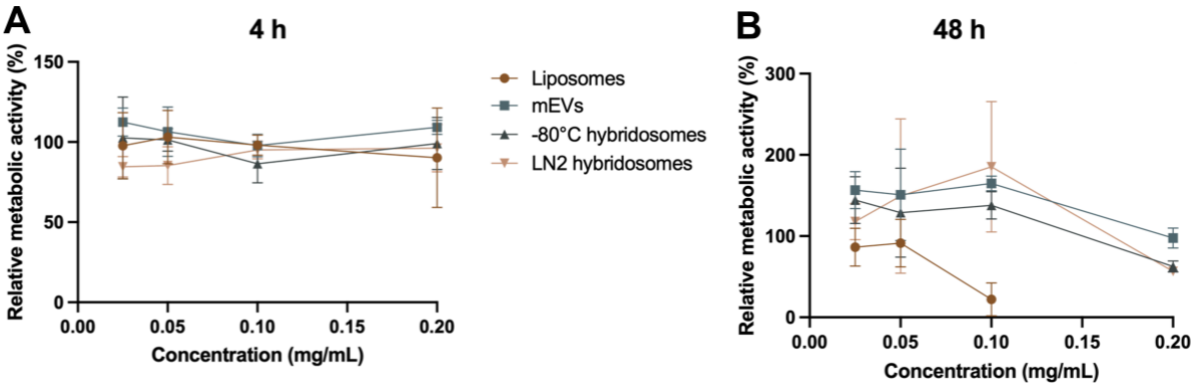

Figure 5-10. Cellular toxicity of different concentrations of bovine milk extracellular vesicles (mEVs), cationic liposomes, -80°C freeze-thaw hybridosomes and liquid nitrogen (LN2) freeze-thaw hybridosomes in Caco-2 cells following 4h (A) and 48h (B) incubation. Data shown as the mean ± SD (n = 3).

5.4.4. Stability of hybridosomes in simulated intestinal fluids

Prior to studying the intestinal epithelial cell uptake and transport of novel hybridosome formulations, we determined their stability in SIFs. We intentionally focused on intestinal

rather than gastric fluids given that the most appropriate way in which such systems would be administered orally is *via* enteric-coated capsules so to ensure that hybridosomes membrane-associated proteins are protected in the harsh environment of stomach biofluid. Therefore, we were interested to ascertain if mEV-based hybridosomes maintain a similar stability to mEVs in SIFs. We used a fluorescence-based assay based on DPH to determine the membrane stability of hybridosomes in SIFs. This assay has not been previously used in EVs research, but has been employed to determine the stability of other lipid membrane-enclosed vesicles such as liposomes [438]. DPH emits fluorescence when positioned in a hydrophobic environment (such as lipid mEVs membranes) and it was postulated that when the membrane of mEVs is disturbed, DPH is released into the hydrophilic phase, whereby its fluorescence signal is significantly reduced. Any decrease in fluorescence of DPH-incorporated mEVs would therefore point to a probable compromise in mEVs membrane integrity. **Figure 5-11** shows the validation of the DPH assay, demonstrating that its application to all vesicle systems (mEVs, liposomes or hybridosomes) resulted in an obvious fluorescence, while fluorescence signal was almost completely absent when DPH was added to a buffer.

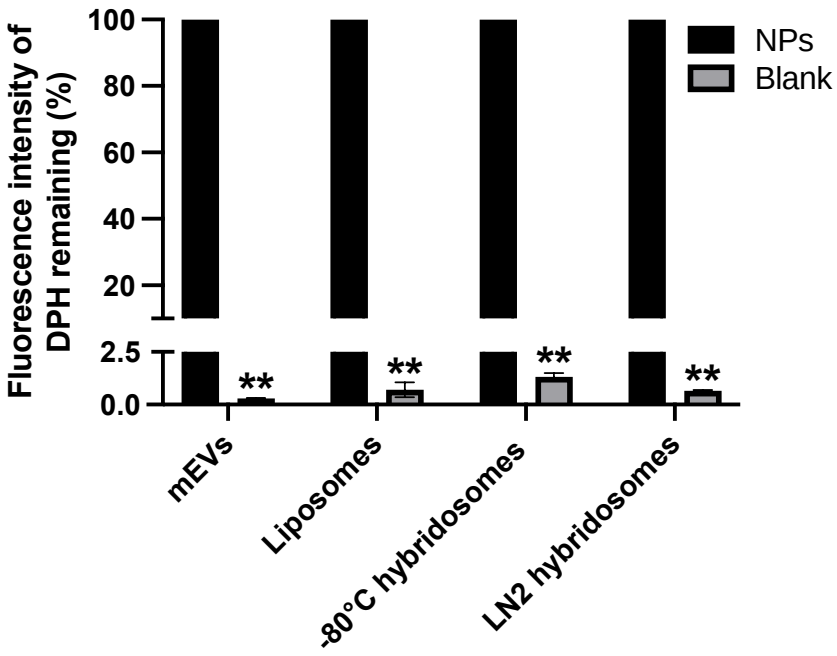

Figure 5-11. Validation of Diphenyl-1,3,5-hexatriene (DPH) with different nanoparticles (NPs), including bovine milk extracellular vesicles (mEVs), cationic liposomes, -80°C freeze-thaw hybridosomes and liquid nitrogen (LN2) freeze-thaw hybridosomes. Blank groups only contained DPH in buffer. NPs were stained with DPH by incubating for 40 minutes at room temperature under gentle shaking in dark. Data are presented as DPH fluorescence intensity remaining of Black group compared with NPs group, mean ± SD (n=3). ** denotes $p < 0.01$.

Data in **Figure 5-12** reveals that, compared with control (PBS), FaSSIF treatment of mEVs did not result in a decrease in DPH fluorescence, while FeSSIF-digested mEVs showed a small but statistically significant loss of fluorescence. Liposome incubation in FaSSIF did not have an impact on DPH fluorescence, while exposure to FeSSIF led to a dramatic loss of fluorescence which was notably higher than that of mEVs (and to similar levels as SDS treatment) (**Figure 5-12A and 5-12B**). The data hence indicates that mEVs are notably more resistant to FeSSIF-induced solubilization than liposomes (DPH fluorescence decrease by 15% in fluorescence *versus* 84%, respectively). Although it is currently not clear why mEVs demonstrate a significantly higher stability than model liposomes in FeSSIF, one could speculate that it may

relate to the high cholesterol content of EVs (over 40% mol % in total lipid extracts) compared to the liposomes employed in this work [456]. From the field of liposome research, cholesterol is known to modulate liposome stability, *via* effects on membrane thickness, fluidity and membrane permeability [457]. Importantly, for hybrid nanovesicles, FeSSIF treatment resulted in a modest (although significant) reduction of DPH fluorescence with LN2 freeze-thaw hybridosomes, while there was no decrease in fluorescence with -80°C freeze-thaw hybridosomes (**Figure 5-12C and 5-12D,** respectively). The stability difference between the two formulations is based on their composition of liposomes to mEVs ratio. The ratio of liposomes:mEVs in -80°C freeze-thaw hybridosomes is 1:5 (w/w) which leads their property closer to mEVs and shows higher stability, while LN2 freeze-thaw hybridosomes demonstrated lower stability due to the high portion of liposomes (liposomes:mEVs is 2:1 (w/w)).

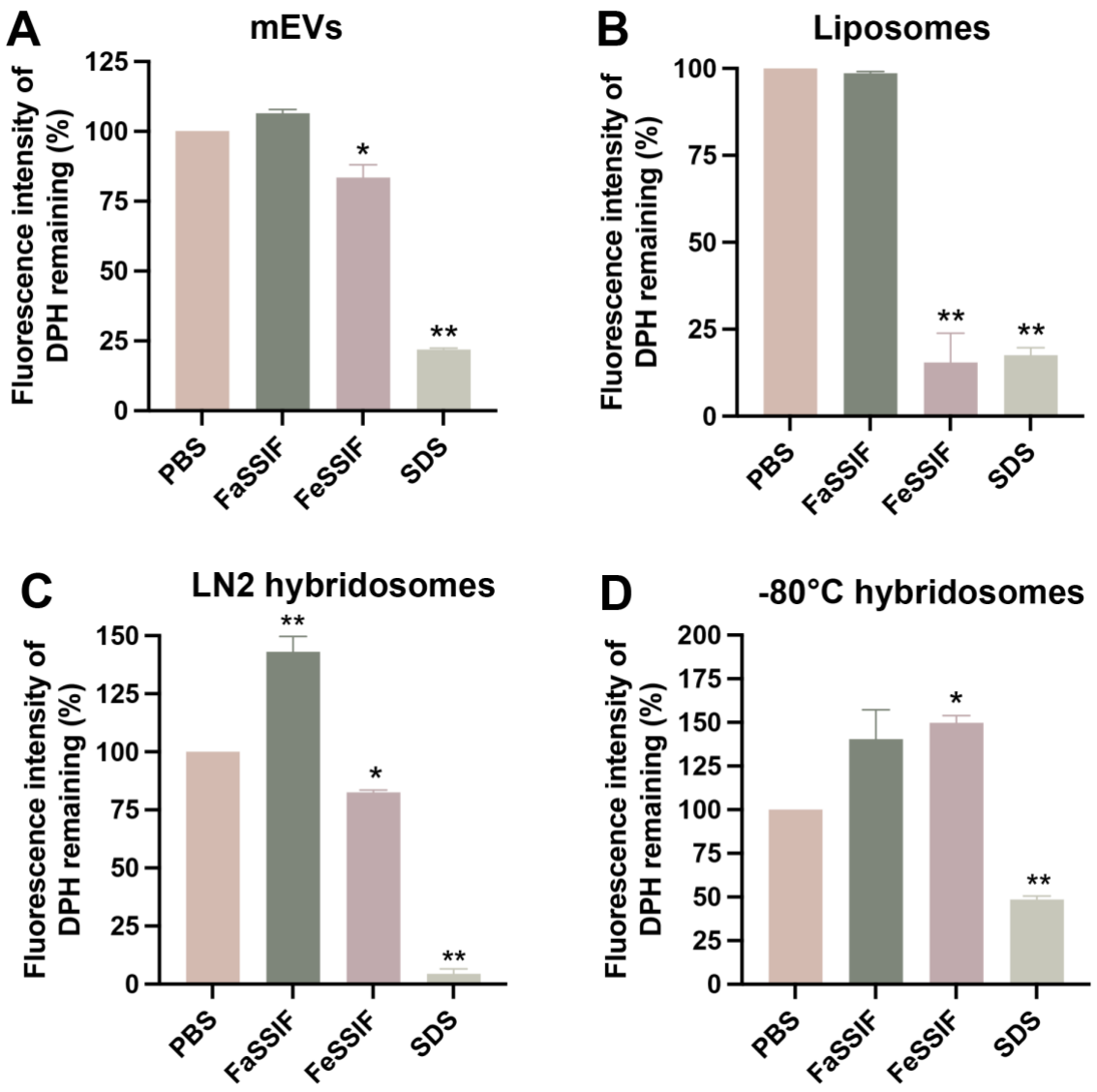

Figure 5-12. Effect of Fasted State Simulated Intestinal Fluid (FaSSIF) and Fed State Simulated Intestinal Fluid (FeSSIF) on membrane stability of bovine milk extracellular vesicles (mEVs) (A), cationic liposomes (B), liquid nitrogen (LN2) freeze-thaw hybridosomes (C), and -80°C freeze-thaw hybridosomes (D). DPH: 1,6-Diphenyl-1,3,5-hexatriene. Sodium dodecyl sulfate (SDS) was used as a control to solubilize the nanoparticles. Data are presented as DPH fluorescence intensity remaining compared with PBS control group, mean ± SD (n=3). * and ** indicate $p < 0.05$ and $p < 0.01$, respectively.

We have further compared the effect of FaSSIF, FeSSIF, or SDS treatment of the four vesicle types on their size. We investigated the effect of SIFs on the size of vesicles since the solubilization of liposomes by the bile salt sodium taurocholate has been shown to involve, depending on the concentration of bile salts, the insertion and partition of detergent (i.e., taurocholate) molecules into the lipid bilayer (at low concentrations), which induces a measurable increase in the size of the liposomes [458], while at higher detergent concentrations vesicles start to break up and fragment into mixed bile salt/lipid micelles [458]. The data in **Table 5-5** highlighting that treatment of hybridosomes with FaSSIF did not result in an increase in particle size, contrary to the outcome with liposomes which demonstrated a statistically significant increase. FeSSIF induced an increase in the size of hybrid vesicles, with the magnitude of this increase being in the range between the size increase of mEVs and liposomes.

Table 5-5. Effect of simulated intestinal fluids on particle size of bovine milk extracellular vesicles (mEVs), -80°C freeze-thaw hybridosomes. liquid nitrogen ('LN2') freeze-thaw hybridosomes and cationic liposomes which were used to fabricate hybridosomes. Vesicles were treated in simulated intestinal fluids at 37°C for 1.5 hours. Size was determined by dynamic light scattering (DLS). Data shown as the mean ± SD (n=3).

Vesicle type	**Particle size in different exposure medium (% of control, PBS)**		
	FaSSIF[a)]	FeSSIF[b)]	SDS[c)]
mEVs	83.97 (±6.88)	126.55 (±15.49)*	92.52 (±13.05)
-80°C hybridosomes	95.25 (±5.64)	169.67 (±18.46)**	91.09 (±4.95)
LN2 hybridosomes	69.91 (±4.4)**	146.59 (±8.9)**	46.4 (±4.93)**
Liposomes	179.09 (±6.39)**	185.42 (±3.39)**	673.56 (±74.8)**

[a)] FaSSIF: Fasted-State Simulated Intestinal Fluids; [b)] FeSSIF: Fed-State Simulated Intestinal Fluids; [c)] SDS: 1% (w/v) sodium dodecyl sulfate in PBS. * and ** indicate $p < 0.05$ and $p < 0.01$, respectively, with comparisons made between vesicle size in PBS and other media.

The moderate increase in DPH fluorescence intensity upon the exposure of LN2 hybridosomes in FaSSIF and −80 °C hybridosomes in FeSSIF may relate to the effect of SIF components on the membrane orientation of DPH [459], instead of particle aggregation. Our data show that there is no relationship between changes in DPH fluorescence and changes in particle size following digestion in these fluids (**Table 5-5**), with FaSSIF inducing a decrease in the size of LN2 hybridosomes and −80 °C hybridosomes increasing in size following FeSSIF treatment, whilst an increase in DPH fluorescence was seen in both scenarios. Future evaluation of the effect of SIFs on these particles should employ additional biophysical techniques (e.g., turbidity measurements and small angle neutron scattering) or imaging (electron microscopy). Although the biological activity of mEVs and mEV-liposome hybrids needs to be confirmed following digestion, our work overall indicates that these systems are more resistant than liposomes to intestinal fluids rich in bile salts such as FeSSIF. This is important as other synthetic lipid nanoparticle drug delivery systems have been shown to possess poor stability in FeSSIF [208].

5.4.5. Transport of siRNA-loaded mEVs and hybridosomes across Caco-2 monolayers

To evaluate the intestinal epithelial delivery potential of hybridosomes, fluorescent Cy5 siRNA was loaded *via* LN2 freeze-thaw and -80°C freeze-thaw process as mentioned above, and the systems were compared with siRNA electroporated-mEVs (**Figure 5-13**), as well as siRNA alone. There was a gradual accumulation of siRNA in the basolateral side in all conditions, however, transport of both hybridosome formulations generally exceeded that of siRNA alone, with LN2 freeze-thaw hybridosomes demonstrating higher transepithelial transport compared to other conditions, including siRNA electroporated-mEVs.

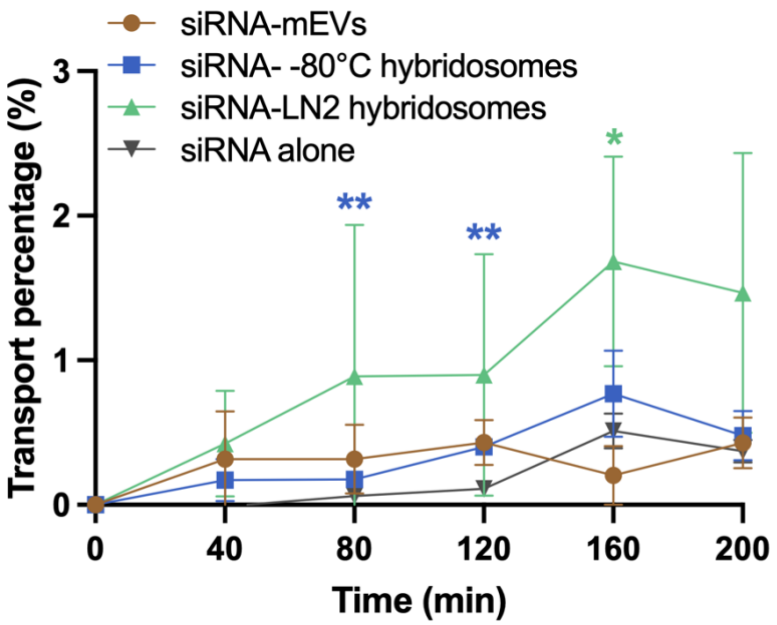

Figure 5-13. Transport of fluorescent Cy5 siRNA electroporated-bovine milk extracellular vesicles (mEVs), siRNA loaded- -80°C freeze-thaw hybridosomes, siRNA loaded-LN2 freeze-thaw hybridosomes, and siRNA alone in differentiated (polarised) Caco-2 monolayers (intestinal epithelium). Transport percentage was calculated by the fluorescent signal of siRNA. Data shown as the mean ± SD (n=3). ** in blue indicates $p < 0.01$ between siRNA loaded (-80°C freeze-thaw hybridosomes) and siRNA alone group, * in green indicates $p < 0.05$ between siRNA loaded-LN2 freeze-thaw hybridosomes and siRNA alone group.

5.4.6. Transfection efficiency of GAPDH siRNA-loaded mEVs and hybridosomes in Caco-2 cells and macrophages

The gene silencing efficiency of siRNA-loaded mEVs, hybridosomes and liposomes was evaluated in Caco-2 cells. A model 'housekeeping' protein, GAPDH, was selected as a target for knock-down as it represents a commonly target for these studies [208, 460]. Two concentrations of mEVs, hybridosomes, and liposomes (0.08 mg/mL and 0.05 mg/mL corresponding to protein or lipids concentration) were applied, loaded with 0.05 nmol/mL and 0.03 nmol/mL siRNA, respectively. As shown in **Figure 5-14**, while siRNA transfected using

a commercial transfection reagent displayed a significant gene silencing efficiency (~30-50%) compared with naked siRNA, siRNA delivered by mEVs, hybridosomes and liposomes did not show obvious gene silencing. In a previous report, siRNA mediated gene silencing at mRNA level was over 80% with lipid-like “lipioid” nanoparticles in Caco-2 cells, and the silencing at protein level was at the highest level 4 days post transfection [450]. The difference in our results from this report can be attributed to the surrogate for silencing efficiency, which is the GAPDH protein, rather than mRNA. However, following a 48-hour transfection period and an additional 48-hour culture period prior to transfection, one would expect that there is cell death due to prolonged culture, which would lead to inaccurate GAPDH measurement, if the cells are cultured for another 24-48 hours post transfection. Additionally, the tertiary amine groups in lipioid nanoparticles from the previous report played a key role in endosomal escape and the siRNA could be released into the cytoplasm for gene silencing induction [450, 461]. However, the mechanism of mEV transport across the intestinal epithelium is thought to be endocytosis based [247] or IgG - FcRn dependent transcytosis (detailed in Section 1.2.3.3) [153, 154] , which would not necessarily guide the mEV based-delivery system to the cytoplasm for siRNA release in intestinal epithelial cells. In summary, while the low transfection efficiency of mEV-based delivery systems in intestinal epithelial cells may preclude the use of these delivery systems to deliver nucleic acid payloads to intestinal epithelial cells, it does not rule out their usefulness in achieving drug (including siRNA) delivery to the subepithelial tissue, including immune cells, which are in fact a primary target in IBD.

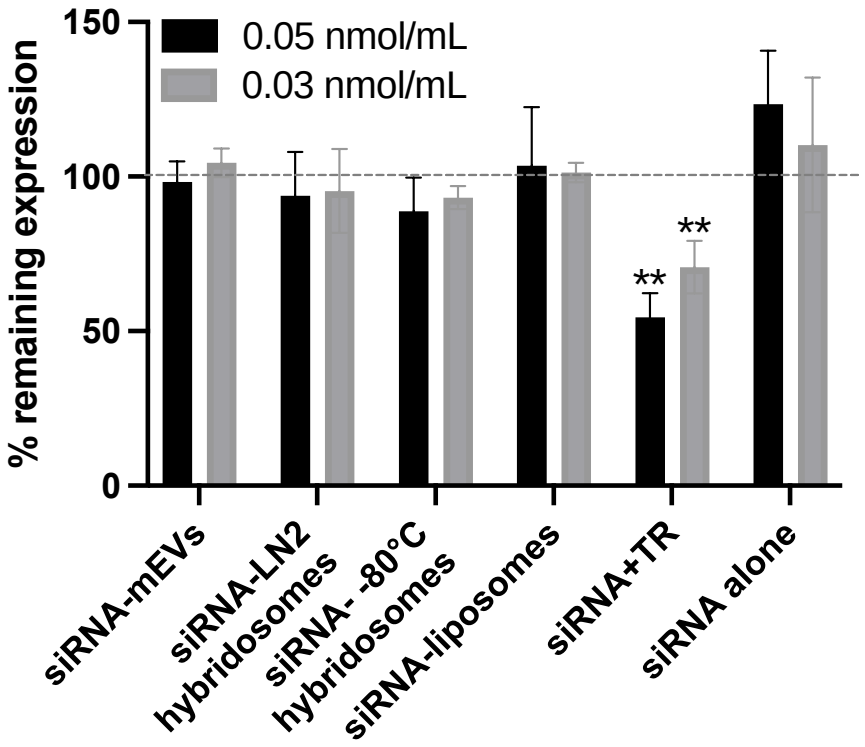

Figure 5-14. GAPDH remaining expression in Caco-2 cells transfected by siRNA electroporated-bovine milk extracellular vesicles (mEVs), siRNA loaded-LN2 freeze-thaw hybridosomes, siRNA loaded- -80°C freeze-thaw hybridosomes, siRNA loaded-liposomes, siRNA transfected by commercial transfection reagent (TR), and siRNA alone for 48 h. The concentration of nanoparticles was 0.08 mg/mL and 0.05 mg/mL corresponding to the siRNA concentration of 0.05 nmol/mL and 0.03 nmol/mL. Data are presented as mean ± SD (n=3). ** indicates $p < 0.01$.

To evaluate the potential of mEVs and hybridosomes for functional biotherapeutic delivery, the gene silencing efficiency of siRNA loaded-hybridosomes was evaluated in J774A.1 macrophages. We selected this cell line since macrophages in the lamina propria (i.e. under the epithelium) are known to play a key role in inflammatory response, and therefore are a potential target of interest in IBD, achieved by a delivery system that permeates the intestinal barrier [462]. The results showed that the higher concentration of GAPDH siRNA loaded hybridosomes (0.08 mg/mL hybridosomes corresponding to 0.05 nmol/mL siRNA loading) prepared *via* the -80°C freeze-thaw method produced approximately 40% gene silencing,

which was significantly higher than that of corresponding siRNA alone and comparable to that achieved by a commercial transfection reagent (TR). Similarly, 0.05 mg/mL GAPDH siRNA electroporated-mEVs (corresponding to 0.03 nmol/mL siRNA loading) showed a higher gene silencing efficiency (~50%) than siRNA alone and also siRNA delivered with a commercial TR (~5% silencing efficiency) (**Figure 5-15A**). As shown in **Figure 5-15B**, 0.05 mg/mL of GAPDH siRNA loaded-LN2 freeze-thaw hybridosomes (with 0.03 nmol/mL siRNA loading) resulted in around 35% gene silencing efficiency, which was significantly higher than that of siRNA alone and comparable to that achieved by siRNA transfected by the commercial TR. There was no significant difference in gene silencing efficiency between siRNA loaded-liposomes and siRNA with TR or siRNA alone. The significant gene silencing of siRNA loaded -mEVs or -hybridosomes compared with naked siRNA in macrophages can be attributed to the systems facilitating cell uptake by endocytosis or direct fusion with the plasma membrane [428]. After endocytosis, the cargo such as siRNA was experimental proved in the previous report to exposure *via* fusion of EVs with endosomes/lysosomes (based on lipid composition changes during the endosomal membrane maturing process), which lead cargo to play their role in cytoplasm, where siRNA can form into the RISC enroute to cleaving the target mRNA and prevent the protein expression [428].

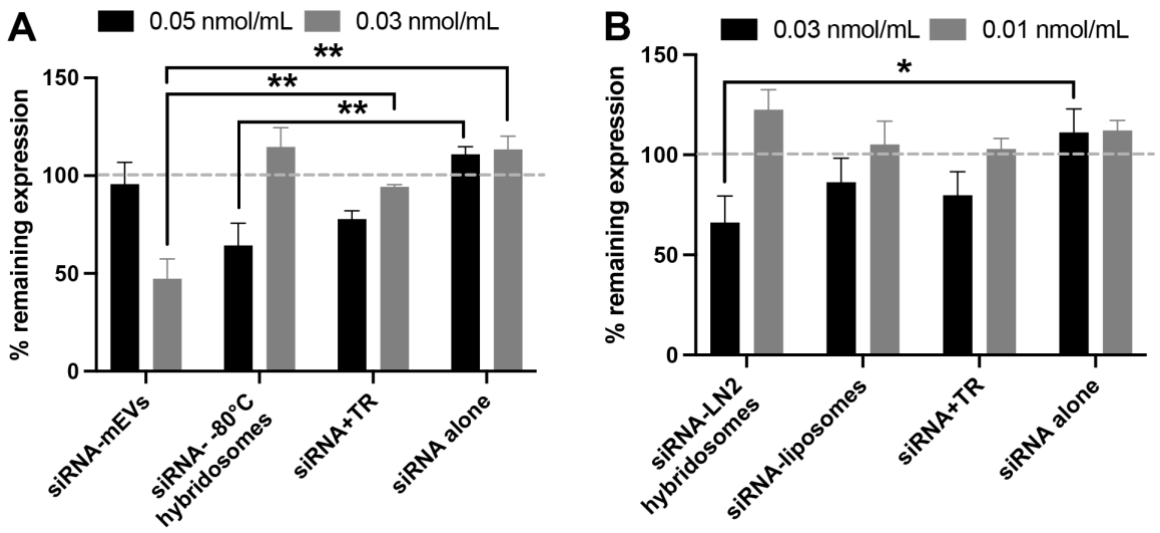

Figure 5-15. Expression levels of GAPDH in macrophages (J774A.1). (A) GAPDH remaining expression in macrophages transfected by siRNA electroporated-bovine milk extracellular vesicles (mEVs), siRNA loaded- -80°C freeze-thaw hybridosomes, siRNA transfected by commercial transfection reagent (TR), and siRNA alone for 48 hours. The concentration of mEVs and hybridosomes was 0.08 mg/mL and 0.05 mg/mL corresponding to the siRNA concentration of 0.05 nmol/mL and 0.03 nmol/mL. **(B)** GAPDH remaining expression in macrophages transfected by siRNA loaded-LN2 freeze-thaw hybridosomes, siRNA loaded-liposomes, siRNA transfected by TR, and siRNA alone for 5 hours (and replaced by culture medium for another 43 hours incubation). The concentration of hybridosomes and liposomes was 0.05 mg/mL and 0.02 mg/mL corresponding to the siRNA concentration of 0.03 nmol/mL and 0.01 nmol/mL. The lower concentrations of LN2 freeze-thaw hybridosomes and liposomes, as well as shorter incubation time, were selected due to the cytotoxic effects observed at higher concentrations during long incubation with macrophages. Data are presented as mean ± SD (n=3). ** indicates $p < 0.01$ and * indicates $p < 0.05$.

5.4.7. Effect of anti-TNFα siRNA-loaded mEVs and hybridosomes on inflammation in an in vitro co-culture model of intestinal inflammation

The abnormal immune response plays a major part in the pathophysiology of IBD. Macrophages, which are the effector immune cells (innate immunity) existing in the lamina

propria under intestinal epithelium, are known to play a key role to maintain the stability of intestinal environment *via* inflammatory response (pro-inflammatory cytokine secretion) [462]. Therefore, an *in vitro* co-culture model of Caco-2 monolayers and macrophages may mimic the homeostatic or inflamed micro-environment of intestine with representation of the immune system [463-466]. We therefore established such a model to enable the testing of the mEV-based formulations. To induce inflammation we used LPS, a molecule found in the outer membrane of Gram-negative bacteria, which is a potent inducer of inflammation and has been used previously in inflammatory co-culture models [464]. LPS can be recognized by various recognition receptors (e.g. Toll-Like Receptor4 (TLR4)) on immune cells, such as macrophages and dendritic cells, leading to the activation of NF-κB signaling pathways and expression of proinflammatory cytokines like TNFα [467].

Figure 5-16A illustrates the set-up process of the *in vitro* co-culture inflamed intestinal model. Briefly, macrophages (J774A.1) were seeded on 12-well plates and cultured for 24 h. Then the inserts supporting intact Caco-2 monolayers (after 21 days culture) were combined with the plates and 100 ng/mL LPS was added to the basolateral side to induce the inflammation from macrophages for additional 24 hours. Subsequently, anti-TNFα siRNA loaded-delivery systems, including electroporated mEVs, -80°C freeze-thaw hybridosomes and LN2 freeze-thaw hybridosomes as well as untreated isolated mEVs, were added to the apical side of Transwells. The samples were collected from the basolateral sides at 0 h, 24 h and 48 h after adding the formulations and TNFα (marker of inflammation) was quantified using an ELISA assay. TNFα released from macrophages at different timepoints is shown in **Figure 5-16B**. At 0 h (after 24 h of adding LPS). The data shows that TNFα concentrations from all groups were relatively low and there was no significant difference between blank with LPS group and blank without LPS group, indicating that the LPS stimulation on macrophages for 24 h was not sufficient to induce detectable inflammation. At 24 h, the significantly higher TNFα concentration of blank

with LPS group compared to the blank without LPS group demonstrated the efficiency of LPS in stimulating inflammation on macrophages after 48 h. However, the treatment by anti-TNFα siRNA loaded-formulations did not show significant inflammation-reducing effects. After 48 h of applying the formulations to cells, the TNFα concentrations of siRNA loaded-mEVs and -80°C freeze-thaw hybridosomes groups were significantly lower than blank with LPS group and showed no difference with blank without LPS group. However, the similar TNFα concentrations between anti-TNFα siRNA loaded-vesicles and negative siRNA loaded-vesicles groups suggested that the inflammation relief may in fact be induced from vesicles rather than the cargo (anti-TNFα siRNA). The inflammation-reducing effect of unmodified mEVs (without siRNA) also supports this hypothesis. On the other hand, the higher inflammation relief efficiency of siRNA loaded, -80°C freeze-thaw hybridosomes than siRNA loaded-LN2 freeze-thaw hybridosomes could be a result of the higher portion of mEVs in -80°C hybridosomes (liposomes:mEVs 1:5 (w/w)) compared to LN2 hybridosomes (liposomes:mEVs 2:1 (w/w)). These findings are consistent with a previous report that demonstrated the capability of mEVs to modulate inflammation in an *in vitro* intestinal model [468]. The mechanism of mEVs to alleviate inflammation is multifaceted, but the main effect can be attributed to the miRNAs found in mEVs, such as miR-141 or miR-155, which have been demonstrated to downregulate the proinflammatory cytokines *via* suppressing NF-κB activation pathway [469, 470]. Moreover, mEVs may also carry antioxidants or factors that protect cells from oxidative stress, which is often associated with inflammation [471]. It was observed that mEVs can carry antioxidant substances or oxides to recipient cells and relieve oxidative stress directly, or deliver regulatory factors in oxidative stress-associated signalling pathways to alleviate oxidative stress indirectly [471].

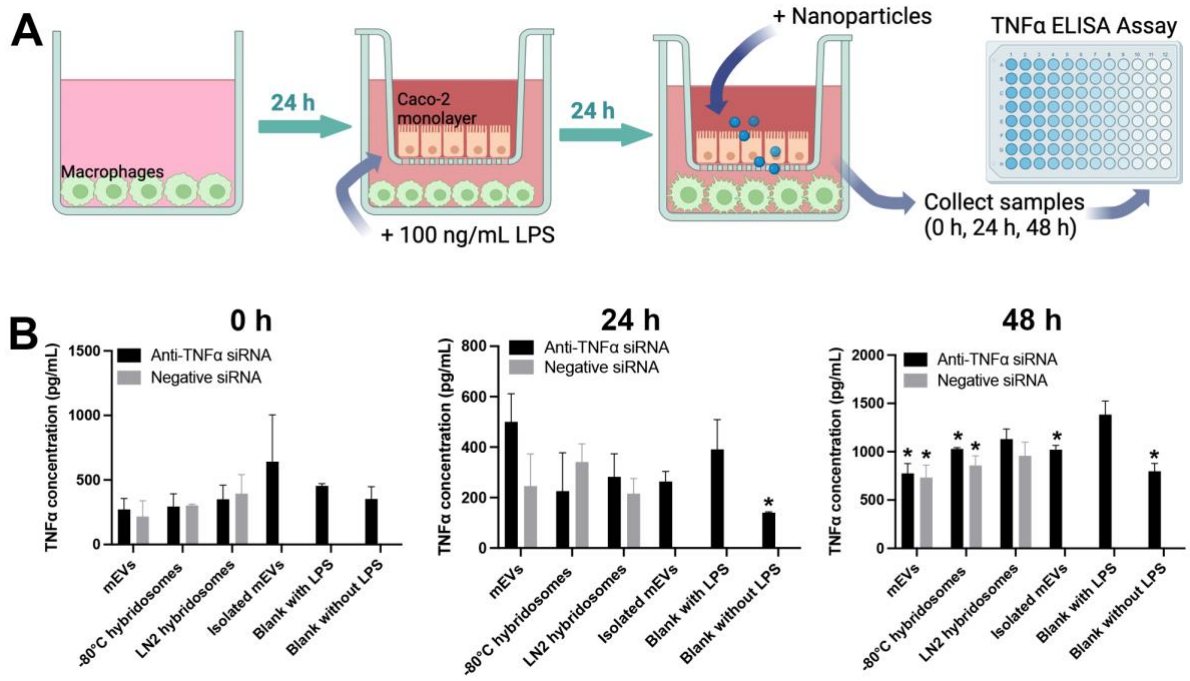

Figure 5-16. Effect of anti-TNFα siRNA-loaded delivery systems on inflammation in an *in vitro* inflamed intestinal model. (A) Schematic description of *in vitro* inflamed intestinal co-culture model set-up by macrophages (J774A.1) and Caco-2 monolayer, and samples collection for inflammatory cytokine (TNFα) ELISA assay. **(B)** Release of TNFα from basolateral side of Transwells after therapeutic delivery systems treatment for 0 h, 24 h, and 48 h. Therapeutic delivery systems include anti-TNFα siRNA electroporated-bovine milk extracellular vesicles (mEVs), anti-TNFα siRNA loaded--80°C freeze-thaw hybridosomes, anti-TNFα siRNA loaded-LN2 freeze-thaw hybridosomes, and isolated mEVs without siRNA. Negative siRNA loaded-delivery systems were applied as negative controls. Blank with lipopolysaccharides (LPS) control group was inflamed co-culture model without therapeutic delivery systems, and blank without LPS control group was uninflamed co-culture model without therapeutic delivery systems. Data are presented as mean ± SD (n=3). * indicates $p < 0.05$ compared with Blank with LPS control group.

It should be noted that the co-culture model established in this study has the potential to be optimized to better replicate relevant IBD conditions. This is due to the observation that the Caco-2 monolayers maintained intact (as evidenced by stable TEER value), which failed to

mimic the dysfunction of intestinal barrier seen in IBD. This was indeed attempted in a previous study [463] in which Caco-2 cells were cultured on Transwell inserts for 18-21 days to form intact monolayers and THP-1 macrophages were differentiated with phorbol 12-myristate 12-acetate (PMA) and seeded on the basolateral sides. With the stimulation of IFN-γ on Caco-2 monolayers, and LPS with IFN-γ on THP-1 cells, a significant but temporary reduction of barrier integrity was observed [463]. Various types of pro-inflammatory cytokines and cytotoxicity markers were identified in this study, providing evidence of the inflamed status of intestine [463]. To simulate IBD conditions more accurately in future studies, the addition of dendritic cells in an *in vitro* co-culture model should also be considered. A co-culture model consisting of immunocompetent macrophages, dendritic cells and Caco-2 monolayer was established in a previous study, where the macrophages and dendritic cells were embedded in a collagen layer on the Transwell membrane, and a Caco-2 monolayer was seeded atop, to mimic inflamed intestinal mucosa [472]. Several combinations of pro-inflammatory stimuli including LPS, interleukin-1β and interferon-γ were evaluated. Interleukin-1β was found to produce the strongest stimulation, with Caco-2 cells responding to this stimulation with significantly decreased (20%) TEER and a moderate increase of proinflammatory markers [472]. Similarly, a co-culture model with Caco-2 cells, macrophages and dendritic cells was developed to test the toxicity of engineered nanoparticles [473]. Therefore, the establishment of an *in vitro* co-culture inflammatory intestinal model involving epithelial cells and immune cells needs careful consideration of several factors. Firstly, the choice of immune cells, their activation status and their interaction with Caco-2 monolayers should be well-defined, since even the subtypes of macrophages like J774A.1 and THP-1 may demonstrate different inflammatory responses. Furthermore, the signaling molecules such as proinflammatory cytokines (or their combinations), are important to induce and sustain the desired inflammatory state. In addition, the model should be adaptable to the research objectives, allowing for the

investigation of desired intestinal inflammation conditions and therapeutic interventions, such as the dysfunction of intestinal barrier under IBD.

5.5. Conclusion

In this chapter, novel mEV-liposome hybrid systems were fabricated for oral siRNA delivery, providing a potential therapeutic approach for IBD. Chemical and mechanical methods to facilitate the formation of hybrids, i.e. PEG and freeze-thaw cycles, respectively, were tested and two hybridosome formulations fabricated by freeze-thaw cycles demonstrated potential as effective carriers for siRNA delivery. These hybridosomes exhibited a major reduction in cytotoxicity when compared to cationic liposomes, which is crucial in ensuring the safety of any therapeutic delivery system. Furthermore, hybridosomes displayed higher stability in a fed-state simulated intestinal fluid compared to liposomes. The hybrid nanovesicles also demonstrated high siRNA loading efficiency and exhibited a notable ability to enhance the permeation of siRNA across the intestinal epithelium. Finally, the systems successfully induced gene silencing (GAPDH) in macrophages. Although anti-TNFα siRNA loaded-hybridosomes were able to downregulate TNFα in an *in vitro* co-culture model of intestinal inflammation, the effect cannot be attributed to their function as carriers of the therapeutic payload but instead it is likely to stem from the inherent effect of mEVs. Overall, mEV-liposome hybridosomes have significant potential to enable oral delivery of siRNA for IBD therapy.

6. Summary and Future Perspective

6.1. Summary

The studies throughout this thesis focus on the development of mEVs-based systems for oral siRNA delivery and the investigation of their potential for IBD therapy.

Initially, in Chapter 3, several methods were optimized to achieve efficient isolation and purification of mEVs from bovine milk. It was found that mEVs obtained by ultracentrifugation and SEC purification exhibited an expected size, good dispersibility, remarkable yield, and high purity. Moreover, the characteristic protein markers and typical cup-shaped morphology for these mEVs were observed, which confirmed their structural integrity. Thereafter, various strategies were assessed for loading siRNA into mEVs. The loading efficiency of siRNA into mEVs *via* commercial transfection kit yielded over 20%, whereas electroporation as the most widely used technology for loading nucleic acids into EVs resulted in 5.05% efficiency.

Chapter 4 investigated the potential of mEVs as oral delivery systems for siRNA. It was found that mEVs demonstrate high permeability in a widely used human intestinal epithelial model (Caco-2 monolayers) and this capability was not compromised after exposure to simulated intestinal fluids, thus confirming their stability in the digestive environment of the intestine. To confirm the intestinal epithelial permeability of mEVs we for the first time utilized a novel human-derived IEO model to determine the intestinal permeation of EVs. To enable this investigation, two relevant *in vitro* IEOs models were initially created: a 3D apical-out IEO model and an IEO monolayer model. Unlike conventional culture of IEOs whereby the apical surface is shielded in the interior of organoids, these models enabled the investigation of apical-to-basolateral permeability of EVs. mEVs demonstrated similar permeability through these highly human-relevant models, demonstrating their potential for oral delivery. In addition, efficient induction of gene silencing in macrophages was observed upon treatment with siRNA

electroporated-mEVs, which demonstrated the therapeutic potential of mEVs as siRNA carriers. Therefore, these results served as an important conformation that mEVs can potentially serve as a safe, stable, and efficient delivery system for oral delivery of siRNA.

Considering that the low siRNA loading efficiency could present the main obstacle to the application of mEVs as nanocarriers, in Chapter 5 new mEV-liposome hybrid systems (hybridosomes) were fabricated. These systems were also investigated for oral delivery of siRNA as IBD therapy. These hybrid systems were developed in two ways, through freeze-thaw fusion of mEVs and cationic liposomes. The hybridosomes demonstrated superior stability in intestinal fluids and reduced cytotoxicity compared with cationic liposomes (and similar to native mEVs). Importantly, the hybridosomes exhibited high siRNA loading efficiency (above 70%) and retained the intestinal epithelial barrier-crossing ability of native mEVs, which significantly increased the permeability of siRNA compared to naked siRNA. Moreover, it was found that GAPDH siRNA loaded-hybridosomes induced efficient gene silencing in macrophages and anti-TNFα siRNA loaded-hybridosomes and mEVs were both able to downregulate TNFα levels and relieve inflammation in an *in vitro* co-culture model of intestinal inflammation. Therefore, mEV-liposome hybrids may be able to overcome some of the issues of mEVs and show promise as oral siRNA delivery systems that could be utilized in IBD therapy.

6.2. Future Perspective

This thesis has shown the potential of mEVs and mEVs-liposome hybrid systems as delivery systems for oral administration of siRNA therapy in IBD. However, to further confirm their potential as therapies, future studies should focus on the following aspects:

i) In our study, the use of hybridosomes demonstrated significantly enhanced loading efficiency for siRNA compared to other loading methods, including transfection reagent, saponin and electroporation. However, the optimization of loading conditions in each method, along with considerations such as the size of delivery systems, and the stability of siRNA and mEVs under different experimental conditions, made it challenging to keep consistency of the concentrations of siRNA and mEVs across different loading methods, which may compromise the comparability of loading efficiencies. Therefore, in future research, efforts should be put into keeping consistency of siRNA and mEVs concentration across various loading methods to ensure that results are directly comparable, despite the inherent difficulties. At least, keeping either the siRNA or mEV concentration constant as a control across different loading methods, while adjusting other conditions, could provide a more reliable basis for comparison.

ii) Our results demonstrated successful incorporation of siRNA into mEVs or hybridosomes. Theoretically, siRNA should be introduced into mEVs by electroporation which induces temporary pores on the vesicle membrane, or by transfection reagent that helps siRNA transport through mEVs membrane. For LN2 freeze-thaw hybridosomes, siRNA is added to the positively charged hybridosomes, and the electrostatic interaction between them leads to siRNA association on mEVs surface. In contrast, siRNA could be encapsulated within the -80 freeze-thaw hybridosomes, given that the siRNA-lipoplexes were formed before fusing with mEVs, and the fusion process (disruption and reassembly) likely provides an opportunity to siRNA to be encapsulated into hybridosomes. However, the exact location of siRNA within or on the surface of mEVs or hybridosomes has not been investigated in this study. Future studies could clarify this by incubating siRNA-vesicle systems with RNase to remove any siRNA attached to the surface of vesicles, followed by assessing the loading efficiency to verify siRNA encapsulation within vesicles [474, 475]. In addition to loading efficiency, fluorescence

microscopy could be used to determine the co-localization percentage of siRNA and vesicles, providing insight into the relationship between them [474].

iii) While mEVs and mEVs-liposomes hybrids were shown to be stable in fasted-state simulated intestinal fluid and possess high permeability across the intestinal epithelium, a notable gap in this study is the absence of a comprehensive stability evaluation in the entire digestion process and permeability assessment across multiple intestinal barriers (as mentioned in 1.2.3) during oral administration. It is necessary to conduct comprehensive *in vitro* digestion tests, including exposure to oral saliva, gastric conditions, and intestinal environments. Even though *in vitro* models in our study, such as IEOs monolayers, contain key intestinal barrier components including various epithelial cells, basement membrane (diluted BME2 on transwell inserts), and mucus from goblet cells, their composition and concentrations do not fully replicate the natural conditions, which should be adjusted and optimized to mimic the complex barriers more accurately. In addition, future *in vivo* studies should incorporate oral administration of these novel delivery systems in an IBD animal model. Furthermore, conducting biodistribution behaviour studies in an IBD animal model using Near-Infrared Fluorescence (NIRF) imaging would provide a valuable insight for determining the localization of our delivery system following oral administration. It would be particularly interesting to establish organ distribution of mEVs and hybrids in order to ascertain whether these systems accumulate in organs other than the intestine (i.e. whether systemic absorption occurs) and determine whether there is a preferential accumulation at the site of intestinal inflammation.

iv) The evaluation of anti-TNFα siRNA-loaded hybridosomes for their efficacy in inflammation relief was conducted in a co-culture intestinal inflammation model (Section 5.4.7.), and it was found that these systems were able to downregulate TNFα. However, the

data indicated that the effect is likely to stem from the inherent effect of mEVs instead of the therapeutic payload they carry. This result may be attributed to the limited siRNA release within the immune cells or the specific conditions of the co-culture model utilized in this study. It should be noted that throughout the incubation of the samples with the co-cultures, the TEER values remained stable, which indicated that the dysfunction in the Caco-2 monolayers through the TNFα induction by LPS was not observed. However, under IBD conditions, the dysfunction of intestinal epithelium is the representative feature, which may also affect the permeation of delivery systems across epithelium. Therefore, this co-culture model should be further optimized to induce temporary barrier dysfunction, such as *via* stimulation by various or combined pro-inflammatory cytokines to both macrophages and Caco-2 monolayers. Furthermore, introducing an additional immune cell type, such as dendritic cells, is considered to potentially simulate IBD conditions more accurately.

v) Two novel human intestinal epithelial models based on IEOs were developed in this study. The IEOs monolayers enable the study of drug delivery systems due to access to the apical side however, in this 2D structure-based model, the natural tissue architecture, namely crypt-villi arrangement, is not represented. Two possible strategies can be considered to overcome these challenges and enhance the relevance of the IEOs monolayers. One approach is to relocate IEOs monolayers onto 3D frameworks, such as scaffolds produced by photolithography, soft-lithography, or 3D printing, which can closely mimic the native structure of the intestinal epithelium in terms of villus and crypt arrangement. Another possibility, which is a technology that has been developing rapidly in recent years, is the incorporation of organoids into an 'organ-on-a-chip' system. The resulting 'gut-on-a-chip' system would replicate the dynamic mechanical stimulation created by shear stress from lumen, and the flow of intestinal fluids, which emulates *in vivo* physiology. Under these dynamic conditions, various types of IEOs

cells are able to differentiate into characteristic populations and structures. Moreover, it is also feasible to incorporate additional components of the intestinal mucosa, such as microbiota and immune cells in the chip to provide a more *in vivo*-relevant environment.

In the future, mEVs and mEV hybrids should also be explored for the delivery of other therapeutic agents, especially other nuclei acid-based systems such as miRNAs and mRNA. For instance, these systems may serve as mRNA carriers in orally-administered vaccines. mRNA-based vaccinations have been regarded as a breakthrough in the field of immunization due to their rapid, scalable and cell-free manufacturing, which enables quicker response to emerging disease outbreaks (e.g. SARS-CoV-2 vaccines). However, their efficacy is often compromised by the need for injection administration, limiting the speed and widespread distribution of these vaccines. Oral administration of mRNA vaccines is considered as effective, pain-free, and convenient method of immunization, however, similar as siRNA, mRNA is unstable and prone to be degraded in the harsh environment of GIT. Therefore, to overcome these challenges, mEVs and mEVs hybrid systems employed in this thesis could be explored as carriers for oral mRNA-based vaccines.

7. Reference

[1] J.R. Korzenik, D.K. Podolsky, Evolving knowledge and therapy of inflammatory bowel disease, Nat. Rev. Drug Discov. 5 (2006) 197-209.

[2] S.C. Ng, et al., Worldwide incidence and prevalence of inflammatory bowel disease in the 21st century: a systematic review of population-based studies, The Lancet 390 (2017) 2769-2778.

[3] S. Alatab, et al., The global, regional, and national burden of inflammatory bowel disease in 195 countries and territories, 1990-2017: a systematic analysis for the Global Burden of Disease Study 2017, Lancet Gastroenterol. Hepatol. 5 (2020) 17-30.

[4] M. Agrawal, E.A. Spencer, J.F. Colombel, R.C. Ungaro, Approach to the management of recently diagnosed inflammatory bowel disease patients: A user's guide for adult and pediatric gastroenterologists, Gastroenterology 161 (2021) 47-65.

[5] E. Szigethy, L. McLafferty, A. Goyal, Inflammatory bowel disease, Child Adolesc. Psychiatr. Clin. N. Am. 19 (2010) 301-318.

[6] I. Ordás, L. Eckmann, M. Talamini, D.C. Baumgart, W.J. Sandborn, Ulcerative colitis, The Lancet 380 (2012) 1606-1619.

[7] D.C. Baumgart, W.J. Sandborn, Crohn's disease, The Lancet 380 (2012) 1590-1605.

[8] B. Xiao, D. Merlin, Oral colon-specific therapeutic approaches toward treatment of inflammatory bowel disease, Expert Opin. Drug Deliv. 9 (2012) 1393-1407.

[9] N.A. Molodecky, et al., Increasing incidence and prevalence of the inflammatory bowel diseases with time, based on systematic review, Gastroenterology 142 (2012) 46-54.

[10] M. Coskun, Intestinal epithelium in inflammatory bowel disease, Front. Med. 1 (2014) 24.

[11] Q. Guan, A comprehensive review and update on the pathogenesis of inflammatory bowel disease, J. Immunol. Res. 2019 (2019) 7247238.

[12] H.L. Huang, et al., Fine-mapping inflammatory bowel disease loci to single-variant resolution, Nature 547 (2017) 173-178.

[13] L.A. Peters, et al., A functional genomics predictive network model identifies regulators of inflammatory bowel disease, Nat. Genet. 49 (2017) 1437-1449.

[14] S. Yamamoto, X.J. Ma, Role of Nod2 in the development of Crohn's disease, Microb. Infect. 11 (2009) 912-918.

[15] W. Strober, A. Kitani, I. Fuss, N. Asano, T. Watanabe, The molecular basis of NOD2 susceptibility mutations in Crohn's disease, Mucosal Immunol. 1 (2008) S5-S9.

[16] W.E. Ek, M. D'Amato, J. Halfvarson, The history of genetics in inflammatory bowel disease, Ann. Gastroenterol. 27 (2014) 294-303.

[17] J.T. Chang, Pathophysiology of inflammatory bowel diseases, N. Engl. J. Med. 383 (2020) 2652-2664.

[18] C.A. Anderson, et al., Investigation of Crohn's Disease Risk Loci in Ulcerative Colitis Further Defines Their Molecular Relationship, Gastroenterology 136 (2009) 523-529.

[19] J.Z. Liu, et al., Association analyses identify 38 susceptibility loci for inflammatory bowel disease and highlight shared genetic risk across populations, Nat. Genet. 47 (2015) 979-986.

[20] T. Hibi, H. Ogata, Novel pathophysiological concepts of inflammatory bowel disease, J. Gastroenterol. 41 (2006) 10-16.

[21] K.T. Dolan, E.B. Chang, Diet, gut microbes, and the pathogenesis of inflammatory bowel diseases, Mol. Nutr. Food Res. 61 (2017) 1600129.

[22] S.M. Ho, et al., Challenges in IBD research: Environmental triggers, Inflamm. Bowel Dis. 25 (2019) S13-S23.
[23] D. Piovani, S. Danese, L. Peyrin-Biroulet, G.K. Nikolopoulos, T. Lytras, S. Bonovas, Environmental risk factors for inflammatory bowel diseases: an umbrella review of meta-analyses, Gastroenterology 157 (2019) 647-659. e644.
[24] G.G. Kaplan, T. Jackson, B.E. Sands, M. Frisch, R.E. Andersson, J. Korzenik, The risk of developing Crohn's disease after an appendectomy: a meta-analysis, Official journal of the American College of Gastroenterology| ACG 103 (2008) 2925-2931.
[25] Y. Sun, et al., The Contribution of Genetic Risk and Lifestyle Factors in the Development of Adult-Onset Inflammatory Bowel Disease: A Prospective Cohort Study, Official journal of the American College of Gastroenterology | ACG 118 (2023) 511-522.
[26] M. Saleh, C.O. Elson, Experimental inflammatory bowel disease: Insights into the host-microbiota dialog, Immunity 34 (2011) 293-302.
[27] J. Ni, G.D. Wu, L. Albenberg, V.T. Tomov, Gut microbiota and IBD: causation or correlation?, Nat. Rev. Gastroenterol. Hepatol. 14 (2017) 573-584.
[28] S. Nell, S. Suerbaum, C. Josenhans, The impact of the microbiota on the pathogenesis of IBD: lessons from mouse infection models, Nat. Rev. Microbiol 8 (2010) 564-577.
[29] M.N. Ince, D.E. Elliott, Immunologic and molecular mechanisms in inflammatory bowel disease, Surg. Clin. North Am. 87 (2007) 681-696.
[30] R. Hodson, Inflammatory bowel disease, Nature 540 (2016) S97-S97.
[31] T. Kucharzik, C. Maaser, A. Lugering, M. Kagnoff, L. Mayer, S. Targan, W. Domschke, Recent understanding of IBD pathogenesis: Implications for future therapies, Inflamm. Bowel Dis. 12 (2006) 1068-1083.
[32] K. Parikh, et al., Colonic epithelial cell diversity in health and inflammatory bowel disease, Nature 567 (2019) 49-55.
[33] S. Danese, Immune and nonimmune components orchestrate the pathogenesis of inflammatory bowel disease, Am. J. Physiol. Gastrointest. Liver Physiol. 300 (2011) G716-G722.
[34] M. Rimoldi, et al., Intestinal immune homeostasis is regulated by the crosstalk between epithelial cells and dendritic cells, Nat. Immunol. 6 (2005) 507-514.
[35] A.L. Hart, H.O. Al-Hassi, R.J. Rigby, S.J. Bell, A.V. Emmanuel, S.C. Knight, M.A. Kamm, A.J. Stagg, Characteristics of intestinal dendritic cells in inflammatory bowel diseases, Gastroenterology 129 (2005) 50-65.
[36] A.M. Mowat, Mucosal macrophages in intestinal homeostasis and inflammation, J. Innate Immun. 3 (2011) 550-564.
[37] S. Thiesen, S. Janciauskiene, H. Uronen-Hansson, W. Agace, C.M. Hogerkorp, P. Spee, K. Hakansson, O. Grip, CD14(hi) HLA-DRdim macrophages, with a resemblance to classical blood monocytes, dominate inflamed mucosa in Crohn's disease, J. Leukocyte Biol. 95 (2014) 531-541.
[38] N. Kamada, et al., Unique CD14(+) intestinal macrophages contribute to the pathogenesis of Crohn disease *via* lL-23/IFN-gamma axis, J. Clin. Invest. 118 (2008) 2269-2280.
[39] E. Meroni, N. Stakenborg, M.F. Viola, G.E. Boeckxstaens, Intestinal macrophages and their interaction with the enteric nervous system in health and inflammatory bowel disease, Acta Physiol. 225 (2019) e13163.
[40] T.T. Pizarro, F. Cominelli, Cytokine therapy for Crohn's disease: Advances in translational research, Annu. Rev. Med. 58 (2007) 433-444.
[41] W. Strober, I.J. Fuss, Proinflammatory cytokines in the pathogenesis of inflammatory bowel diseases, Gastroenterology 140 (2011) 1756-1782.

[42] F.J. Baert, P.R. Rutgeerts, Anti-TNF strategies in Crohn's disease: mechanisms, clinical effects, indications, Int. J. Colorectal Dis. 14 (1999) 47-51.
[43] B. Ngo, C. P Farrell, M. Barr, K. Wolov, R. Bailey, J. M Mullin, J. J Thornton, Tumor necrosis factor blockade for treatment of inflammatory bowel disease: efficacy and safety, Curr. Mol. Pharmacol. 3 (2010) 145-152.
[44] M.G. Bouma, W.A. Buurman, Soluble TNF receptors, in: H. Redl, G. Schlag (Eds.) Cytokines in Severe Sepsis and Septic Shock, Birkhäuser Basel, Basel, 1999, pp. 121-132.
[45] T. van der Poll, J. Jansen, D. van Leenen, M. von der Mohlen, M. Levi, H. ten Cate, H. Gallati, J.W. ten Cate, S.J. van Deventer, Release of soluble receptors for tumor necrosis factor in clinical sepsis and experimental endotoxemia, J. Infect. Dis. 168 (1993) 955-960.
[46] C. Kriegel, M. Amiji, Oral TNF-alpha gene silencing using a polymeric microsphere-based delivery system for the treatment of inflammatory bowel disease, J. Control. Release 150 (2011) 77-86.
[47] O.H. Nielsen, M.A. Ainsworth, Tumor necrosis factor inhibitors for inflammatory bowel disease, New Engl. J. Med. 369 (2013) 754-762.
[48] S.M. Vindigni, T.L. Zisman, D.L. Suskind, C.J. Damman, The intestinal microbiome, barrier function, and immune system in inflammatory bowel disease: a tripartite pathophysiological circuit with implications for new therapeutic directions, Therap. Adv. Gastroenterol. 9 (2016) 606-625.
[49] J.K. Triantafillidis, E. Merikas, F. Georgopoulos, Current and emerging drugs for the treatment of inflammatory bowel disease, Drug Des. Devel. Ther. 5 (2011) 185-210.
[50] A. Viscido, A. Capannolo, G. Latella, R. Caprilli, G. Frieri, Nanotechnology in the treatment of inflammatory bowel diseases, J. Crohns. Colitis 8 (2014) 903-918.
[51] M.T.J. Olesen, B. Ballarin-Gonzalez, K.A. Howard, The application of RNAi-based treatments for inflammatory bowel disease, Drug Deliv. Transl. Res. 4 (2014) 4-18.
[52] S. Ardizzone, G.B. Porro, Biologic therapy for inflammatory bowel disease, Drugs 65 (2005) 2253-2286.
[53] F. Magro, F. Portela, Management of inflammatory bowel disease with infliximab and other anti-tumor necrosis factor alpha therapies, Biodrugs 24 (2010) 3-14.
[54] J. Mantaj, D. Vllasaliu, Recent advances in the oral delivery of biologics, Pharm. J. 304 (2020) No 7933.
[55] T.E.M. Manuc, M.M. Manuc, M.M. Diculescu, Recent insights into the molecular pathogenesis of Crohn's disease: a review of emerging therapeutic targets, Clin. Exp. Gastroenterol. 9 (2016) 59-70.
[56] H.C. Chan, S.C. Ng, Emerging biologics in inflammatory bowel disease, J. Gastroenterol. 52 (2017) 141-150.
[57] A. Di Paolo, G. Luci, Personalized medicine of monoclonal antibodies in inflammatory bowel disease: pharmacogenetics, therapeutic drug monitoring, and beyond, Front. Pharmacol. 11 (2020) 610806.
[58] E. Cruz, V. Kayser, Monoclonal antibody therapy of solid tumors: clinical limitations and novel strategies to enhance treatment efficacy, Biol.: Targets Ther. 13 (2019) 33-51.
[59] A. Schroeder, C.G. Levins, C. Cortez, R. Langer, D.G. Anderson, Lipid-based nanotherapeutics for siRNA delivery, J. Intern. Med. 267 (2010) 9-21.
[60] A. Khvorova, siRNAs—A New Class of Medicines, JAMA 329 (2023) 2185-2186.
[61] S.C. Humphreys, et al., Considerations and recommendations for assessment of plasma protein binding and drug–drug interactions for siRNA therapeutics, Nucleic Acids Res. 50 (2022) 6020-6037.

[62] W. Alshaer, H. Zureigat, A. Al Karaki, A. Al-Kadash, L. Gharaibeh, M.M. Hatmal, A.A.A. Aljabali, A. Awidi, siRNA: Mechanism of action, challenges, and therapeutic approaches, Eur. J. Pharmacol. 905 (2021) 174178.
[63] P.D. Zamore, T. Tuschl, P.A. Sharp, D.P. Bartel, RNAi double-stranded RNA directs the ATP-dependent cleavage of mRNA at 21 to 23 nucleotide intervals, Cell 101 (2000) 25-33.
[64] M. Friedrich, A. Aigner, Therapeutic siRNA: State-of-the-art and future perspectives, BioDrugs 36 (2022) 549-571.
[65] S. Gao, F. Dagnaes-Hansen, E.J. Nielsen, J. Wengel, F. Besenbacher, K.A. Howard, J. Kjems, The effect of chemical modification and nanoparticle formulation on stability and biodistribution of siRNA in mice, Mol. Ther. 17 (2009) 1225-1233.
[66] P. Ventura, et al., Efficacy and safety of givosiran for acute hepatic porphyria: 24-month interim analysis of the randomized phase 3 ENVISION study, Liver International 42 (2022) 161-172.
[67] F.J. Raal, et al., Inclisiran for the Treatment of Heterozygous Familial Hypercholesterolemia, New Engl. J. Med. 382 (2020) 1520-1530.
[68] H. Laroui, D. Geem, B. Xiao, E. Viennois, P. Rakhya, T. Denning, D. Merlin, Targeting intestinal inflammation with CD98 siRNA/PEI-loaded nanoparticles, Mol. Ther. 22 (2014) 69-80.
[69] E.E. Ioachim, K.H. Katsanos, M.C. Michael, E.V. Tsianos, N.J. Agnantis, Immunohistochemical expression of cyclin D1, cyclin E, p21/waf1 and p27/kip1 in inflammatory bowel disease: correlation with other cell-cycle-related proteins (Rb, p53, ki-67 and PCNA) and clinicopathological features, Int. J. Colorectal Dis. 19 (2004) 325-333.
[70] D. Peer, E.J. Park, Y. Morishita, C.V. Carman, M. Shimaoka, Systemic leukocyte-directed siRNA delivery revealing cyclin D1 as an anti-inflammatory target, Science 319 (2008) 627-630.
[71] Y. Zhu, L. Zhu, X. Wang, H. Jin, RNA-based therapeutics: an overview and prospectus, Cell Death Dis. 13 (2022) 644.
[72] A. Stallmach, S. Hagel, T. Bruns, Adverse effects of biologics used for treating IBD, Best Pract. Res. Clin. Gastroenterol. 24 (2010) 167-182.
[73] F. Schnitzler, et al., Long-term outcome of treatment with infliximab in 614 patients with Crohn's disease: results from a single-centre cohort, Gut 58 (2009) 492-500.
[74] D. Vllasaliu, M. Thanou, S. Stolnik, R. Fowler, Recent advances in oral delivery of biologics: nanomedicine and physical modes of delivery, Expert Opin. Drug Deliv. 15 (2018) 759-770.
[75] B. Loretz, F. Foger, M. Werle, A. Bernkop-Schnurch, Oral gene delivery: Strategies to improve stability of pDNA towards intestinal digestion, J. Drug Target. 14 (2006) 311-319.
[76] M.J. O'Neill, L. Bourre, S. Melgar, C.M. O'Driscoll, Intestinal delivery of non-viral gene therapeutics: physiological barriers and preclinical models, Drug Discov. Today 16 (2011) 203-218.
[77] Y. Zhang, M. Thanou, D. Vllasaliu, Exploiting disease-induced changes for targeted oral delivery of biologics and nanomedicines in inflammatory bowel disease, Eur. J. Pharm. Biopharm. 155 (2020) 128-138.
[78] M.A. McGuckin, R. Eri, L.A. Simms, T.H. Florin, G. Radford-Smith, Intestinal barrier dysfunction in inflammatory bowel diseases, Inflamm. Bowel Dis. 15 (2009) 100-113.
[79] S. Prasad, R. Mingrino, K. Kaukinen, K.L. Hayes, R.M. Powell, T.T. MacDonald, J.E. Collins, Inflammatory processes have differential effects on claudins 2, 3 and 4 in colonic epithelial cells, Lab. Invest. 85 (2005) 1139-1162.

[80] J.R. Turner, Intestinal mucosal barrier function in health and disease, Nat. Rev. Immunol. 9 (2009) 799-809.
[81] C. Buning, N. Geissler, M. Prager, A. Sturm, D.C. Baumgart, J. Buttner, S. Buhner, V. Haas, H. Lochs, Increased small intestinal permeability in ulcerative colitis: rather genetic than environmental and a risk factor for extensive disease?, Inflamm. Bowel Dis. 18 (2012) 1932-1939.
[82] D.F. Evans, G. Pye, R. Bramley, A.G. Clark, T.J. Dyson, J.D. Hardcastle, Measurement of gastrointestinal pH profiles in normal ambulant human subjects, Gut 29 (1988) 1035-1041.
[83] A. Allen, G. Flemstrom, A. Garner, E. Kivilaakso, Gastroduodenal mucosal protection, Physiol. Rev. 73 (1993) 823-857.
[84] J.M. Gamboa, K.W. Leong, *In vitro* and *in vivo* models for the study of oral delivery of nanoparticles, Adv. Drug Del. Rev. 65 (2013) 800-810.
[85] A. Effinger, C.M. O'Driscoll, M. McAllister, N. Fotaki, Impact of gastrointestinal disease states on oral drug absorption - implications for formulation design - a PEARRL review, J. Pharm. Pharmacol. 71 (2019) 674-698.
[86] V.C. Ibekwe, H.M. Fadda, E.L. McConnell, M.K. Khela, D.F. Evans, A.W. Basit, Interplay between intestinal pH, transit time and feed status on the *in vivo* performance of pH responsive ileo-colonic release systems, Pharm. Res. 25 (2008) 1828-1835.
[87] S.F. Zhang, R. Langer, G. Traverso, Nanoparticulate drug delivery systems targeting inflammation for treatment of inflammatory bowel disease, Nano Today 16 (2017) 82-96.
[88] T.A. Winter, S.J.D. O'Keefe, M. Callanan, N. Dip, T. Marks, Impaired gastric acid and pancreatic enzyme secretion in patients with Crohn's disease may be a consequence of a poor nutritional state, Inflamm. Bowel Dis. 10 (2004) 618-625.
[89] G. Angelini, G. Cavallini, P. Bovo, G. Brocco, A. Castagnini, E. Lavarini, F. Merigo, N. Tallon, L.A. Scuro, Pancreatic function in chronic inflammatory bowel disease, Int. J. Pancreatol. 3 (1988) 185-193.
[90] N. Vergnolle, Protease inhibition as new therapeutic strategy for GI diseases, Gut 65 (2016) 1215-1224.
[91] R.B. Sartor, G.D. Wu, Roles for intestinal bacteria, viruses, and fungi in pathogenesis of inflammatory bowel diseases and therapeutic approaches, Gastroenterology 152 (2017) 327-339.
[92] J.J. Qin, et al., A human gut microbial gene catalogue established by metagenomic sequencing, Nature 464 (2010) 59-65.
[93] O. Carrette, C. Favier, C. Mizon, C. Neut, A. Cortot, J.F. Colombel, J. Mizon, Bacterial enzymes used for colon-specific drug delivery are decreased in active Crohn's disease, Dig. Dis. Sci. 40 (1995) 2641-2646.
[94] A.P. Corfield, A.J.K. Williams, J.R. Clamp, S.A. Wagner, R.A. Mountford, Degradation by bacterial enzymes of colonic mucus from normal subjects and patients with inflammatory bowel disease: The role of sialic acid metabolism and the detection of a novel *O*-acetylsialic acid esterase, Clin. Sci. 74 (1988) 71-78.
[95] C. Atuma, V. Strugala, A. Allen, L. Holm, The adherent gastrointestinal mucus gel layer: thickness and physical state in vivo, Am. J. Physiol. Gastrointest. Liver Physiol. 280 (2001) G922-G929.
[96] M.E. Johansson, et al., Composition and functional role of the mucus layers in the intestine, Cell. Mol. Life Sci. 68 (2011) 3635-3641.
[97] J.Y. Lock, T.L. Carlson, R.L. Carrier, Mucus models to evaluate the diffusion of drugs and particles, Adv. Drug Del. Rev. 124 (2018) 34-49.

[98] T.L. Carlson, J.Y. Lock, R.L. Carrier, Engineering the Mucus Barrier, in: M.L. Yamush (Ed.) Annual review of biomedical engineering, Vol 20, 2018, pp. 197-220.
[99] S.P. Bandi, Y.S. Kumbhar, V.V.K. Venuganti, Effect of particle size and surface charge of nanoparticles in penetration through intestinal mucus barrier, J. Nanopart. Res. 22 (2020) 62.
[100] G.M. Birchenough, M.E. Johansson, J.K. Gustafsson, J.H. Bergstrom, G.C. Hansson, New developments in goblet cell mucus secretion and function, Mucosal Immunol. 8 (2015) 712-719.
[101] X. Murgia, B. Loretz, O. Hartwig, M. Hittinger, C.M. Lehr, The role of mucus on drug transport and its potential to affect therapeutic outcomes, Adv. Drug Del. Rev. 124 (2018) 82-97.
[102] B.H. Bajka, N.M. Rigby, K.L. Cross, A. Macierzanka, A.R. Mackie, The influence of small intestinal mucus structure on particle transport ex vivo, Colloids Surf. B. Biointerfaces 135 (2015) 73-80.
[103] H.M. Yildiz, C.A. McKelvey, P.J. Marsac, R.L. Carrier, Size selectivity of intestinal mucus to diffusing particulates is dependent on surface chemistry and exposure to lipids, J. Drug Target. 23 (2015) 768-774.
[104] S.K. Lai, D.E. O'Hanlon, S. Harrold, S.T. Man, Y.-Y. Wang, R. Cone, J. Hanes, Rapid transport of large polymeric nanoparticles in fresh undiluted human mucus, Proc. Natl. Acad. Sci. U.S.A. 104 (2007) 1482-1487.
[105] B.B. González, E.B. Nielsen, T.B. Thomsen, K.A. Howard, Mucosal delivery of RNAi therapeutics, in: RNA Interference from Biology to Therapeutics, 2013, pp. 97-125.
[106] F. Laffleur, F. Hintzen, G. Shahnaz, D. Rahmat, K. Leithner, A. Bernkop-Schnürch, Development and in vitro evaluation of slippery nanoparticles for enhanced diffusion through native mucus, Nanomedicine 9 (2014) 387-396.
[107] C. Schultsz, F.M. van den Berg, F.W. ten Kate, G.N.J. Tytgat, J. Dankert, The intestinal mucus layer from patients with inflammatory bowel disease harbors high numbers of bacteria compared with controls, Gastroenterology 117 (1999) 1089-1097.
[108] M. Boegh, H.M. Nielsen, Mucus as a Barrier to Drug Delivery – Understanding and Mimicking the Barrier Properties, Basic Clin. Pharmacol. Toxicol. 116 (2015) 179-186.
[109] L.A. Sellers, A. Allen, E. Morris, S.R. Murphy, Rheological studies on pig gastrointestinal mucous secretions, in, Portland Press Ltd., 1983.
[110] M. Van Allen, Handbook of Physiology: A Critical, Comprehensive Presentation of Physiological Knowledge and Concepts, Arch. Intern. Med. 106 (1960) 580-581.
[111] L.M. Ensign, A. Henning, C.S. Schneider, K. Maisel, Y.-Y. Wang, M.D. Porosoff, R. Cone, J. Hanes, Ex Vivo Characterization of Particle Transport in Mucus Secretions Coating Freshly Excised Mucosal Tissues, Mol. Pharm. 10 (2013) 2176-2182.
[112] R.D. Pullan, G.A.O. Thomas, M. Rhodes, R.G. Newcombe, G.T. Williams, A. Allen, J. Rhodes, Thickness of adherent mucus gel on colonic mucosa in humans and its relevance to colitis, Gut 35 (1994) 353-359.
[113] M. Derrien, M.W.J. van Passel, J.H.B. van de Bovenkamp, R.G. Schipper, W.M. de Vos, J. Dekker, Mucin-bacterial interactions in the human oral cavity and digestive tract, Gut Microbes 1 (2010) 254-268.
[114] A.H. Raouf, H.H. Tsai, N. Parker, J. Hoffman, R.J. Walker, J.M. Rhodes, Sulphation of colonic and rectal mucin in inflammatory bowel disease: reduced sulphation of rectal mucus in ulcerative colitis, Clin. Sci. 83 (1992) 623-626.
[115] M.E.V. Johansson, et al., Bacteria penetrate the normally impenetrable inner colon mucus layer in both murine colitis models and patients with ulcerative colitis, Gut 63 (2014) 281-291.

[116] I. Arijs, et al., Mucosal gene expression of antimicrobial peptides in inflammatory bowel disease before and after first infliximab treatment, Plos One 4 (2009) e7984.
[117] J. Wehkamp, M. Schmid, K. Fellermann, E.F. Stange, Defensin deficiency, intestinal microbes, and the clinical phenotypes of Crohn's disease, J. Leukocyte Biol. 77 (2005) 460-465.
[118] M. Karner, et al., First multicenter study of modified release phosphatidylcholine "LT-02" in ulcerative colitis: a randomized, placebo-controlled trial in mesalazine-refractory courses, Am. J. Gastroenterol. Suppl. 109 (2014) 1041-1051.
[119] R. Ehehalt, J. Wagenblast, G. Erben, W.D. Lehmann, U. Hinz, U. Merle, W. Stremmel, Phosphatidylcholine and lysophosphatidylcholine in intestinal mucus of ulcerative colitis patients. A quantitative approach by nanoelectrospray-tandem mass spectrometry, Scand. J. Gastroenterol. 39 (2004) 737-742.
[120] A. Braun, et al., Alterations of phospholipid concentration and species composition of the intestinal mucus barrier in ulcerative colitis: a clue to pathogenesis, Inflamm. Bowel Dis. 15 (2009) 1705-1720.
[121] E. Theodoratou, et al., The role of glycosylation in IBD, Nat. Rev. Gastroenterol. Hepatol. 11 (2014) 588-600.
[122] J.M.H. Larsson, H. Karlsson, J.G. Crespo, M.E.V. Johansson, L. Eklund, H. Sjovall, G.C. Hansson, Altered *O*-glycosylation profile of MUC2 mucin occurs in active ulcerative colitis and is associated with increased inflammation, Inflamm. Bowel Dis. 17 (2011) 2299-2307.
[123] N.J. Simmonds, R.E. Allen, T.R.J. Stevens, R.N.M. Vansomeren, D.R. Blake, D.S. Rampton, Chemiluminescence assay of mucosal reactive oxygen metabolites in inflammatory bowel disease, Gastroenterology 103 (1992) 186-196.
[124] C. Yang, D. Merlin, Nanoparticle-mediated drug delivery systems for the treatment of IBD: current perspectives, Int. J. Nanomedicine 14 (2019) 8875-8889.
[125] J.M. Allaire, S.M. Crowley, H.T. Law, S.Y. Chang, H.J. Ko, B.A. Vallance, The intestinal epithelium: central coordinator of mucosal immunity, Trends Immunol. 39 (2018) 677-696.
[126] J.Y. Lee, V.C. Wasinger, Y.Y. Yau, E. Chuang, V. Yajnik, R.W. Leong, Molecular pathophysiology of epithelial barrier dysfunction in inflammatory bowel diseases, Proteomes 6 (2018) 17.
[127] Y. Merga, B.J. Campbell, J.M. Rhodes, Mucosal barrier, bacteria and inflammatory bowel disease: possibilities for therapy, Dig. Dis. 32 (2014) 475-483.
[128] S.J. Brown, M.T. Abreu, Antibodies to tumor necrosis factor-alpha in the treatment of Crohn's disease, Curr. Opin. Drug Discov. Dev. 8 (2005) 160-168.
[129] F. Heller, et al., Interleukin-13 is the key effector Th2 cytokine in ulcerative colitis that affects epithelial tight junctions, apoptosis, and cell restitution, Gastroenterology 129 (2005) 550-564.
[130] A.H. Gitter, F. Wullstein, M. Fromm, J.D. Schulzke, Epithelial barrier defects in ulcerative colitis: Characterization and quantification by electrophysiological imaging, Gastroenterology 121 (2001) 1320-1328.
[131] R. Kiesslich, et al., Local barrier dysfunction identified by confocal laser endomicroscopy predicts relapse in inflammatory bowel disease, Gut 61 (2012) 1146-1153.
[132] S. Zeissig, et al., Changes in expression and distribution of claudin 2, 5 and 8 lead to discontinuous tight junctions and barrier dysfunction in active Crohn's disease, Gut 56 (2007) 61-72.
[133] P. Nava, et al., Interferon-γ regulates intestinal epithelial homeostasis through converging beta-catenin signaling pathways, Immunity 32 (2010) 392-402.

[134] T.S. Olson, et al., The primary defect in experimental ileitis originates from a nonhematopoietic source, J. Exp. Med. 203 (2006) 541-552.
[135] S. Amasheh, N. Meiri, A.H. Gitter, T. Schoneberg, J. Mankertz, J.D. Schulzke, M. Fromm, Claudin-2 expression induces cation-selective channels in tight junctions of epithelial cells, J. Cell Sci. 115 (2002) 4969-4976.
[136] T. Oshima, H. Miwa, T. Joh, Changes in the expression of claudins in active ulcerative colitis, J. Gastroenterol. Hepatol. 23 (2008) S146-S150.
[137] X.Y. Si, D. Merlin, B. Xiao, Recent advances in orally administered cell-specific nanotherapeutics for inflammatory bowel disease, World J. Gastroenterol. 22 (2016) 7718-7726.
[138] M. Zhang, D. Merlin, Nanoparticle-based oral drug delivery systems targeting the colon for treatment of ulcerative colitis, Inflamm. Bowel Dis. 24 (2018) 1401-1415.
[139] S.F. Zhang, et al., An inflammation-targeting hydrogel for local drug delivery in inflammatory bowel disease, Sci. Transl. Med. 7 (2015) 300ra128.
[140] B. Tirosh, N. Khatib, Y. Barenholz, A. Nissan, A. Rubinstein, Transferrin as a luminal target for negatively charged liposomes in the inflamed colonic mucosa, Mol. Pharm. 6 (2009) 1083-1091.
[141] U. Testa, E. Pelosi, C. Peschle, The transferrin receptor, Crit. Rev. Oncogen. 4 (1993) 241-276.
[142] J.M. Yong, J. Mantaj, Y.Y. Cheng, D. Vllasaliu, Delivery of nanoparticles across the intestinal epithelium *via* the transferrin transport pathway, Pharmaceutics 11 (2019) 298.
[143] E. Harel, A. Rubinstein, A. Nissan, E. Khazanov, M. Nadler Milbauer, Y. Barenholz, B. Tirosh, Enhanced transferrin receptor expression by proinflammatory cytokines in enterocytes as a means for local delivery of drugs to inflamed gut mucosa, PLoS ONE 6 (2011) e24202.
[144] H.T. Nguyen, D. Merlin, Homeostatic and innate immune responses: role of the transmembrane glycoprotein CD98, Cell. Mol. Life Sci. 69 (2012) 3015-3026.
[145] S.A. Ingersoll, S. Ayyadurai, M.A. Charania, H. Laroui, Y.T. Yan, D. Merlin, The role and pathophysiological relevance of membrane transporter PepT1 in intestinal inflammation and inflammatory bowel disease, Am. J. Physiol. Gastrointest. Liver Physiol. 302 (2012) G484-G492.
[146] S.Y. Vafaei, M. Esmaeili, M. Amini, F. Atyabi, S.N. Ostad, R. Dinarvand, Self assembled hyaluronic acid nanoparticles as a potential carrier for targeting the inflamed intestinal mucosa, Carbohydr. Polym. 144 (2016) 371-381.
[147] X.W. Zhang, W. Wu, Ligand-mediated active targeting for enhanced oral absorption, Drug Discov. Today 19 (2014) 898-904.
[148] T.E. Wileman, M.R. Lennartz, P.D. Stahl, Identification of the macrophage mannose receptor as a 175-kDa membrane protein, Proc. Natl. Acad. Sci. U. S. A. 83 (1986) 2501-2505.
[149] H.L. Jiang, M.L. Kang, J.S. Quan, S.G. Kang, T. Akaike, H.S. Yoo, C.S. Cho, The potential of mannosylated chitosan microspheres to target macrophage mannose receptors in an adjuvant-delivery system for intranasal immunization, Biomaterials 29 (2008) 1931-1939.
[150] A. Jain, A. Agarwal, S. Majumder, N. Lariya, A. Khaya, H. Agrawal, S. Majumdar, G.P. Agrawal, Mannosylated solid lipid nanoparticles as vectors for site-specific delivery of an anti-cancer drug, J. Control. Release 148 (2010) 359-367.
[151] L. Hashem, M. Swedrowska, D. Vllasaliu, Intestinal uptake and transport of albumin nanoparticles: potential for oral delivery, Nanomedicine 13 (2018) 1255-1265.

[152] E.M. Pridgen, F. Alexis, T.T. Kuo, E. Levy-Nissenbaum, R. Karnik, R.S. Blumberg, R. Langer, O.C. Farokhzad, Transepithelial transport of Fc-targeted nanoparticles by the neonatal fc receptor for oral delivery, Sci. Transl. Med. 5 (2013) 213ra167.
[153] J. Roerig, L. Schiller, H. Kalwa, G. Hause, C. Vissiennon, M.C. Hacker, C. Wölk, M. Schulz-Siegmund, A focus on critical aspects of uptake and transport of milk-derived extracellular vesicles across the Caco-2 intestinal barrier model, Eur. J. Pharm. Biopharm. 166 (2021) 61-74.
[154] J.L. Betker, B.M. Angle, M.W. Graner, T.J. Anchordoquy, The potential of exosomes from cow milk for oral delivery, J. Pharm. Sci. 108 (2019) 1496-1505.
[155] S.K. Ramadass, S.L. Jabaris, R.K. Perumal, V.I. HairulIslam, A. Gopinath, B. Madhan, Type I collagen and its daughter peptides for targeting mucosal healing in ulcerative colitis: A new treatment strategy, Eur. J. Pharm. Sci. 91 (2016) 216-224.
[156] E.A. Abou Neel, L. Bozec, J.C. Knowles, O. Syed, V. Mudera, R. Day, J.K. Hyun, Collagen - Emerging collagen based therapies hit the patient, Adv. Drug Del. Rev. 65 (2013) 429-456.
[157] R. Jayadev, D.R. Sherwood, Basement membranes, Curr. Biol. 27 (2017) R207-R211.
[158] P. Mestres, L.L. Gomez, T.N. Lopez, G. del Rosario, S.W. Lukas, U. Hartmann, The basement membrane of the isolated rat colonic mucosa. A light, electron and atomic force microscopy study, Ann. Anat. 196 (2014) 108-118.
[159] J. Mantaj, T. Abu-Shams, Z. Enlo-Scott, M. Swedrowska, D. Vllasaliu, Role of the basement membrane as an intestinal barrier to absorption of macromolecules and nanoparticles, Mol. Pharm. 15 (2018) 5802-5808.
[160] M.C. Alfano, A.I. Chasens, C.W. Masi, Autoradiographic study of the penetration of radiolabelled dextrans and inulin through non-keratinized oral mucosa *in vitro*, J. Periodontal Res. 12 (1977) 368-377.
[161] E. Shimshoni, D. Yablecovitch, L. Baram, I. Dotan, I. Sagi, ECM remodelling in IBD: innocent bystander or partner in crime? The emerging role of extracellular molecular events in sustaining intestinal inflammation, Gut 64 (2015) 367-372.
[162] L. Stronati, F. Palone, A. Negroni, E. Colantoni, A.B. Mancuso, S. Cucchiara, V. Cesi, S. Isoldi, R. Vitali, Dipotassium glycyrrhizate improves intestinal mucosal healing by modulating extracellular matrix remodeling genes and restoring epithelial barrier functions, Front. immunol. 10 (2019) 939.
[163] A. Derkacz, P. Olczyk, K. Olczyk, K. Komosinska-Vassev, The Role of Extracellular Matrix Components in Inflammatory Bowel Diseases, J. Clin. Med. 10 (2021) 1122.
[164] A. Gaggar, P.L. Jackson, B.D. Noerager, P.J. O'Reilly, D.B. McQuaid, S.M. Rowe, J.P. Clancy, J.E. Blalock, A novel proteolytic cascade generates an extracellular matrix-derived chemoattractant in chronic neutrophilic inflammation, J. Immunol. 180 (2008) 5662-5669.
[165] F. Rieder, J.R. de Bruyn, B.T. Pham, K. Katsanos, V. Annese, P.D. Higgins, F. Magro, I. Dotan, Results of the 4th scientific workshop of the ECCO (Group II): markers of intestinal fibrosis in inflammatory bowel disease, J. Crohns Colitis 8 (2014) 1166-1178.
[166] L. Mäkitalo, T. Sipponen, P. Kärkkäinen, K.-L. Kolho, U. Saarialho-Kere, Changes in matrix metalloproteinase (MMP) and tissue inhibitors of metalloproteinases (TIMP) expression profile in Crohn's disease after immunosuppressive treatment correlate with histological score and calprotectin values, Int. J. Colorectal Dis. 24 (2009) 1157-1167.
[167] J.R. de Bruyn, et al., Intestinal fibrosis is associated with lack of response to Infliximab therapy in Crohn's disease, PLOS ONE 13 (2018) e0190999.

[168] D.G. Vartak, R.A. Gemeinhart, Matrix metalloproteases: Underutilized targets for drug delivery, J. Drug Target. 15 (2007) 1-20.
[169] S. Zhang, R. Langer, G. Traverso, Nanoparticulate drug delivery systems targeting inflammation for treatment of inflammatory bowel disease, Nano Today 16 (2017) 82-96.
[170] M. Sobczak, Enzyme-Responsive Hydrogels as Potential Drug Delivery Systems—State of Knowledge and Future Prospects, Int. J. Mol. Sci. 23 (2022) 4421.
[171] A. Wittrup, A. Ai, X. Liu, P. Hamar, R. Trifonova, K. Charisse, M. Manoharan, T. Kirchhausen, J. Lieberman, Visualizing lipid-formulated siRNA release from endosomes and target gene knockdown, Nat. Biotechnol. 33 (2015) 870-876.
[172] T. Tieu, Y. Wei, A. Cifuentes-Rius, N.H. Voelcker, Overcoming Barriers: Clinical Translation of siRNA Nanomedicines, Adv. Ther. 4 (2021) 2100108.
[173] S. Zhang, H. Gao, G. Bao, Physical principles of nanoparticle cellular endocytosis, ACS nano 9 (2015) 8655-8671.
[174] C. Wang, T. Zhao, Y. Li, G. Huang, M.A. White, J. Gao, Investigation of endosome and lysosome biology by ultra pH-sensitive nanoprobes, Adv. Drug Del. Rev. 113 (2017) 87-96.
[175] G. Sahay, et al., Efficiency of siRNA delivery by lipid nanoparticles is limited by endocytic recycling, Nat. Biotechnol. 31 (2013) 653-658.
[176] C.R. Brown, et al., Investigating the pharmacodynamic durability of GalNAc–siRNA conjugates, Nucleic Acids Res. 48 (2020) 11827-11844.
[177] K.A. Lennox, M.A. Behlke, Chemical modification and design of anti-miRNA oligonucleotides, Gene Ther. 18 (2011) 1111-1120.
[178] W.J. Kim, S.W. Kim, Efficient siRNA Delivery with Non-viral Polymeric Vehicles, Pharm. Res. 26 (2009) 657-666.
[179] M. Jafari, P. Chen, Peptide mediated siRNA delivery, Curr. Top. Med. Chem. 9 (2009) 1088-1097.
[180] S.S. Ali Zaidi, F. Fatima, S.A. Ali Zaidi, D. Zhou, W. Deng, S. Liu, Engineering siRNA therapeutics: challenges and strategies, J. Nanobiotechnology 21 (2023) 381.
[181] Viral Vector Systems for Gene Therapy: A Comprehensive Literature Review of Progress and Biosafety Challenges, Appl. Biosaf. 25 (2020) 7-18.
[182] A.N. Lukashev, A.A. Zamyatnin, Viral vectors for gene therapy: Current state and clinical perspectives, Biochemistry (Moscow) 81 (2016) 700-708.
[183] K. Lundstrom, Viral Vectors in Gene Therapy, Diseases 6 (2018) 42.
[184] R. Buckinx, J.-P. Timmermans, Targeting the gastrointestinal tract with viral vectors: state of the art and possible applications in research and therapy, Histochem. Cell Biol. 146 (2016) 709-720.
[185] J.C. Steel, G. Di Pasquale, C.A. Ramlogan, V. Patel, J.A. Chiorini, J.C. Morris, Oral vaccination with adeno-associated virus vectors expressing the Neu oncogene inhibits the growth of murine breast cancer, Mol. Ther. 21 (2013) 680-687.
[186] Oral Administration of Recombinant Adeno-Associated Virus Elicits Human Immunodeficiency Virus-Specific Immune Responses, Hum. Gene Ther. 13 (2002) 1571-1581.
[187] W. Huang, T. McMurphy, X. Liu, C. Wang, L. Cao, Genetic Manipulation of Brown Fat Via Oral Administration of an Engineered Recombinant Adeno-associated Viral Serotype Vector, Mol. Ther. 24 (2016) 1062-1069.
[188] S. Singh, S.S. Ray, Polylactide based nanostructured Biomaterials and their applications, J. Nanosci. Nanotechnol. 7 (2007) 2596-2615.

[189] F. Danhier, E. Ansorena, J.M. Silva, R. Coco, A. Le Breton, V. Preat, PLGA-based nanoparticles: An overview of biomedical applications, J. Control. Release 161 (2012) 505-522.
[190] D. Chenthamara, S. Subramaniam, S.G. Ramakrishnan, S. Krishnaswamy, M.M. Essa, F.-H. Lin, M.W. Qoronfleh, Therapeutic efficacy of nanoparticles and routes of administration, Biomater. Res. 23 (2019) 20.
[191] B. Begines, T. Ortiz, M. Pérez-Aranda, G. Martínez, M. Merinero, F. Argüelles-Arias, A. Alcudia, Polymeric Nanoparticles for Drug Delivery: Recent Developments and Future Prospects, Nanomaterials (Basel) 10 (2020).
[192] H. Laroui, E. Viennois, B. Xiao, B.S. Canup, D. Geem, T.L. Denning, D. Merlin, Fab'-bearing siRNA TNFα-loaded nanoparticles targeted to colonic macrophages offer an effective therapy for experimental colitis, J. Control. Release 186 (2014) 41-53.
[193] Y. Huang, J. Guo, S. Gui, Orally targeted galactosylated chitosan poly(lactic-co-glycolic acid) nanoparticles loaded with TNF-α siRNA provide a novel strategy for the experimental treatment of ulcerative colitis, Eur. J. Pharm. Sci. 125 (2018) 232-243.
[194] H. Laroui, A.L. Theiss, Y. Yan, G. Dalmasso, H.T. Nguyen, S.V. Sitaraman, D. Merlin, Functional TNFalpha gene silencing mediated by polyethyleneimine/TNFalpha siRNA nanocomplexes in inflamed colon, Biomaterials 32 (2011) 1218-1228.
[195] A. Frede, B. Neuhaus, R. Klopfleisch, C. Walker, J. Buer, W. Muller, M. Epple, A.M. Westendorf, Colonic gene silencing using siRNA-loaded calcium phosphate/PLGA nanoparticles ameliorates intestinal inflammation *in vivo*, J. Control. Release 222 (2016) 86-96.
[196] X. Xu, W. Yang, Q. Liang, Y. Shi, W. Zhang, X. Wang, F. Meng, Z. Zhong, L. Yin, Efficient and targeted drug/siRNA co-delivery mediated by reversibly crosslinked polymersomes toward anti-inflammatory treatment of ulcerative colitis (UC), Nano Res. 12 (2019) 659-667.
[197] H. Nsairat, D. Khater, U. Sayed, F. Odeh, A. Al Bawab, W. Alshaer, Liposomes: structure, composition, types, and clinical applications, Heliyon 8 (2022) e09394.
[198] L. Maja, K. Željko, P. Mateja, Sustainable technologies for liposome preparation, J. Supercrit. Fluids 165 (2020) 104984.
[199] X. Ming, K. Sato, R.L. Juliano, Unconventional internalization mechanisms underlying functional delivery of antisense oligonucleotides via cationic lipoplexes and polyplexes, J. Control. Release 153 (2011) 83-92.
[200] Y.J. Zhang, et al., Engineering mucosal RNA interference *in vivo*, Mol. Ther. 14 (2006) 336-342.
[201] Y. Guo, X. He, R.M. Zhao, H.Z. Yang, Z. Huang, J. Zhang, X.Q. Yu, Zn-dipicolylamine-based reactive oxygen species-responsive lipids for siRNA delivery and in vivo colitis treatment, Acta Biomater. 147 (2022) 287-298.
[202] M. Zhang, X. Wang, M.K. Han, J.F. Collins, D. Merlin, Oral administration of ginger-derived nanolipids loaded with siRNA as a novel approach for efficient siRNA drug delivery to treat ulcerative colitis, Nanomedicine 12 (2017) 1927-1943.
[203] A. Wittrup, A. Ai, X. Liu, P. Hamar, R. Trifonova, K. Charisse, M. Manoharan, T. Kirchhausen, J. Lieberman, Visualizing lipid-formulated siRNA release from endosomes and target gene knockdown, Nat. Biotechnol. 33 (2015) 870-876.
[204] H. Lv, S. Zhang, B. Wang, S. Cui, J. Yan, Toxicity of cationic lipids and cationic polymers in gene delivery, J. Control. Release 114 (2006) 100-109.
[205] W. Liu, A. Ye, F. Han, J. Han, Advances and challenges in liposome digestion: Surface interaction, biological fate, and GIT modeling, Adv. Colloid Interface Sci. 263 (2019) 52-67.

[206] W. Liu, F. Wei, A. Ye, M. Tian, J. Han, Kinetic stability and membrane structure of liposomes during in vitro infant intestinal digestion: Effect of cholesterol and lactoferrin, Food Chem. 230 (2017) 6-13.
[207] M.-L. Binderup, L. Bredsdorff, V.M. Beltoft, A. Mortensen, K. Löschner, K. Löschner, E.H. Larsen, F.D. Eriksen, Systemic Absorption of Nanomaterials by Oral Exposure, in: Better control of nano, DTU library, 2013.
[208] R.L. Ball, P. Bajaj, K.A. Whitehead, Oral delivery of siRNA lipid nanoparticles: Fate in the GI tract, Sci. Rep. 8 (2018) 2178.
[209] G. Alp, N. Aydogan, Lipid-based mucus penetrating nanoparticles and their biophysical interactions with pulmonary mucus layer, Eur. J. Pharm. Biopharm. 149 (2020) 45-57.
[210] L.M. Doyle, M.Z. Wang, Overview of extracellular vesicles, their origin, composition, purpose, and methods for exosome isolation and analysis, Cells 8 (2019).
[211] B. Jurgielewicz, S. Stice, Y. Yao, Therapeutic potential of nucleic acids when combined with extracellular vesicles, Aging Dis. 12 (2021) 1476-1493.
[212] R. Sanwlani, P. Fonseka, S.V. Chitti, S. Mathivanan, Milk-derived extracellular vesicles in inter-organism, cross-species communication and drug delivery, Proteomes 8 (2020) 11.
[213] A. Jafari, A. Babajani, M. Abdollahpour-Alitappeh, N. Ahmadi, M. Rezaei-Tavirani, Exosomes and cancer: from molecular mechanisms to clinical applications, Med. Oncol. 38 (2021) 45.
[214] M. Xu, et al., The biogenesis and secretion of exosomes and multivesicular bodies (MVBs): Intercellular shuttles and implications in human diseases, Genes & Diseases 10 (2023) 1894-1907.
[215] X. Xu, Y. Lai, Z.C. Hua, Apoptosis and apoptotic body: disease message and therapeutic target potentials, Biosci. Rep. 39 (2019).
[216] M. Frydrychowicz, A. Kolecka-Bednarczyk, M. Madejczyk, S. Yasar, G. Dworacki, Exosomes - structure, biogenesis and biological role in non-small-cell lung cancer, Scand. J. Immunol. 81 (2015) 2-10.
[217] Z. Yang, et al., Functional exosome-mimic for delivery of siRNA to cancer: *in vitro* and *in vivo* evaluation, J. Control. Release 243 (2016) 160-171.
[218] C. Tucher, K. Bode, P. Schiller, L. Claßen, C. Birr, M.M. Souto-Carneiro, N. Blank, H.M. Lorenz, M. Schiller, Extracellular Vesicle Subtypes Released From Activated or Apoptotic T-Lymphocytes Carry a Specific and Stimulus-Dependent Protein Cargo, Front. immunol. 9 (2018) 534.
[219] P. Stejskal, H. Goodarzi, J. Srovnal, M. Hajdúch, L.J. van 't Veer, M.J.M. Magbanua, Circulating tumor nucleic acids: biology, release mechanisms, and clinical relevance, Mol. Cancer 22 (2023) 15.
[220] K.C. Miranda, D.T. Bond, M. McKee, J. Skog, T.G. Păunescu, N. Da Silva, D. Brown, L.M. Russo, Nucleic acids within urinary exosomes/microvesicles are potential biomarkers for renal disease, Kidney Int. 78 (2010) 191-199.
[221] M.J. Haney, et al., Exosomes as drug delivery vehicles for Parkinson's disease therapy, J. Control. Release 207 (2015) 18-30.
[222] E. Segura, S. Amigorena, C. Thery, Mature dendritic cells secrete exosomes with strong ability to induce antigen-specific effector immune responses, Blood Cells Mol. Dis. 35 (2005) 89-93.
[223] R.W.Y. Yeo, R.C. Lai, B. Zhang, S.S. Tan, Y. Yin, B.J. Teh, S.K. Lim, Mesenchymal stem cell: an efficient mass producer of exosomes for drug delivery, Adv. Drug Del. Rev. 65 (2013) 336-341.

[224] M. Kou, et al., Mesenchymal stem cell-derived extracellular vesicles for immunomodulation and regeneration: a next generation therapeutic tool?, Cell Death Dis. 13 (2022) 580.
[225] N.M. Mahaweni, M.E.H. Kaijen-Lambers, J. Dekkers, J.G.J.V. Aerts, J.P.J.J. Hegmans, Tumour-derived exosomes as antigen delivery carriers in dendritic cell-based immunotherapy for malignant mesothelioma, J. Extracell. Vesicles 2 (2013) 22492.
[226] S.M. Kim, Y. Yang, S.J. Oh, Y. Hong, M. Seo, M. Jang, Cancer-derived exosomes as a delivery platform of CRISPR/Cas9 confer cancer cell tropism-dependent targeting, J. Control. Release 266 (2017) 8-16.
[227] F. Ma, J. Vayalil, G. Lee, Y. Wang, G. Peng, Emerging role of tumor-derived extracellular vesicles in T cell suppression and dysfunction in the tumor microenvironment, J. immunotherap. cancer 9 (2021) e003217.
[228] X. Luan, K. Sansanaphongpricha, I. Myers, H. Chen, H. Yuan, D. Sun, Engineering exosomes as refined biological nanoplatforms for drug delivery, Acta Pharmacol. Sin. 38 (2017) 754-763.
[229] B. Oliviero, et al., Ceramide present in cholangiocarcinoma-derived extracellular vesicle induces a pro-inflammatory state in monocytes, Sci. Rep. 13 (2023) 7766.
[230] R. Du, C. Wang, L. Zhu, Y. Yang, Extracellular vesicles as delivery vehicles for therapeutic nucleic acids in cancer gene therapy: Progress and challenges, Pharmaceutics 14 (2022) 2236.
[231] S. Raimondo, et al., Citrus limon-derived nanovesicles inhibit cancer cell proliferation and suppress CML xenograft growth by inducing TRAIL-mediated cell death, Oncotarget 6 (2015) 19514.
[232] S. Raimondo, et al., Preliminary results of CitraVes™ effects on low density lipoprotein cholesterol and waist circumference in healthy subjects after 12 Weeks: a pilot open-label study, Metabolites 11 (2021) 276.
[233] S. Ju, et al., Grape exosome-like nanoparticles induce intestinal stem cells and protect mice from DSS-induced colitis, Mol. Ther. 21 (2013) 1345-1357.
[234] Q.L. Wang, et al., Grapefruit-derived nanovectors use an activated leukocyte trafficking pathway to deliver therapeutic agents to inflammatory tumor sites, Cancer Res. 75 (2015) 2520-2529.
[235] C. Hildreth, Exosomes: Company Spotlights from “A” to “Z”, BioInformant (2023).
[236] ClinicalTrials.gov, in, 2023.
[237] S. Reif, Y. Elbaum-Shiff, N. Koroukhov, I. Shilo, M. Musseri, R. Golan-Gerstl, Cow and human milk-derived exosomes ameliorate colitis in DSS murine model, Nutrients 12 (2020) 2589.
[238] R. Golan-Gerstl, Y. Elbaum Shiff, V. Moshayoff, D. Schecter, D. Leshkowitz, S. Reif, Characterization and biological function of milk-derived miRNAs, Mol. Nutr. Food Res. 61 (2017) 1700009.
[239] B.C. Pieters, et al., Commercial cow milk contains physically stable extracellular vesicles expressing immunoregulatory TGF-beta, PLoS One 10 (2015) e0121123.
[240] M.P. Zaborowski, L. Balaj, X.O. Breakefield, C.P. Lai, Extracellular vesicles: Composition, biological relevance, and methods of study, Bioscience 65 (2015) 783-797.
[241] J. Wahlgren, T.D.L. Karlson, M. Brisslert, F. Vaziri Sani, E. Telemo, P. Sunnerhagen, H. Valadi, Plasma exosomes can deliver exogenous short interfering RNA to monocytes and lymphocytes, Nucleic Acids Res. 40 (2012) e130-e130.
[242] Y. Rong, et al., Engineered extracellular vesicles for delivery of siRNA promoting targeted repair of traumatic spinal cord injury, Bioact. Mater. 23 (2023) 328-342.

[243] L. Xu, et al., Exosome-mediated RNAi of PAK4 prolongs survival of pancreatic cancer mouse model after loco-regional treatment, Biomaterials 264 (2021) 120369.
[244] M. Piffoux, J. Volatron, A.K.A. Silva, F. Gazeau, Thinking quantitatively of RNA-based information transfer *via* extracellular vesicles: Lessons to learn for the design of RNA-loaded EVs, Pharmaceutics 13 (2021) 1931.
[245] J. Zhong, B. Xia, S. Shan, A. Zheng, S. Zhang, J. Chen, X.J. Liang, High-quality milk exosomes as oral drug delivery system, Biomaterials 277 (2021) 121126.
[246] B. Zeng, T. Chen, M.Y. Xie, J.Y. Luo, J.J. He, Q.Y. Xi, J.J. Sun, Y.L. Zhang, Exploration of long noncoding RNA in bovine milk exosomes and their stability during digestion in vitro, J. Dairy Sci. 102 (2019) 6726-6737.
[247] T. Wolf, S.R. Baier, J. Zempleni, The intestinal transport of bovine milk exosomes is mediated by endocytosis in human colon carcinoma Caco-2 cells and rat small intestinal IEC-6 cells, J. Nutr. 145 (2015) 2201-2206.
[248] M.R. Warren, C. Zhang, A. Vedadghavami, K. Bokvist, P.K. Dhal, A.G. Bajpayee, Milk exosomes with enhanced mucus penetrability for oral delivery of siRNA, Biomater. Sci. 9 (2021) 4260-4277.
[249] G. Carobolante, J. Mantaj, E. Ferrari, D. Vllasaliu, Cow milk and intestinal epithelial cell-derived extracellular vesicles as systems for enhancing oral drug delivery, Pharmaceutics 12 (2020) 226.
[250] P. Rani, M. Vashisht, N. Golla, S. Shandilya, S.K. Onteru, D. Singh, Milk miRNAs encapsulated in exosomes are stable to human digestion and permeable to intestinal barrier *in vitro*, J. Funct. Foods 34 (2017) 431-439.
[251] Y. Liao, X. Du, J. Li, B. Lonnerdal, Human milk exosomes and their microRNAs survive digestion *in vitro* and are taken up by human intestinal cells, Mol. Nutr. Food Res. 61 (2017).
[252] M. Vashisht, P. Rani, S.K. Onteru, D. Singh, Curcumin encapsulated in milk exosomes resists human digestion and possesses enhanced intestinal permeability *in vitro*, Appl. Biochem. Biotechnol. 183 (2017) 993-1007.
[253] R.J. Kusuma, S. Manca, T. Friemel, S. Sukreet, C. Nguyen, J. Zempleni, Human vascular endothelial cells transport foreign exosomes from cow's milk by endocytosis, Am. J. Physiol. Cell Physiol. 310 (2016) C800-807.
[254] A. Matsuda, T. Patel, Milk-derived extracellular vesicles for therapeutic delivery of small interfering RNAs, in: T. Patel (Ed.) Extracellular RNA: Methods and Protocols, Springer New York, New York, NY, 2018, pp. 187-197.
[255] S.R. Marsh, K.J. Pridham, J. Jourdan, R.G. Gourdie, Novel protocols for scalable production of high quality purified small extracellular vesicles from bovine milk, Nanotheranostics 5 (2021) 488-498.
[256] B. Adriano, N.M. Cotto, N. Chauhan, M. Jaggi, S.C. Chauhan, M.M. Yallapu, Milk exosomes: Nature's abundant nanoplatform for theranostic applications, Bioact. Mater. 6 (2021) 2479-2490.
[257] Y. Hu, J. Thaler, R. Nieuwland, Extracellular vesicles in human milk, Pharmaceuticals (Basel) 14 (2021) 1015.
[258] R. Munagala, F. Aqil, J. Jeyabalan, R.C. Gupta, Bovine milk-derived exosomes for drug delivery, Cancer Lett. 371 (2016) 48-61.
[259] A.K. Agrawal, et al., Milk-derived exosomes for oral delivery of paclitaxel, Nanomedicine 13 (2017) 1627-1636.
[260] R. Weiskirchen, S.K. Schröder, S. Weiskirchen, E.M. Buhl, B. Melnik, Isolation of Bovine and Human Milk Extracellular Vesicles, Biomedicines 11 (2023) 2715.
[261] S. Gupta, S. Rawat, V. Arora, S.K. Kottarath, A.K. Dinda, P.K. Vaishnav, B. Nayak, S. Mohanty, An improvised one-step sucrose cushion ultracentrifugation method for

exosome isolation from culture supernatants of mesenchymal stem cells, Stem Cell Res. Ther. 9 (2018) 180.
[262] M.K. Maghraby, et al., Extracellular vesicles isolated from milk can improve gut barrier dysfunction induced by malnutrition, Sci. Rep. 11 (2021) 7635.
[263] M. Kesimer, M. Scull, B. Brighton, G. DeMaria, K. Burns, W. O'Neal, R.J. Pickles, J.K. Sheehan, Characterization of exosome-like vesicles released from human tracheobronchial ciliated epithelium: a possible role in innate defense, FASEB J. 23 (2009) 1858-1868.
[264] F.N. Faruqu, L. Xu, K.T. Al-Jamal, Preparation of exosomes for siRNA delivery to cancer cells, J. Vis. Exp. 142 (2018) e58814.
[265] R.P. Alexander, N.-T. Chiou, K.M. Ansel, Improved exosome isolation by sucrose gradient fractionation of ultracentrifuged crude exosome pellets, Protoc. Exch. (2016).
[266] M.Y. Tian, D.X. Hao, Y. Liu, J. He, Z.H. Zhao, T.Y. Guo, X. Li, Y. Zhang, Milk exosomes: an oral drug delivery system with great application potential, Food Funct. 14 (2023) 1320-1337.
[267] R.J. Lobb, M. Becker, S.W. Wen, C.S. Wong, A.P. Wiegmans, A. Leimgruber, A. Moller, Optimized exosome isolation protocol for cell culture supernatant and human plasma, J. Extracell. Vesicles 4 (2015) 27031.
[268] K. Vaswani, Y.Q. Koh, F.B. Almughlliq, H.N. Peiris, M.D. Mitchell, A method for the isolation and enrichment of purified bovine milk exosomes, Reprod. Biol. 17 (2017) 341-348.
[269] D.C. Bickmore, J.J. Miklavcic, Characterization of extracellular vesicles isolated from human milk using a precipitation-based method, Front Nutr. 7 (2020) 22.
[270] R. Kandimalla, F. Aqil, N. Tyagi, R. Gupta, Milk exosomes: A biogenic nanocarrier for small molecules and macromolecules to combat cancer, Am. J. Reprod. Immunol. 85 (2021) e13349.
[271] B.J. Tauro, D.W. Greening, R.A. Mathias, H. Ji, S. Mathivanan, A.M. Scott, R.J. Simpson, Comparison of ultracentrifugation, density gradient separation, and immunoaffinity capture methods for isolating human colon cancer cell line LIM1863-derived exosomes, Methods 56 (2012) 293-304.
[272] H. Shao, H. Im, C.M. Castro, X. Breakefield, R. Weissleder, H. Lee, New technologies for analysis of extracellular vesicles, Chem. Rev. 118 (2018) 1917-1950.
[273] P. Li, M. Kaslan, S.H. Lee, J. Yao, Z. Gao, Progress in exosome isolation techniques, Theranostics 7 (2017) 789.
[274] D. Iannotta, A. A, A. Lai, S. Nair, N. Koifman, M. Lappas, C. Salomon, J. Wolfram, Chemically-Induced Lipoprotein Breakdown for Improved Extracellular Vesicle Purification, Small (2023) e2307240.
[275] R.E. Ghebosu, J. Pendiuk Goncalves, J. Wolfram, Extracellular Vesicle and Lipoprotein Interactions, Nano Lett. (2023).
[276] E. Lozano-Andres, et al., Physical association of low density lipoprotein particles and extracellular vesicles unveiled by single particle analysis, J. Extracell. Vesicles 12 (2023) e12376.
[277] M.I. Gonzalez, B. Gallardo, C. Ceron, E. Aguilera-Jimenez, M. Cortes-Canteli, H. Peinado, M. Desco, B. Salinas, Isolation of goat milk small extracellular vesicles by novel combined bio-physical methodology, Front Bioeng. Biotechnol. 11 (2023) 1197780.
[278] D. Ter-Ovanesyan, et al., Improved isolation of extracellular vesicles by removal of both free proteins and lipoproteins, Elife 12 (2023).

[279] M. Wu, C. Chen, Z. Wang, H. Bachman, Y. Ouyang, P.H. Huang, Y. Sadovsky, T.J. Huang, Separating extracellular vesicles and lipoproteins via acoustofluidics, Lab Chip 19 (2019) 1174-1182.
[280] Y. Zhang, et al., High-Efficiency Separation of Extracellular Vesicles from Lipoproteins in Plasma by Agarose Gel Electrophoresis, Anal. Chem. 92 (2020) 7493-7499.
[281] S. Walker, et al., Extracellular vesicle-based drug delivery systems for cancer treatment, Theranostics 9 (2019) 8001-8017.
[282] D. Sun, et al., A novel nanoparticle drug delivery system: the anti-inflammatory activity of curcumin is enhanced when encapsulated in exosomes, Mol. Ther. 18 (2010) 1606-1614.
[283] M.S. Kim, et al., Development of exosome-encapsulated paclitaxel to overcome MDR in cancer cells, Nanomed. Nanotechnol. Biol. Med. 12 (2016) 655-664.
[284] G. Fuhrmann, A. Serio, M. Mazo, R. Nair, M.M. Stevens, Active loading into extracellular vesicles significantly improves the cellular uptake and photodynamic effect of porphyrins, J. Control. Release 205 (2015) 35-44.
[285] S.L. Peswani Sajnani, Y. Zhang, D. Vllasaliu, Exosome-based therapies for mucosal delivery, Int. J. Pharm. 608 (2021) 121087.
[286] S. Estes, K. Konstantinov, J.D. Young, Manufactured extracellular vesicles as human therapeutics: challenges, advances, and opportunities, Curr. Opin. Biotechnol. 77 (2022) 102776.
[287] T.R. Lunavat, S.C. Jang, L. Nilsson, H.T. Park, G. Repiska, C. Lasser, J.A. Nilsson, Y.S. Gho, J. Lotvall, RNAi delivery by exosome-mimetic nanovesicles - Implications for targeting c-Myc in cancer, Biomaterials 102 (2016) 231-238.
[288] S. Shandilya, P. Rani, S.K. Onteru, D. Singh, Natural ligand-receptor mediated loading of siRNA in milk derived exosomes, J. Biotechnol. 318 (2020) 1-9.
[289] J. Wahlgren, L.K.T. De, M. Brisslert, F. Vaziri Sani, E. Telemo, P. Sunnerhagen, H. Valadi, Plasma exosomes can deliver exogenous short interfering RNA to monocytes and lymphocytes, Nucleic Acids Res. 40 (2012) e130.
[290] S. Shandilya, P. Rani, S.K. Onteru, D. Singh, Small interfering RNA in milk exosomes is resistant to digestion and crosses the intestinal barrier *in vitro*, J. Agric. Food. Chem. 65 (2017) 9506-9513.
[291] S. Manca, B. Upadhyaya, E. Mutai, A.T. Desaulniers, R.A. Cederberg, B.R. White, J. Zempleni, Milk exosomes are bioavailable and distinct microRNA cargos have unique tissue distribution patterns, Sci. Rep. 8 (2018) 11321.
[292] R.A.K. Tatyana A Shtam, Elena Yu Varfolomeeva, Evgeny M Makarov, Yury V Kil & Michael V Filatov, Exosomes are natural carriers of exogenous siRNA to human cells *in vitro*, Cell Commun. Signal. 11 (2013) 88.
[293] F. Aqil, R. Munagala, J. Jeyabalan, A.K. Agrawal, A.H. Kyakulaga, S.A. Wilcher, R.C. Gupta, Milk exosomes - Natural nanoparticles for siRNA delivery, Cancer Lett. 449 (2019) 186-195.
[294] M.-C. Didiot, et al., Exosome-mediated delivery of hydrophobically modified siRNA for huntingtin mRNA silencing, Mol. Ther. 24 (2016) 1836-1847.
[295] A. Familtseva, N. Jeremic, S.C. Tyagi, Exosomes: cell-created drug delivery systems, Mol. Cell. Biochem. 459 (2019) 1-6.
[296] T.N. Lamichhane, A. Jeyaram, D.B. Patel, B. Parajuli, N.K. Livingston, N. Arumugasaamy, J.S. Schardt, S.M. Jay, Oncogene knockdown *via* active loading of small RNAs into extracellular vesicles by sonication, Cell Mol. Bioeng. 9 (2016) 315-324.
[297] D.S. Sutaria, et al., Low active loading of cargo into engineered extracellular vesicles results in inefficient miRNA mimic delivery, J. Extracell. Vesicles 6 (2017) 1333882.

[298] C. Aslan, S.H. Kiaie, N.M. Zolbanin, P. Lotfinejad, R. Ramezani, F. Kashanchi, R. Jafari, Exosomes for mRNA delivery: a novel biotherapeutic strategy with hurdles and hope, BMC Biotechnol. 21 (2021) 20.
[299] S. Fu, Y. Wang, X. Xia, J.C. Zheng, Exosome engineering: Current progress in cargo loading and targeted delivery, NanoImpact 20 (2020) 100261.
[300] O.G. de Jong, S.A.A. Kooijmans, D.E. Murphy, L. Jiang, M.J.W. Evers, J.P.G. Sluijter, P. Vader, R.M. Schiffelers, Drug delivery with extracellular vesicles: From imagination to innovation, Acc. Chem. Res. 52 (2019) 1761-1770.
[301] M. Lu, Y. Huang, Bioinspired exosome-like therapeutics and delivery nanoplatforms, Biomaterials 242 (2020) 119925.
[302] A. Liu, G. Yang, Y. Liu, T. Liu, Research progress in membrane fusion-based hybrid exosomes for drug delivery systems, Front Bioeng. Biotechnol. 10 (2022) 939441.
[303] M.J.W. Evers, S.I. van de Wakker, E.M. de Groot, O.G. de Jong, J.J.J. Gitz-Francois, C.S. Seinen, J.P.G. Sluijter, R.M. Schiffelers, P. Vader, Functional siRNA delivery by extracellular vesicle-liposome hybrid nanoparticles, Adv. Healthc. Mater. (2021) e2101202.
[304] L. Cheng, X. Zhang, J. Tang, Q. Lv, J. Liu, Gene-engineered exosomes-thermosensitive liposomes hybrid nanovesicles by the blockade of CD47 signal for combined photothermal therapy and cancer immunotherapy, Biomaterials 275 (2021) 120964.
[305] Y. Lin, J. Wu, W. Gu, Y. Huang, Z. Tong, L. Huang, J. Tan, Exosome–liposome hybrid nanoparticles deliver CRISPR/Cas9 system in MSCs, Adv. Sci. 5 (2018) 1700611.
[306] M. Piffoux, A.K.A. Silva, C. Wilhelm, F. Gazeau, D. Tareste, Modification of extracellular vesicles by fusion with liposomes for the design of personalized biogenic drug delivery systems, ACS Nano 12 (2018) 6830-6842.
[307] L. Sun, M. Fan, D. Huang, B. Li, R. Xu, F. Gao, Y. Chen, Clodronate-loaded liposomal and fibroblast-derived exosomal hybrid system for enhanced drug delivery to pulmonary fibrosis, Biomaterials 271 (2021) 120761.
[308] L. Li, et al., Exosome-liposome hybrid nanoparticle codelivery of TP and miR497 conspicuously overcomes chemoresistant ovarian cancer, J. Nanobiotechnology 20 (2022) 50.
[309] M.J.W. Evers, S.I. van de Wakker, E.M. de Groot, O.G. de Jong, J.J.J. Gitz-François, C.S. Seinen, J.P.G. Sluijter, R.M. Schiffelers, P. Vader, Functional siRNA delivery by extracellular vesicle–liposome hybrid nanoparticles, Adv. Healthc. Mater. 11 (2022) 2101202.
[310] K. Vaswani, M.D. Mitchell, O.J. Holland, Y. Qin Koh, R.J. Hill, T. Harb, P.S.W. Davies, H. Peiris, A method for the isolation of exosomes from human and bovine milk, J. Nutr. Metab. 2019 (2019) 5764740.
[311] R. Munagala, F. Aqil, J. Jeyabalan, R.C. Gupta, Bovine milk-derived exosomes for drug delivery, Cancer Lett. 371 (2016) 48-61.
[312] N.-T. Chiou, K.M. Ansel, Improved exosome isolation by sucrose gradient fractionation of ultracentrifuged crude exosome pellets, Protoc. Exch. (2016) 057.
[313] C. Théry, et al., Minimal information for studies of extracellular vesicles 2018 (MISEV2018): a position statement of the International Society for Extracellular Vesicles and update of the MISEV2014 guidelines, J. Extracell. Vesicles 7 (2018) 1535750.
[314] T.A. Shtam, R.A. Kovalev, E.Y. Varfolomeeva, E.M. Makarov, Y.V. Kil, M.V. Filatov, Exosomes are natural carriers of exogenous siRNA to human cells *in vitro*, Cell Commun. Signal. 11 (2013).
[315] J. Hou, H. Ci, P. Wang, C. Wang, B. Lv, L. Miao, G. You, Nanoparticle tracking analysis versus dynamic light scattering: Case study on the effect of Ca2+ and

alginate on the aggregation of cerium oxide nanoparticles, J. Hazard. Mater. 360 (2018) 319-328.
[316] V. Filipe, A. Hawe, W. Jiskoot, Critical evaluation of Nanoparticle Tracking Analysis (NTA) by NanoSight for the measurement of nanoparticles and protein aggregates, Pharm. Res. 27 (2010) 796-810.
[317] J. Aarts, et al., Flood Control: How Milk-Derived Extracellular Vesicles Can Help to Improve the Intestinal Barrier Function and Break the Gut–Joint Axis in Rheumatoid Arthritis, Front. immunol. 12 (2021).
[318] H. Miyake, C. Lee, S. Chusilp, M. Bhalla, B. Li, M. Pitino, S. Seo, D.L. O'Connor, A. Pierro, Human breast milk exosomes attenuate intestinal damage, Pediatr. Surg. Int. 36 (2020) 155-163.
[319] L. Zhu, S. Fu, L. Li, Y. Liu, Changes of extracellular vesicles in goat milk treated with different methods, LWT 170 (2022) 114038.
[320] K.M. Howard, R. Jati Kusuma, S.R. Baier, T. Friemel, L. Markham, J. Vanamala, J. Zempleni, Loss of miRNAs during Processing and Storage of Cow's (Bos taurus) Milk, J. Agric. Food. Chem. 63 (2015) 588-592.
[321] T.A. Hartjes, S. Mytnyk, G.W. Jenster, V. van Steijn, M.E. van Royen, Extracellular vesicle quantification and characterization: Common methods and emerging approaches, Bioengineering (Basel) 6 (2019) 7.
[322] W.-J. Li, H. Chen, M.-L. Tong, J.-J. Niu, X.-Z. Zhu, L.-R. Lin, Comparison of the yield and purity of plasma exosomes extracted by ultracentrifugation, precipitation, and membrane-based approaches, Open Chem. 20 (2022) 182-191.
[323] J. Webber, A. Clayton, How pure are your vesicles?, J. Extracell. Vesicles 2 (2013) 19861.
[324] C. Théry, et al., Minimal information for studies of extracellular vesicles 2018 (MISEV2018): a position statement of the International Society for Extracellular Vesicles and update of the MISEV2014 guidelines, J. Extracell. Vesicles 7 (2018) 1535750.
[325] M. Samuel, et al., Bovine milk-derived exosomes from colostrum are enriched with proteins implicated in immune response and growth, Sci. Rep. 7 (2017) 5933.
[326] A. Kupsco, D. Prada, D. Valvi, L. Hu, M.S. Petersen, B. Coull, P. Grandjean, P. Weihe, A.A. Baccarelli, Human milk extracellular vesicle miRNA expression and associations with maternal characteristics in a population-based cohort from the Faroe Islands, Sci. Rep. 11 (2021) 5840.
[327] M.J. van Herwijnen, M.I. Zonneveld, S. Goerdayal, E.N. Nolte-'t Hoen, J. Garssen, B. Stahl, A.F. Maarten Altelaar, F.A. Redegeld, M.H. Wauben, Comprehensive Proteomic Analysis of Human Milk-derived Extracellular Vesicles Unveils a Novel Functional Proteome Distinct from Other Milk Components, Mol. Cell. Proteomics 15 (2016) 3412-3423.
[328] H. Kim, et al., Harnessing the Natural Healing Power of Colostrum: Bovine Milk-Derived Extracellular Vesicles from Colostrum Facilitating the Transition from Inflammation to Tissue Regeneration for Accelerating Cutaneous Wound Healing, Adv. Healthc. Mater. 11 (2022) e2102027.
[329] Y. Tian, et al., Protein Profiling and Sizing of Extracellular Vesicles from Colorectal Cancer Patients via Flow Cytometry, ACS Nano 12 (2018) 671-680.
[330] C. Théry, S. Amigorena, G. Raposo, A. Clayton, Isolation and characterization of exosomes from cell culture supernatants and biological fluids, Curr. Protoc. Cell Biol. Chapter 3 (2006) Unit 3.22.

[331] E. Serrano-Pertierra, M. Oliveira-Rodríguez, M. Matos, G. Gutiérrez, A. Moyano, M. Salvador, M. Rivas, M.C. Blanco-López, Extracellular Vesicles: Current Analytical Techniques for Detection and Quantification, Biomolecules 10 (2020) 824.
[332] K.C. French, M.A. Antonyak, R.A. Cerione, Extracellular vesicle docking at the cellular port: Extracellular vesicle binding and uptake, Semin. Cell Dev. Biol. 67 (2017) 48-55.
[333] M.M. Jørgensen, R. Bæk, K. Varming, Potentials and capabilities of the Extracellular Vesicle (EV) Array, J. Extracell. Vesicles 4 (2015) 26048.
[334] T. Cloet, N. Momenbeitollahi, H. Li, Recent advances on protein-based quantification of extracellular vesicles, Anal. Biochem. 622 (2021) 114168.
[335] S. Zhou, T. Hu, F. Zhang, D. Tang, D. Li, J. Cao, W. Wei, Y. Wu, S. Liu, Integrated microfluidic device for accurate extracellular vesicle quantification and protein markers analysis directly from human whole blood, Anal. Chem. 92 (2019) 1574-1581.
[336] A.R. Brisson, S. Tan, R. Linares, C. Gounou, N. Arraud, Extracellular vesicles from activated platelets: a semiquantitative cryo-electron microscopy and immuno-gold labeling study, Platelets 28 (2017) 263-271.
[337] M. Colombo, et al., Analysis of ESCRT functions in exosome biogenesis, composition and secretion highlights the heterogeneity of extracellular vesicles, J. Cell Sci. 126 (2013) 5553-5565.
[338] M.K. Jung, J.Y. Mun, Sample preparation and imaging of exosomes by transmission electron microscopy, J. Vis. Exp. 4 (2018) 56482.
[339] F. Aqil, R. Munagala, J. Jeyabalan, A.K. Agrawal, A.-H. Kyakulaga, S.A. Wilcher, R.C. Gupta, Milk exosomes - Natural nanoparticles for siRNA delivery, Cancer Lett. 449 (2019) 186-195.
[340] K. O'Brien, K. Breyne, S. Ughetto, L.C. Laurent, X.O. Breakefield, RNA delivery by extracellular vesicles in mammalian cells and its applications, Nat. Rev. Mol. Cell Biol. 21 (2020) 585-606.
[341] M. Piffoux, J. Volatron, A.K.A. Silva, F. Gazeau, Thinking Quantitatively of RNA-Based Information Transfer via Extracellular Vesicles: Lessons to Learn for the Design of RNA-Loaded EVs, Pharmaceutics 13 (2021).
[342] M.Y. Konoshenko, E.A. Lekchnov, A.V. Vlassov, P.P. Laktionov, Isolation of Extracellular Vesicles: General Methodologies and Latest Trends, Biomed Res. Int. 2018 (2018) 8545347.
[343] B.J. Benedikter, et al., Ultrafiltration combined with size exclusion chromatography efficiently isolates extracellular vesicles from cell culture media for compositional and functional studies, Sci. Rep. 7 (2017) 15297.
[344] D.L. Sparks, C. Chatterjee, E. Young, J. Renwick, N.R. Pandey, Lipoprotein charge and vascular lipid metabolism, Chem. Phys. Lipids 154 (2008) 1-6.
[345] I. Podolak, A. Galanty, D. Sobolewska, Saponins as cytotoxic agents: a review, Phytochem. Rev. 9 (2010) 425-474.
[346] T. Batista Napotnik, T. Polajzer, D. Miklavcic, Cell death due to electroporation - A review, Bioelectrochemistry 141 (2021) 107871.
[347] M.A.C. Pomatto, B. Bussolati, S. D'Antico, S. Ghiotto, C. Tetta, M.F. Brizzi, G. Camussi, Improved loading of plasma-derived extracellular vesicles to encapsulate antitumor miRNAs, Mol. Ther. Methods Clin. Dev. 13 (2019) 133-144.
[348] J. Ahmad, et al., Solid matrix based lipidic nanoparticles in oral cancer chemotherapy: applications and pharmacokinetics, Curr. Drug Metab. 16 (2015) 633-644.

[349] Y. Wang, C. Pi, X. Feng, Y. Hou, L. Zhao, Y. Wei, The Influence of Nanoparticle Properties on Oral Bioavailability of Drugs, Int. J. Nanomedicine 15 (2020) 6295-6310.
[350] Y.Y. Luo, X.Y. Xiong, Y. Tian, Z.L. Li, Y.C. Gong, Y.P. Li, A review of biodegradable polymeric systems for oral insulin delivery, Drug Deliv. 23 (2016) 1882-1891.
[351] A. Banerjee, J. Qi, R. Gogoi, J. Wong, S. Mitragotri, Role of nanoparticle size, shape and surface chemistry in oral drug delivery, J. Control. Release 238 (2016) 176-185.
[352] D. Vllasaliu, M. Thanou, S. Stolnik, R. Fowler, Recent advances in oral delivery of biologics: nanomedicine and physical modes of delivery, Expert Opin. Drug Deliv. 15 (2018) 759-770.
[353] D.S. Wilson, G. Dalmasso, L.X. Wang, S.V. Sitaraman, D. Merlin, N. Murthy, Orally delivered thioketal nanoparticles loaded with TNF-alpha-siRNA target inflammation and inhibit gene expression in the intestines, Nat. Mater. 9 (2010) 923-928.
[354] C.H. Yang, G. Alpini, S. Glaser, D. Merlin, Lipid nanoparticles for oral delivery of nucleic acids for treating inflammatory bowel disease, Nanomedicine 17 (2022) 1501-1509.
[355] M. Zhang, D. Merlin, Nanoparticle-based oral drug delivery systems targeting the colon for treatment of ulcerative colitis, Inflamm. Bowel Dis. 24 (2018) 1401-1415.
[356] H. Clevers, The intestinal crypt, a prototype stem cell compartment, Cell 154 (2013) 274-284.
[357] F. Antunes, F. Andrade, F. Araújo, D. Ferreira, B. Sarmento, Establishment of a triple co-culture *in vitro* cell models to study intestinal absorption of peptide drugs, Eur. J. Pharm. Biopharm. 83 (2013) 427-435.
[358] J. Creff, L. Malaquin, A. Besson, *In vitro* models of intestinal epithelium: Toward bioengineered systems, J. Tissue Eng. 12 (2021) 2041731420985202.
[359] H. Sun, E.C.Y. Chow, S. Liu, Y. Du, K.S. Pang, The Caco-2 cell monolayer: usefulness and limitations, Expert Opin. Drug Metab. Toxicol. 4 (2008) 395-411.
[360] C. Pontier, J. Pachot, R. Botham, B. Lenfant, P. Arnaud, HT29-MTX and Caco-2/TC7 monolayers as predictive models for human intestinal absorption: role of the mucus layer, J. Pharm. Sci. 90 (2001) 1608-1619.
[361] O. Reale, A. Huguet, V. Fessard, Co-culture model of Caco-2/HT29-MTX cells: A promising tool for investigation of phycotoxins toxicity on the intestinal barrier, Chemosphere 273 (2021) 128497.
[362] A.F.G. Strugari, M.S. Stan, S. Gharbia, A. Hermenean, A. Dinischiotu, Characterization of nanoparticle intestinal transport using an *in vitro* co-culture model, Nanomaterials 9 (2019) 5.
[363] Y. Zhang, S. Huang, W. Zhong, W. Chen, B. Yao, X. Wang, 3D organoids derived from the small intestine: An emerging tool for drug transport research, Acta Pharm. Sin. B. 11 (2021) 1697-1707.
[364] T. Sato, et al., Single Lgr5 stem cells build crypt-villus structures in vitro without a mesenchymal niche, Nature 459 (2009) 262-265.
[365] A. Ootani, et al., Sustained *in vitro* intestinal epithelial culture within a Wnt-dependent stem cell niche, Nat. Med. 15 (2009) 701-706.
[366] A. Singh, H.M. Poling, J.R. Spence, J.M. Wells, M.A. Helmrath, Gastrointestinal organoids: a next-generation tool for modeling human development, Am. J. Physiol. Gastrointest. Liver Physiol. 319 (2020) G375-G381.
[367] T. Sato, et al., Long-term expansion of epithelial organoids from human colon, adenoma, adenocarcinoma, and Barrett's epithelium, Gastroenterology 141 (2011) 1762-1772.

[368] T. Sato, H. Clevers, Growing self-organizing mini-guts from a single intestinal stem cell: Mechanism and applications, Science 340 (2013) 1190-1194.
[369] S.S. Wilson, A. Tocchi, M.K. Holly, W.C. Parks, J.G. Smith, A small intestinal organoid model of non-invasive enteric pathogen-epithelial cell interactions, Mucosal Immunol. 8 (2015) 352-361.
[370] J.Y. Co, M. Margalef-Catala, X. Li, A.T. Mah, C.J. Kuo, D.M. Monack, M.R. Amieva, Controlling epithelial polarity: A human enteroid model for host-pathogen interactions, Cell Rep. 26 (2019) 2509-2520.
[371] J.Y. Co, M. Margalef-Catala, D.M. Monack, M.R. Amieva, Controlling the polarity of human gastrointestinal organoids to investigate epithelial biology and infectious diseases, Nat. Protoc. 16 (2021) 5171-5192.
[372] C. Moon, K.L. VanDussen, H. Miyoshi, T.S. Stappenbeck, Development of a primary mouse intestinal epithelial cell monolayer culture system to evaluate factors that modulate IgA transcytosis, Mucosal Immunol. 7 (2014) 818-828.
[373] C.A. Thorne, I.W. Chen, L.E. Sanman, M.H. Cobb, L.F. Wu, S.J. Altschuler, Enteroid monolayers reveal an autonomous WNT and BMP circuit controlling intestinal epithelial growth and organization, Dev. Cell 44 (2018) 624-633.
[374] G. Altay, E. Larranaga, S. Tosi, F.M. Barriga, E. Batlle, V. Fernandez-Majada, E. Martinez, Self-organized intestinal epithelial monolayers in crypt and villus-like domains show effective barrier function, Sci. Rep. 9 (2019) 10140.
[375] Y. Wang, et al., Self-renewing monolayer of primary colonic or rectal epithelial cells, Cell. Mol. Gastroenterol. Hepatol. 4 (2017) 165-182.
[376] M. Anderson, A. Omri, The Effect of Different Lipid Components on the In Vitro Stability and Release Kinetics of Liposome Formulations, Drug Deliv. 11 (2004) 33-39.
[377] Z. Du, M.M. Munye, A.D. Tagalakis, M.D. Manunta, S.L. Hart, The role of the helper lipid on the DNA transfection efficiency of lipopolyplex formulations, Sci. Rep. 4 (2014) 7107.
[378] J. Kraiczy, et al., DNA methylation defines regional identity of human intestinal epithelial organoids and undergoes dynamic changes during development, Gut 68 (2019) 49-61.
[379] W.T.M. van Dooremalen, M. Derksen, J.L. Roos, C. Higuera Baron, C.S. Verissimo, R.G.J. Vries, S.F. Boj, F. Pourfarzad, Organoid-derived epithelial monolayer: A clinically relevant *in vitro* model for intestinal barrier function, J. Vis. Exp. 29 (2021) 62074.
[380] A. Benmoussa, C.H. Lee, B. Laffont, P. Savard, J. Laugier, E. Boilard, C. Gilbert, I. Fliss, P. Provost, Commercial dairy cow milk microRNAs resist digestion under simulated gastrointestinal tract conditions, J. Nutr. 146 (2016) 2206-2215.
[381] H. Izumi, N. Kosaka, T. Shimizu, K. Sekine, T. Ochiya, M. Takase, Bovine milk contains microRNA and messenger RNA that are stable under degradative conditions, J. Dairy Sci. 95 (2012) 4831-4841.
[382] M. Kokkona, P. Kallinteri, D. Fatouros, S.G. Antimisiaris, Stability of SUV liposomes in the presence of cholate salts and pancreatic lipases: effect of lipid composition, Eur. J. Pharm. Sci. 9 (2000) 245-252.
[383] B. Wuyts, D. Riethorst, J. Brouwers, J. Tack, P. Annaert, P. Augustijns, Evaluation of fasted and fed state simulated and human intestinal fluids as solvent system in the Ussing chambers model to explore food effects on intestinal permeability, Int. J. Pharm. 478 (2015) 736-744.

[384] D. Riethorst, P. Baatsen, C. Remijn, A. Mitra, J. Tack, J. Brouwers, P. Augustijns, An in-depth view into human intestinal fluid colloids: Intersubject variability in relation to composition, Mol. Pharm. 13 (2016) 3484-3493.
[385] D. Riethorst, J. Brouwers, J. Motmans, P. Augustijns, Human intestinal fluid factors affecting intestinal drug permeation *in vitro*, Eur. J. Pharm. Sci. 121 (2018) 338-346.
[386] B. Srinivasan, A.R. Kolli, M.B. Esch, H.E. Abaci, M.L. Shuler, J.J. Hickman, TEER measurement techniques for *in vitro* barrier model systems, J. Lab. Autom. 20 (2015) 107-126.
[387] C.L. Pires, C. Praça, P.A.T. Martins, A.L.M. Batista de Carvalho, L. Ferreira, M.P.M. Marques, M.J. Moreno, Re-Use of Caco-2 Monolayers in Permeability Assays-Validation Regarding Cell Monolayer Integrity, Pharmaceutics 13 (2021).
[388] Y. Wang, J.B. Mumm, R. Herbst, R. Kolbeck, Y. Wang, IL-22 Increases Permeability of Intestinal Epithelial Tight Junctions by Enhancing Claudin-2 Expression, J. Immun. 199 (2017) 3316-3325.
[389] N.J. Darling, C.L. Mobbs, A.L. González-Hau, M. Freer, S. Przyborski, Bioengineering Novel in vitro Co-culture Models That Represent the Human Intestinal Mucosa With Improved Caco-2 Structure and Barrier Function, Front Bioeng. Biotechnol. 8 (2020).
[390] J. Ukkola, et al., Enrichment of bovine milk-derived extracellular vesicles using surface-functionalized cellulose nanofibers, Carbohydr. Polym. 297 (2022) 120069.
[391] M. Montanari, et al., Extracellular Vesicles from Campylobacter jejuni CDT-Treated Caco-2 Cells Inhibit Proliferation of Tumour Intestinal Caco-2 Cells and Myeloid U937 Cells: Detailing the Global Cell Response for Potential Application in Anti-Tumour Strategies, Int. J. Mol. Sci. 24 (2022).
[392] J.B. Simonsen, Pitfalls associated with lipophilic fluorophore staining of extracellular vesicles for uptake studies, J. Extracell. Vesicles 8 (2019) 1582237.
[393] S. Sukreet, C.P. Braga, J. Adamec, J. Cui, J. Zempleni, The absorption of bovine milk small extracellular vesicles largely depends on galectin 3 and galactose ligands in human intestinal cells and C57BL/6J mice, Am. J. Physiol. Cell Physiol. 325 (2023) C1421-C1430.
[394] S. Hu, M. Niu, F. Hu, Y. Lu, J. Qi, Z. Yin, W. Wu, Integrity and stability of oral liposomes containing bile salts studied in simulated and *ex vivo* gastrointestinal media, Int. J. Pharm. 441 (2013) 693-700.
[395] W. Liu, A. Ye, W. Liu, C. Liu, J. Han, H. Singh, Behaviour of liposomes loaded with bovine serum albumin during *in vitro* digestion, Food Chem. 175 (2015) 16-24.
[396] J.N. Tian, B.Q. Ge, Y.F. Shen, Y.X. He, Z.X. Chen, Thermodynamics and structural evolution during a reversible vesicle-micelle transition of a vitamin-derived bolaamphiphile induced by sodium cholate, J. Agric. Food. Chem. 64 (2016) 1977-1988.
[397] M.H. Richards, C.R. Gardner, Effects of bile salts on the structural integrity of liposomes, Biochim. Biophys. Acta 543 (1978) 508-522.
[398] M. Kokkona, P. Kallinteri, D. Fatouros, S.G. Antimisiaris, Stability of SUV liposomes in the presence of cholate salts and pancreatic lipases: effect of lipid composition, Eur. J. Pharm. Sci. 9 (2000) 245-252.
[399] G. Midekessa, et al., Zeta Potential of Extracellular Vesicles: Toward Understanding the Attributes that Determine Colloidal Stability, ACS Omega 5 (2020) 16701-16710.
[400] H.K. Kleinman, K. Kim, H. Kang, Matrigel uses in cell biology and for the identification of thymosin β4, a mediator of tissue regeneration, Appl. Biol. Chem. 61 (2018) 703-708.
[401] T. Sato, et al., Single Lgr5 stem cells build crypt-villus structures *in vitro* without a mesenchymal niche, Nature 459 (2009) 262-265.

[402] E. Suarez-Martinez, I. Suazo-Sanchez, M. Celis-Romero, A. Carnero, 3D and organoid culture in research: physiology, hereditary genetic diseases and cancer, Cell Biosci. 12 (2022) 39.
[403] T.Q. Crawford, H. Roelink, The Notch response inhibitor DAPT enhances neuronal differentiation in embryonic stem cell-derived embryoid bodies independently of sonic hedgehog signaling, Dev. Dyn. 236 (2007) 886-892.
[404] J.A. Grondin, Y.H. Kwon, P.M. Far, S. Haq, W.I. Khan, Mucins in Intestinal Mucosal Defense and Inflammation: Learning From Clinical and Experimental Studies, Front. immunol. 11 (2020).
[405] S.A. Jelinsky, et al., Molecular and Functional Characterization of Human Intestinal Organoids and Monolayers for Modeling Epithelial Barrier, Inflamm. Bowel Dis. 29 (2022) 195-206.
[406] T. Roodsant, et al., A Human 2D Primary Organoid-Derived Epithelial Monolayer Model to Study Host-Pathogen Interaction in the Small Intestine, Front. cell. infect. microbiol. 10 (2020).
[407] G.A. Kim, N.J. Ginga, S. Takayama, Integration of Sensors in Gastrointestinal Organoid Culture for Biological Analysis, Cell. Mol. Gastroenterol. Hepatol. 6 (2018) 123-131.e121.
[408] K. Kozuka, et al., Development and Characterization of a Human and Mouse Intestinal Epithelial Cell Monolayer Platform, Stem Cell Reports 9 (2017) 1976-1990.
[409] J.P. Gleeson, H.Q. Estrada, M. Yamashita, C.N. Svendsen, S.R. Targan, R.J. Barrett, Development of physiologically responsive human iPSC-derived intestinal epithelium to study barrier dysfunction in IBD, Int. J. Mol. Sci. 21 (2020) 1438.
[410] P. Artursson, A.-L. Ungell, J.-E. Löfroth, Selective paracellular permeability in two models of intestinal absorption: cultured monolayers of human intestinal epithelial cells and rat intestinal segments, Pharm. Res. 10 (1993) 1123-1129.
[411] M. Vertzoni, et al., Impact of regional differences along the gastrointestinal tract of healthy adults on oral drug absorption: An UNGAP review, Eur. J. Pharm. Sci. 134 (2019) 153-175.
[412] Z. Lu, L. Ding, Q. Lu, Y.H. Chen, Claudins in intestines: Distribution and functional significance in health and diseases, Tissue Barriers 1 (2013) e24978.
[413] A. Sjoberg, M. Lutz, C. Tannergren, C. Wingolf, A. Borde, A.L. Ungell, Comprehensive study on regional human intestinal permeability and prediction of fraction absorbed of drugs using the Ussing chamber technique, Eur. J. Pharm. Sci. 48 (2013) 166-180.
[414] G. Huang, et al., Functional and biomimetic materials for engineering of the three-dimensional cell microenvironment, Chem. Rev. 117 (2017) 12764-12850.
[415] J.H. Sung, J. Yu, D. Luo, M.L. Shuler, J.C. March, Microscale 3-D hydrogel scaffold for biomimetic gastrointestinal (GI) tract model, Lab Chip 11 (2011) 389-392.
[416] J. Yu, S. Peng, D. Luo, J.C. March, *In vitro* 3D human small intestinal villous model for drug permeability determination, Biotechnol. Bioeng. 109 (2012) 2173-2178.
[417] S.H. Kim, M. Chi, B. Yi, S.H. Kim, S. Oh, Y. Kim, S. Park, J.H. Sung, Three-dimensional intestinal villi epithelium enhances protection of human intestinal cells from bacterial infection by inducing mucin expression, Integr. Biol. 6 (2014) 1122-1131.
[418] L.R. Madden, et al., Bioprinted 3D primary human intestinal tissues model aspects of native physiology and ADME/Tox functions, IScience 2 (2018) 156-167.
[419] Y. Wang, D.B. Gunasekara, M.I. Reed, M. DiSalvo, S.J. Bultman, C.E. Sims, S.T. Magness, N.L. Allbritton, A microengineered collagen scaffold for generating a

polarized crypt-villus architecture of human small intestinal epithelium, Biomaterials 128 (2017) 44-55.
[420] S.N. Bhatia, D.E. Ingber, Microfluidic organs-on-chips, Nat. Biotechnol. 32 (2014) 760-772.
[421] H.J. Kim, H. Li, J.J. Collins, D.E. Ingber, Contributions of microbiome and mechanical deformation to intestinal bacterial overgrowth and inflammation in a human gut-on-a-chip, Proc. Natl. Acad. Sci. U.S.A. 113 (2016) E7-E15.
[422] X. Han, S. Ding, H. Jiang, G. Liu, Roles of macrophages in the development and treatment of gut inflammation, Front. Cell Dev. Biol. 9 (2021) 625423.
[423] L. Alvarez-Erviti, Y. Seow, H. Yin, C. Betts, S. Lakhal, M.J. Wood, Delivery of siRNA to the mouse brain by systemic injection of targeted exosomes, Nat. Biotechnol. 29 (2011) 341-345.
[424] A. Wadhwa, A. Aljabbari, A. Lokras, C. Foged, A. Thakur, Opportunities and Challenges in the Delivery of mRNA-based Vaccines, Pharmaceutics 12 (2020).
[425] D.W. Hagey, et al., The cellular response to extracellular vesicles is dependent on their cell source and dose, Science Advances 9 (2023) eadh1168.
[426] M. Dominska, D.M. Dykxhoorn, Breaking down the barriers: siRNA delivery and endosome escape, J. Cell Sci. 123 (2010) 1183-1189.
[427] S. Oliveira, I. van Rooy, O. Kranenburg, G. Storm, R.M. Schiffelers, Fusogenic peptides enhance endosomal escape improving siRNA-induced silencing of oncogenes, Int. J. Pharm. 331 (2007) 211-214.
[428] B.S. Joshi, M.A. de Beer, B.N.G. Giepmans, I.S. Zuhorn, Endocytosis of extracellular vesicles and release of their cargo from endosomes, ACS Nano 14 (2020) 4444-4455.
[429] T.T. Pham, H. Chen, P.H.D. Nguyen, M.K. Jayasinghe, A.H. Le, M.T.N. Le, Endosomal escape of nucleic acids from extracellular vesicles mediates functional therapeutic delivery, Pharmacol. Res. 188 (2023) 106665.
[430] R. Laís, J. Bhagyashree, G. Jie, Z. Inge, Breaking free: endocytosis and endosomal escape of extracellular vesicles, Extracellular Vesicles and Circulating Nucleic Acids 4 (2023) 283-305.
[431] Y. Jiang, et al., Quantitating Endosomal Escape of a Library of Polymers for mRNA Delivery, Nano Lett. 20 (2020) 1117-1123.
[432] P. Paramasivam, et al., Endosomal escape of delivered mRNA from endosomal recycling tubules visualized at the nanoscale, J. Cell Biol. 221 (2021).
[433] Y. Zhang, M. Belaid, X. Luo, A. Daci, R. Limani, J. Mantaj, M. Zilbauer, K. Nayak, D. Vllasaliu, Probing milk extracellular vesicles for intestinal delivery of RNA therapies, J. Nanobiotechnology 21 (2023) 406.
[434] T. Imai, Y. Takahashi, M. Nishikawa, K. Kato, M. Morishita, T. Yamashita, A. Matsumoto, C. Charoenviriyakul, Y. Takakura, Macrophage-dependent clearance of systemically administered B16BL6-derived exosomes from the blood circulation in mice, J. Extracell. Vesicles 4 (2015) 26238.
[435] D. Zhang, H. Lee, X. Wang, A. Rai, M. Groot, Y. Jin, Exosome-Mediated Small RNA Delivery: A Novel Therapeutic Approach for Inflammatory Lung Responses, Mol. Ther. 26 (2018) 2119-2130.
[436] J. Zempleni, S. Sukreet, F. Zhou, D. Wu, E. Mutai, Milk-derived exosomes and metabolic regulation, Annu. Rev. Anim. Biosci. 7 (2019) 245-262.
[437] M. Mevel, et al., DODAG; a versatile new cationic lipid that mediates efficient delivery of pDNA and siRNA, J. Control. Release 143 (2010) 222-232.
[438] E. Caudron, J.Y. Zhou, P. England, M. Ollivon, P. Prognon, Some insights about 1,6-diphenyl-1,3,5-hexatriene-lipid supramolecular assemblies by steady-state fluorescence measurements, Appl. Spectrosc. 61 (2007) 963-969.

[439] B.R. Lentz, PEG as a tool to gain insight into membrane fusion, Eur. Biophys. J. 36 (2007) 315-326.
[440] B.R. Lentz, J.K. Lee, Poly(ethylene glycol) (PEG)-mediated fusion between pure lipid bilayers: a mechanism in common with viral fusion and secretory vesicle release?, Mol. Membr. Biol. 16 (1999) 279-296.
[441] S.W. Burgess, T.J. McIntosh, B.R. Lentz, Modulation of poly (ethylene glycol)-induced fusion by membrane hydration: importance of interbilayer separation, Biochemistry 31 (1992) 2653-2661.
[442] Y. Xia, J. Tian, X. Chen, Effect of surface properties on liposomal siRNA delivery, Biomaterials 79 (2016) 56-68.
[443] A. Zeb, S.T. Arif, M. Malik, F.A. Shah, F.U. Din, O.S. Qureshi, E.-S. Lee, G.-Y. Lee, J.-K. Kim, Potential of nanoparticulate carriers for improved drug delivery via skin, J. Pharm. Investig. 49 (2019) 485-517.
[444] C.-Y. Hsu, et al., An overview of nanoparticles in drug delivery: Properties and applications, S. Afr. J. Chem. Eng. 46 (2023) 233-270.
[445] P. Verma, K. Pathak, Therapeutic and cosmeceutical potential of ethosomes: An overview, J. adv. pharm. technol res. 1 (2010) 274.
[446] X. Han, H. Zhang, K. Butowska, K.L. Swingle, M.-G. Alameh, D. Weissman, M.J. Mitchell, An ionizable lipid toolbox for RNA delivery, Nat. Commun. 12 (2021) 7233.
[447] R.P. Hickerson, A.V. Vlassov, Q. Wang, D. Leake, H. Ilves, E. Gonzalez-Gonzalez, C.H. Contag, B.H. Johnston, R.L. Kaspar, Stability study of unmodified siRNA and relevance to clinical use, Oligonucleotides 18 (2008) 345-354.
[448] P. Yadava, M. Gibbs, C. Castro, J.A. Hughes, Effect of Lyophilization and Freeze-thawing on the Stability of siRNA-liposome Complexes, AAPS PharmSciTech 9 (2008) 335-341.
[449] C. Chen, C. Chen, Y. Li, R. Gu, X. Yan, Characterization of lipid-based nanomedicines at the single-particle level, Fundamental Research 3 (2023) 488-504.
[450] R.L. Ball, C.M. Knapp, K.A. Whitehead, Lipidoid nanoparticles for siRNA delivery to the intestinal epithelium: *In vitro* investigations in a Caco-2 model, PLoS One 10 (2015) e0133154.
[451] T. Celius, P. Garberg, B. Lundgren, Stable suppression of MDR1 gene expression and function by RNAi in Caco-2 cells, Biochem. Biophys. Res. Commun. 324 (2004) 365-371.
[452] K. Romøren, B.J. Thu, N.C. Bols, Ø. Evensen, Transfection efficiency and cytotoxicity of cationic liposomes in salmonid cell lines of hepatocyte and macrophage origin, Biochim. Biophys. Acta 1663 (2004) 127-134.
[453] S. Cui, Y. Wang, Y. Gong, X. Lin, Y. Zhao, D. Zhi, Q. Zhou, S. Zhang, Correlation of the cytotoxic effects of cationic lipids with their headgroups, Toxicol. Res. 7 (2018) 473-479.
[454] S. Matic, V.P. Dia, Bovine milk exosomes affected proliferation of macrophages under hypoxia, Curr. Res. Food Sci. 5 (2022) 2108-2113.
[455] T. Chen, et al., Porcine milk-derived exosomes promote proliferation of intestinal epithelial cells, Sci. Rep. 6 (2016) 33862.
[456] K. Suga, D. Matsui, N. Watanabe, Y. Okamoto, H. Umakoshi, Insight into the exosomal membrane: From viewpoints of membrane fluidity and polarity, Langmuir 37 (2021) 11195-11202.
[457] S. Kaddah, N. Khreich, F. Kaddah, C. Charcosset, H. Greige-Gerges, Cholesterol modulates the liposome membrane fluidity and permeability for a hydrophilic molecule, Food Chem. Toxicol. 113 (2018) 40-48.

[458] P. Garidel, A. Hildebrand, K. Knauf, A. Blume, Membranolytic activity of bile salts: influence of biological membrane properties and composition, Molecules 12 (2007) 2292-2326.
[459] C. Poojari, N. Wilkosz, R.B. Lira, R. Dimova, P. Jurkiewicz, R. Petka, M. Kepczynski, T. Róg, Behavior of the DPH fluorescence probe in membranes perturbed by drugs, Chem. Phys. Lipids 223 (2019) 104784.
[460] L. Alvarez-Erviti, Y. Seow, H. Yin, C. Betts, S. Lakhal, M.J. Wood, Delivery of siRNA to the mouse brain by systemic injection of targeted exosomes, Nat Biotechnol 29 (2011) 341-345.
[461] A.K. Varkouhi, M. Scholte, G. Storm, H.J. Haisma, Endosomal escape pathways for delivery of biologicals, J. Control. Release 151 (2011) 220-228.
[462] X. Han, S. Ding, H. Jiang, G. Liu, Roles of Macrophages in the Development and Treatment of Gut Inflammation, Front Cell Dev Biol 9 (2021) 625423.
[463] A.A.M. Kampfer, P. Urban, S. Gioria, N. Kanase, V. Stone, A. Kinsner-Ovaskainen, Development of an *in vitro* co-culture model to mimic the human intestine in healthy and diseased state, Toxicol. In Vitro 45 (2017) 31-43.
[464] X. Hu, Q. Yu, K. Hou, X. Ding, Y. Chen, J. Xie, S. Nie, M. Xie, Regulatory effects of Ganoderma atrum polysaccharides on LPS-induced inflammatory macrophages model and intestinal-like Caco-2/macrophages co-culture inflammation model, Food Chem. Toxicol. 140 (2020) 111321.
[465] A.W.-S. Zongo, D. Zogona, M. Youssef, S. Ye, F. Zhan, J. Li, B. Li, Senegalia macrostachya seed polysaccharides attenuate inflammation-induced intestinal epithelial barrier dysfunction in a Caco-2 and RAW264.7 macrophage co-culture model by inhibiting the NF-κB/MLCK pathway, Food Funct. 13 (2022) 11676-11689.
[466] H. Liu, J. Liang, G. Xiao, L. Ma, Q. Wang, Dendrobine suppresses lipopolysaccharide-induced gut inflammation in a co-culture of intestinal epithelial Caco-2 cells and RAW264.7 macrophages, eFood 2 (2021) 92-99.
[467] A.U. Ahmed, An overview of inflammation: mechanism and consequences, Front. Biol. 6 (2011) 274-281.
[468] S. Mecocci, et al., Cow milk extracellular vesicle effects on an *in vitro* model of intestinal inflammation, Biomedicines 10 (2022) 10030570.
[469] T.M. Bui, L.A. Mascarenhas, R. Sumagin, Extracellular vesicles regulate immune responses and cellular function in intestinal inflammation and repair, Tissue Barriers 6 (2018) e1431038.
[470] H. Zhang, L. Wang, C. Li, Y. Yu, Y. Yi, J. Wang, D. Chen, Exosome-induced regulation in inflammatory bowel disease, Front. immunol. 10 (2019) 1464.
[471] H. Qi, Y. Wang, S. Fa, C. Yuan, L. Yang, Extracellular vesicles as natural delivery carriers regulate oxidative stress under pathological conditions, Front Bioeng. Biotechnol. 9 (2021) 752019.
[472] F. Leonard, E.-M. Collnot, C.-M. Lehr, A three-dimensional coculture of enterocytes, monocytes and dendritic cells to model inflamed intestinal mucosa *in vitro*, Mol. Pharm. 7 (2010) 2103-2119.
[473] J. Susewind, C. de Souza Carvalho-Wodarz, U. Repnik, E.-M. Collnot, N. Schneider-Daum, G.W. Griffiths, C.-M. Lehr, A 3D co-culture of three human cell lines to model the inflamed intestinal mucosa for safety testing of nanomaterials, Nanotoxicology 10 (2016) 53-62.
[474] Y. Diao, et al., Loading of "cocktail siRNAs" into extracellular vesicles via TAT-DRBD peptide for the treatment of castration-resistant prostate cancer, Cancer Biol. Ther. 23 (2022) 163-172.

[475] A.A. Mokhtarieh, J. Lee, S. Kim, M.K. Lee, Preparation of siRNA encapsulated nanoliposomes suitable for siRNA delivery by simply discontinuous mixing, Biochim. Biophys. Acta 1860 (2018) 1318-1325.